Czech Technical University in Prague
Faculty of Nuclear Sciences and Physical Engineering


# Dissertation

## Role of Data Representation in Modeling of Pedestrian Flow

2021 Marek Bukáček

Bibliografický záznam

| | |
|---|---|
| Autor | Ing. Marek Bukáček<br>České vysoké učení technické v Praze<br>Fakulta jaderná a fyzikálně inženýrská<br>Katedra matematiky |
| Název práce | Role datových reprezentací při modelování pohybu chodců |
| Studijní program | Aplikace přírodních věd |
| Studijní obor | Matematické inženýrství |
| Školitel | Doc. Milana Krbálek, Ph.D.<br>České vysoké učení technické v Praze<br>Fakulta jaderná a fyzikálně inženýrská<br>Katedra matematiky |
| Školitel specialista | Doc. Ing. Jaromír Kukal, Ph.D.<br>České vysoké učení technické v Praze<br>Fakulta jaderná a fyzikálně inženýrská<br>Katedra softwarového inženýrství |
| Akademický rok | 2020/2021 |
| Počet stran | 176 |
| Klíčová slova | Pohyb chodců<br>Celulární model<br>Evakuační experiment |

Bibliographic Entry

| | |
|---|---|
| Author | Ing. Marek Bukáček<br>Czech Technical University in Prague<br>Faculty of Nuclear Sciences and Physical Engineering<br>Department of Mathematics |
| Title of Dissertation | Role of Data Representation in Modeling of Pedestrian Flow |
| Degree Programme | Applications of Natural Sciences |
| Field of Study | Mathematical Engineering |
| Supervisor | Doc. Milana Krbálek, Ph.D.<br>Czech Technical University in Prague<br>Faculty of Nuclear Sciences and Physical Engineering<br>Department of Mathematics |
| Supervisor specialist | Doc. Ing. Jaromír Kukal, Ph.D.<br>Czech Technical University in Prague<br>Faculty of Nuclear Sciences and Physical Engineering<br>Department of Software Engineering |
| Academic Year | 2020/2021 |
| Number of Pages | 176 |
| Keywords | Pedestrian Movement<br>Cellular Model<br>Evacuation Experiment |

**Abstrakt** Předkládaná disertační práce si klade za cíl vylepšit mikroskopické vlastnosti celulárních modelů pohybu chodců, především se zaměřuje na individuální vlastnosti chodce a jejich heterogenní povahu. Byla implementována vlastní varianta Floor field modelu se zakomponovanými originální prvky které přiblížily model realitě. Z důvodu kalibrace modelu a popsání standardního chování chodců autor navrhl a zrealizoval čtyři evakuační experimenty; analýza dat extrahovaných z kamer a dalších detektorů poukázala na dosud nepopsané jevy jejichž podrobná studie představuje další těžiště této práce. Konktétněji, pozorovaná heterogenita v rychlosti, agresivitě a volbě dráhy byla promítnuta do vylepšeného modelu, což přineslo lepší shodu distribuce pozorovaných veličin, především evakuačního času. Při matematickém popisu experimentálních pozorování se autor zabýval vytvořením obecného konceptu hustoty zastřešující různé metody výpočtu. Vlastnosti těchto metod jsou podrobně prozkoumány a ilustovány na experimentálních datech. Kromě vyhodnocování vlastních experimentů se autor podílel také na realizaci a vyhodnocování dvou experimentů evakuace vlakové jednotky a organizoval dva experimenty slučování chodeckých proudů cílených na složitější infrastrukturu. V rámci této komplexní geometrie proběhla také validace modelu, a to nejen na vlastních datech, ale i na datech měřených zahraniční výzkumnou skupinou.

**Abstract** The presented dissertation aims to improve the microscopic properties of cellular models of pedestrian movement, focusing mainly on the individual pedestrian characteristics and their heterogeneous nature. A custom variant of the Floor field model was implemented with incorporated original elements that brought the model closer to the reality. In order to calibrate the model and describe the standard behavior of pedestrians, author designed and performed four evacuation experiments; analysis of data extracted from cameras and other detectors pointed to several undescribed phenomena – their detailed study become another pillar of the thesis. To be more specific, the observed heterogeneity in speed, aggressiveness and path selection was projected into the custom model resulting in a better fit of the observed quantities distribution, especially the evacuation time. In the mathematical description of experimental observations, the author dealt with the creation of a general concept of density covering various calculation methods. The properties of these methods are investigated in detail and illustrated on experimental data. In addition to evaluating calibration experiments, the author also participated in the organization and evaluation of two train unit egress experiments and he organized two merging pedestrian streams experiments focusing to more complex infrastructure. Using such complex geometry, the custom model was validated on in-house measured data as well as the data measured by a foreign research group.

# Contents

# Chapter 1

# Introduction

The dynamic of socio-physical systems or in particular pedestrian movement is a progressive interdisciplinary research field. With respect to the process of data acquisition and consecutive analysis, to the development of both analytic and numerical models, to the statistical validation and finally to the interpretation of results, presented research combines applied mathematics and statistics with software engineering and eve theoretical physics.

Even the initial goal was set to the model development for one specific situation, multiple sub-tasks occurred an the project become much wider. To calibrate and validate any model the reliable testing data are crucial. Unfortunately public datasets appeared too late thus we had to introduce own experiment and develop video processing tools. Then we had to query fundamental statistics from raw data, facing the issues with various definitions of basic quantities, therefore we had to bring our own "universal" approach. Actually analyzing all aspects of the process is a beneficial for the thesis, it has prevented us from misinterpretation of different studies.

The author has been working on this topic since his bachelor thesis [1] where the crowd motion is analyzed as a special case of granular system dynamics. Within this work, the basic version of Floor Field model is introduced – the first brick of this thesis was placed.

In following master thesis [2], the author extends this model by several original features, using the data from two egress experiments he organized. Model was calibrated to mimic the free flow and congested state from macroscopic and even microscopic point of view. The drawback of this model was the lack of individual aspects enabling to implement the heterogeneity of pedestrians.

Therefore the dissertation has ambitions to rise the analytic background and the model itself to another level, where individual pedestrian characteristics would affect the results. To handle that, the right quantities characterizing individual features have to be defined, extracted from experimental data and implemented to the model.

The strategy of research follows simple pattern to reach above mentioned goal. An unknown phenomena is spotted in existing observations. A measurable quantity is defined and evaluated on available data, if possible. Otherwise, a new experiment is designed and realized. After quantification, the model is extended to cover given feature, parameters are calibrated on measured data and whole concept is validated.

Such approach was used to study the heterogeneity in free flow velocity, the different ability to push through the dense crowd and even the different strategy in path selection. Even each phenomenon required specific modification of the model, its cellular core remained. The crucial element is the right heterogeneity in parameters.

The whole research was conducted in cooperation with Pavel Hrabák who has contributed mainly as a model development and calibration consultant. Fruits of this cooperation are visible in publication list – together we have written 15 articles accepted be prestigious journals.

The experimental data were not used only as the support for calibration of developed model or illustrating crowd behavior. In cooperation with Milan Krbálek, we have applied advanced statistical analysis on pedestrian headways data resulting in general conclusions about the social forces that may affect the crows dynamic [18].

Even this work focuses on the one room analysis, complex geometries were engaged as well. Two experiments focusing on merging of pedestrian streams were organized by our group and another one was conducted at AGH Krakow under the lead of Jaroslaw Was. Both experimental setups were implemented into our cellular model as well as into polish social distance model and all results were compared [16, 13]. Moreover, the measurements in Prague were supported by Peter Kielar from TU Munich who enveloped pedestrian tracking technique using wifi in mobile phones [25].

In parallel, we are contributing to train evacuation study introduced by the Hana Najmanová from UCEEB CTU. Two train experiments were organized focusing on the total evacuation time under various boundary and internal conditions. Our role was to help with the experimental setup and mainly with the data processing and analysis [17, 20, 22].

We should mention even the systematization of fundamental definitions and playbooks to apply them. This effort was conducted in cooperation with undergraduate students Matěj Kotrba and Marina Džabarjan whose bachelor and master thesis [33, 35] were supervised by the author. The concept of density distribution that generalize standadly used pedestrian density was developed, calibrated and analyzed in detail on experimental data.

Few years ago, Jana Vacková has joined the group to cooperate on the project "Pedestrian reaction to changes in his/her surroundings". The leading point was set to the relation of velocity and local density, but the detected complexity of this task lead to the design and implementation of continuous rule based model of pedestrian movement [27, 32]. Jana is working on this topic within her dissertation, the progress is frequently consulted.

The document will be organized as follows: In this introduction chapter, both modeling and analytic effort will be summarized, including the review of published papers. The body of research is covered by pedestrian quantities definition and analyses chapter, crowd motion analysis chapter and model review, design and simulation chapters. After the conclusion and reference sections, few more details about realized experiments will be provided.

Even the author spend a lot of time unifying 10 years of research and publications into one compact book, a reader may found sections that differs by the writing style, level of language or even in the way how the argumentation is lead. I hope such inconveniences won't damage the experience taken.

As mentioned above, the author had the privilege to collaborate with multiple colleagues whose contribution should be credited. I would like to thank to my supervisors, GAMS team members and all my student whose support or inspired my research. For this reason, the author's plural will be used wherever appropriate.

## 1.1 Analytic Areas

The dynamics of pedestrian crowd is an attractive object of study for researchers from a variety of scientific fields providing a great opportunity for interdisciplinary dialogues [80, 119, 128, 130].

In general, public events with large number of participants are quite common. Well designed infrastructure must be able to handle traffic peaks as well as some emergency cases, e.g. evacuation. To fulfill this goal, many requirements should be fulfilled, each of the would represent independent block to study. In this work (especially in chapter 3 dedicated to analytic studies), will focus on following three:

### 1.1.1 Phase Transition

To achieve reasonable evacuation time, a pedestrian should be able to keep his/her preferred free flow velocity. Any significant slow down caused e.g. by the dense crowd around would dramatically extend total evacuation time.

Therefore the key task is to determine conditions when adjust they behavior due to the crowd and when slow down or stop. This question may be addressed both from macroscopic perspective (analyzing the occupancy in the area and the flow through) and microscopic (analyzing the velocity of specific pedestrian and the density around him).

The density-flow relation, resp. density-velocity relation are critical for pedestrian dynamic, thus they are referred to as fundamental diagrams [123, 118]. Their shape is influenced by the geometry of infrastructure, by the attributes of pedestrians and even by their culture. Therefore published researches significantly differ, as shown further.

The transition from micro to macro is natural using some mean value approximations or distribution estimates (e.g. kernel technique). The second way is at least partially possible, with construction of the most likely behavior of pedestrian fulfilling a number of macroscopic observations.

Any observation approach indicates that the pedestrian system (similarly to particle systems) may occur in several states (phases). Free flow state is characterized by low density allowing independent motion of pedestrians (could be compared to gas). On the other side of spectrum is congested state where, similarly to crystals, are pedestrians packed into a cluster without a possibility of independent movement. Typically the congestion is characterized by low density, but is is not a rule. Highly synchronized cluster may move forward, at least to the first obstacle on the route [126].

The phase transition (from congestion to free flow and vice versa) itself is not a jump like dynamic, but more continuously (through some liquid phase). Moreover, the system indicates significant hysteresis [125], thus the point of transition is hard to identify. It

seems beneficial to use some indirect quantities dependent on the state, e.g. travel time that reflects the state if the system with high sensitivity.

Such complexity in the system implies various complication, thus we have decided to start with single bottleneck and check complicated geometries later.

### 1.1.2 Bottleneck Effects

Bottleneck is understand as a part of corridor when the width changes. The capacity of bottleneck (i.e. the maximal capacity) is given not only by the minimal width, but by the width before and even after narrowest point. As validated in [150], the important is even the length of narrow segment. Pedestrians are capable to temporarily accept the high density, thus the short bottleneck (e.g. the door) is less limiting than several meters long corridor of the same width.

The state of the system in front of the bottleneck is (from mid or long term perspective) determined by the incoming flow. In theory, any inflow higher than capacity has to result in congested state and on the other hand, any crowd should occur when the capacity is not reached. This is the exact behavior of liquids, thus this concept is know as the hydrodynamic approximation.

As will be shown further, the reality is more complicated. The experiments with inflow fixed near the value of bottleneck capacity detected a state where a relatively small cluster occurred. Slightly higher inflow produced slightly larger cluster, but again the cluster size stabilized. It seems that the bottleneck capacity is affected even by the conditions in front of it, i.e. the crowd size and even the gradient of crowd size.

Such dynamic motivated us to introduce the third phase of the system as "matastable phase".

### 1.1.3 Complex Phenomena

Even the complex infrastructure may be considered as the system of connected bottlenecks, several observed phenomena go beyond such simplified concept. The complex geometry is characterized by the interaction of pedestrians streams (i.e. a group of pedestrians wanking the same direction) that includes merging, crossing of counter flow [44].

In all these cases, the synchronicity of a pedestrian stream is crucial. It is known that a more harmonic, organized group is efficient in motion, even the group itself is not instructed to behave in organized manner. The rules used in collision avoidance on crossroad or in case of counter flow, the zip rule or the counter flow oscillation at bottleneck segment are generally known.

A pedestrian tends to apply these rules optimizing the motion of all group not only because it is beneficially for them self, but even because they feel a kind of connection within the crowd. The collective behavior roots in deep instincts and its impact grows when the situation deviates from routine, see experimental study of motion under limited visibility [62].

As detected within our merging experiments, each bottleneck may be considered as a synchronization segment, positively affecting the performance. Bottlenecks closer to the start-

ing point produced higher time headways as well as their higher variance. This observation is in agreement with previous ideas that a kind of established order in crowd limited conflicts and other effects comparable to physical friction.

The highly risky situations may cause panic (i.e. the state of selfish behavior at the edge of rationality) when individualistic aspects prevail. It is stated that such behavior is counterproductive, but it differs with the point of view. Imagine a strong person at the end of the crowd in case of fire. He/she could push through the crowd (in panic), caused several conflicts and eventually save himself, even several other people may die or be injured. Imagine the other case, when this last person does not use his potential in order to keep the evacuation as smooth as possible. Imagine for simplification that this man will be the only victim comparing to the multiple victims in the first case. Even the total numbers are better for the smooth evacuation, it would be much productive for him try to save himself.

The observation from real life catastrophes illustrates existence of both patters, stampedes occurred many times during the Mecca pilgrimage [113] as well as the football match disasters motivating organizers to improve the infrastructure. On the other hand, during the bomb attack in London 2012 only minor part of affected people left the undergrounds in panic while majority stays there to help others. The key feature determining the situation is the immediate estimate of individual risk as well as the behavior of others.

The ability of crowd to avoid panic and to follow the evacuation guidance may be raised by regular evacuation drills and other methods increasing the level knowledge among the citizens/participants.

Anyway, the goal of all engineering, starting with legislative through architects to fire engineers is to develop such infrastructure that would decrease the risk in case of any kind of disaster. That would prevent the panic or at least decrease its negative impact.

## 1.2 Applied Models

With respect to the above mentioned ambitions of this scientific discipline, the practical outcome is a prediction model of pedestrian flow. There are various kinds of models where chosen approach differs with the purpose (summarized in Chapter 4). This project focused on following sample:

### 1.2.1 Hand Calculation

Macroscopic flow approximation frequently called “Hand calculations” is based on iterative process:

$$J_i(t) = f(N_i(t)), \tag{1.1}$$

$$N_i(t) = N_i(t-1) - \sum_i J_i^{out}(t-1) + \sum_i J_i^{in}(t-1). \tag{1.2}$$

where typically $f(N) = \min(N, C)$ with $N_i(t)$ denoting the number of pedestrians in front of the bottleneck $i$ in time $t$ (i.e. the occupancy) and $C$ refers to the capacity within the one time unit. The flow through the bottleneck is constant if there is sufficient number of pedestrians in front of it.

Such model is very useful for complex structure simulations described by oriented graph, where each vertex represents one bottleneck. The value of vertex may be interpreted as the occupancy an the value of the edge could be the free flow time distance of consecutive bottlenecks $t_{ij}$. Enhancing the (1.1) by the substitution $J_i^{out}(t) = J_j^{in}(t + t_{ij})$, the system is transparent and after few technical corrections (e.g. maximal occupancy of a bottleneck) covers all information needed.

The drawback of this method is ignoring the deviations characteristic for social systems, nerveless the calculation is simple and the results aren't far form reality.

We have applied this approach on merging study, comparing hand calculation with experimental data (section 3.5.12) and floor field model (section 6.5). After quick calibration, total evacuation time and curves visualizing the progress of the evacuation were provided.

### 1.2.2 Cellular Automata

Cellular automata represents a model family discrete in time and space, with dynamic implemented as a set of rules. The size of one cell mostly corresponds to the size of a pedestrian, thus the motion is quite similar to the chessboard simulation. Based on the state of the surrounding an agent (virtual pedestrian) chooses the most profitable cell assessed with respect to some probabilistic function.

The floor field model [45, 77, 110, 96] is the most popular representative implemented, enhanced and used for simulations in Chapters 5 and 6.

Such approach is widely used and modified for specific purposes, thus we can find models enhanced by the other pedestrian movement anticipation, physic forces or inertial effects [41, 50, 53, 69, 78].

We have focused on the improvements of individual characteristics thus we have enhanced basic model by the concepts of heterogeneous velocity, aggressiveness and path selection [3, 4, 14].

**Heterogeneity in Time** The key point to establish heterogeneity in velocity is to separate the agent's actualization frequency from the actualization frequency of the whole model. Then, each agent could have its own frequency simulating its velocity. Then the actualization of an agent does not happen each step but it is driven by more complex algorithm.

The first approach related to the asynchronous cellular automata introduces the adaptive model time span [5]. Global frequency is not defined at all, the time of the next model update is set to the nearest agent update time (or the inflow to the system or another action in general). To keep a certain level of synchronicity, such approach requires wise selection of individual frequencies as explained in the section 5.3.

The other method is based on the global actualization frequency cutting the timeline to the actualization frames. All agents with their time of next update are manipulated at once, but their time of next update is recalculated based on the exact previous values. Such approach solves all potential issues thus it is used in most of the simulations. The only limit is technical – the global actualization frequency shouldn't be lower than the frequency of the fastest pedestrian.

**Conflicts** The velocity of agents defines their performance in the free flow, but its effects vanishes under congestion. Analytically, we have introduced the statistics "aggressiveness" defined as the linear fit slope of travel time – occupancy model (see section 3.2.1 for details.

The ability of efficient movement is more related to the ability to win conflicts, i.e. the situation when multiple agents select the same cell. With the probability $(1 - \mu)$), one of the agents is selected for the motion and other stand; with the probability $\mu$, no one moves. Such "friction" is critical for a successful socio-physical systems.

Then the individual parameter "aggressiveness" deforms the random selection of the agent to move from uniform distribution towards more aggressive agent [12]. Moreover, we have generalize the parameter $\mu$ in order to decrease the friction $\mu$ with increasing difference of aggressiveness among conflicted pedestrians.

**Path Selection** Based on microscopic observations, the path selection task can be simplified to the decision whether an agent prefers to join the crow or it tries to overtake it. In presented model, such choice is realized by the option to select an occupied cell. In case and agent selected occupied cell, a bond between him and blocking agent is created [4]. Due to the bond, the next motion of blocking agent triggers the motion of bonded agent thus they become synchronous. Therefore a line (or the whole crow) may efficiently move as one pack.

In case of removing the occupied cells from the decision, an agent has to overtake blocking person, i.e. it is realizing the other strategy. It is not needed to limit the model to binary choice, the individually parametrized penalization of occupied cells enables the full scale between mentioned extremes [14].

### 1.2.3 Agent Systems

Agent systems continuous in time and space are mostly rule based engines combining social aspects and classical mechanics to provide microscopically reliable simulation. Within a dissertation of Jana Vacková, we have decided to develop such model covering all observed behavior. This model is in the calibration phase (that is interesting itself), yet several results (and this introduction) has been published in [31, 32].

To capture the agent moving process properly [39, 104], we choose to let the pedestrians make their own decisions in accordance with conditions in their neighborhood. There are many benefits of this choice – since heterogeneity in pedestrian behavior is observable (see section 3.2 or e.g. [119, 66]), the decision-based pedestrian model can be simply generalized to predict the movement of many different groups of people [100]. The choice behavior during evacuation process in a building [152] and pedestrian competitiveness [56] can be also considered. Developing of pedestrian models with simple and realistic principles [74] or capturing rational behavior using perception and decision stages of pedestrian movement [39] are examples of the contemporary topics.

Model, even implemented for simple room, assumes independent strategic, tactic and operational phases. Strategy is globally defined as "leave the room by the only door". Tactical phase provides a set of checkpoint navigating an agent around obstacles and potentially around the crowd. An finally, the operational phase realize the movement from one checkpoint oa another. As a rule based model, the update (on the operational) is defined by set

of rules:

**Blind Velocity** Firstly, the pedestrian tries to find their new position using the optimum (i.e. blind) direction, which is calculated as the one to the current checkpoint, and they keep moving with the desired speed or accelerate

**Collision Avoidance** If the blind velocity fails, i.e. the optimal position is not available, the pedestrian needs to change the optimal direction due to the possible collision with the room equipment or the other pedestrians. As we still want the pedestrian to profit as much as it is possible, the change of the course is minimized if there are more possibilities and changing their course is examined primarily (it does not change the pedestrian speed which can be still increased. If the change in the pedestrian course does not solve the conflict, the slowing down is admitted.If there is more than one admissible position after the pedestrian slows down, the deceleration is minimized, see illustration in Figure 1.1.

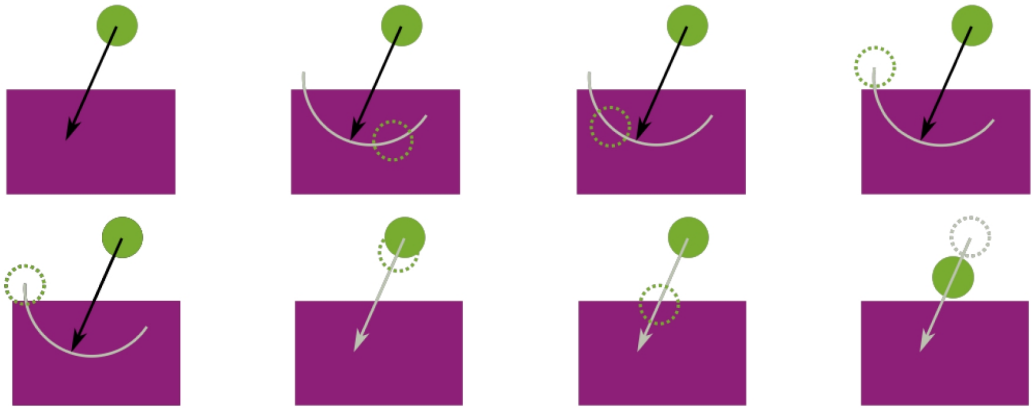

Figure 1.1: Top: collision avoidance by course change - the blind velocity, searching for admissible positions, the final position. Bottom: collision avoidance by slowing down - the course change does not work, searching for positions by shortening the blind distance, the final position.

**Dense Crowd Behavior** To avoid clogging, we allow agents to change their (social) size used in free flow for collision avoidance up to their physical size. Such behavior is in agreement with observations, pedestrians are able to squeeze through a space even smaller than the shoulder distance. Finally in case an arch occurs causing a deadlock in the model, a jump through rule is applied for appropriate pedestrian, see Figure 1.2.

**Calibration Results** As mentioned, this model is the calibration phase, we are working on calibration episodes that focuses on particular parameters. So far it seem we are on the right path - a modification of parameters reflects into the monitored quantities expected way (see Figure 1.3), thus a wise choice of parametric set up should generate correct outcomes.

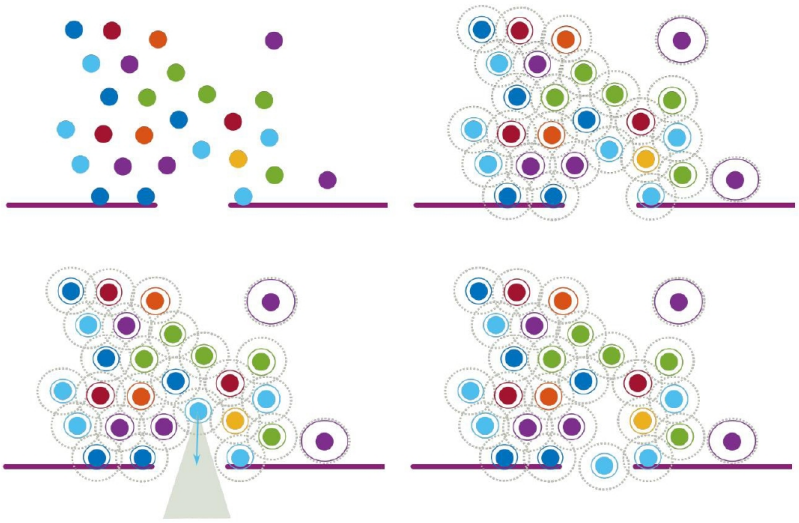

Figure 1.2: Dense crowd behavior - when an arch occurs in the exit area and the solution by crisis model rules is provided. Solid circles around pedestrians represent the pedestrian social size which changes in time, dotted circles depict the initial size.

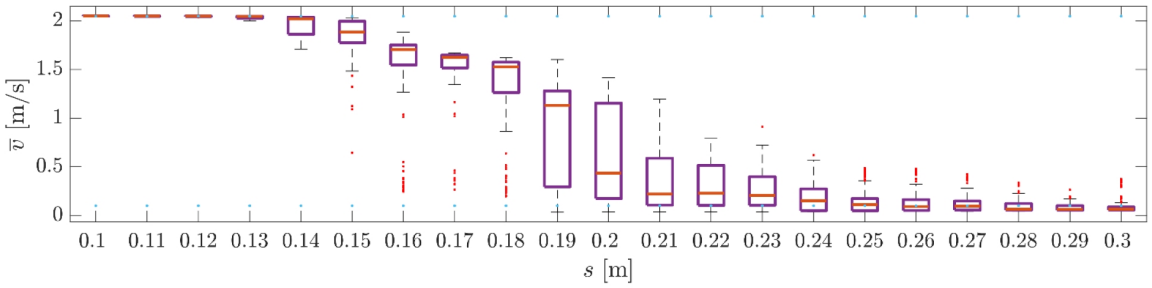


Figure 1.3: Calibration study: mean speed with respect to parametric settings of pedestrian (initial) size.

## 1.3 Conducted Experiments

As mentioned earlier, 8 experiments organized or co-organized by the author have been performed to support this study. Both the ambitions and the quality were increasing in time, the first issue in 2012 consists only of observing predefined group of 30 volunteers leaving rectangular room without any obstacles. On the other hand, latest experiments are performed in artificial room or or special object, boundary conditions are controlled to get demanded situations and the data from camera records are extracted by advanced image processing tools. The basic information of performed experiments is summarized in Table 1.1.

| ID | type | date | phenomena | image processing |
|---|---|---|---|---|
| E1 | leave the room | 28/02/2012 | crowd formation | manual |
| E2 | passing through | 10/12/2012 | individual FD | automatic detection (basic) |
| E3 | passing through | 13/05/2013 | phase transition | automatic detection |
| E4 | passing through | 29/04/2014 | heterogeneity | automatic identification |
| E5 | multiple bottlenecks | 07/03/2016 | crowd merging | developed semiautomatic tool |
| ET | train evacuation | /06/2015 | crowd merging | developed semiautomatic tool |
| E6 | multiple bottlenecks | 20/12/2016 | crowd merging | developed semiautomatic tool |
| T2 | train evacuation | /03/2018 | heterogeneity | developed semiautomatic tool |

Table 1.1: Review of performed experiments.

### 1.3.1 Experiment 1

The first experiment was organized as a part of author's research project to support developed cellular automata model. To calibrate several parameters, a group consisting of 70 undergraduate students was arranged into the predefined formation and instructed to leave the room (study hall of FNSPE) as fast as possible, without running or pushing each other by the exit situated in the opposite wall. In last four runs, the running was allowed (only volunteers instructed to be cautious participated).

This process repeated 29 times with different initial shape and position, to get sufficient amount of data. The experiment was monitored by cameras enabling rear view, side view and view from the top of the exit. Camera records did not enable the automatic detection of pedestrians, thus only macroscopic observations were performed. Moreover, the time headways at the exit were recorded manually that enables numerical analysis.

**Results:** Even without the trajectory data we were able to bring several observations published in [3, 4]:

- behavior is rather deterministic, participants kept their initial formation until the exit area
- at the exit, the funnel-like shape of crowd was observed for all walking rounds. The semicircular crowd appeared for rounds where running was allowed – these rounds performed much more competitiveness. These observations motivated us to introduce different shapes of potential generated by the exit
- average velocity: 1.46 m/s
- the flow through the 0.6 m wide exit: (1.1 ped/s, 1.7 ped/s), lower flow at the end of each round

Even the results were sufficient to basic calibration of designed model, we learned that without image recognition system and some factor increasing motivation, there is no way to get reliable microscopic data.

### 1.3.2 Experiment 2 & 3

The place and participants remained the same (FNSPE study hall, second year students), several enhancements were implemented to mimic real conditions.

First, an artificial room (7.8 m $\times$ 5.5 m) from paper and wooden construction was build inside the study hall. This room had one entrance (width 2 m) and one exit (width 0.6 m), that enabled circulation of participants.

For each of 9 E2 rounds and 11 E3 rounds, pedestrians entered the room according to traffic lights in front of the entrance, passed the room and leave it (as fast as possible, without running or pushing each other). The green signal was alternated by randomly long period of red light, intervals were generated from trimmed normal distribution (var $= 1$, $\mu \in (1.3, 1.8)$). Once they left the room, they moved back to the pool in front of the entrance. This continuous process significantly improved the motivation of participants because no one could wait in front of the exit for better conditions.

Moreover, signalization device together with variable number of entering pedestrians on one green signal enabled to control the conditions inside the room. For each round, a specific parameters were set and held for few minutes, optimally to reach the steady state.

The last modification improved the monitoring system. One panoramic camera was installed on the ceiling in the middle of the experimental room. Pedestrians were equipped by red paper hat with written number for recognition (E2) resp. white paper hat with red circle in the middle (E3). Even though this number was not readable by automatic system, developed image processing tool enabled to extract pedestrian trajectories. The accuracy of detection was significantly higher in E3, due to the absence of hat overlapping.

**Results:** These results motivated the first set of improvements implemented into cellular model including spontaneous line formation, prediction of the motions in the surroundings and asynchronous update.

Evaluation of velocity and density for each point of the trajectory enabled to assign the space coordinates to measured quantities, thus the spatial maps of dynamic quantities were provided [6]:

- the drop of velocity appeared 3 meters ahead of high density area
- the lowest velocity is reached 1 meter in front of the exit. Then, the velocity increased even the density was constant
- in the crowd area, the velocity is higher near walls comparing to the inner location, even the density is the same

Inflow driven phase transition from free flow to congested state indicated the metastable zone in the interval $J_{\text{in}} \in (1.3, 1.7)$.

The detail analysis uncovered significant differences among the individual paths observed under the same conditions, but without pedestrian identification it is not possible to distinguish personal preference from random element. Thus the identification system has to be introduced ...

### 1.3.3 Experiment 4

This time, the artificial room was equipped by three cameras, one for global overview and two to monitor inflow and outflow. The central camera was used mainly for synchronization, the automatic data processing was applied to border cameras. The exit from the room was extended by the corridor of the same width (0.6 m) to study even post-exit behavior.

Previous experiments were affected by the differences between expected and realized inflow and by the injecting pedestrians in pairs or triplets. In the E4, three parallel entries were build along one side, each controlled by independent signalization device.

In total 10 runs of passing through scenario were performed, the range of inflow parameter covered different phases of the system, the duration of each round varied from 3 to 5 minutes.

**Results:** This experiment finalized the room evacuation project. Video processing methods and inflow control brought the high quality data that enabled to perform all designed studies.

- phase transition induced by inflow from free flow to congested state in band (1.35, 1.5) ped/s through meta-stable state [8]
- capacity of bottleneck influenced by the size of the crowd [8]
- individual travel time modeled by the piece wise linear model reflecting the occupancy [11]
$$TT(i_\alpha) = \frac{S}{v_0} + \mathbf{1}_{\{\overline{N}(i_\alpha)>7\}}(\overline{N}(i_\alpha) - 7) \cdot \text{slope}(i_\alpha) + \text{noise}$$
- exit angle distribution study with respect to the occupancy and its effect to the travel time [15]
- lower travel time reached by trajectories along the walls [11]
- movement synchronization evaluated from the time headways at the exit and behind [11, 17]
- movement heterogeneity increment with occupancy [8]
- heterogeneity used for model calibration [12, 14]

### 1.3.4 Experiment 5 & 6

This set of experiments focused on the motion in complex geometry especially on the merging of four pedestrian streams, see details in section 3.5.12. The E4 experiment shown that the headway distribution measured at the exit is the same for different value of inflow (producing a crowd in front of the exit) and that the consecutive produced lower and lower variance. These experiments aimed to check whether such synchronicity would be observed even for geometry that differs from corridor.

To conduct these experiment, we have leveraged the geometry of stidy hall T-201, where four stairways led to the two doors to the adjacent room with one door to the platform. Both realizations consisted of 6 rounds, each with approximately 60 participants.

Experiments were monitored by cameras on top of the doors and by main camera in the lecture hall. The data were processed by semi-manual software. Moreover, E6 was monitored by the beta version of wi-fi technology communicating with participants mobile phones [25].

**Results:** Time headways distribution analysis confirmed the role of bottleneck as a synchronization unit. Consecutive exits indicated not only lower variance, but even lower mean value, thus observed synchronization improved the performance of the evacuation [17].

Other than that, measured data were used to (successfully) validate developed model on the complex infrastructure. Results were shared with the AGH Krakow, where similar experiment was conducted, the comparison of both experimental datasets and two implemented model was published in [16].

### 1.3.5 Train evacuation experiments

Two train egress experiments were organized by the UCEEB CTU, our contribution was to help with the realization of second experiment and the overall data analysis. As described in section 3.3, a double-deck electric unit class EPJ 671 (CityElefant) intended for passenger service in the vicinity of city agglomerations was available for more than 10 rounds in each experiment, covering six independent parameters to total evacuation time, namely exit width, exit type, exit availability, heterogeneity of passengers, distribution of passengers and time to stop effect [17, 20, 22].

The train was equipped by cameras focusing on all potentially significant areas, but the low ceiling disabled automatic detection thus the semi-manual software was used.

**Results:** The time headway analysis at the main exit up to 1.2 m wide studied the effect of two pedestrian rows that may pass almost independently. Their distribution represents the mixture of headways in one row and the phase shift between them. The pillow like pattern indicating egress in pairs is alternated by the constant like pattern representing the phase shift equal to the one half of period.

These time headway trends were used to explain the differences in total evacuation time measured for different settings. Generally we can say that a “standard headway” is the same for all occasions, and that the performance is given by the occurrences of extremely high headways observed for heterogeneous population (kids, old people) and for the exit to the open terrain [17].

The other analysis focused on the individual pedestrian performance. The lower deck passenger were significantly prioritized due to the distance of their initial position and the exit room. The lower deck passengers occupied this room thus the upper deck passengers had to wait at stairs and started their evacuation later.

## 1.4 (Un)related Activities

The research on the pedestrian dynamics covers a wide set of analytic, stochastic or modeling tools thus it shouldn't be a surprise that author have applied some of them on completely different task when a chance appeared. From all such distributions, three projects wort mentioning.

### 1.4.1 Analytic Activities for Škoda Auto

Škoda Auto and Czech Academy of Science participated on many research activities under TACR foundation. Author has been working on few of them.

One typical example is the estimate of road surface features from data continuously evaluated by car sensors. Based on the wheel circulation velocity, the loss of the torque or the tangential velocity, the slid detector was designed. After the calibration on the data generated within the driving test on the testing circuit with predefined road surface conditions, the tool was able to identify the dangerous conditions after the firs symptoms. Further the project continued with the proposal of some system to warn the driver even earlier, but it was stopped at the beginning.

The other project focused on the velocity control of self driven vehicle. Assuming the profile of altitude is known as well as the known speed limits on the route, the goal on the strategic was to propose the optimal velocity for each point of the planned trajectory. On the tactical level, the algorithm was supposed to deliver instructions to accelerate, break or to shift off to follow toleration band around proposed velocity. The criteria assessing the model quality combine the fuel consumption with the travel time.

### 1.4.2 Analysis of Egyptologic Data

In 2018, the cooperation with Radek Mařík (FEL ČVUT) and the Egyptology group of Miroslav Bárta was initiated. Through a hundred years of research, they collect dataset summarizing thousands of historical persons of the Old kingdom of Egypt. The overall goal of this project is to describe dynamics within the society and to study the punctuated equilibrium observed not only in the historical empires but even in modern society.

The emphasis is put especially to analysis of titles which were possessed by individual people and searching for mutual relationships between them. The personal data from tombs are used as the main source of information, especially the inscription (hieroglyphs) on false doors. Any (important) person depicted their name, titles and information about related persons there. Veronika Dulíková (CIE, CUNI) has provided expert classification to categories are based on profession, location, linked person or privileges. Any title might be assigned just to one category or it may be linked multiple times. Any shared title indicates an interaction between categories or in any aspect of real life.

After initial data analysis, we have studied the join occurrence of selected title categories [28]. As shown in Figure 1.4, even there is no title that would be shared by administrative and priestly title categories, significant number of officials held at least one title from each category. Such trivial observation from mathematical perspective can be interpreted as a proof of overlap between civil and religious government.

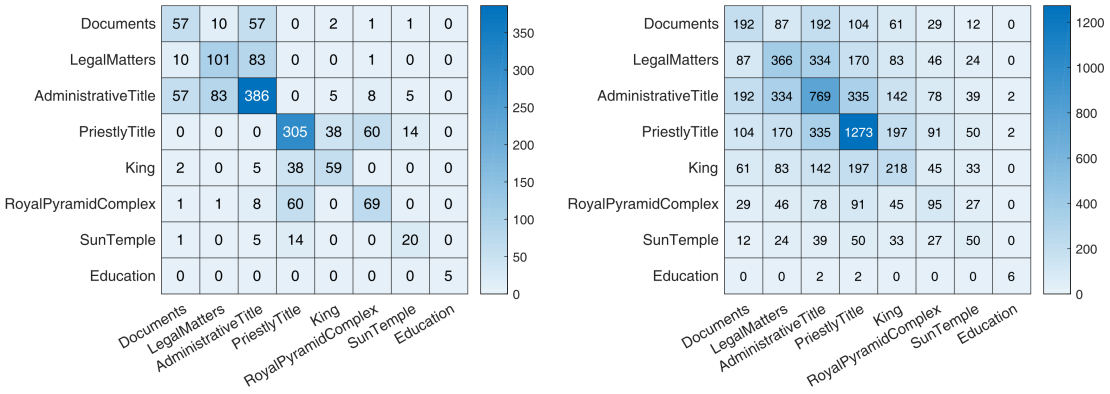


Figure 1.4: Left: the number of titles in selected categories. Right: the number of people holding a title from selected categories.

The successful proof of concept motivated us to apply more advanced methods. Decision trees, K-medoids and t-Distributed Stochastic Neighbor Embedding algorithms applied to the person – title – class data (as the student project of Martin Oharek and Benjamin Páterek) brought additional information about title similarity [29, 30].

Among other studies, K-medoids algorithm was applied to arrange each person to a cluster (interpreted as a clan) using the title – category assignment. Each person was characterized by 69 dimensional vector, the value of each dimension was derived from the number of titles from given category. 13 produced clusters were interpreted with Egyptologists, identifying correspondence to different ranks of administrative officials, priests or king's relative. To visualize the 69 dimensional space, we used the TSNE that compressed the information into three space coordinates. In the visualization on Figure 1.5 combines TSNE with the color taken from the K-medoids algorithm. We can see that significant portion of persons tends to from groups and these groups were independently detected by both algorithms. The remaining group is too complex to visualize in 3D, but even here clustering was able to separate specific subpopulation.

Now we are preparing another projects focusing to larger dataset adding artifacts and morphological information and covering larger historical period.

### 1.4.3 Medical Data Analysis

A brief cooperation with Oaks consulting was established in summer 2019 to analyze medical data related to the lungs cancer treatment. Within one year of collaboration, we have helped to build the data model storing the information about patient diagnosis, prescribed treatments and their results formulated as a time to progression, where progression might be the cancer grow, propagation or death. Based on that it was possible to compare treatments applied in different phases and to check that a cure follows guidelines.

With Jana Vacková we have used Kaplan-Meier estimate of survival curves comparing the proportion of events in time or hazard curve development, see Figure 1.6. This approach is capable to detect differences among treatments in arbitrary time after the application.

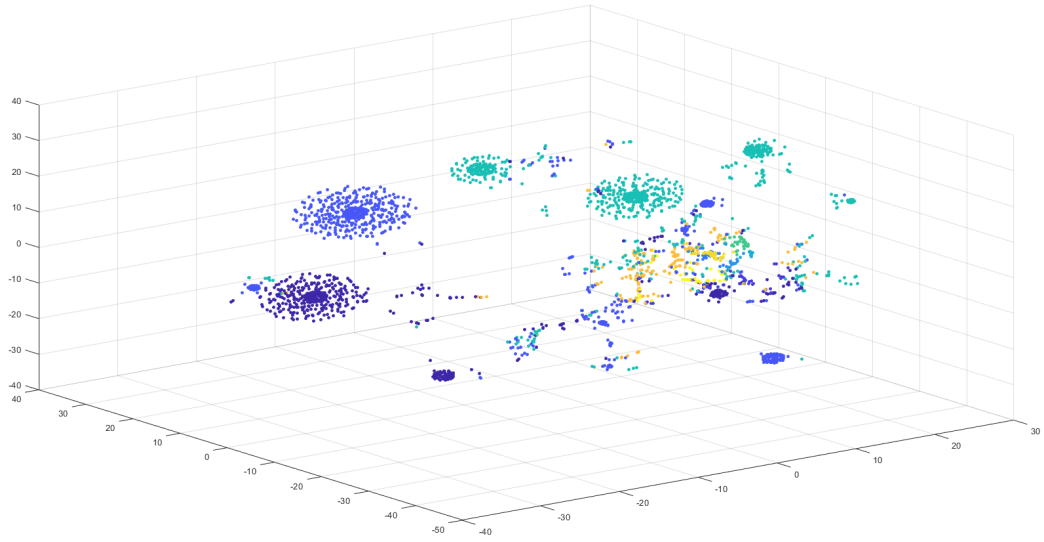

Figure 1.5: Left: the number of titles in selected categories. Right: the number of people holding a title from selected categories.

With assumption of similar diagnosis (and after consultation with a medical specialist), the recommendation to prefer given treatment might be formulated.

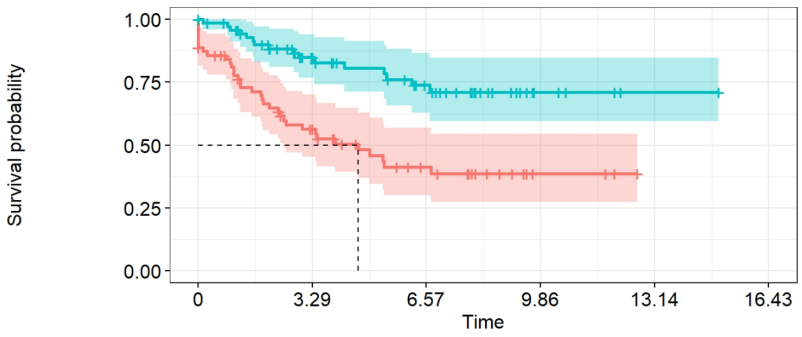


Figure 1.6: The Kaplan-Mayer estimate of survival probability for two selected lungs cancer treatments.

The other project over described data was solved within the master thesis of Martin Oharek [34]. Combining random forest and neural networks, we have proposed a treatment based on detected diagnosis clusters. As tested on toy datasets, even on these data was shown that developed classification algorithm performs better than high end classification tools. This project would detect any treatment that does not meet the expectations, but unfortunately the partner decided to continue only with internal employees.

# Chapter 2

# Definitions

There are wide spectrum of quantities that may be used to express a feature of pedestrian movement, mostly taken from different scientific branches and adjusted for specific conditions. In this section, time based quantities together with density and flow will be introduced as definitions presented here were (partially) invented and deeply analyzed during the whole research process. Other quantities will be defined where needed.

## 2.1 Time Based Quantities

As one of the purposes of pedestrian modeling is to prevent fatal outcomes of critical situations, the time required to evacuate a facility is the natural quantity to evaluate. Safety engineers distinguish ASET (available safety egress time) consisting of RSET (required safety time) and safety margin. Furthermore the RSET consists of preliminary steps (fire detection, alarm activation or the interpretation of the situation) and action steps (preparing for evacuation and movement).

In this work, we are focusing mainly on the egress itself, participants of the experiments are prepared to move on the signal, thus the travel time from their initial position to the exit is evaluated. To be more specific, the travel time $TT(i)$ assigned to path $i \in I$ is defined as

$$TT(i) = T_{\text{out}}(i) - T_{\text{in}}(i)\,, \tag{2.1}$$

where $T_{\text{out}}$ is the exit time and $T_{\text{in}}$ stands for entry or the time when the movement was initiated.

Another quantity influencing the path's properties is the mean occupation of the room denoting average number of pedestrians in the room. The mean occupancy $\overline{N}(i)$ assigned to path $i$ is defined as time average of the actual occupancy $N(t)$, i.e.

$$\overline{N}(i) = \frac{1}{TT(i)} \int_{T_{\text{in}}(i)}^{T_{\text{out}}(i)} N(t)\mathrm{d}t\,. \tag{2.2}$$

Here we note that the integral in the definition above is rather formal, since the camera records are limited by the frame-rate, and technically the average occupancy is calculated using a sum. On the other hand, this representation enables to calculate the mean occupancy even for event driven updates or records.

To compare the travel time measured under different conditions, scaling based on mean occupancy is introduced. For each occupancy bin $(N-1, N]$, $N \in 1 \dots N_{\max}$, the mean travel time $TT_N$ is defined as

$$TT_N = \text{average}\left\{TT(i) \mid i \in I,\ \overline{N}(i) \in (N-1, N]\right\}\ . \tag{2.3}$$

Then the relative travel time $TT_R(i)$ for each path $i \in I$ is defined

$$TT_R(i) = \frac{TT(i)}{TT_N}\,. \tag{2.4}$$

Let us denote by $TT_{R,\alpha}$ the set of all relative travel times of paths corresponding to pedestrian $\alpha$, i.e.

$$TT_{R,\alpha} = \{TT_R(i) \mid i \in I_\alpha\}\,. \tag{2.5}$$

To unify all path records, we scale real time to the normalized one

$$t_N(i) = \frac{t(i) - T_{\text{in}}(i)}{TT(i)}\,. \tag{2.6}$$

The value of normalized time (denoted globally as $t_N$) is in the interval $\langle 0, 1\rangle$ where $t_N = 0$ and $t_N = 1$ corresponds for each pedestrian to the entry and exit time, respectively.

## 2.2 Internal Variables

Historically the description of pedestrian dynamics is based on point approximation where the position ($\vec{x}_\alpha$) of a pedestrian $\alpha$ is defined by the center of the head or it is derived from shoulders' position. Using this simplification, quantities defined in classical physics may be used on both, microscopic and macroscopic level. As usual, we will start with density $\rho$ and flow $J$:

$$\rho = \frac{N}{|A|}, \qquad\qquad J = \frac{\Delta N}{\Delta t}, \tag{2.7}$$

where N is the number of particles (pedestrians, cars, ...) in given area A, respectively number of particles passing given cross-section in time unit $\Delta t$ [119].

Such approach can be used in socio-physical systems only when the system itself is large enough to neglect inaccuracy caused by point approximation on borders. As a limit we can consider area larger than 20 $m^2$ or the time interval larger than 5 $s$.

This restriction does not affect many practical application, but microscopical analysis and individual approach require more detail methods respecting physical and even psychical requirements to personal space. The real body mass or e.g. social zones should be considered.

Moreover, there are other phenomena to consider, namely the personal space overlapping or irregular body shape, changeable in time.

With respect to all mentioned ideas, it seems logical to convert from point approximation to the distribution approach, where each particle can be considered as a source of individual density.

### 2.2.1 Pedestrian Distribution

As the density distribution $p(\vec{x})$ over the area $A$ where is placed N pedestrians, we will understand any non-negative function which fulfills

$$\int_A p(\vec{x})\mathrm{d}\vec{x} = N. \tag{2.8}$$

Obviously some functions are more appropriate than others. The right distributions should reflect the localization of particles, but it is not clear how to do it.

The kernel estimate approach seems suitable place to start with. Assuming each pedestrian is a source of some density distribution, we can construct density distribution form individual components:

$$p(\vec{x}) = \sum_{\alpha=1}^{N} p_\alpha(\vec{x}), \tag{2.9}$$

where $p_\alpha(\vec{x})$ is the individual density generated by pedestrian $\alpha$.

Such distribution has to fulfill common requirement $\int_\infty p_\alpha(\vec{x})\mathrm{d}\vec{x} = 1$ that can be interpret as the maximal contribution. With respect to further research directions, it is beneficial to define the support of distribution $A_\alpha$ set of of all points where the individual distribution function is strictly positive, i.e.

$$A_\alpha = \{\vec{x} \in A | p_\alpha(\vec{x}) > 0\}. \tag{2.10}$$

In the other words, pedestrian $\alpha$ contributes only to area $A_\alpha$:

$$\int_{A_\alpha} p_\alpha(\vec{x})\mathrm{d}\vec{x} = 1. \tag{2.11}$$

Furthermore let us define the contribution of pedestrian $\alpha$ to area $A$:

$$N_A^\alpha = \int_A p_\alpha(\vec{x})\mathrm{d}\vec{x}. \tag{2.12}$$

Here should be notes that the occupancy in any area $A$ does not have to be an integer – the "partial presence" is a feature of presented approach. Then the occupancy in area $A$ consists of individual contributions, i.e.

$$, N_A = \sum_{\alpha=1}^{N} N_A^\alpha. \tag{2.13}$$

The properties of density distributions are driven by the applied kernel, the most relevant are listed bellow:

1. Point approximation

   $$p_\alpha(\vec{x}) = \delta_{x,x_\alpha}, \tag{2.14}$$

   where:

   $$\int_A \delta_{\vec{x},\vec{x_\alpha}}\mathrm{d}\vec{x} = \begin{cases} 1 & \text{when} \quad \vec{x_\alpha} \in A, \\ 0 & \text{otherwise.} \end{cases} \tag{2.15}$$

   Obviously original definition is a special case of presented general approach.

2. Constant distribution

$$p_\alpha(\vec{x}) = \begin{cases} \frac{1}{|A_\alpha|} & \text{when} \quad \vec{x} \in A_\alpha, \\ 0 & \text{otherwise.} \end{cases} \tag{2.16}$$

Cylindrical variant

$$p_\alpha(\vec{x}) = \begin{cases} \frac{1}{r^2\pi} & \text{when} \quad \|\vec{x} - \vec{x_\alpha}\| < r, \\ 0 & \text{otherwise,} \end{cases} \tag{2.17}$$

where a circular neighborhood with radius $r$ is assigned to each pedestrian. The density distribution is constant over the whole neighborhood.

3. Voronoi distribution [129] is a special case of constant distribution using adaptive neighborhood. So called Voronoi diagram split the area into pedestrian related cells the way that each point of the area is assigned to nearest pedestrian. To evaluate the density it is sufficient to express the volume of Voronoi cell $|A_\alpha| = \int_{A_\alpha} d\vec{x}$. By definition the cells do not overlap thus each pedestrian has ell defined individual space.

4. Conic distribution

$$p_\alpha(\vec{x}) = \begin{cases} \frac{3}{r^3\pi}(r - ||\vec{x} - \vec{x_\alpha}|\,|) & \text{when} \quad \|\vec{x} - \vec{x_\alpha}\| < r, \\ 0 & \text{otherwise,} \end{cases} \tag{2.18}$$

here $\frac{3}{r^3\pi}$ is the normalization constant.

Even here a pedestrian is represented by circular area, but the value of distribution linearly grows from zero at the edge to the maximum in the center. With increasing "blur" parameter $r$, pedestrian becomes more foggy. On the other hand in case the blur tends to zero, the distribution moves toward point approximation.

5. Gaussian distribution

$$p_\alpha(\vec{x}) = \frac{1}{2\pi \cdot \sqrt{\Sigma}} e^{-\frac{1}{2}(\vec{x}-\vec{x_\alpha})^T \Sigma (\vec{x}-\vec{x_\alpha})}, \tag{2.19}$$

with covariance matrix $\Sigma = \sigma \cdot \begin{pmatrix} 1 & 0 \\ 0 & 1 \end{pmatrix}$. Parameter $\sigma$ plays role of "blur" – even the support $A_\alpha$ is limited only by the boundaries of the hole area $A$.

## 2.3 Density

Applying above mentioned ideas to the basic density (2.7), we can derive individual density formula just by generalization:

$$\rho_B = \frac{N}{|B|} = \frac{\int_B p(\vec{x})\,\mathrm{d}\vec{x}}{|B|} = \frac{\int_B \sum_{\alpha=1}^{N} p_\alpha(\vec{x})\,\mathrm{d}\vec{x}}{|B|} = \sum_{\alpha=1}^{N} \frac{\int_B p_\alpha(\vec{x})\,\mathrm{d}\vec{x}}{|B|}. \tag{2.20}$$

Please note that we have switched notation related to area from $A$ denoting "whole area" or "whole pedestrian support" to $B$ related to the "detector" or the "area that a pedestrian perceives".

In this paper, we consider several shape of detectors as well as the individual approach.

### 2.3.1 Detector Approach

The most simple approach starts with rectangular detector area $B$, thus equation 2.20 might be applied straight forwardly.

It happens quite often that the area is defined only vaguely, one may be interested in the "density in front of the exit" or "density inside the corridor". In such case, we have to define it our self. Rather than placing a rectangle in front of the exit, we may use the agent based definition of the area.

Assuming we have selected a set of pedestrians to define the area (e.g. pedestrians that are close to the exit or pedestrians with their head inside an area). Then, we can define detector area $B_\alpha = \cup_{\alpha=1}^{N} A_\alpha$.

Moreover, lets assume other pedestrians do not contribute to $B$. As all pedestrians inside contributes by all their volume, the relation (2.20) may be significantly simplify:

$$\rho_v = \frac{N}{|\cup_{\alpha=1}^{N} A_\alpha|}, \tag{2.21}$$

that is quite similar to (2.7), but the produced density is smoother due to the smooth changes of $B$.

Furthermore, if $A_\alpha$ is disjunctive $A_\alpha \cap A_\beta = \varnothing \quad \forall \alpha \neq \beta$ (e.g. Voronoi approach), then:

$$|A| = |\cup_{\alpha=1}^{N} A_\alpha| = \sum_{\alpha} |A_\alpha|. \tag{2.22}$$

Applying to (2.21) we can get:

$$\rho_v = \frac{N}{\sum_\alpha |A_\alpha|} = \frac{1}{\frac{1}{N}\sum_\alpha |A_\alpha|} = \frac{1}{\langle A_\alpha \rangle_N}. \tag{2.23}$$

Under such constraints to the density kernel, standard density $\rho$ in area $B$ may be approximated by $\rho_v$ calculated over area $B_\alpha$. Instead of evaluating the pedestrian contribution to given area, the task is transformed to measuring the area covered by them. Such approach has benefits from implementation perspective, there is no need to construct the distribution at all.

Finally, it remains to asses methods how to select the set of pedestrians to approximate desired area (denoting $A_0$). There are to approaches to consider, see illustration in Figure 2.1:

a) all pedestrians with head in $A_0$ are incorporated – referred to as $A_{in}$

b) all pedestrians interfering by their $A_\alpha$ to $A_0$ are incorporated – referred to as $A_{out}$

Any of mentioned methods have its benefits as will be illustrated in next sections. In general, area $A_{in}$ is smaller and better approximates the density $\rho$, when the amount of pedestrian is high enough. On the other hand in case if low density, area $A_{in}$ may be frequently empty. Area $A_{out}$ expanding target area thus the chance of empty area is lower. But this approach incorporates pedestrians at the edge that have larger personal space, thus the density could be underestimated.

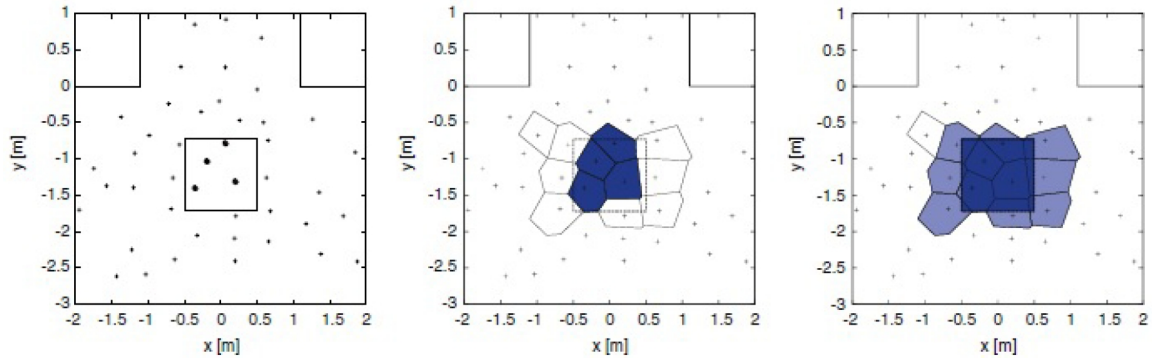


Figure 2.1: Illustration of several Voronoi based methods.

Therefore the choice of $A_0$ and method of approximation depend always on the conditions in the pedestrian system. Following sections will discuss the differences between methods and propose appropriate parameters.

### 2.3.2 Individual Approach

Quite interesting is the research studying the individual perception of density, i.e. the density "around" given pedestrian. Simple but the frequently used variant is the density calculated according to 2.20 over the circular neighborhood

$$B_\alpha = \{\vec{x} \in A | \|\vec{x} - \vec{x}_\alpha\| \leq R\}. \tag{2.24}$$

Parameter $R$ defines the range of pedestrian perception.

For purposes of pedestrian perception analysis it is beneficial to remove pedestrian itself:

$$\rho_{B\alpha} =: \rho_\alpha := \sum_{\beta=1,\beta\neq\alpha}^{N} \frac{\int_B p_\beta(\vec{x})\,\mathrm{d}\vec{x}}{|B|}. \tag{2.25}$$

More fancy shapes might be proposed – very popular idea occurring during theoretical conferences discussions is the elliptical shape with pedestrian sitting in the focus and the eccentricity dynamically adjusted with respect to the velocity. The point of this idea is to highlight the are in front of the pedestrian.

In this study, we have implemented alternative approach limiting $B_\alpha$ to the wedge shape. Pedestrian is sitting at the vertex and the axis of the wedge is oriented toward the direction of motion.

There is not metrics to decide which density is better than the other one. In following sections, the calibration process and measurable features of selected approaches are analyzed.

## 2.4 Density Detector-base Features

In this section, the analysis provided in [33] will be summarized. The differences between density evaluation methods will be illustrated on experimental data E4.

Lets consider several detectors virtually placed around exit as visualized in Figure 2.2. For each of them, we will evaluate density using above mentioned methods and check either the absolute values and trends or the stability in time.

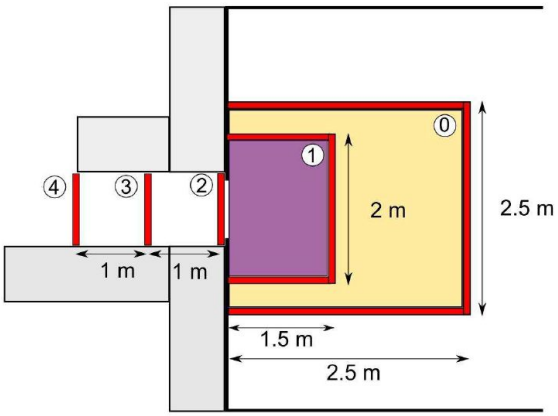


Figure 2.2: Placement of virtual detectors.

Namely, we will study standard density (refer to as $\rho_{stand}$) calculated according to (3.4), for which we need to know just the count of pedestrians in the detector.

Then, we will evaluate Voronoi density[1] within distribution approach (2.16), i.e. integrated over exact detector area (refer to as $\rho_{ex}$). This exact approach will be compared with pedestrian area approximation (2.23) using both cases: pedestrian with head in the detector area $\rho_{in}$ and then all pedestrians whose cell overlap the detector $\rho_{out}$.

Finally, conic approach (2.18) $\rho_{kuz}$ will be evaluated. In this case, only exact case makes sense as pedestrian supports $A_\alpha$ do overlap.

Mentioned methods will be assessed with respect to the trend of measured values and the smoothness expressed by the mean differences between consecutive values $\overline{\Delta\rho}$:

$$\overline{\Delta\rho} = \frac{\sum_{i=2}^{n} |\rho(t_i) - \rho(t_{i-1})|}{n}, \tag{2.26}$$

where $n$ is the length of time series produced by each experimental round.

### 2.4.1 Density in Front of the Exit

**Detector D0** was designed to cover almost all monitoring area, thus the densities tend to jump any time, when a pedestrian entered the room (as shown in Figure 2.3). We should notice as well that Voronoi approach underestimates the density with respect to the standard or conic method.

In case of relatively small D1, $\rho_{kuz}$ and $\rho_{ex}$ are almost smooth (remaining jumps may be driven by data issues), but the other methods remained jump-like (depicted on Figure 2.4). It is coded in their nature, any time a pedestrian leave the detector, the value significantly

[1] From practical purposes, the maximal size of pedestrian cell was limited to radius 1.5 m .

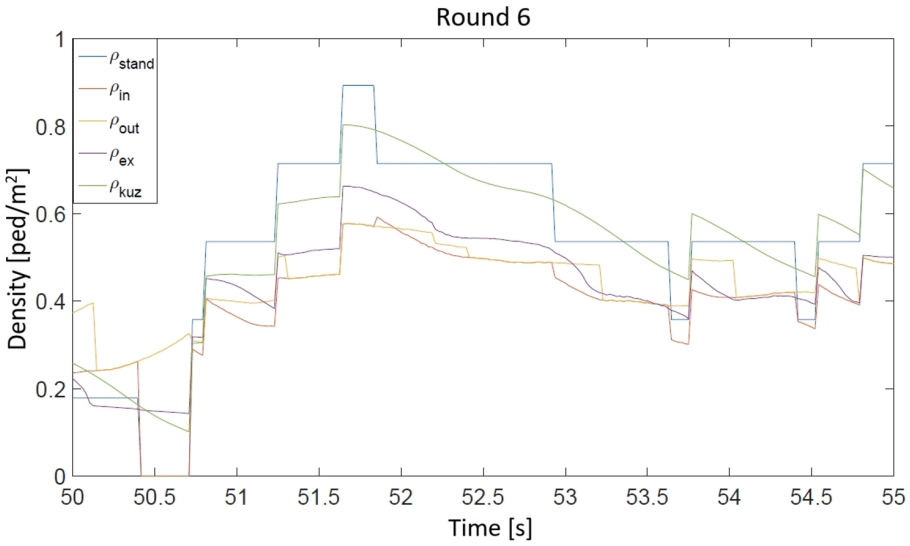


Figure 2.3: Results of different density evaluation methods in detector D0, E4, run 6, 50 – 55 sec.

moves. Voronoi methods are more smooth than standard approach, but even there some jumps may appear as new voronoi cell is incorporated to detector.

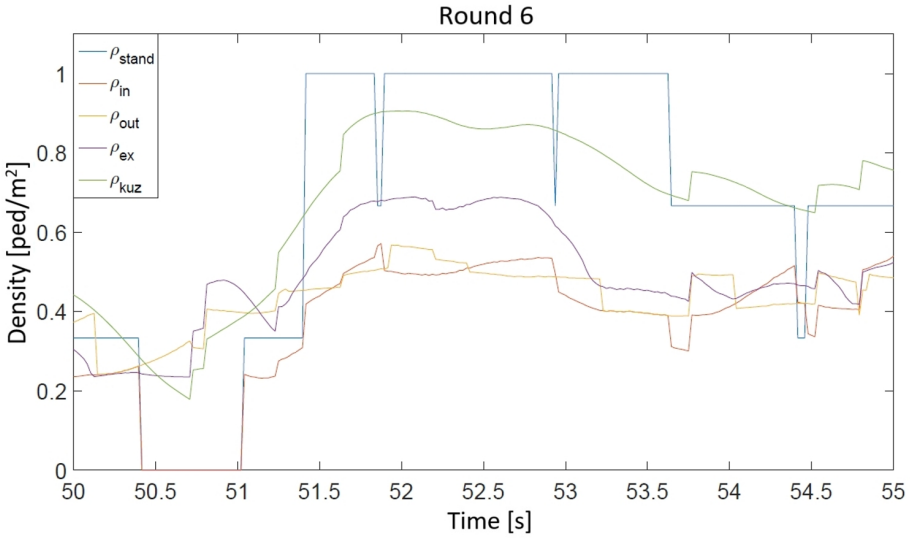


Figure 2.4: Results of different density evaluation methods in detector D1, E4, run 6, 50 – 55 sec.

Jumpy behavior may be significantly improved by filtering. There are large amount of methods, but we can keep it simple. In this work, we will use central rolling average accumulating data 2 seconds before and 2 seconds after the event.

Even from large time frame view, mentioned approaches perform differently. As illustrated

in Figure 2.5, the highest values were reached by $\rho_{stand}$, followed by $\rho_{kuz}$ and $\rho_{ex}$. On the other hand, lowest values ere generated by voronoi approximation $\rho_{in}$ and $\rho_{out}$. Even the time series are shifted, the trend is the same.

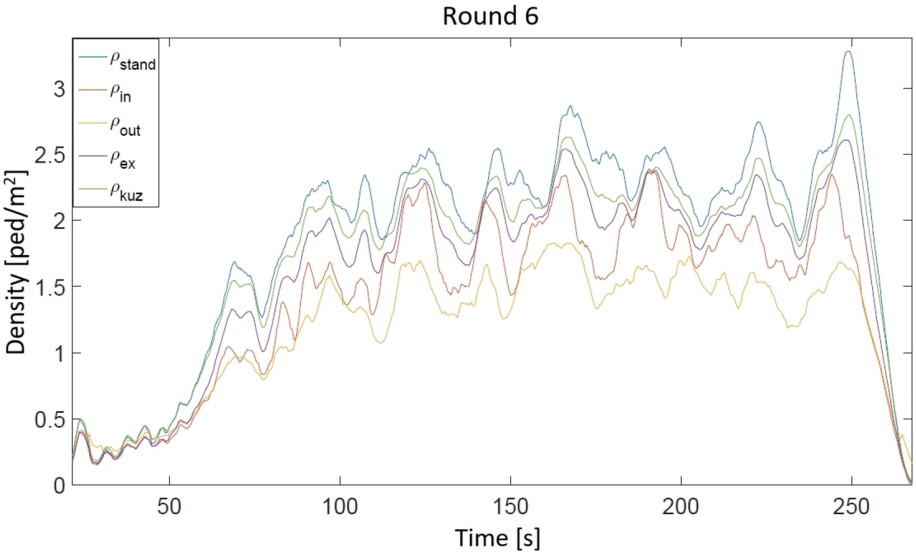


Figure 2.5: Results of different density evaluation methods in detector D1, E4, run 6.

Such shift is undesirable, even for approxamative methods – the value should be close to $\rho_{stand}$. To fulfill this requirement, pedestrian should be distributed around the detector similarly as they are distributed inside. When the conditions changes at the edge of detector, voronoi approximations fails.

With respect to the positions of D0 and D1, this requirement is hard to fulfill – detectors are in the way toward the exit, capturing all passing pedestrians. But the situation at its edges is different, the density there is lower.

Figure 2.6 summarizes the performance of investigated methods for different modes of the system, starting with free flow and ending with congestion. Density evaluation methods performs similarly for all high density rounds. Comparing free flow and high density rounds, only $\rho_{out}$ significantly differs.

In free flow case, higher density is reached when a detector can extend its size to incorporate approaching pedestrian. Lets imagine empty detector and a pedestrian one meter far. Method $\rho_{out}$ extends detector size because voronoi cell overlap the detector area. Therefore measured value is large comparing to zeros produced by other methods. The same effect causes increase of values measured at the end of experiment. Even when the last pedestrian passed the detector, $\rho_{out}$ extension may track him/her a bit longer producing non zero value.

On the other hand, in crowd situations, extension of detector incorporates large voronoi cells of pedestrians at edges of crowd. These cells decrease the value of density produced by the group of pedestrian crowded in the middle of detector.

Table 2.1 enumerates $\overline{\Delta\rho}$ criterion (2.26):

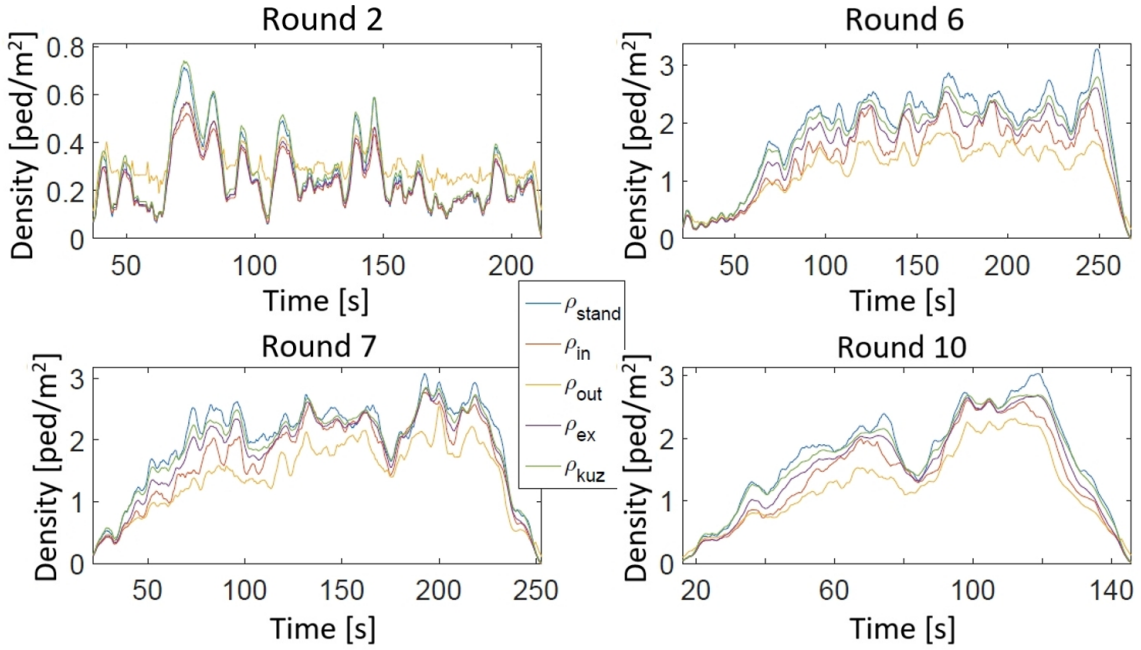


Figure 2.6: Different density evaluation methods in detector D0 within four experimental rounds.

| Round | 2 | 3 | 4 | 5 | 6 | 7 | 8 | 9 | 10 | 11 |
|---|---|---|---|---|---|---|---|---|---|---|
| $\rho_{stand}$ | 7.0 | 9.5 | 9.7 | 8.6 | 9.3 | 10.0 | 9.8 | 9.6 | 9.2 | 10.0 |
| $\rho_{in}$ | 6.8 | 8.1 | 9.5 | 6.2 | 9.4 | 9.2 | 8.6 | 8.0 | 8.5 | 8.9 |
| $\rho_{out}$ | 6.4 | 6.3 | 6.4 | 5.7 | 7.0 | 7.8 | 6.8 | 6.6 | 7.2 | 6.4 |
| $\rho_{ex}$ | 4.9 | 5.6 | 5.4 | 5.6 | 5.1 | 4.9 | 5.0 | 4.9 | 5.0 | 5.2 |
| $\rho_{kuz}$ | 6.1 | 5.7 | 5.5 | 6.9 | 4.8 | 4.5 | 4.9 | 4.8 | 4.8 | 5.1 |

Table 2.1: $[10^{-3}$ ped/m$^2]$ $\overline{\Delta\rho}$ measured in D0 during all experiment rounds.

Focusing on $\rho_{stand}$, it is obviously the least smooth method. That confirms our expectations and verify proposed approaches.

The smoothness of Voronoi methods differs with the applied approach. $\rho_{ex}$ performs better than other two, due to the fixed detector position. Incoming pedestrian's contribution slowly increases as he/she is approaching. Conversely approximative approaches instantly adapts its size to cover all voronoi cell once it fulfills acceptance criterion. $\rho_{out}$ performs better than $\rho_{in}$, due to the larger area more robust to sudden changes.

Conic approach $\rho_{kuz}$ performs similarly to $\rho_{ex}$, they differ with the level of congestion. In free flow cases (rounds 2 and 5), $\rho_{kuz}$ is significantly worse than $\rho_{ex}$. Results in rounds 3 and 4 are almost same and in other rounds (with dense crowd situation), $\rho_{kuz}$ seems to be the smoothest method

Furthermore, the Table 2.1 illustrates the impact of crowd size to the smoothness of methods. While $\rho_{stand}$ and $\rho_{in}$ behave more jumpy with increased density, $\rho_{kuz}$ becomes more

stable. Methods $\rho_{out}$ and especially $\rho_{ex}$ are not sensitive to the state of the system.

To conclude, we can recommend to use $\rho_{ex}$ for the free flow systems and $\rho_{kuz}$ for crowd systems.

**Detector D1** is smaller, designed to focus on the are in front of the exit. Therefore it measured higher values of density, but the trends are almost the same, see Figure 2.7.

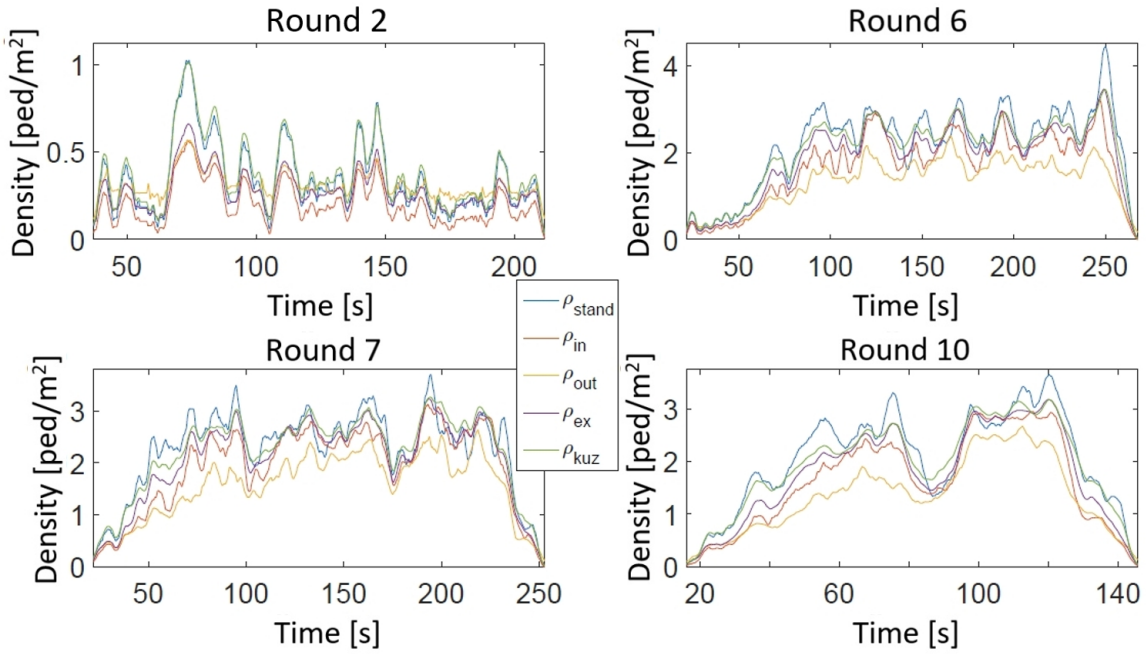


Figure 2.7: Different density evaluation methods in detector D1 within four experimental rounds.

On the other side, the differences in smoothness $\overline{\Delta\rho}$ summarized in Table 2.2 are more dramatic.

| Round | 2 | 3 | 4 | 5 | 6 | 7 | 8 | 9 | 10 | 11 |
|---|---|---|---|---|---|---|---|---|---|---|
| $\rho_{stand}$ | 12.8 | 17.4 | 16.8 | 16.0 | 17.1 | 18.4 | 16.9 | 17.1 | 17.4 | 18.1 |
| $\rho_{in}$ | 7.4 | 12.9 | 13.6 | 8.7 | 14.0 | 13.8 | 13.3 | 12.6 | 13.9 | 14.0 |
| $\rho_{out}$ | 6.4 | 8.1 | 8.7 | 5.9 | 9.3 | 10.3 | 8.1 | 8.4 | 8.7 | 9.2 |
| $\rho_{ex}$ | 4.9 | 5.6 | 5.4 | 5.6 | 5.5 | 5.7 | 5.5 | 5.9 | 5.9 | 5.8 |
| $\rho_{kuz}$ | 5.4 | 4.0 | 3.9 | 4.9 | 3.8 | 3.8 | 3.9 | 4.1 | 4.1 | 4.0 |

Table 2.2: $[10^{-3}$ ped/m$^2]$ $\overline{\Delta\rho}$ measured in D1 during all experiment rounds.

Density evaluation methods $\rho_{stand}$, $\rho_{in}$ and $\rho_{out}$ are the most sensitive to the number of pedestrians inside the detector. As the detector D1 is much smaller, jumps in measured values are higher. Both $\rho_{ex}$ and $\rho_{kuz}$ don't suffer by jumps he a pedestrian approaches the detector area, thus the data quality is the same as before.

Moreover, $\rho_{kuz}$ is even smoother. Front edge of D0 copied the border of monitored area thus pedestrians appeared in D0 instantly. In case of D1, pedestrian's distribution is modeled sufficiently around the detector therefore the entry of new pedestrian to the detector is as smooth as the definition 2.18 allows.

To summarize these observations, distribution approaches $\rho_{kuz}$ and $\rho_{ex}$ present good fit to $\rho_{stand}$ and minimize jumps in measured values. They are beneficial especially when the detector is surrounded by monitored area. Exact Voronoi method is appropriate for low densities while conic kernels are better in crowd situations.

### 2.4.2 Density at the Exit and Behind

Detectors dedicated to the Exit (D2) and consecutive corridor (D3, D4) are specific by the area 0.06 $m^2$. Due to such small size, these detectors are empty most of the time, thus standard approach without smoothing is not applicable at all (Figure 2.8). Voronoi approach $\rho_{in}$ produces zero value any time $\rho_{stand}$ does. Voronoi methods $\rho_{ex}$ and $\rho_{out}$ together with $\rho_{kuz}$ can handle empty detector area thus they perform much better.

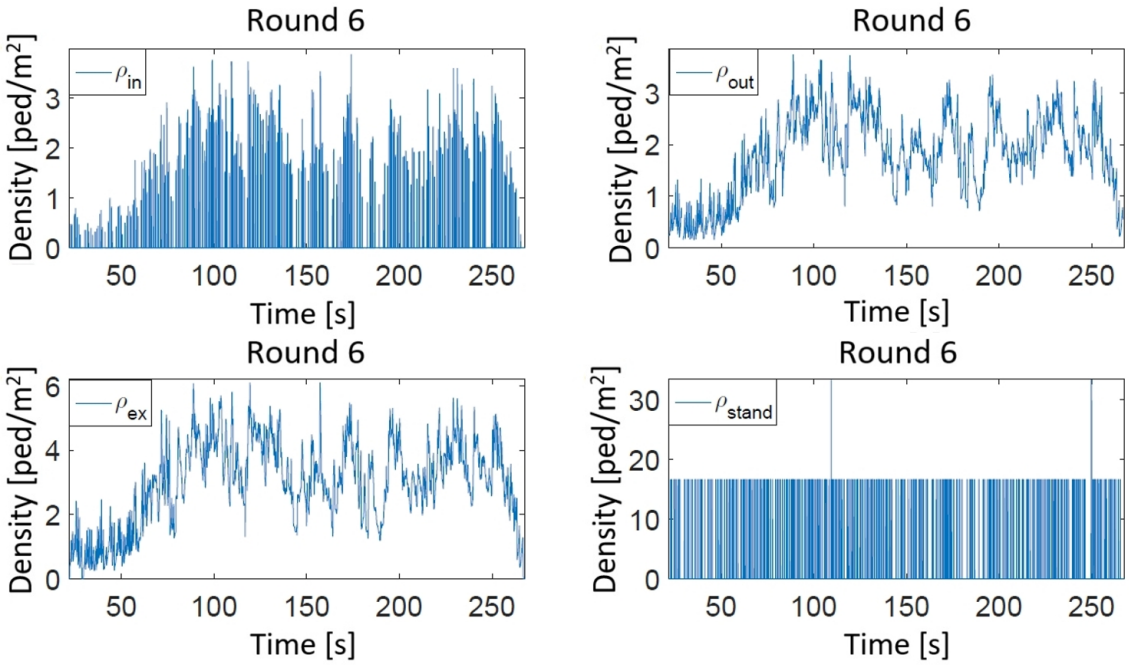


Figure 2.8: Standard and Voronoi based density evaluation methods in detector D2 within round 6.

After smoothing (still central rolling average, smoothing period 8 second) the differences among approaches described in previous section can be observed (Figure 2.9).

In this case, exact and conic approach overestimate the standard method, but it does not mean they are wrong. Presence of one pedestrian in area 0.06 $m^2$ produces a density $16.6 ped/m^2$. Smoothing in time cuts the peak and fill gaps between pedestrians, but the number of non-zero values is dependent on pedestrians velocity – therefore the behavior

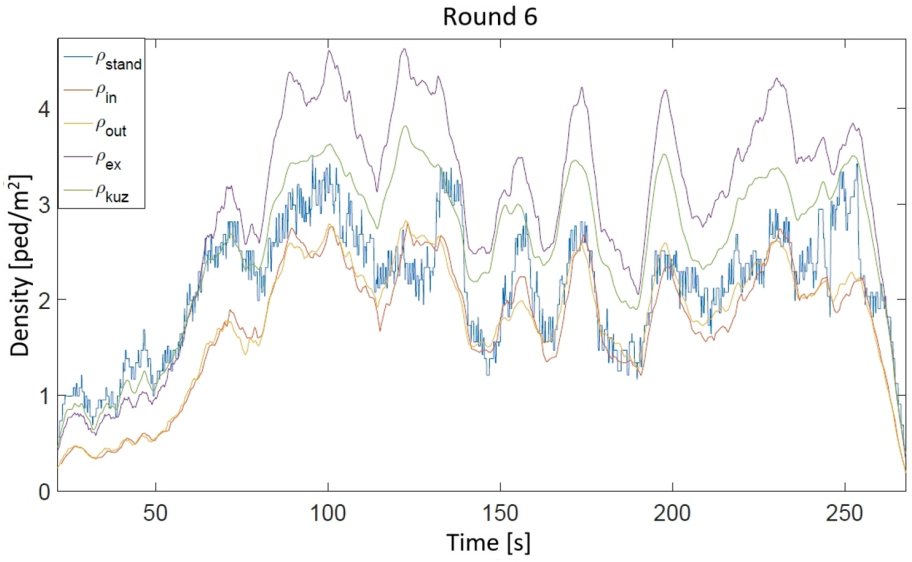


Figure 2.9: Different density evaluation methods after smoothing in detector D2 within round 6.

of this estimate varies with the mode in the corridor. Distribution approaches smooth the data over the are by definition, thus they are more reliable by nature of the situation.

From the smoothness perspective $\overline{\Delta\rho}$ (summarized in Tables 2.3, 2.4 and 2.5), we can observe dramatically worse performance of $\rho_{stand}$. As expected, this method produces ten times worse values than other approaches.

Other methods have not change much comparing to large detectors in front of the exit. Only $\rho_{out}$ relatively improves and beats exact voronoi method. As the detector is small, it is beneficial to extend detector area to all voronoi cells of overlapping pedestrians.

Moving from D2 through D3 toward D4, criterion $\overline{\Delta\rho}$ produces gradually worse values for approach for $\rho_{kuz}$. This is more technological issue than a feature of the method – pedestrians leave scene soon after they leave the detectors. That time, they still partially contribute to the density in the detector. This contribution suddenly vanishes, causing a jump in the density time series.

| Round | 2 | 3 | 4 | 5 | 6 | 7 | 8 | 9 | 10 | 11 |
|---|---|---|---|---|---|---|---|---|---|---|
| $\rho_{stand}$ | 65.4 | 83.9 | 80.5 | 80.5 | 76.5 | 78.3 | 75.7 | 75.3 | 77.5 | 80.4 |
| $\rho_{in}$ | 2.0 | 8.6 | 7.8 | 4.5 | 9.0 | 9.2 | 8.2 | 8.5 | 9.2 | 10.3 |
| $\rho_{out}$ | 2.4 | 3.1 | 3.1 | 3.6 | 3.1 | 3.1 | 3.2 | 3.2 | 3.3 | 3.6 |
| $\rho_{ex}$ | 4.6 | 4.9 | 4.8 | 6.1 | 5.0 | 4.9 | 5.0 | 4.8 | 5.2 | 5.5 |
| $\rho_{kuz}$ | 1.6 | 1.2 | 1.2 | 1.2 | 1.1 | 1.2 | 1.3 | 1.2 | 1.3 | 1.3 |

Table 2.3: $[10^{-2}$ ped/m$^2]$ $\overline{\Delta\rho}$ measured in D2 during all experiment rounds.

In general we can conclude that it is not appropriate to use standard approach for small detectors. Conic distribution approach is again a good choice, especially hen the detector is

| Round | 2 | 3 | 4 | 5 | 6 | 7 | 8 | 9 | 10 | 11 |
|---|---|---|---|---|---|---|---|---|---|---|
| $\rho_{stand}$ | 64.6 | 81.2 | 77.7 | 78.3 | 72.5 | 69.5 | 68.8 | 67.6 | 67.3 | 67.5 |
| $\rho_{in}$ | 3.8 | 7.8 | 7.0 | 7.0 | 7.7 | 7.2 | 6.2 | 6.9 | 6.6 | 7.1 |
| $\rho_{out}$ | 2.4 | 3.3 | 3.3 | 3.1 | 3.2 | 3.3 | 2.9 | 3.1 | 3.3 | 3.5 |
| $\rho_{ex}$ | 4.0 | 5.0 | 5.1 | 4.6 | 4.9 | 4.9 | 4.4 | 5.0 | 5.0 | 5.2 |
| $\rho_{kuz}$ | 2.9 | 2.5 | 2.5 | 2.4 | 2.3 | 2.4 | 2.6 | 2.4 | 2.7 | 2.7 |

Table 2.4: [$10^{-2}$ ped/m$^2$] $\overline{\Delta\rho}$ measured in D3 during all experiment rounds.

| Round | 2 | 3 | 4 | 5 | 6 | 7 | 8 | 9 | 10 | 11 |
|---|---|---|---|---|---|---|---|---|---|---|
| $\rho_{stand}$ | 52.2 | 68.9 | 69.8 | 72.5 | 60.1 | 62.0 | 52.9 | 50.7 | 49.0 | 52.3 |
| $\rho_{in}$ | 3.6 | 5.8 | 5.7 | 5.9 | 5.2 | 5.4 | 4.4 | 4.4 | 4.4 | 4.3 |
| $\rho_{out}$ | 3.3 | 4.9 | 4.5 | 4.8 | 4.4 | 4.6 | 4.0 | 4.3 | 4.2 | 4.4 |
| $\rho_{ex}$ | 6.3 | 7.8 | 7.6 | 7.7 | 7.3 | 7.5 | 6.7 | 7.2 | 7.4 | 7.4 |
| $\rho_{kuz}$ | 7.2 | 9.1 | 8.8 | 8.8 | 8.3 | 8.4 | 8.0 | 8.1 | 8.2 | 8.5 |

Table 2.5: [$10^{-2}$ ped/m$^2$] $\overline{\Delta\rho}$ measured in D4 during all experiment rounds.

far enough from the edge of monitored area. Voronoi approaches can produce good results as well, $\rho_{out}$ produces reliable results.

## 2.5 Individual Density Features

Lets imagine for now that a detector is not fixed in given area, but it can move. E.g. we can consider a pedestrian (more precisely a neighborhood around a pedestrian) as the density detector.

Let us start with a trivial observation illustrated the trend of conic density approach on one selected path, Figure 2.10. The overall trend of four density curves is similar, but the features corresponding to specific set of parameters are visible. Short range densities ($r = 0.5$ m) present lower values in crowd approaching phase and they are more sensitive to temporal approach of another pedestrian as seen in interval $(247, 248)$ s when a density increase is followed by a drop. Small radius densities ($R = 0.2$ m) are characteristic by high frequency fluctuations – pedestrian mass is more concentrated, therefore even a small deviation in distance to the other pedestrian brings a change in density.

From the smoothness perspective, we can pick long range large radius variant (yellow) as the best option.

Similarly to the corridor research studying the dependency of flow on the density inside, we should select the best method evaluating density using more than smoothness. The reflection of natural velocity – density relation would play role of a accuracy criterion.

Within the master thesis of Marina Dzabarjan [35], we have analyzed Conic and Gaussian distribution method together with Voronoi approach and developed concept of minimal

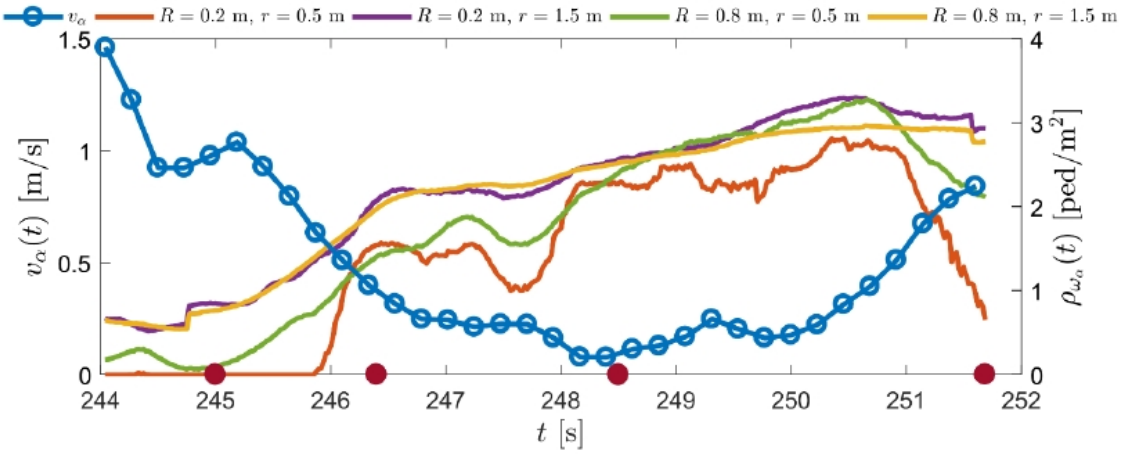


Figure 2.10: Velocity and four densities with different blur $R$ and range $r$ parameters. First drop of velocity (1.5 m/s to 1 m/s) at the beginning of avoiding the crowd is followed by continuous decrease of velocity (1 m/s to 0.2 m/s) while joining the crowd, meanwhile the density increases from 0.5 ped/m$^2$ up to 3 ped/m$^2$ based on parameters.

distance. Moreover, the effect of narrowing of the detector along the moving direction was analyzed as one of the studied parameter.

Assuming a pedestrian $\alpha$ reacts to the conditions is his surrounding $\omega_\alpha$ described by density $\rho_{\omega_\alpha}$) by his velocity $v_\alpha$, we could measure strength of this relation using the Pearson correlation coefficient

$$R(\rho_{\omega_\alpha}, v_\alpha) = \frac{\mathrm{Cov}\,(\rho_{\omega_\alpha}, v_\alpha)}{\sqrt{\mathrm{Var}\,(\rho_{\omega_\alpha})\ \mathrm{Var}\,(v_\alpha)}}\,. \tag{2.27}$$

### 2.5.1 Perception Angle

The firs experiment focuses on the determining the best setting of the perception angle for the nearest pedestrian density approximation.

As seen in the Figure 2.11, measured values cover all spectrum of possible correlation values. The velocity model is obviously too complex to be explained just by the distance to the nearest pedestrian, but the trend of mean values fulfills the expectation.

First, the mean value of correlation is positive, i.e. velocity tends to increase with increasing distance to the nearest pedestrian. Moreover, the correlation is highest in the perception angle band $\langle 120°, 160° \rangle$ that is in agreement with the human eye angle of vision [67].

Unfortunately the absolute value of correlation is low, lower than measured values for other density evaluation methods (as will be shown in next sections). This method could be more successful in corridors than in the fully 2D motion in the room, thus we will stick with more standard methods.

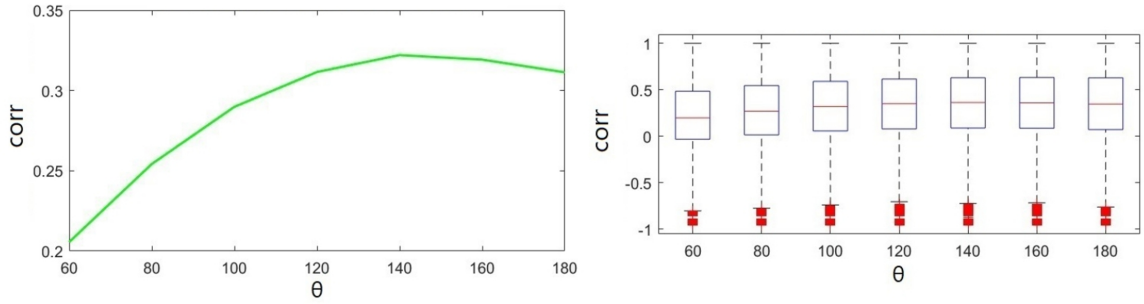


Figure 2.11: Mean value and boxplot of correlation coefficient between velocity and the distance to the nearest pedestrian evaluated for different perception angles.

### 2.5.2 Individual Density Parametric Study

Both distribution approaches have similar trend of correlation with respect to the both, radius and range parameters as illustrated in the Figure 2.12. Extra short range and extra short range parametric set performs worse than a symmetric ridge around one meter. This circle of optimal setting reaches the velocity – density correlation values around -0.5, indicating relatively strong negative correlation.

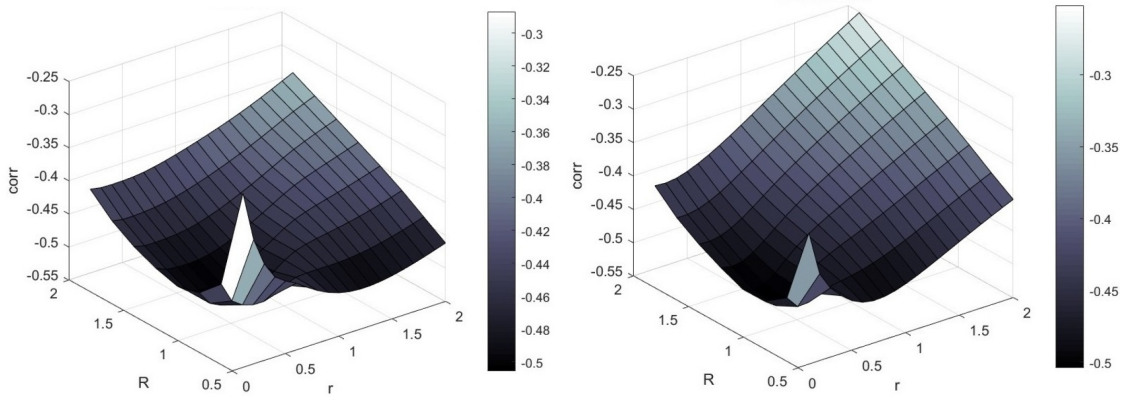


Figure 2.12: Mean velocity - density correlation evaluated for various parameters of density, whole trajectory. Left: Conic density, Right: Gauss density.

Correlation considering all trajectory may mix several phases of motion. To make a closer look, lets split the trajectory into three parts. The trajectory was cut at the distance 1.5 m to the exit and then right at the exit line.

Figure 2.13 visualizes three completely different profiles. In the first section covering typically free flow mode, the maximal correlation is reached in the large range part of parametric space. Obviously the short range density parametric setup is not appropriate in the low density areas, medium and long range settings don't differ much.

The second section is the most similar to the whole trajectory picture. The optimal ridge has slightly different shape, but still the medium radius and range seems to the the best choice. Here should be noted that the value of correlation is lower comparing to the whole

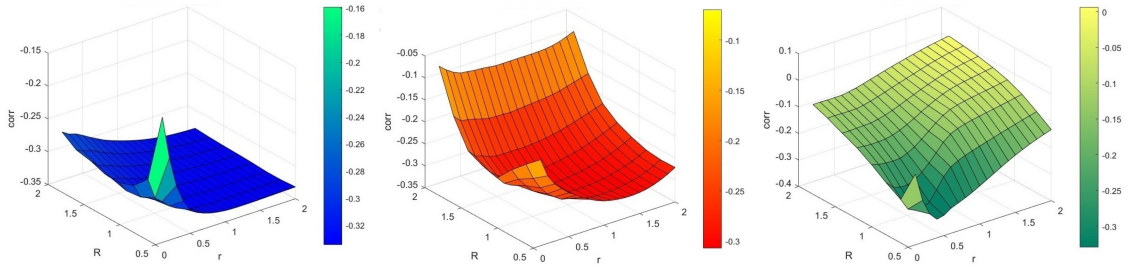


Figure 2.13: Mean velocity - density correlation evaluated for various parameters of conic density. Left: Free flow area, Middle: Crowd area, Right: Corridor behind the exit.

trajectory, approximately by 20 points. The correlation between velocity and density is carried by the whole trajectory – all pedestrians started in low density area, walking with relatively large velocity. At the exit area and behind, most of them significantly slowed down due to the high density. Cutting the trajectory to pieces, this information is depreciated and the correlation is based on more local velocity-density changes. These changes are less stable, therefore the mean value of correlation is lower.

The third section completed the shift from long range to short range parametrization. Optimal values moved below 0.5 m that indicates hard body approximation combined with nearest pedestrian neighborhood. Interestingly even here the point approximation brought worse correlation, but not that much as in case of other sections.

Finally, the same analysis was performed for Voronoi method. This approach is parametrized just by the radius as the size of pedestrian area is defined by Voronoi cell. Even for this method, correlation curves indicates the same behavior as the conic approach, see the Figure 2.14. The correlation of whole trajectory and second sector are optimized by medium range set up, while starting area prefers long range and corridor short range setup. The absolute values are similar, whole trajectory reached -0.5 and the sections move around -0.3.

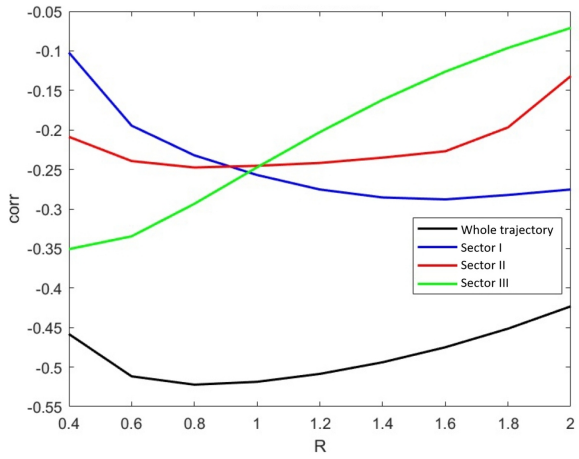


Figure 2.14: Mean velocity - density correlation evaluated for various parameters of voronoi density. Curves are related to the whole trajectory, free flow sector, crowd area and Corridor behind the exit.

### 2.5.3 Factors Affecting Correlation

Previous section worked with averaged velocity-density correlation over all trajectories. Naturally, trajectory significantly differs thus it worth's analyzing possible factors affecting the value. To avoid combining too many information, followed analysis was performed just for the second sector of trajectory.

We will consider three possible factors, all of them designed as categorical variables:

- $TT_R$ defining fast trajectories ($TT_R < 0.8$), regular ($0.8 <= TT_R < 1.2$) and slow ($1.2 <= TT_R$)
- trajectory shape: straight (no crossing of 1.5 m distance of entrance - exit axis) vs peripheral
- occupancy: low (0-12), medium (12-19), high (19-30), extra high (30+)

Such design produces 24 categories of trajectories, their coding is defined in Table 2.6

| Trajectory | straight | | | | peripheral | | | |
|---|---|---|---|---|---|---|---|---|
| Occupancy | 0-12 | 12-19 | 19-30 | 30+ | 0-12 | 12-19 | 19-30 | 30+ |
| Fast groups | 1 | 2 | 3 | 4 | 5 | 6 | 7 | 8 |
| Regular groups | 9 | 10 | 11 | 12 | 13 | 14 | 15 | 16 |
| Slow groups | 17 | 18 | 19 | 20 | 21 | 22 | 23 | 24 |

Table 2.6: Indexation of parametric groups based on trajectory, occupancy and travel time.

The influence of factors is visualized in Figure 2.15. The sequences of four, respectively eight similar groups is well visible. Repeatable patters indicates strong effects of all proposed factors.

First, we should distinguish straight and peripheral trajectories. Peripheral trajectories are characteristic by lower level of correlation. While the peripheral trajectories does not change with occupancy, straight trajectories increase negative correlation with increased occupancy. And finally, higher correlation is frequently reached by slower passing's, for all types of trajectories.

To go even more deep with the analysis why pedestrians behave this way, please see section 3.4. In this chapter, we will continue with the analysis of defined quantities.

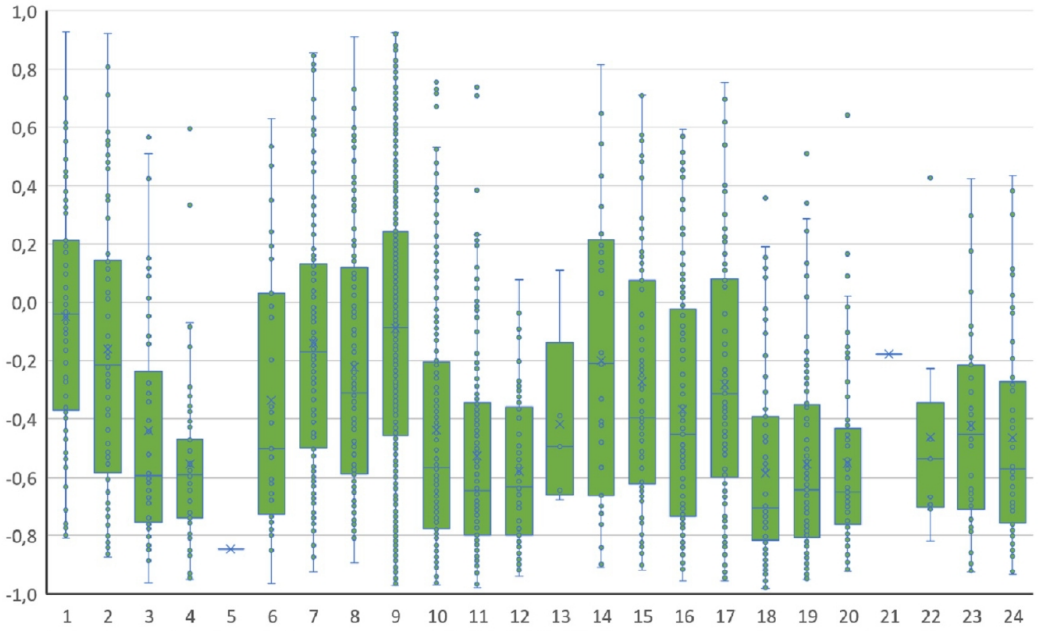


Figure 2.15: Boxplot of velocity - density correlation evaluated for groups of trajectories as defined in Table 2.6.

## 2.6 Flow

The dynamic quantity "Flow" $J$ is always related to the given cross-section, a virtual barrier splitting analyzed area $A$ into two parts. Let us denote the area in front of the cross-section as $A_1$ and the area behind as $A_2$, when the front and rear area is defined with respect to the sense of movement. The flow from front area to rear area will be considered as positive.

The pedestrian flow is by nature vector quantity with value and direction. Its coordinates are defined as the value of flow through the cross-section orthogonal to given direction:

$$\vec{J} = (J_x, J_y, \dots). \tag{2.28}$$

In this work, we are interested in the flow through linear cross-section and, more over, the flow can be considered as unidirectional. Thus we can identify $J := J_x$ and work only with the value of flow.

Assuming the area $A$ is closed (there is no flow through the border), the increase of occupancy in $A_1$ has to be the same the decrease of occupancy in $A_2$ and vice versa. Therefore for the evaluation of the (scalar) flow, we will use the increase of occupancy in $A_2$.

Even it is quite frequent to evaluate the flow through the area $A$ instead the cross-section, such term is not well defined. We will always evaluate the flow through the the cross-section, possibly defined by border(s) of $A$.

Similarly to the density, even flow can be defined applying pedestrian distribution 2.20 to fundamental definition 2.7:

$$J = \frac{\Delta N_{A_2}}{\Delta t} = \frac{N_{A_2}(t+\Delta t) - N_{A_2}(t)}{\Delta t} = \frac{\int_{A_2} \sum_\alpha p_\alpha(x, t+\Delta t) - p_\alpha(x,t)\,\mathrm{d}x}{\Delta t} \tag{2.29}$$

that in case of actual flow, i.e. when $\Delta t \to 0$, gives:

$$J_{akt}(t) = \lim_{\Delta t \to 0} \frac{\int_{A_2} \sum_\alpha p_\alpha(x, t+\Delta t) - p_\alpha(x,t) \mathrm{d}x}{\Delta t} = \int_{A_2} \sum_\alpha p\prime_\alpha(x,t) \mathrm{d}x \,. \tag{2.30}$$

Again, the performance of method is defined by the shape of kernel:

**Conic & Gauss distribution** Event the complex distribution are well applicable, just the kernel (2.18), resp. (2.19) would be injected to (2.29).

**Constant distribution (e.g. cylindrical, voronoi)** Using the linear relation between area and density (2.16) the equation (2.29) may be rewritten with the pedestrian support in front and behind the cross-section:

$$\begin{aligned} J(t) &= \frac{\sum_\alpha N^\alpha_{A_2}(t+\Delta t) - N^\alpha_{A_2}(t)}{\Delta t} = \frac{\sum_\alpha \dfrac{N^\alpha_{A_2}(t+\Delta t)}{N^\alpha_A} - \dfrac{N^\alpha_{A_2}(t)}{N^\alpha_A}}{\Delta t} \\ &= \frac{\sum_\alpha \dfrac{A^2_\alpha(t+\Delta t)}{A_\alpha(t+\Delta t)} - \dfrac{A^2_\alpha(t)}{A_\alpha(t)}}{\Delta t}, \end{aligned} \tag{2.31}$$

where $A^2_\alpha = A_\alpha \cap A_2$ refer to as pedestrian support if front and behind the cross-section.

Here should be noted that Voronoi flow may be affected be affected by several technical issues that should be prevented on the implementation level:

- voronoi cell doesn't have to be compact. Imagine a point behind the obstacle may be assigned to the cell of pedestrian in front of it just due to the shortest Euclidean distance, even there are other pedestrians closer with respect to "walk distance". Such detached part of cell used to be unstable in time, thus it should be avoided by modifying the voronoi cell assignment.
- voronoi cell is defined in the context of other pedestrians. It can happen that a fraction of voronoi cell in front of the cross-section increase even pedestrian is moving forward, just because of some random movement in the crowd. Such behavior could cause repeatedly addition of partial flow. This issue can be prevented by normalizing a flow contribution from one pedestrian to 1 ped.

**Point approximation** Applying Dirac kernel (2.15), the flow calculated from pedestrian distribution returns back to standard shape:

$$\begin{aligned} J &= \frac{\sum_\alpha \int_{A_2} p_\alpha(x, t+\Delta t) - p_\alpha(x,t) \mathrm{d}x}{\Delta t} = \frac{\sum_\alpha \int_{A_2} \delta_{x,x_\alpha}(t+\Delta t) - \delta_{x,x_\alpha}(t) \mathrm{d}x}{\Delta t} \\ &= \frac{\sum_\alpha \mathcal{I}_{\mathrm{pass}}(t, t+\Delta t)}{\Delta t} \end{aligned} \tag{2.32}$$

where $\mathcal{I}_{\mathrm{pass}}(t, t+\Delta t)$ stands for identifier of pedestrian's passing the cross-section in given time interval.

Therefore the mean value of flow in measured interval fulfills $\langle t_1, t_2)$ fundamental expectations

$$\bar{J}(t_1, t_2) = \frac{\sum_\alpha \mathcal{I}_{\text{pass}}(t_1, t_2)}{t_2 - t_1}, \tag{2.33}$$

with the drawback in badly defined actual flow

$$\lim_{\Delta t \to 0} J = \begin{cases} \inf & \exists \alpha : t_\alpha \in \langle t, t + \Delta t) \\ 0 & \text{otherwise,} \end{cases} \tag{2.34}$$

that is useless in practical applications.

From known times of passing the cross-section, it is possible to define actual flow using following transformation of flow:

$$J(t_1, t_2) = \frac{\sum_\alpha \mathcal{I}_{\text{pass}}(t_1, t_2)}{t_2 - t_1} = \frac{1}{\frac{(t_2 - t_1)}{\sum_\alpha \mathcal{I}_{\text{pass}}(t_1, t_2)}} = \frac{1}{\langle \Delta t_\alpha \rangle_t}, \tag{2.35}$$

where $\Delta t_\alpha$ is the time distance of pedestrian $\alpha$ to his/her predecessor. The mean value of flow is therefore proportional to inverse value of mean time distance.

But even this approach does not define actual flow – in case of time interval shorter than time distance it is not clear how to execute the mean value. We can define actual flow using wisely selected time distance $\Delta t(t)$ relevant in time $t$:

$$J(t) = \frac{1}{\Delta t(t)}. \tag{2.36}$$

The most simple method would use the time distance of nearest passing pedestrian

$$\Delta t(t) = \Delta t_\alpha, \quad \alpha = \text{argmin}(|t - t_\alpha|). \tag{2.37}$$

Such approach generates jump in measured values in times of switch from one nearest pedestrian to another. Therefore the smooth approach keeping focus on actual values is accomplished by linear interpolation on the time distance level, i.e.

$$\begin{aligned} \Delta t(t) &= \frac{|t - t_\alpha| \cdot \Delta t_\alpha + |t - t_{\alpha+1}| \cdot \Delta t_{\alpha+1}}{|t - t_\alpha| + |t - t_{\alpha+1}|} \\ &= \frac{|t - t_\alpha| \cdot \Delta t_\alpha + |t - t_{\alpha+1}| \cdot \Delta t_{\alpha+1}}{\Delta t_{\alpha+1}}, \quad \alpha = \text{argmin}(t_\alpha - t) | \, t_\alpha \leq t. \end{aligned} \tag{2.38}$$

It may be beneficial to use higher level of interpolation, but it would shift the actual picture toward the mean value.

## 2.7 Flow Detector-based Features

To compare performance of presented methods, we will again calculate flow on the E4 data through the detectors defined in 2.2, through their front edge to be more specific.

Two distribution and two passing-times approaches will be analyzed:

1. Standard method (referred to as $J_{stand}$) calculated by (2.32). With respect to the time interval $\Delta t = 1/48$ s equal to the frame rate, each entering pedestrian generates flow 48 ped/s in the time of his/her first detection
2. Voronoi approach denoted as $J_{vor}$ calculated by (2.31). For each voronoi cell in the detector it is evaluated the fraction of cell area inside vs. outside the detector
3. Distribution approach with conic kernel referred to as $J_{kuz}$
4. Time headway approach denoted as $J_{roz}$ calculated by (2.37). Each measured time, the flow is equal to the inverse value of time headway of nearest pedestrian

Again, the quality will be assessed by the smoothness criterion $\overline{\Delta J}$ defined as mean difference of consecutive values:

$$\overline{\Delta J} = \frac{\sum_{i=2}^{n} |J(t_i) - J(t_{i-1})|}{n}, \tag{2.39}$$

where $n$ is the number of measured data points. Note that this value is extracted from non-smoothed values.

Moreover, we will check the agreement with macroscopic mean value. For each round, mean flow $J_{macro}$ is calculated using (3.4) from the time interval between the first and the last pedestrian an the total number of pedestrians. Values are summarized in Table 2.7.

| Round | 2 | 3 | 4 | 5 | 6 | 7 | 8 | 9 | 10 | 11 |
|---|---|---|---|---|---|---|---|---|---|---|
| $J_{macro}$ | 0.91 | 1.21 | 1.16 | 1.14 | 1.10 | 1.13 | 1.08 | 1.09 | 1.11 | 1.17 |

Table 2.7: [ped/s] Macroscopic flow is all rounds of E4.

### 2.7.1 Flow in front of the Exit

**Detector D0** is characteristic by the jumpy results of all methods, see Figure 2.16. We should distinguish jumps implicated by definition, i.e. $J_{stand}$ method and jumps caused by sudden entry of new pedestrian to analyzed area affecting mainly $J_{kuz}$ a $J_{vor}$. The reason is the same as in case of density – the front side of detector D0 matches the border of monitored area, thus all pedestrian cell appears instantly inside the detector, there is no benefit of distribution approach.

Consequently the flow of pedestrians leaving the detector is rather smooth, as visualized in Figure 2.17. Anyway, to get applicable results for D0 in the whole timeline, smoothing is needed. Central rolling correlation over time window 4 s completely removed jumps and uncovered very good fit among all methods, as illustrated in Figure 2.18.

Even in term of the macroscopic fit criterion summarized in Table 2.8, all flow evaluation methods produced mean value closed to macroscopic measurements. Only in the case of round with the lowest density, the errors reaches 3%. Otherwise the difference does not exceed 1%.

The second criterion $\overline{\Delta J}$ measuring smoothness of produced data (Table 2.9) confirms the observation that only $J_{roz}$ is not affected by the position of detector. Moreover, even the

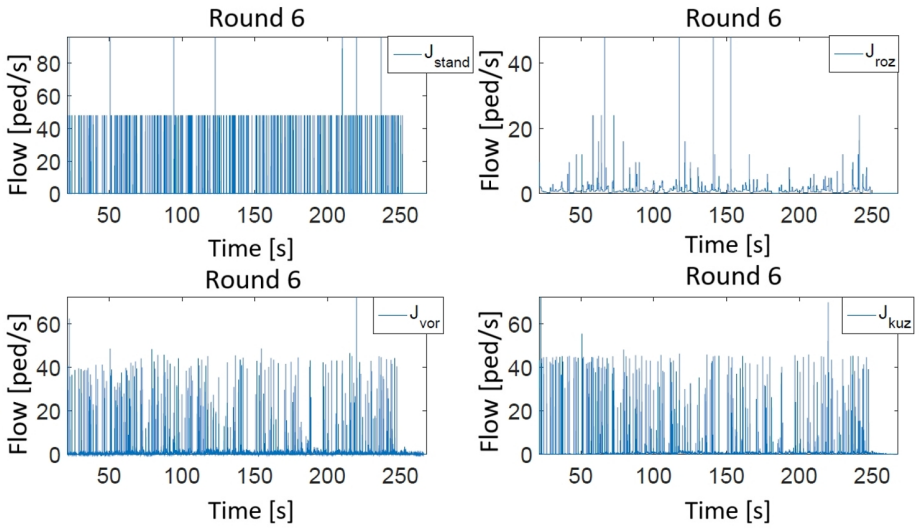


Figure 2.16: Non-smoothed results of all analyzed methods, detector D0, round 6.

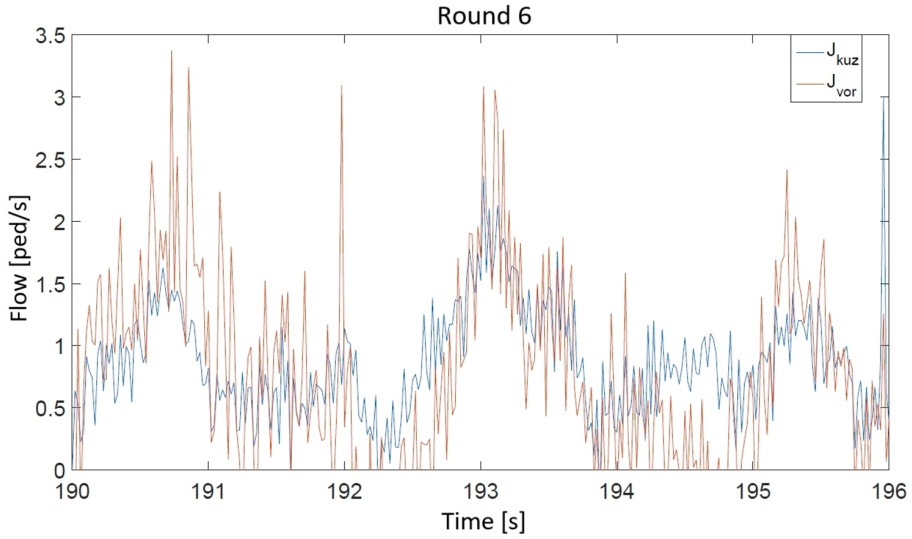


Figure 2.17: Non-smoothed results of distribution approaches, detector 0, short time interval without any pedestrian entry.

distribution approaches were affected by mentioned issue, they better results than standard approach, mainly in more dense rounds.

**Detector D1** is supposed to bring more smooth results due to its position inside the room. Comparison of distribution approaches on both, short (Figure 2.19) and long (Figure 2.20) time scale confirms the expectations, but even here jumps occurred.

After smoothing (visualized in 2.21), apparent difference appears between trends in time-based and distribution approaches. In case of standard of headway based flow, a pedestrian

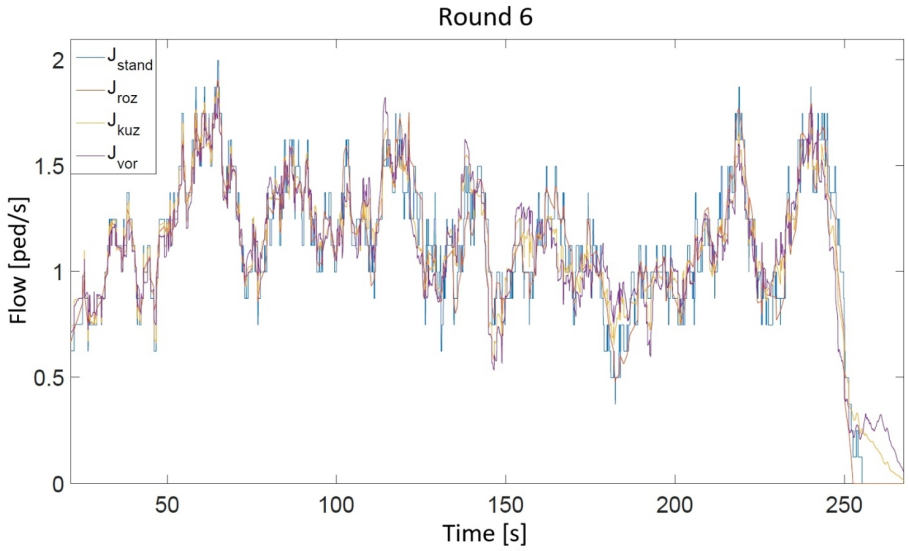


Figure 2.18: Smoothed results of all analyzed methods, detector D0, round 6.

| Round | 2 | 3 | 4 | 5 | 6 | 7 | 8 | 9 | 10 | 11 |
|---|---|---|---|---|---|---|---|---|---|---|
| $J_{macro}$ | 0.91 | 1.21 | 1.16 | 1.14 | 1.10 | 1.13 | 1.08 | 1.09 | 1.11 | 1.17 |
| $J_{stand}$ | 0.94 | 1.20 | 1.15 | 1.15 | 1.09 | 1.12 | 1.08 | 1.08 | 1.11 | 1.16 |
| $J_{roz}$ | 0.93 | 1.20 | 1.15 | 1.14 | 1.09 | 1.12 | 1.07 | 1.08 | 1.11 | 1.16 |
| $J_{vor}$ | 0.94 | 1.21 | 1.16 | 1.15 | 1.10 | 1.13 | 1.08 | 1.09 | 1.12 | 1.17 |
| $J_{kuz}$ | 0.94 | 1.21 | 1.16 | 1.16 | 1.10 | 1.13 | 1.07 | 1.09 | 1.12 | 1.17 |

Table 2.8: [ped/s] Mean value of flow of all analyzed method, detector D0.

| Round | 2 | 3 | 4 | 5 | 6 | 7 | 8 | 9 | 10 | 11 |
|---|---|---|---|---|---|---|---|---|---|---|
| $J_{stand}$ | 4.65 | 7.16 | 7.48 | 5.99 | 7.23 | 8.15 | 7.96 | 7.26 | 7.11 | 7.83 |
| $J_{roz}$ | 1.98 | 2.74 | 2.59 | 2.61 | 2.63 | 2.71 | 2.66 | 2.45 | 2.64 | 2.93 |
| $J_{vor}$ | 4.05 | 4.96 | 4.86 | 4.73 | 4.61 | 4.48 | 4.36 | 4.44 | 4.54 | 4.61 |
| $J_{kuz}$ | 4.38 | 4.70 | 4.64 | 5.36 | 4.07 | 3.98 | 4.01 | 4.06 | 4.10 | 4.29 |

Table 2.9: [$10^{-3}$ ped/s] Criterion $\overline{\Delta J}$ evaluated for all analyzed method, detector D0.

is detected at once, after coming to the detector area. Distribution approaches $J_{vor}$ and $J_{kuz}$ contributes to the detector flow continuously since pedestrian support touches the detector edge until it is fully incorporated into the detector area. Therefore significant portion of the flow may be delayed, especially in the crowd situations. Such behavior is rather a feature than a bug – it was a goal to develop a method blurring pedestrian flow in time and moreover, the mean value is still conserved as showed in Table 2.10. On the other hand in case the goal is just to approximate $J_{stand}$ by some smoother method as close as possible, $J_{roz}$ is the best idea.

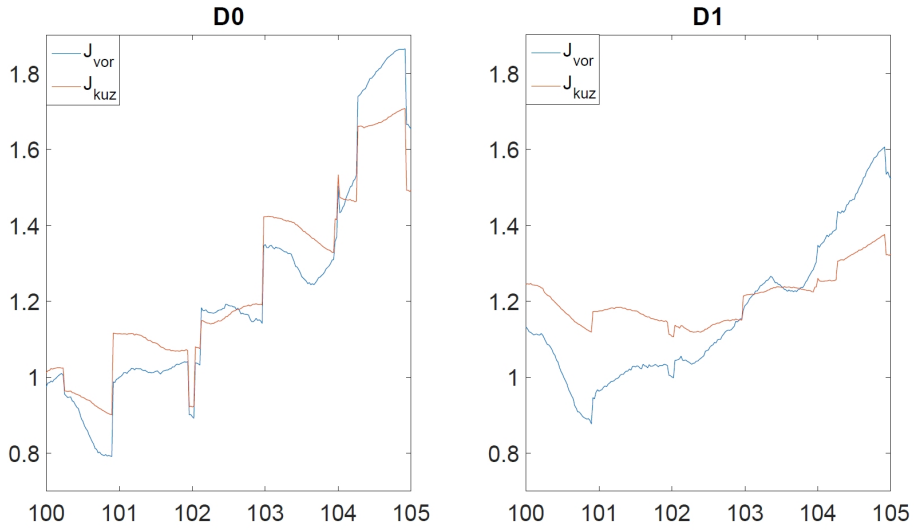


Figure 2.19: Distribution based flow evaluation methods in detector D0 (left) and D1 (right) within short interval round 6.

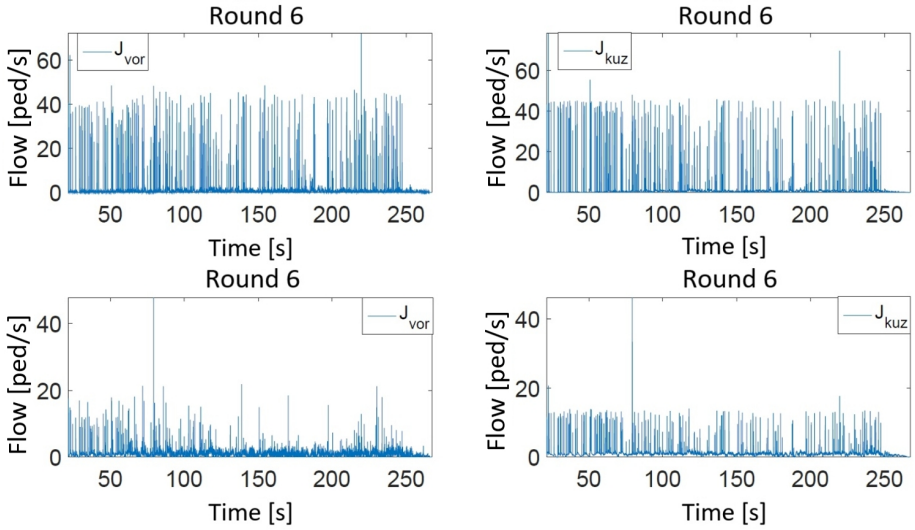


Figure 2.20: Distribution based flow evaluation methods in detector D0 (upper) and D1 (lower) within round 6.

From the smoothing criterion $\overline{\Delta J}$, situation illustrated in Table 2.11 become more complex. Standard approach is several times worse, but remaining three methods bring competitive results. Results of Voronoi method are stable no matter the density, while headway based approach is getting worse $J_{roz}$ and conic approach is getting better with increasing density.

To conclude, conic distribution approach is again the best one if the detector is well inside the resoled area. Otherwise, headway based method produced satisfied results no matter the condition are.

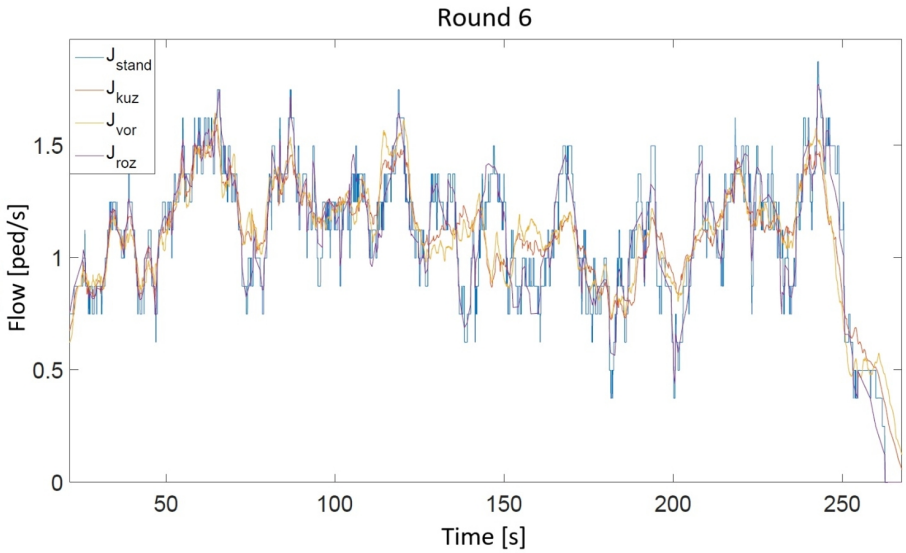


Figure 2.21: Smoothed results of all analyzed methods, detector D1, round 6.

| Round | 2 | 3 | 4 | 5 | 6 | 7 | 8 | 9 | 10 | 11 |
|---|---|---|---|---|---|---|---|---|---|---|
| $J_{macro}$ | 0.91 | 1.21 | 1.16 | 1.14 | 1.10 | 1.13 | 1.08 | 1.09 | 1.11 | 1.17 |
| $J_{stand}$ | 0.94 | 1.21 | 1.16 | 1.15 | 1.10 | 1.13 | 1.08 | 1.09 | 1.12 | 1.17 |
| $J_{roz}$ | 0.93 | 1.21 | 1.16 | 1.15 | 1.09 | 1.13 | 1.07 | 1.09 | 1.11 | 1.17 |
| $J_{vor}$ | 0.94 | 1.21 | 1.16 | 1.15 | 1.10 | 1.13 | 1.08 | 1.09 | 1.12 | 1.17 |
| $J_{kuz}$ | 0.94 | 1.21 | 1.16 | 1.16 | 1.10 | 1.13 | 1.07 | 1.09 | 1.12 | 1.17 |

Table 2.10: [ped/s] Mean value of flow of all analyzed method, detector D1.

| Round | 2 | 3 | 4 | 5 | 6 | 7 | 8 | 9 | 10 | 11 |
|---|---|---|---|---|---|---|---|---|---|---|
| $J_{stand}$ | 4.77 | 7.18 | 6.61 | 5.84 | 7.24 | 7.91 | 7.17 | 7.05 | 7.23 | 7.27 |
| $J_{roz}$ | 1.83 | 2.71 | 2.72 | 2.45 | 2.59 | 2.82 | 2.55 | 2.45 | 2.60 | 2.92 |
| $J_{vor}$ | 2.49 | 2.68 | 2.63 | 2.74 | 2.56 | 2.68 | 2.62 | 2.88 | 2.64 | 2.64 |
| $J_{kuz}$ | 2.36 | 1.99 | 2.00 | 2.56 | 1.80 | 1.83 | 1.84 | 2.02 | 1.85 | 1.96 |

Table 2.11: [$10^{-3}$ ped/s] Criterion $\overline{\Delta J}$ evaluated for all analyzed method, detector D1.

### 2.7.2 Flow at the Exit and Behind

Small detectors in the corridor brings smooth and stable data, as visualized in overview in Figure2.22. Putting aside standard method, there are only few events causing high values.

In case of headway approach, high values are caused by passing two pedestrians with minimal distance. Even with the exit width equal to 0.6 m, the lowest headway reached 0.06 s producing the flow over 16 ped/s.

Distribution approaches $J_{vor}$ a $J_{kuz}$ were affected by data issues, it happened several times that a pedestrian were not detected for few seconds. Then, sudden appearance causes instantly high flow.

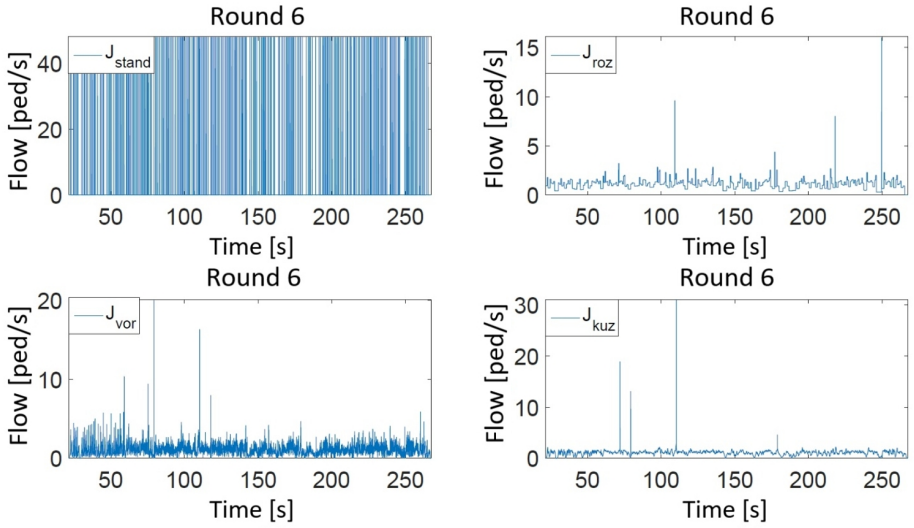


Figure 2.22: Non-smoothed results of all analyzed methods, detector D2, round 6.

Due to the high data quality, the consecutive smoothing was applied over shorter time window, only 4 seconds were used (see Figure 2.23). Final curves have very similar trends, mean values are almost the same (Table 2.12).

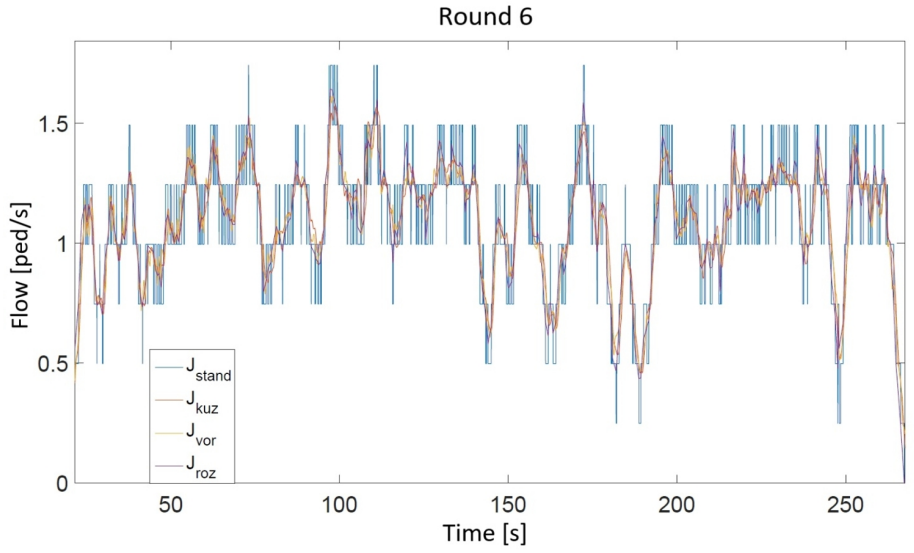


Figure 2.23: Smoothed results of all analyzed methods, detector D2, round 6.

The smoothness criterion just confirmed the observation indicating that standard method is significantly worse than other three. In case of detector D2, the conic method is the best for all rounds but the first one (Table 2.13.

| Round | 2 | 3 | 4 | 5 | 6 | 7 | 8 | 9 | 10 | 11 |
|---|---|---|---|---|---|---|---|---|---|---|
| $J_{macro}$ | 0.91 | 1.21 | 1.16 | 1.14 | 1.10 | 1.13 | 1.08 | 1.09 | 1.11 | 1.17 |
| $J_{stand}$ | 0.94 | 1.21 | 1.16 | 1.15 | 1.10 | 1.13 | 1.08 | 1.09 | 1.12 | 1.16 |
| $J_{roz}$ | 0.93 | 1.21 | 1.16 | 1.15 | 1.10 | 1.13 | 1.07 | 1.09 | 1.11 | 1.16 |
| $J_{vor}$ | 0.94 | 1.21 | 1.16 | 1.15 | 1.10 | 1.13 | 1.08 | 1.09 | 1.12 | 1.17 |
| $J_{kuz}$ | 0.94 | 1.21 | 1.16 | 1.16 | 1.10 | 1.13 | 1.07 | 1.09 | 1.12 | 1.17 |

Table 2.12: [ped/s] Mean value of flow of all analyzed method, detector D2.

Similarly to the density case, the distribution approaches suffer from worse data quality at the edge of monitored area, therefore for detector 3 (Table 2.14) and mainly for detector 4 (Table 2.15), it would be better to use headway approach.

| Round | 2 | 3 | 4 | 5 | 6 | 7 | 8 | 9 | 10 | 11 |
|---|---|---|---|---|---|---|---|---|---|---|
| $J_{stand}$ | 9.52 | 12.1 | 11.6 | 11.7 | 11.1 | 11.2 | 10.8 | 10.9 | 10.8 | 11.3 |
| $J_{roz}$ | 2.88 | 2.38 | 2.41 | 2.38 | 2.82 | 2.99 | 2.82 | 2.82 | 2.99 | 3.13 |
| $J_{vor}$ | 4.92 | 3.60 | 3.79 | 4.86 | 3.58 | 3.62 | 3.64 | 3.58 | 3.69 | 4.04 |
| $J_{kuz}$ | 3.45 | 2.11 | 2.34 | 2.30 | 2.34 | 2.60 | 2.59 | 2.59 | 2.81 | 2.83 |

Table 2.13: [$10^{-3}$ ped/s] Criterion $\overline{\Delta J}$ evaluated for all analyzed method, detector D2.

| Round | 2 | 3 | 4 | 5 | 6 | 7 | 8 | 9 | 10 | 11 |
|---|---|---|---|---|---|---|---|---|---|---|
| $J_{stand}$ | 9.40 | 11.8 | 11.6 | 11.1 | 10.7 | 10.3 | 9.78 | 9.54 | 9.46 | 9.70 |
| $J_{roz}$ | 2.70 | 2.31 | 2.31 | 2.14 | 2.52 | 2.85 | 2.72 | 2.71 | 3.05 | 2.86 |
| $J_{vor}$ | 3.59 | 3.59 | 3.56 | 3.35 | 3.51 | 3.63 | 3.66 | 3.69 | 3.93 | 3.81 |
| $J_{kuz}$ | 3.24 | 2.29 | 2.41 | 2.24 | 2.39 | 2.80 | 2.78 | 2.75 | 3.08 | 3.08 |

Table 2.14: [$10^{-3}$ ped/s] Criterion $\overline{\Delta J}$ evaluated for all analyzed method, detector D3.

| Round | 2 | 3 | 4 | 5 | 6 | 7 | 8 | 9 | 10 | 11 |
|---|---|---|---|---|---|---|---|---|---|---|
| $J_{stand}$ | 8.78 | 10.3 | 11.2 | 11.1 | 9.15 | 9.46 | 8.48 | 8.31 | 7.88 | 8.27 |
| $J_{roz}$ | 2.44 | 2.68 | 2.68 | 2.23 | 2.37 | 2.54 | 2.55 | 2.41 | 2.61 | 2.59 |
| $J_{vor}$ | 4.38 | 6.16 | 5.78 | 5.79 | 5.74 | 5.76 | 5.33 | 5.40 | 5.41 | 5.85 |
| $J_{kuz}$ | 5.77 | 6.45 | 6.23 | 5.93 | 5.99 | 6.26 | 6.15 | 6.17 | 6.34 | 6.64 |

Table 2.15: [$10^{-3}$ ped/s] Criterion $\overline{\Delta J}$ evaluated for all analyzed method, detector D4.

To conclude, headway approach $J_{roz}$ is suitable for all investigated cases. This method can be alternated by conic distribution approach $J_{kuz}$ for detectors surrounded by monitored area. Distribution methods may diverge from standard methodology, but this difference is well explained and it may be more appropriate for some interpretation.

# Chapter 3

# Crowd Motion

The description and analysis of pedestrian behavior will be illustrated on several rather simple situations, where individual phenomena visibility is better.

First sections are based on "passing through a room" situation. The data from several experimental trials supports topics "phase transition", "heterogeneity" and "local behavior". Then, more complex geometry covering the join of pedestrian streams will be used to demonstrate the effect of synchronization. At the end, the evacuation of double deck rail car unit was realized focusing on features affecting the travel time.

Studied situations were simulated by developed cellular automata model, where innovative approaches were implemented to reproduce observed behavior.

## 3.1 Phase Transition

From the safety engineering perspective, the prediction of "the state" of any part of infrastructure with respect to the boundary conditions given by inflow and outflow is the most crucial question. The term state refers to the set of observables, generally we can meet free flow state and the congestion on the other side of the scale, however the exact definition of this states is not unified in the literature so far. The conditions of phase transition or the existence of other states between is the subjects of this section.

All rounds of the experiments performed to support this study started with an empty room, therefore the free flow phase was observed every time. Controlled inflow rate $J_{in}$ constant for all round covered the interval both below and above expected capacity of the exit, therefore phase congestion was observed as well.

### 3.1.1 Bottleneck Capacity

The term capacity $J_c$ defined as the maximal flow through given bottleneck is supposed be determined by its width denoted as $d$. To get better insight, we may use the concept $J = 1/\langle \delta T \rangle$, the flow is determined by mean time headway. For the narrow bottleneck (pedestrians go in line), the time headway is given by the space headway and velocity $\delta T = v \cdot \delta L$. This two quantities are linked together $v = v(\delta L)$.

The empiric relation

$$J_c = 1.9 \cdot d \tag{3.1}$$

proposed as average of many experimental studies [105, 107, 106, 94, 123] (see Figure 3.1) neglects all other effects as the motivation or heterogeneity of humans and the geometry of the exit.

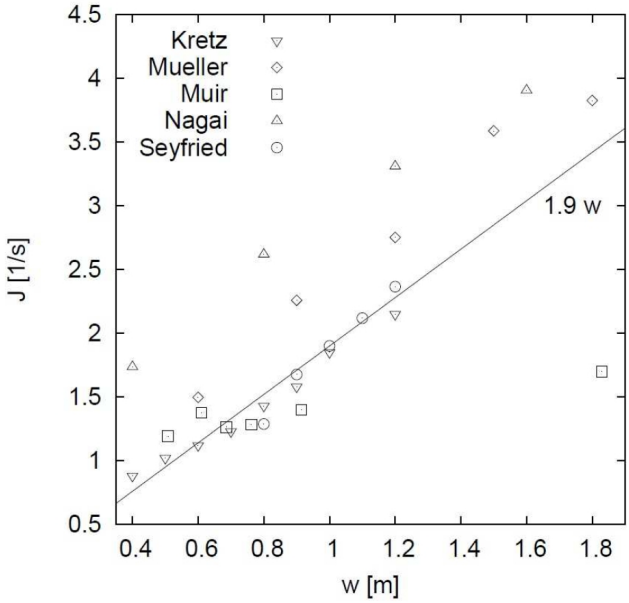


Figure 3.1: The values of flow with respect to the bottleneck width. Taken from [123].

As shown further, with higher motivation, pedestrian could go faster even when the space headway is relatively low. The potential contacts between them (that they try to avoid under normal condition) are less relevant in case of emergency situation.

### 3.1.2 States of the System

From the most macroscopic perspective, there are only two possible scenarios with respect to the inflow rate:

- $J_{in} < J_c$ Initially empty room stays empty, pedestrians walk freely, there is no crowd in front the exit, $J_{out} = J_{in}$
- $J_{in} > J_c$ Initially empty room is filled by people, pedestrians stands in the crowd in front the exit, the size of cluster linearly grows with time (the growing speed is expressed by difference $J_{in} - J_c$), $J_{out} = J_c$

The presence of these modes is well observable on microscopic level as well. The histogram of velocity evaluated for leave the room experiment in E2 (Fig. 3.2) visualizes two local maxims: The high peak on value 0.5 m/s corresponds to the congestion, while the wide peak on value 2 m/s is linked to the free flow. The histogram of density does not exhibit two

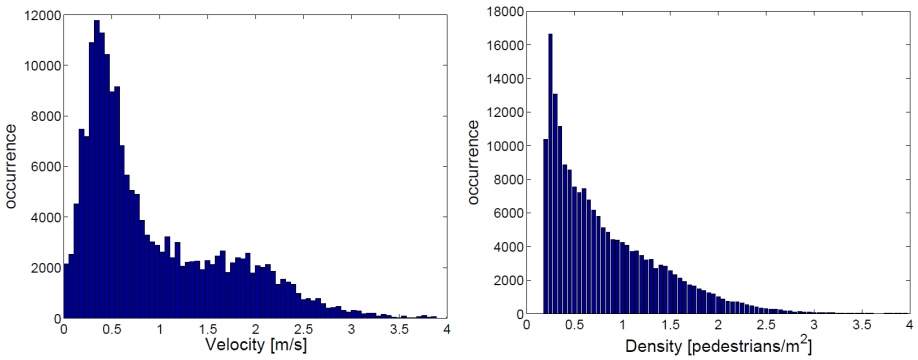


Figure 3.2: The histogram of velocity (left) and density (right).

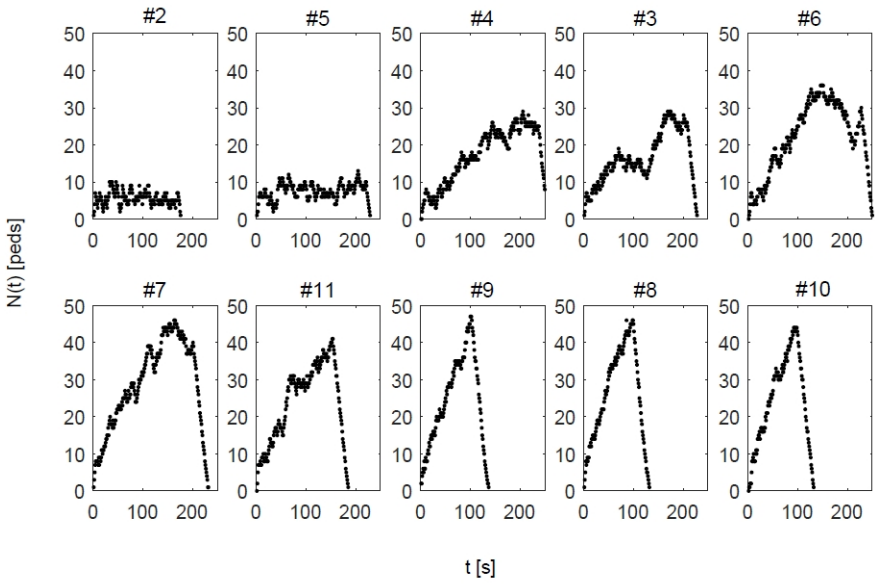


Figure 3.3: The occupancy of the experimental room in time, measured during E4.

modes, indicating that density changes smoothly. A pedestrian keeps his optimal velocity, until it the density around reaches critical value. Then, he must slow down or stop.

This approximation simplifies the pedestrians to granular matter, ignoring their ability to adapt behavior to the conditions around. In realized experiment E4, we observed more complex development of occupancy than expected, as visualized in Figure 3.3.

### 3.1.3 Steady State

As the experiment always started with the empty room, the beginning of all rounds is the same. The occupancy in the room increased according to the inflow – outflow balance and the system becomes stabilize. In the language of mathematics, the system variables do not change in time. Finally, the inflow is stopped thus the occupancy drops to zero.

For microscopical analysis (and not only), the conclusions related to some state should be derived only over the steady state data. That means in case of E4 to make the cut off illustrated in Table 3.1.

| Round | 2 | 3 | 4 | 5 | 6 | 7 | 8 | 9 | 10 | 11 |
|---|---|---|---|---|---|---|---|---|---|---|
| Beginning [s] | 40 | 100 | 110 | 80 | 100 | 80 | 50 | 70 | 100 | 120 |
| End [s] | 200 | 220 | 250 | 230 | 250 | 220 | 120 | 120 | 120 | 180 |

Table 3.1: Steady state intervals in E4.

Obviously the impact of evaluating stats over steady state is the most significant in the most crowded rounds, i.e. in the rounds with the highest inflow as visualized in Table 3.2.

| Round | 2 | 3 | 4 | 5 | 6 | 7 | 8 | 9 | 10 | 11 |
|---|---|---|---|---|---|---|---|---|---|---|
| $\rho_{kuz}$ (whole round) | 0.86 | 2.31 | 2.19 | 1.54 | 2.57 | 2.66 | 2.40 | 2.48 | 2.50 | 2.70 |
| $\rho_{kuz}$ (steady state) | 0.78 | 2.49 | 2.59 | 1.66 | 2.91 | 2.92 | 2.69 | 2.90 | 3.01 | 3.00 |
| $\alpha$ [ped/s] | 1.20 | 1.50 | 1.50 | 1.35 | 1.65 | 1.95 | 2.25 | 2.25 | 2.40 | 1.94 |

Table 3.2: Mean conic density $\rho_{kuz}$ for all runs of D0 evaluated for the all round (upward) and steady state (downward) and the inflow to the system.

### 3.1.4 Free Flow

The first two runs represent the free flow state, the occupancy in the room fluctuated around seven, resp. nine pedestrians. Even the free flow steady state occupancy depends on the inflow, these values express the average number of pedestrians enter the room during the passing of one person:

$$N_{ff} = \frac{\bar{TT}}{\Delta t_{in}} = TT \cdot J_{in}, \tag{3.2}$$

where $\bar{TT}$ refers to mean travel time and $\Delta t_{in}$ to pedestrians headway at the entrance, the relation uses the flow definition (2.35). In the E4 free flow case, $\bar{TT} = 7$ s, therefore the $N_{ff} = 7$ ped for $J_{in} = 0.99$ ped/s, resp. $N_{ff} = 9$ ped for $J_{in} = 1.22$ ped/s.

The equation was derived using the fact, that the outflow in free flow state is equal to the inflow. The phase of increasing occupancy is quite short, takes only few second until the first pedestrian reaches the exit. Then, the frequency of entering is the same as the frequency of leaving that brings equilibrium, i.e. steady state.

### 3.1.5 Congestion

The last 5 runs are classified as congestion, the crowd accumulates in front of the bottleneck. As the inflow exceeds outflow, the number of people would fill all room (or, in experimental case, all participants entered and the round had to be finished). The trend of occupancy

extends the free flow relation by the difference of inflow and outflow:

$$N_{con} = (J_{in} - J_{out}) \cdot t \tag{3.3}$$

where $J_{out}$ is assumed to be equal to $J_c$.

This assumption should be further discussed, because both, records of occupancy fitted to (3.1.5) and direct outflow measurement presented in Figure 3.4 indicate more complex behavior of outflow than presented hydrodynamic approximation.

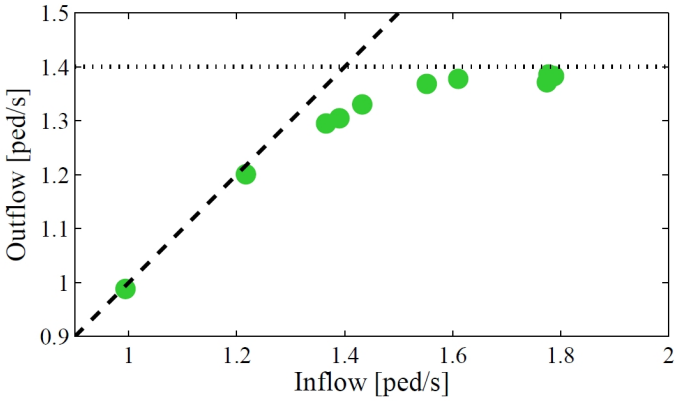


Figure 3.4: The relation of outflow and inflow measured for each round of E4.

As seen in the Figure 3.4, the inflow-outflow trend deviated from identity since the value exceeds 1.3 ped/s (add specific flow). If this value expresses the capacity of the exit, the outflow should level, but this is not observed yet. The outflow grows until the inflow reaches 1.6 ped/s, then the value stabilizes at 1.4 ped/s.

Outflow measured within E4 hits the interval measured by the other research groups dealing with the same exit width (d = 0.6 m), namely Kretz [94], Muir [105] and Müller [106], see Table 3.3. The empiric relation 3.1 predicts the flow equal to 1.14 ped/s, slightly over Kretz values.

| Study | $J_c$ [ped/s] |
|---|---|
| Kretz [94] | 1.1 |
| Muir [105] | 1.4 |
| Müller [106] | 1.5 |

Table 3.3: Mean flow corresponding to exit width 0.6 m referenced in selected publications.

As we can see, the values in table significantly differs as the experimental conditions were not unified. The lower limit near 1.1 ped/s corresponds to the long corridor in front of the exit, while the upper bound around 1.5 was reached by different geometry more similar to E4 - a room with the exit as the bottleneck.

Moreover, Müller [106] started the experiment with dense crowd, the density in all room reaches 5 ped/m$^2$.. In the article [107] proposes that the outflow is more influenced by the initial density than the bottleneck width.

### 3.1.6 Metastable State

Aside the discussions about the precise value of capacity with respect to the geometry or initial conditions, the non-linear part of inflow-outflow curve visualize in 3.4 indicates that the whole concept of (static) capacity as a product of hydrodynamic approach should be reviewed.

The observed non-linearity suggests that "dynamic capacity" (defined as the maximal congested flow under given conditions, i.e. $J_c(\rho)$) moves with number of pedestrians in the cluster.

Therefore the phase transition from free flow to congested state driven by the inflow is not jump-like, but the system passes through relatively long transition interval. As the behavior of crowd in this transition interval differs to the both free flow and congestion phase, we propose to define "metastable phase".

In this state, observed when inflow is between low and high capacity limits, occupation fluctuates and all characteristics less stable. In the range of inflow close to the static capacity, small crowd in front of the exit increases the motivation of pedestrian, which increases the flow through the exit and therefore the cluster stops growing.

This phenomena was observed in detail during rounds 3, 4 and 6. As seen in Figure 3.3, the occupancy increased up to 20 resp. 30 pedestrian, that corresponds to 15 resp. 25 people in the crowd in front of the exit. After that, the occupancy levels or even decreases and after while eventually starts growing again. This behavior indicates the high sensitivity to fluctuations of the inflow as well as to other internal or external factors.

While all pedestrians walk in free flow and (almost) all pedestrians stay at congestion, the metastable state supports individual behavior. More fast and aggressive people still walk rather fast, but others stay and spend much more time by passing. Therefore it is still walk or stay on the individual level, but the projection to crowd level produce described complex behavior and verifies the need of adding metastable state into the system classification.

### 3.1.7 Fundamental Diagram

So far, the inflow was used as the only variable explaining the flow through a room. The deviations from hydrodynamic approach motivate us to analyze the effects of intern variables as occupancy, density or density distribution. These quantities obviously affect both, macroscopic behavior expressed by the flow and individual velocity representing microscopic feature.

The essential characteristic of pedestrian movement represents the fundamental diagram, the dependence of the flow on the density ($J = J(\rho)$) or the velocity on the density ($v = v(\rho)$), see [70] or [126].

In theory, the motion of mass of people might be modeled similarly to a fluid matter – at least the same fundamental dependence can be derived from the basic definitions (2.7) for the one-directional movement in the corridor:

$$J = \frac{N}{T} = \frac{N}{A}\frac{A}{T} = \rho\,\frac{l\,b}{T} = \rho b v, \tag{3.4}$$

where $b$ is the width of the corridor. The specific flow $J_s = J/b = \rho v$ reflects the flow

standardized to unit of width.

As seen in Figure 3.5, the shape of fundamental diagram differs with respect to the experimental condition or to the setting of simulation. Regardless to these differences, the extreme values of specific flow and densities for one dimensional motion are estimated (see [118], [119]):

- $J_{\max} \in (1.2,\ 1.8)\,(\mathrm{ms})^{-1}$,
- $\rho_{\max} \in (1.75,\ 7)\,\mathrm{m}^{-2}$ (the density which maximizes the flow),
- $\rho_0 \in (3.8,\ 10)\,\mathrm{m}^{-2}$ (the density which disables the movement).

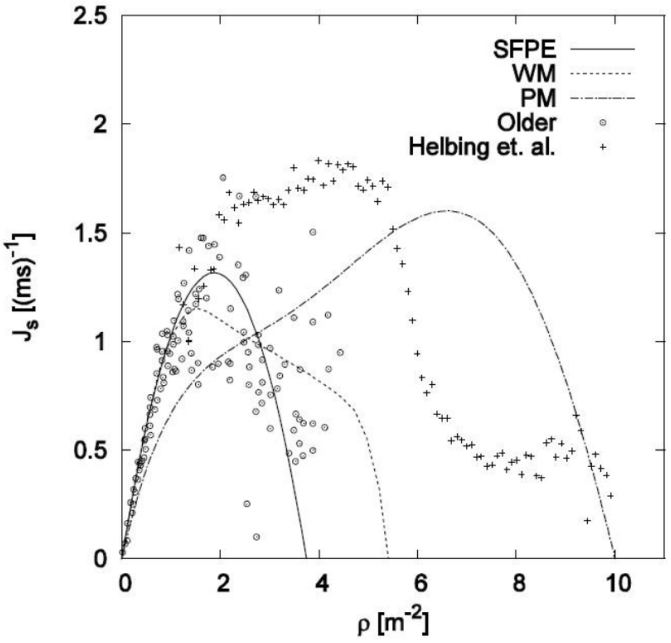


Figure 3.5: The visualization of several fundamental diagrams (taken from [118]). Lines represent modeled data, points refer to experimental values.

Juelich group organized many pedestrian flow experiments and classified different geometry into three groups [151]:

- **open:** the length bottleneck is low, the width of area behind and in front is much higher than bottleneck width. The example is the door.
- **semi-closed:** the area in front of the bottleneck is wide, but the width behind corresponds with the bottleneck width. The example is the beginning of a hallway
- **closed:** both the width in front and behind the bottleneck corresponds to the bottleneck width. The example is the corridor itself, considering any cross-section as a bottleneck.

Open geometries achieve highest flow as the discomfort caused by the short interval of narrow bottleneck is more acceptable than permanently narrow corridor. Anyway it seems that the geometry itself adds a lot of variance into the fundamental diagram curves.

Our experiments may be characterized as semi-closed, thus we can expect rather higher flow for given density. During the experiment E4, we have evaluated density using multiple methods (see section 2.3). For standard density, voronoi exact density and conic density evaluation approaches there are matching flow evaluation techniques. Generated fundamental diagrams are visualized on Figure 3.6. Standard approach density and flow was smoothed using rolling average with central 8 s window, distribution approaches are visualized in raw form.

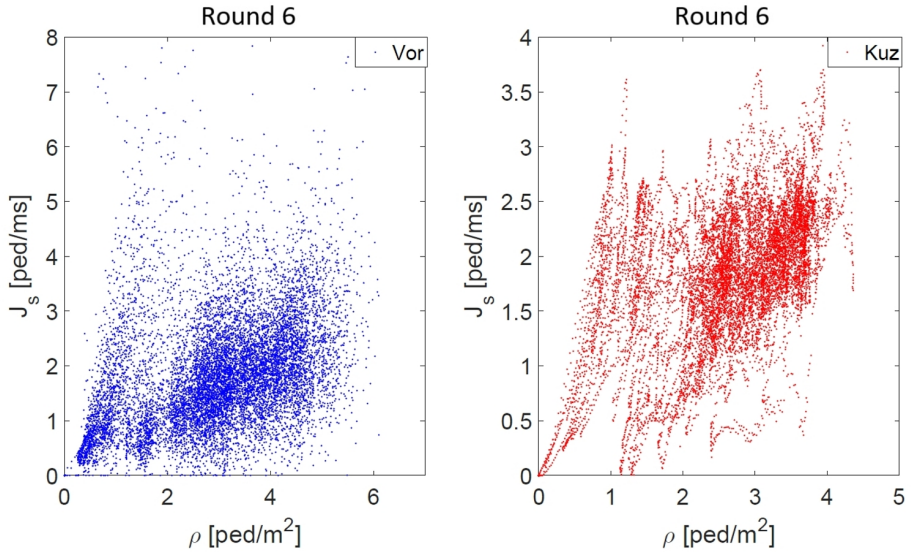


Figure 3.6: Fundamental diagrams evaluated in D2, round 2 of experiment E4.

From the microscopic perspective, the same relation may be expressed by the relation of velocity and individual density, visualizing the density areas where pedestrians are able to walk freely or they have to adjust their velocity to the conditions around.

Apparently, velocity should decreases with the increasing density. This trend is well visible for all studied publications, see Figure 3.7. Presented curves differ just by maximal values of density or velocity. Expect of SFPE [108] where velocity decreases linearly, the trend is characterized by a density interval, where the decrease of velocity slow down.

Or data from E4 (detector D2) copies this trend as shown in Figure 3.8. With maximal density around 5 ped/m$^2$ for voronoi approach (2.23) or 4 ped/m$^2$ for conic approach (2.18) and steep velocity decrease until the density reached 2 ped/m$^2$, or data corresponds to the WM and Older results. The difference between our data and selected publications roots in the maximal velocity. Volunteers participated in conducted experiment we motivated to walk fast to he exit when they have a change.

The three dimensional fundamental diagram evaluated for leave the room experiment E2 (fig. 3.9) clearly describes this dependency adding the information of the frequency of occurrence.

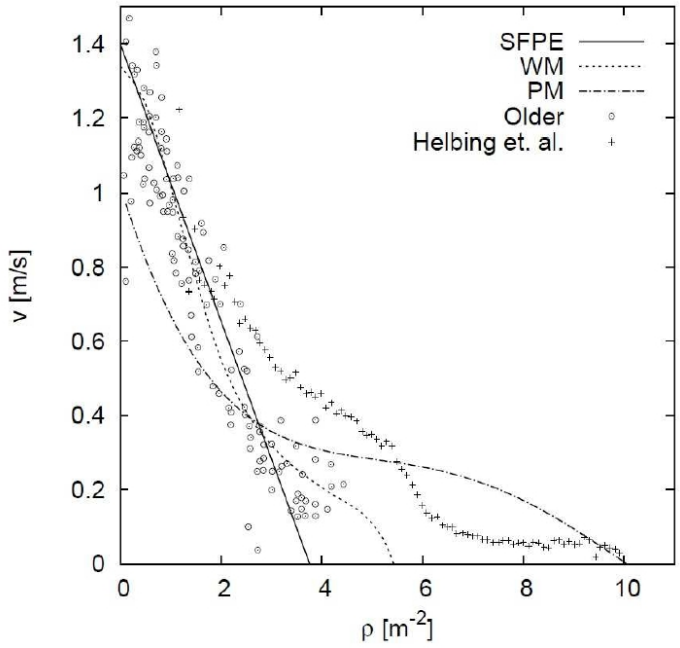


Figure 3.7: Velocity – density fundamental diagram evaluated in selected models: [117] (PM), [141] (WM) and [108] (SPFE), and experimental studies: [111] (Older) and [72] (Helbing). Taken from [124].

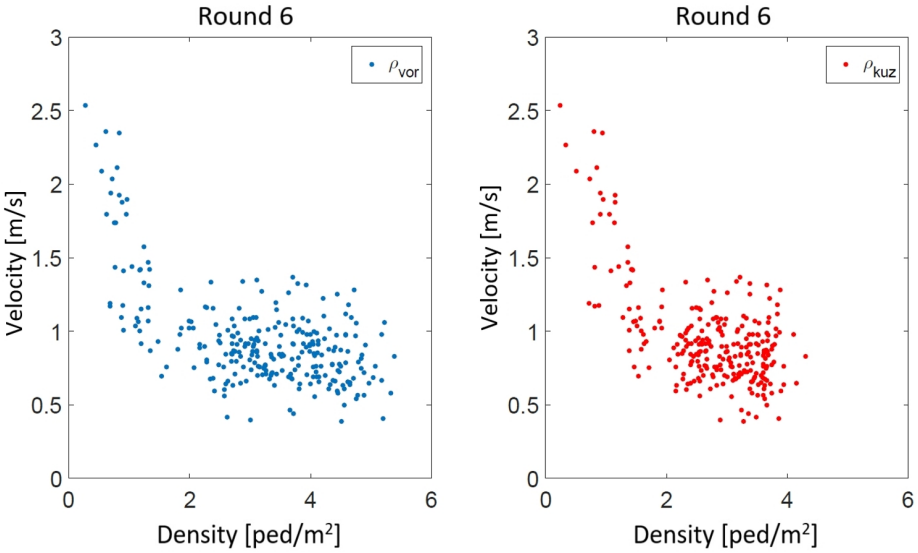


Figure 3.8: Velocity – density fundamental diagram evaluated in D2, round 6 of E4. One point represents one passing through the detector. The pedestrian velocity is averaged over the period that a pedestrian spend in the detector, the detector density is averaged over the same interval. Left: Voronoi approach, right: conic approach.

As mentioned above, pedestrian may walk freely or they must adjust their velocity. The

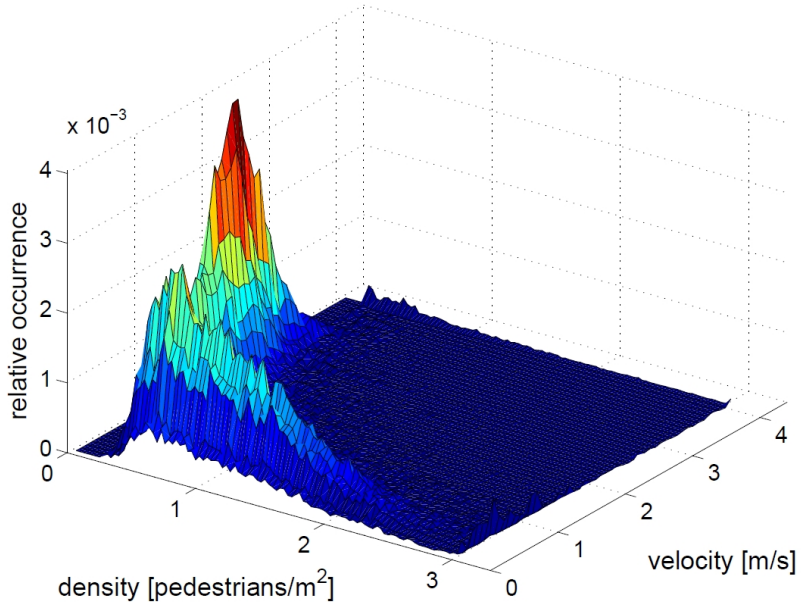


Figure 3.9: The three dimensional fundamental diagram, E2.

free flow occurs until the density reaches 0.3 ped/m$^2$, participants walked with velocity 1.5 – 2.5 m/s. The high variation of velocity in this area of densities demonstrates individual aspect of the movement.

Conversely, when density exceeded 0.5 pedestrians/m$^2$, congestion appeared. In this state, the velocity fluctuates between 0 and 0.7 m/s, with slowly decreasing trend and low variance. The highest observable density in E2 reached 3 ped/m$^2$.

The transition from free flow phase to congestion was observed for the density interval 0.3 – 0.5 ped/m$^2$. The width of this range indicates individual perception of near by conditions. While some pedestrian are able to walk freely even the density reaches 0.5 m/s, others are slowing down much earlier.

Here we note that the described microscopic phase transition is not related to the phase transition detected at the exit. This density driven individual phase relates only to personal preferences, without any reference to geometry or the reason for individual conditions. On the other hand previously mentioned inflow driven transition describes global features at some specific geometry.

The only common observation refers to foggy transition between phases instead of sharp jump. This behavior is typical for socio-physical systems where people's decision making process with elements of uncertainty or randomness appears.

### 3.1.8 Spacial Distribution

The motivation of pedestrians is (aside the geometry of the room) the most important factor defining the shape if crowd in front of the bottleneck.

As we observed during E1, when the motivation to leave the room is low, pedestrians keep

the initial shape. Generally a queue with one line or multiple lines was observed.

When the motivation is higher, crowd is formed into a funnel-like shape (Figure 3.10), where the number of queue lines rapidly increases with increasing distance to the exit. Again, the width of the funnel depends on motivation, the funnel become more width as more people try to overtake the others.

Figure 3.10: The shapes of crowd observed during E1.

The final shape of a crowd in competing situations is a semi-circle, but the occupancy inside the crowd doesn't have to be uniform. As presented by the density profile form E2 (Figure 3.11), the transition from free flow to congested state mentioned in previous section is rather smooth.

Moreover, four critical checkpoints indicate the velocity adjustments well before the real density increment:

- 6 m to the exit: the velocity begin to decrease
- 4 m to the exit: the density begin to increase
- 3 m to the exit: velocity reaches the minimum
- 1 m to the exit: density reaches the maximum

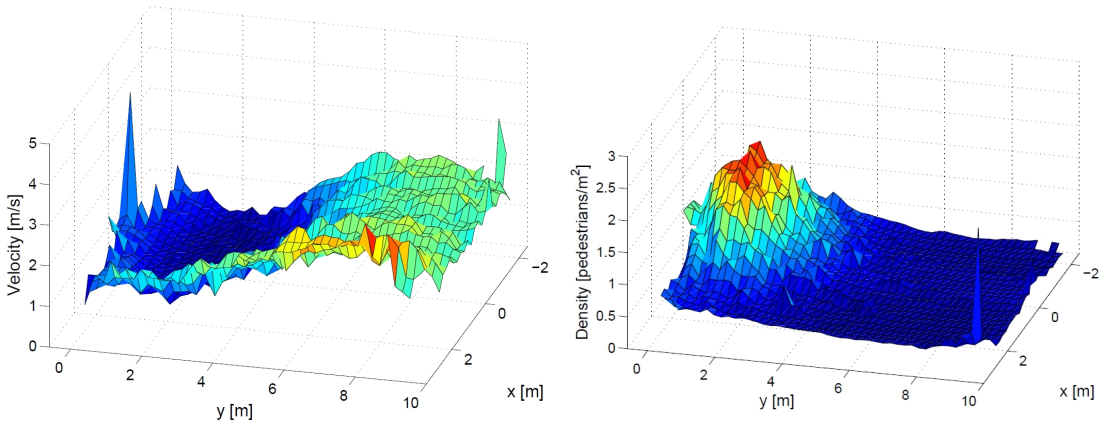


Figure 3.11: The distribution of velocity and density and in the room.

Nonetheless the specific values are related to the experimental set-up, we may generalize three phenomena:

1. The density in crowd is not homogeneous, the dense center is surrounded by area with linearly decreasing density towards the edge.

2. Pedestrians slow down much earlier than the density rises, in anticipation to the future conditions.

3. The deceleration of pedestrian is rather gradual, even people are physically able to stop almost immediately.

All effects should be taken into account for modeling.

## 3.2 Heterogeneity

From microscopic (individual) perspective, the travel time is the most crucial quantity describing the performance of an infrastructure. As is shown in this section, the travel time reached by different pedestrians dramatically differs due to many individual features.

### 3.2.1 Travel Time Analysis

This section focuses on the properties of the travel time (2.1). Our aim is to show that the travel time is mainly influenced by the size of the clogging in front of the exit represented by the mean occupancy (2.2). The data was taken from E4.

For each path $i \in I$, the pair $(\overline{N}(i), TT(i))$ is plotted in Figure 3.12. The mean travel time $TT_N$ increases almost linearly with increasing occupancy $N$.

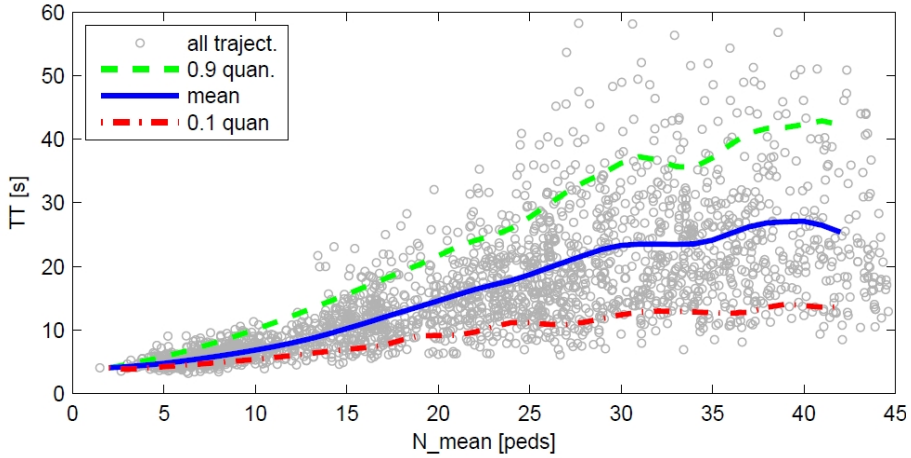


Figure 3.12: Travel time – occupancy relation, mean, top 10% and bottom 10% quantiles highlighted. E4

This linear increase of mean travel time $\overline{TT}$ is accompanied with increasing variance of the measured travel-time, which is not proportional to the absolute value of the mean. Indeed, comparing the relative travel time (2.3) of free flow ($\overline{N} \leq 7$) to the relative travel time

corresponding to regime involving interactions ($\overline{N} > 7$), we can observe significant increase of variability, as shown in Figure 3.13.

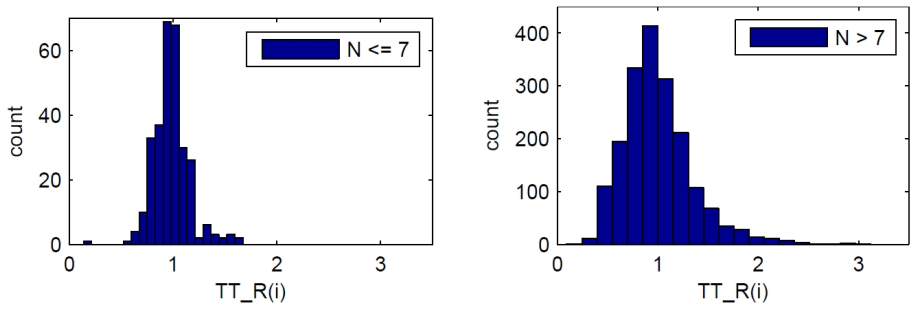


Figure 3.13: Histograms of relative travel time, data filtered over different modes. E4

This fact motivated us to investigate the dependence from the individual pedestrians $\alpha \in A$ perspective. In Figure 3.14, box-plots of $TT_R$ related to all individuals (2.5) are plotted, the participants are ordered according to the average of their relative travel time.

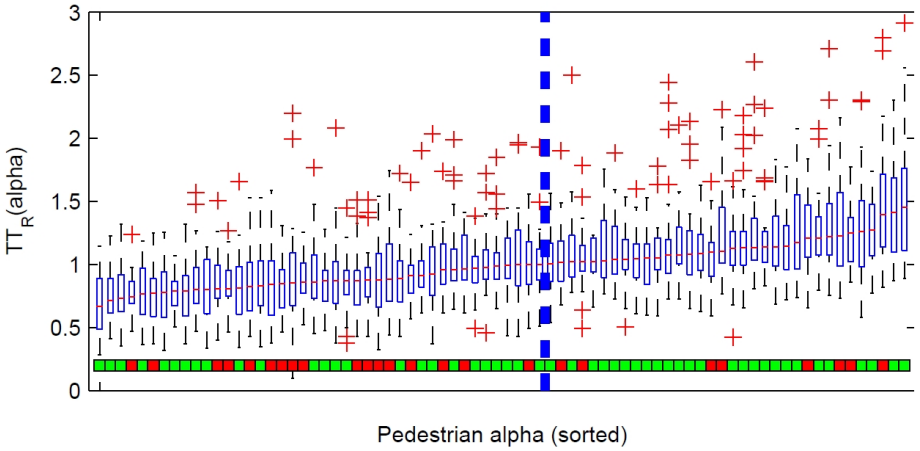


Figure 3.14: Boxplot of $TT$ for each pedestrian, ordered by mean value. Colored squares represent gender (red – women, green – men). E4

From this graph it is evident that the increasing variance in $TT$ is caused by heterogeneity of individual properties of individual participants. This motivates us to handle the $TT - \overline{N}$ dependence separately for each participant.

Let us now consider one arbitrary but fixed pedestrian $\alpha$. We assume that the relation between $TT(i)$ and $\overline{N}(i)$ for $i \in I_\alpha$ can be expressed by means of piece-wise linear model

$$TT(i) = \mathbf{a}_\alpha + \mathbf{1}_{\{\overline{N}(i)>7\}}(\overline{N}(i) - 7) \cdot \mathbf{b}_\alpha + \text{noise}\,, \tag{3.5}$$

where the intercept $\mathbf{a}_\alpha$ can be understood as $\mathbf{a}_\alpha = S/v_{0,\alpha}$, $S$ being the distance between entrance and exit, $v_{0,\alpha}$ desired free-flow velocity. The parameters $\mathbf{a}_\alpha$ and $\mathbf{b}_\alpha$ are unique for each participant. The factor $(\overline{N} - 7)$ has been derived from the data in order to distinguish

situation without and with interactions. From the analysis it follows that for $\overline{N} \leq 7$, the pedestrians are scattered in the room without significant interaction. The situation $\overline{N} > 7$ is accompanied with positive number of pedestrians in the clogging in front of the exit. Three representatives are visualized in Figure 3.15.

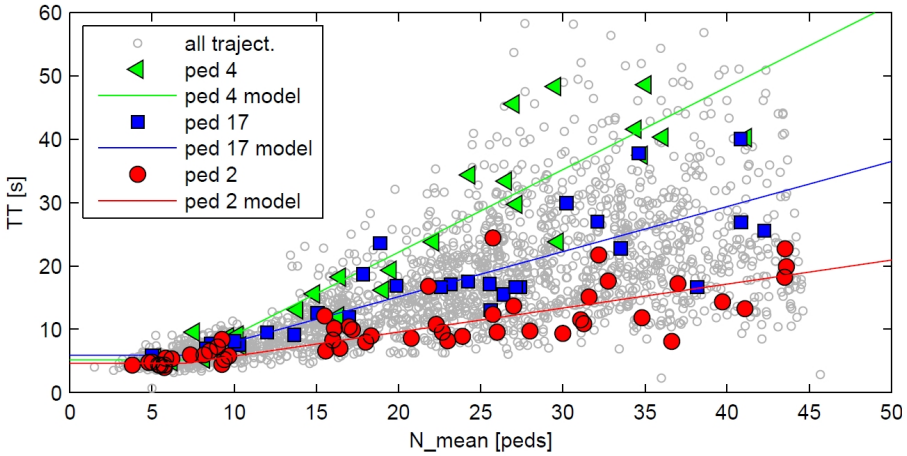


Figure 3.15: Dependency of TT to occupancy. Three pedestrians with evaluated linear model were highlighted. E4

The inverse of the slope $\mathbf{b}_\alpha$ can be interpreted as the ability of pedestrian $\alpha$ to push trough the crowd in order to reach lower travel time. The lower the slope is, the less influenced by the number of pedestrians in the clogging the travel-time of the pedestrian is.

Here should be noticed that the value of intercept and slope are not correlated. In other words, the free flow velocity and the ability to go through dense crowd are two different features. We have frequently observed slow pedestrians succeed in crowd situations and vice verse.

The correctness of the linear model has been checked using the $R^2$ statistics. The average $R^2$ statistics is 0.688 with the minimum 0.386 and maximum 0.936. The low values of $R^2$ statistics were obtained for pedestrians with low value of the slope $\mathbf{b}_\alpha$, which is expected, since low slope means that the dependence of $TT$ on $\overline{N}$ is not significant.

### 3.2.2 Route Choice

Let us make deeper look at the factors explaining the variety of slopes of the linear dependence of $TT$ on $\overline{N}$. An important aspect influencing the $TT$ is the choice of the route, more specifically, whether the participant pushes through the crowd or rather tries to walk around the crowd.

The route choice differences and patterns are visualized in Figure 3.16. Upper row visualizes all trajectories with given properties in one plot. To avoid optical illusion, we introduce the term path density, illustrating, how many trajectories passed through given area (3.6).

More precisely, let the whole area $A$ of the room be artificially divided to disjoint sub-areas $A_j$ covering the room, i.e., $A = \bigcup_j A_j$. The path-density $\varrho(A_j)$ [path/m$^2$] of the sub-area

$A_j$ is then defined as

$$\varrho(A_j) = \frac{|W(A_j)|}{|A_j|}, \quad W(A_j) = \{i \in I \mid \exists t \in T_i\,;\, (x_i(t), y_i(t)) \in A_j\}\,, \tag{3.6}$$

where $|\cdot|$ refers to the number of elements of a finite set or a size of a continuous set. The path density is given in lower row of Figure 3.16.

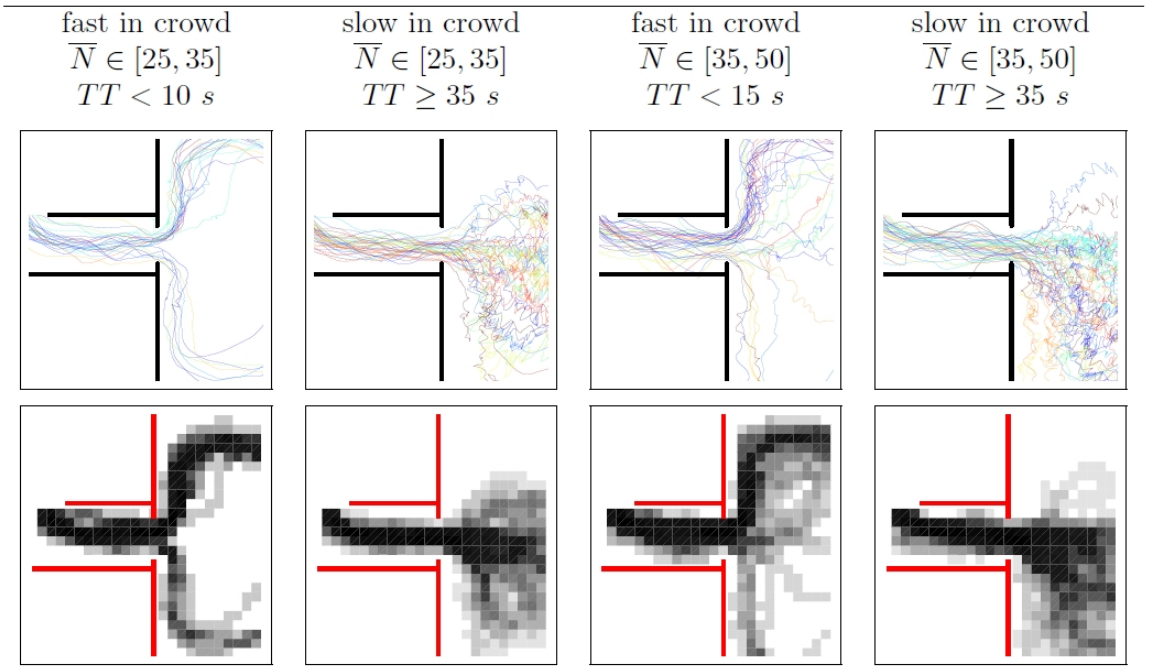


Figure 3.16: Paths (first row) and path density (second row) visualized for two different conditions metastable cluster ($\overline{N} \in [25, 35]$) and congested crowd $\overline{N} \in [35, 50]$. For both traffic modes, trajectories of slow and fast pedestrians are compared. Here we note that the density was evaluated on a grid 0.2 m $\times$ 0.2 m, each trajectory contributed to any segment maximally ones. The darker color, the higher density. Data from E4 were used.

For purpose of the discussion, paths related to free-flow were excluded. The remaining paths were divided into four groups according to mean occupancy $\overline{N}$ and travel-time $TT$. Two traffic modes are distinguished: metastable cluster for $\overline{N} \in [25, 35]$ and congested crowd $\overline{N} \in [35, 50]$. Path are then further divided to slow and fast.

Following observations can be drawn from the graphs. In metastable regime, the crowd size enabled to some participants to run around the crowd, which led to significantly lower travel time. However, in the congested regime, the crowd size caused that the running-around strategy was not so efficient and several fast participants pushed through the crowd in order to reach low travel time. Further, we can see that fast participants preferred the right-hand side of the room. This can be caused by the asymmetry of experiment outside the room or imprinted behavior.

Now we can question whether the slope of the linear model (3.5) is determined by the ability to push through the crowd, or rather by the willingness of participants to run around the crowd. Deeper insight to this question gives the study of the exit angle $\vartheta(i)$.

### 3.2.3 Angle Analysis

The exit angle $\vartheta(i)$ defined in Figure 3.17 has been investigated mainly using data from experiment E4. The conclusions were supported by data from congested regime of experiment E2.

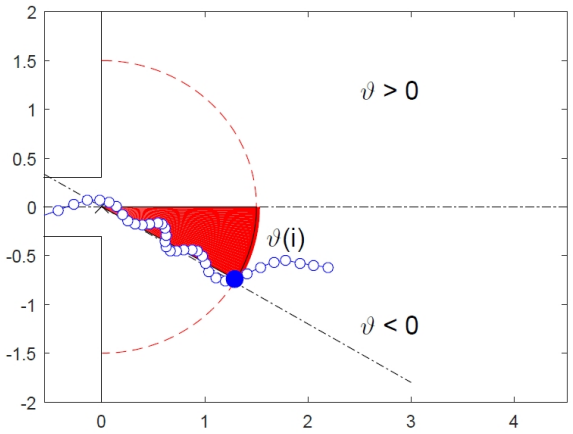


Figure 3.17: Illustration of exit angle definition. Since the moment of joining the crowd is automatically hard to recognize, the angle while passing a semicircle with center in the exit $\vec{e}$ and radius of 1.5 m was used. Direct trajectory from the entrance to the exit has the angle $\vartheta \sim 0\,\text{deg}$, trajectories along the walls have $\vartheta \sim \pm 80\,\text{deg}$, positive sign refers to right side from the flow direction.

In this section two occupancy regimes are considered: without clogging in front of the exit (referred to as free-flow) and with clogging in front of the exit (referred to as congestion). The free-flow is characterized by the low occupancy $\overline{N} \leq 15$, under which the interactions are present, but do not sufficiently affect the route-choice. The congestion is characterized by high occupancy $\overline{N} > 15$, under which a significant clogging in front of the exit is formed, which motivates some participants to run around the crowd. (Compare this division with the division for purposes of the linear model, where the presence of interactions was important).

The frequency of path with given angles is depicted in Figure 3.18 for two regimes separately. As expected, in free-flow regime the exit angles $\vartheta(i)$ diverge from 0° only rarely, 90 % of the angles are in the interval $(-45°, +45°)$, which corresponds to the straight route between the entrance and the exit. In congested regime, the angles from the whole range $(-90°, +90°)$ are distributed almost uniformly.

The effect of exit angle to travel time are illustrated using boxplots in Figure 3.19. From these graphs we may conclude that in average the path approaching the exit under higher angle (in absolute value) reached lower travel time. In the language of relative travel time, the difference between the worst and the best angle reaches 50%. Observed asymmetry of the average travel-time may be related to the shape of the corridor behind the exit.

Very similar situation was observed during the experiment E2, where the design was the same, only the corridor behind the exit was missing. This modification may caused no observable preference of left or right side. In this experiment the paths with high $|\vartheta(i)|$ (related to motion along the walls) were even more frequent (see Figure 3.20). Here we note

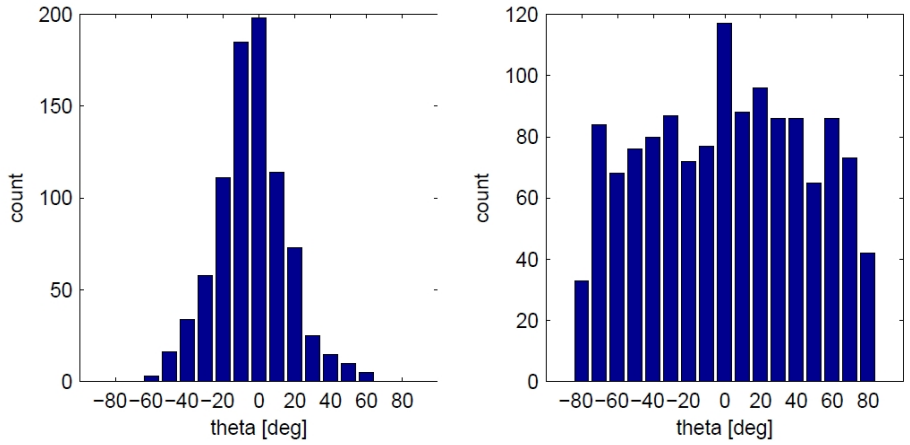


(a) Free flow (b) Congested

Figure 3.18: Histograms of measured exit angles. Left: free flow $\overline{N} \leq 15$. Right: congestion $\overline{N} > 15$. Data from E4.

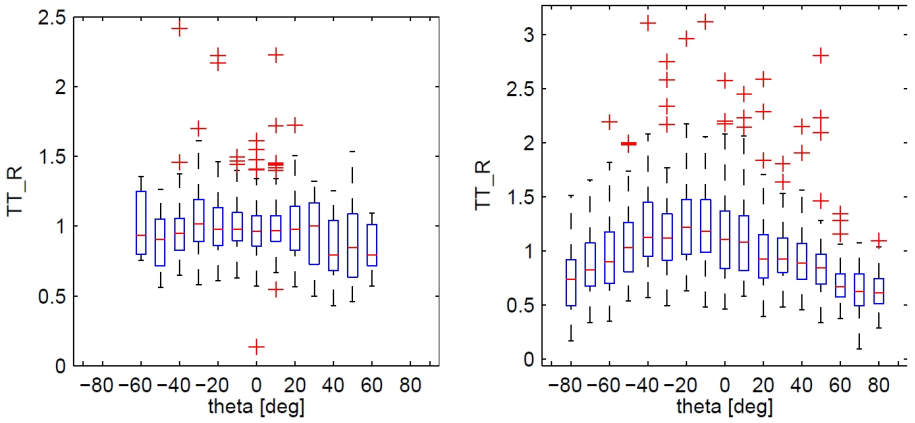


Figure 3.19: Dependency of TT to exit angle sampled by 10 deg. E4

that the data of E2 stem from one round with rather high occupancy and therefore all the paths were measured in congestion regime.

Similarly to the travel-time analysis, the dependence of chosen angle $\vartheta$ and mean occupancy $\overline{N}$ has been investigated. At first instance, the individual linear model for each participant $\alpha$ has been tested. We assume that for all path $i \in I_\alpha$ the absolute value of $\vartheta(i)$ is given by linear model

$$|\vartheta(i)| = \vartheta_{\alpha,0} + \overline{N}(i) \cdot \mathbf{c}_\alpha + \text{noise}\,, \tag{3.7}$$

where $\vartheta_{\alpha,0}$ can be interpreted as participant's preferred deviation from straight direction ($\vartheta_{\alpha,0} \geq 0$), $\mathbf{c}_\alpha$ is the slope of anticipated dependence.

Studying the $R^2$ statistics expressing, how much the use of the linear model decreases the variance in $\vartheta(i)$, we found out that for majority of participants the value of the statistics is rather low ($R^2 < 0.3$). The visualization is provided in Figure 3.21.

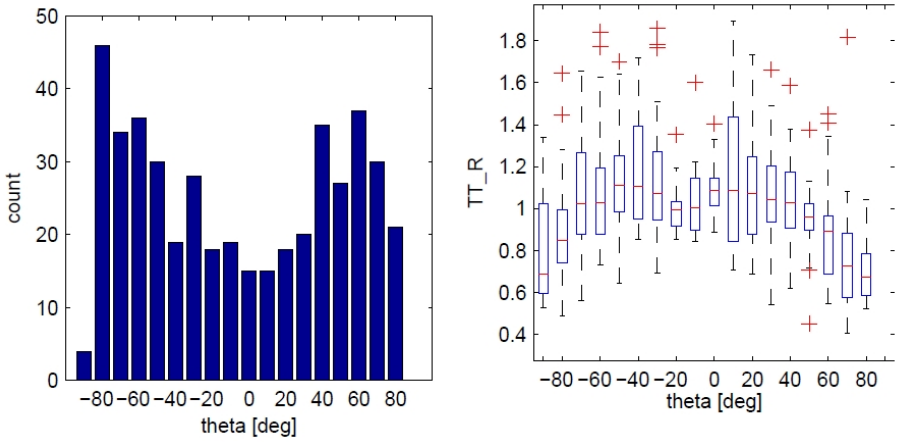


Figure 3.20: Study of $TT$ with respect to exit angle, data from high density phase. E2

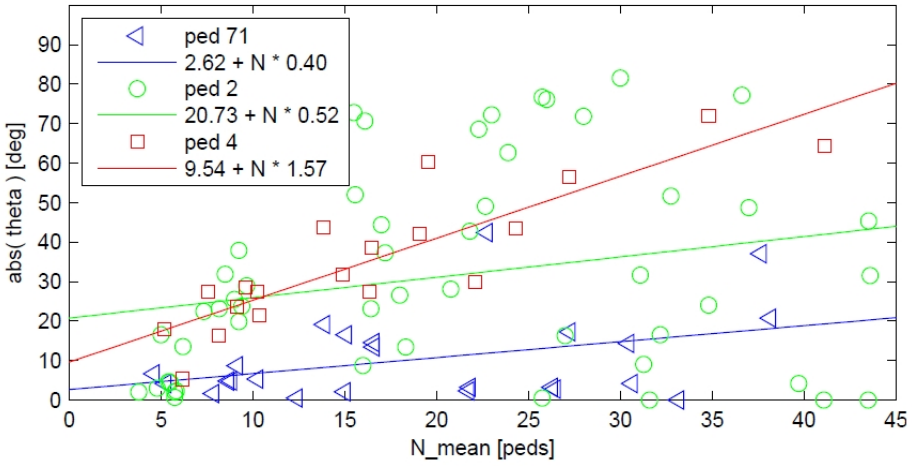


Figure 3.21: Linear model $\vartheta$ – occupancy for selected representatives of different strategy groups.

The linear model corresponds well to data related to participants with consistent strategy, i.e., preferring overtaking the crowd (ped 4) or preferring straight movement (pushing through the crowd – ped 71). Nevertheless, many participants tried to follow both strategies (ped 2). For those the linear model gives nonsensical results.

### 3.2.4 Strategy Classification

The previous section shows that in contrast to $TT$-$\overline{N}$ dependence the linear model fails to characterize the dependence of chosen angle on the mean occupancy. In this section we try to explain the relation between $\overline{N}(i)$, $\vartheta(i)$, and $TT(i)$ with respect to chosen strategy. The study presented in this section is based on data from experiment E4.

Firstly, let us put information of all trajectories to one overview graph presented in Fig-

ure 3.22. Each trajectory $i \in I$ is represented by one point, x-axis shows the average occupancy $\overline{N}(i)$, y-axis the exit angle $\vartheta(i)$, the color reflects the travel time $TT(i)$.

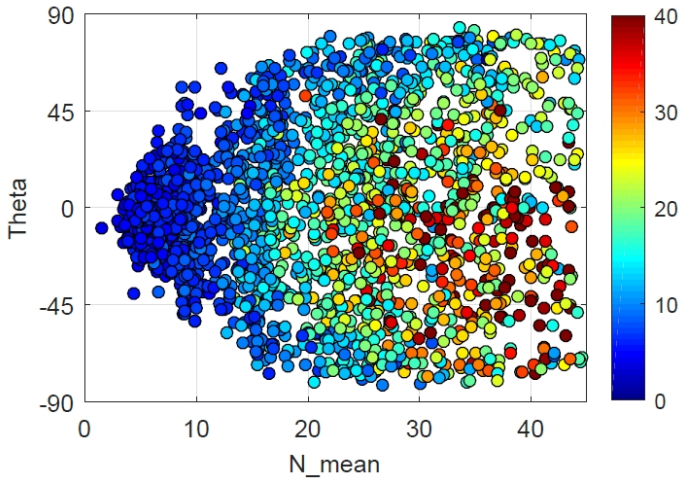


Figure 3.22: Travel time visualized with respect to average occupancy and exit angle. Each point represents one path.

This graph supports the hypothesis that the trajectories leading around the crowd are "faster" then those going directly towards the exit. This effect is getting stronger while the mean occupancy $\overline{N}$ increases. Further, the clustering of the data justifies the division to free-flow and congested regime using the boarder $\overline{N} = 15$ pedestrians.

Let us look closer on individual participants. We assume that there are two possible route-choices to be followed: walking straight towards the exit regardless to the size of the clogging and walking around the crowd once the clogging gets bigger. In both route-choices, the pedestrians travel time $TT$ is (1) or is not (0) significantly affected by the mean occupancy $\overline{N}$. Therefore, the pedestrians strategy (and performance) can be described by a triplet

$$\text{Strategy}_\alpha = \left(\text{direct}_\alpha, \text{around}_\alpha, \text{preferred}_\alpha\right), \tag{3.8}$$

where direct and around are boolean variables denoting whether the participant's travel time is significantly affected by the occupancy, while walking directly or around respectively, or not. The variable preferred $\in \{\text{direct}, \text{around}, \text{both}\}$ denotes the preferred route-choice of the participant.

The possible strategies can be then interpreted as follows:

- (1,1,?) Slow in crowd regardless to route-choice.
- (1,0,?) Slow while pushing through, but fast while walking around the crowd.
- (0,0,?) Fast regardless to route-choice.

The frequency of observed strategies is given in Table 3.4. The classification has been performed by naked eye.

Representative $\vartheta - \overline{N} - TT$ graphs are provided for illustration in Figure 3.23. Graphs belonging to the pedestrians with combined strategies are depicted in Figure 3.24.

| Type | Path | Count | |
|---|---|---|---|
| $0,1$ | – | 0 | |
| $0,0$ | direct | 3 | |
| | around | 9 | 17 |
| | both | 5 | |
| $1,0$ | direct | 6 | |
| | around | 9 | 19 |
| | both | 4 | |
| $1,1$ | direct | 22 | |
| | around | 10 | 39 |
| | both | 7 | |

Table 3.4: Number of participants using strategies $(\text{direct}_\alpha, \text{around}_\alpha, \text{preferred}_\alpha)$. Data from E4.

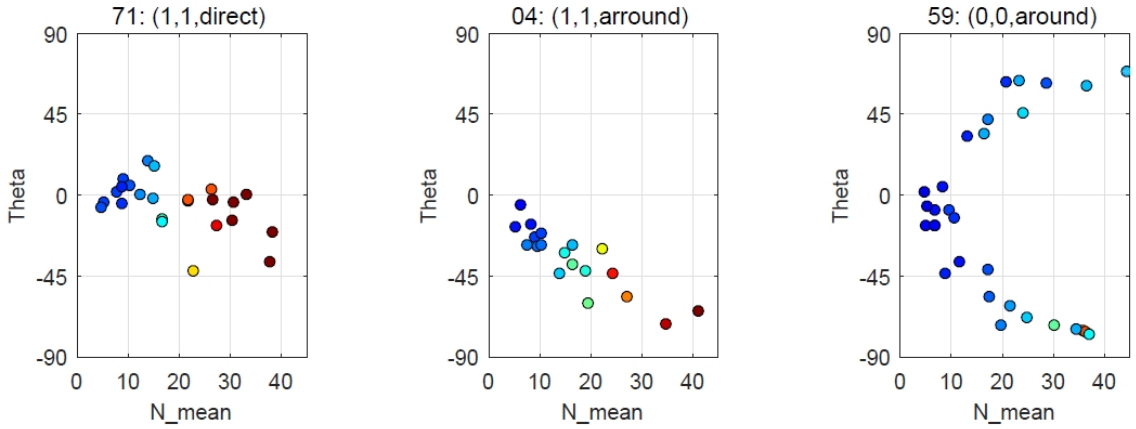


Figure 3.23: $\vartheta - \overline{N} - TT$ graphs for three representatives of studied strategies. Colormap reflects $TT$ and is the same as in Figure 3.22

From the provided graphs and table we can draw following conclusions.

- Approximately one half of participants can be considered as non-aggressive in the sense that they do not push or walk around the crowd in order to reach low travel time.
- Approximately one quarter of participants can be considered as aggressive in the sense that they push through or walk around the crowd effectively to reach low travel time.
- Approximately one quarter of participants cannot push effectively through the crowd, but is successive in reaching lower travel time while walking around.

The concept of aggressiveness as pedestrian's property fits well presented observations. We found out many tokens of aggressive behavior from the camera records as pushing, rude overtaking or blocking each other.

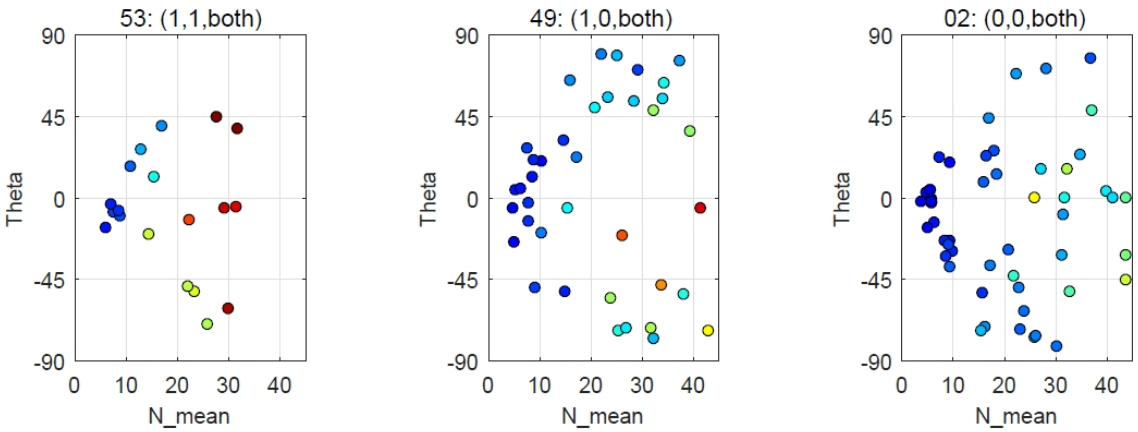


Figure 3.24: $\vartheta - \overline{N} - TT$ graphs for three representatives of combined strategies. Colormap reflects $TT$ and is the same as in Figure 3.22

As will be demonstrated in following chapter, this study is applicable in the field of microscopic simulations of pedestrian flow. The introduction of heterogeneity as the ability to win conflicts and reaction to the occupancy enables to reproduce some patterns observable in pedestrian egress experiments, as e.g. line formation, running around the crowd, getting trapped in the clogging close to the exit door.

The description of pedestrian strategy using boolean triplet categorizes participants into 12 strategy groups. More smooth approach using the coefficient of "aggressiveness" instead of boolean identifiers would describe pedestrian's performance in detail, the usage depends on application. As will be shown in simulation section, the essential is just the existence of heterogeneous groups. The shape of heterogeneity is not that important.

## 3.3 Evacuation of Train

While pedestrian motion in simple geometries with bottlenecks [19], counter-flow [44] or even complex city infrastructure [150], has been studied, the field of train unit evacuation suffers from the lack of data.

There are several difficulties that complicate optimization of train evacuation. Mainly the geometry of trains is mostly given, each inch adding to corridor width decreases the comfort of seats. The number of the exit is limited as well, therefore the total evacuation time is strictly controlled when a new train unit is developed.

This project focuses on a double-deck electric unit class EPJ 671 (CityElefant) intended for passenger service in the vicinity of city agglomerations. The aims is to quantify the effect of six independent parameters to total evacuation time, namely exit width, exit type, exit availability, heterogeneity of passengers, distribution of passengers and time to stop effect.

To handle this task, two train egress experiment were organized within the cooperation of CTU and VÚKV a.s. (Research Institute of Railway Rolling Stock), each covering three parameters – see details in articles [17, 20, 21, 22]. Concerning both experiment, more than 130 volunteers participated the evacuation and more than 10 organizers were engaged.

Train units were equipped by wide angle cameras covering most of the experiment area, see snapshots in Figure 3.25. The passing times of each pedestrian through the critical bottlenecks (illustrated in Figure 3.26) were extracted manually.

Figure 3.25: Illustration of both experiments.

Such data enables not only to evaluate total evacuation time, but the progress of occupancy in all sections and the time headways [18] as well. This article summarizes this "microscopic" point of view, trying to explain observed total evacuation times by means of individual behavior [11].


Figure 3.26: Layout of the first experiment.

### 3.3.1 Time Headways

To handle the microscopic behavior, the time headways were evaluated at the main exit. Here should be noted that the main exit width varies form 0.6 m to 1.34 m, which enables independent motion of two pedestrian lines. In this case, the headway itself does not carry all information. The mutual orientation of such lines is expressed as the "phase shift", see illustration in Figure 3.27.

When people are moving side by side, the phase shift is equal to zero. This phase is detected by the saw-like pattern (the side by side walkers have time headways are close to zero, while the next pair keeps the distance).

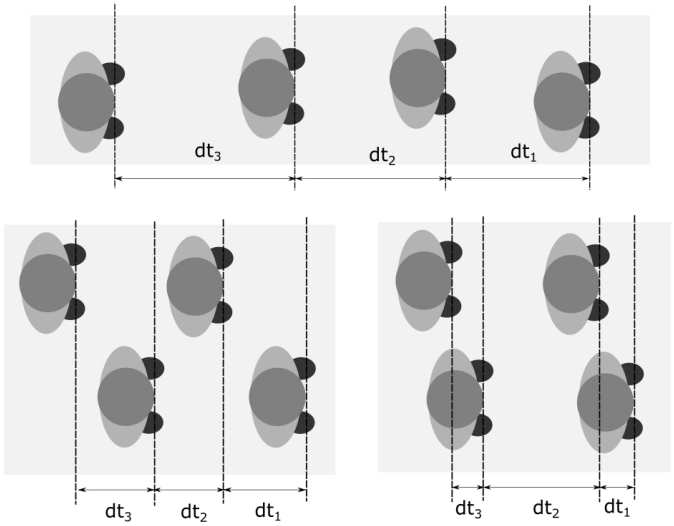


Figure 3.27: Top: Time headway definition in narrow corridor. Bottom: Two possible settings of lines – The right one is almost synchronous (phase shift close to zero) while the left one is asynchronous (phase shift close to $\pi/2$).

On the other hand, when the lines are shifted by half of the period, the distance to the predecessor is the same as to the follower. In this case, constant trend is observed.

As any of line behavior is spontaneous, phase shift between lines evolves dynamically. The line motion may be temporally synchronous, but due to the random people behavior, the asynchronism can occur instantly.

It should be noted that the phase shift itself has no effect to the flow or total evacuation time. The understanding of this effect is needed to read the charts correctly as the time shift dynamics represents most of the variance in the data.

In the next sections, the time development of pedestrian headways will be used to explain the total travel time. Following charts would combine several type of trends. Aside of mentioned fluctuations of time shift, the time headway is affected by situation in front of the bottleneck. To evaluate effects of different settings, we have to compare corresponding phases of the evacuation. Generally one can distinguish:

1. initial phase – the fastest participants are egressing, the queue (crowd) has not been formed yet in front of the exit. The outflow does not reach the capacity, therefore time headways are relatively high
2. stable phase – the core of the passengers is leaving. They have formed a queue (crowd) thus the outflow fluctuates around the capacity. The time headways are relatively low
3. closing phase – the last passengers are egressing. The pool of remaining people does not saturate the capacity thus the time headways are higher again

First, the phase transition (driven by the time time development) itself may explain the value of total evacuation time. Second, the evaluation of headway statistics just in given phase will help to focus on relevant data.

### 3.3.2 Egress Experiment 1

The first train experiment simulating an emergency egress was organized in June 2015. It involved 56 volunteers at the age of 21 to 51 years (18 women, 38 men) and focused on three binomial parameters:

- occupancy distribution: both decks (A) / lower deck only (B)
- exit availability: both sides (1) / one side only (2)
- time to stop effect: no delay (I) / 50 s delay (II)

Time to stop effect simulates the situation when the evacuation starts in the moving train. It may take several minutes to stop the train from operational velocity, thus the passengers may prepare for evacuation, move closer the exit or at least leave area affected by fire.

For purposes of this study, only (A) settings were processed. The exit availability affects the size of crowd in front of the exit as the number of participants is the same in both cases. The time to stop represents potential delay between start of evacuation and opening the door simulating the time needed to stop the train.

The Table 3.5 summarizes the macroscopic quantities selected to quantify each evacuation trial: the total evacuation time defined as the leaving time of the last participant ($T_{first}$), the total number of participants passing through given exit (N) and the time of first passing $T_{first}$ as the scenarios differs by the door-opening time. From these quantities, mean flow and mean headway may be extracted by simple formulas

$$J_{mean} = \frac{N}{t_{Last} - t_{first}}, \qquad dt_{mean} = \frac{t_{Last} - t_{first}}{N - 1}. \tag{3.9}$$

The evacuation time obviously differs with the scenario, but the mechanism is hardly visible.

| Scenario | $T_{first}$ [s] | $T_{last}$ [s] | N [peds] | $J_{mean}$ [ped/s] | $dt_{mean}$ [s/ped] |
|---|---|---|---|---|---|
| A-1-I | 7.61 | 28.52 | 28 | 1.36 | 0.75 |
| A-1-II | 52.64 | 69.67 | 28 | 1.64 | 0.61 |
| A-2-I | 11.70 | 46.98 | 56 | 1.59 | 0.63 |
| A-2-II | 52.42 | 87.82 | 56 | 1.59 | 0.63 |

Table 3.5: Macroscopic results of Experiment E1. Values were averaged over two trials and two main exits, where available.

Applying the headway approach, we can get more detail insight, see the the progress of one round visualized in Figure 3.28. The headway time series may be characterized by the three statistics:

- mean headway value within main phase
- mean headway within tail phase
- proportion of phases

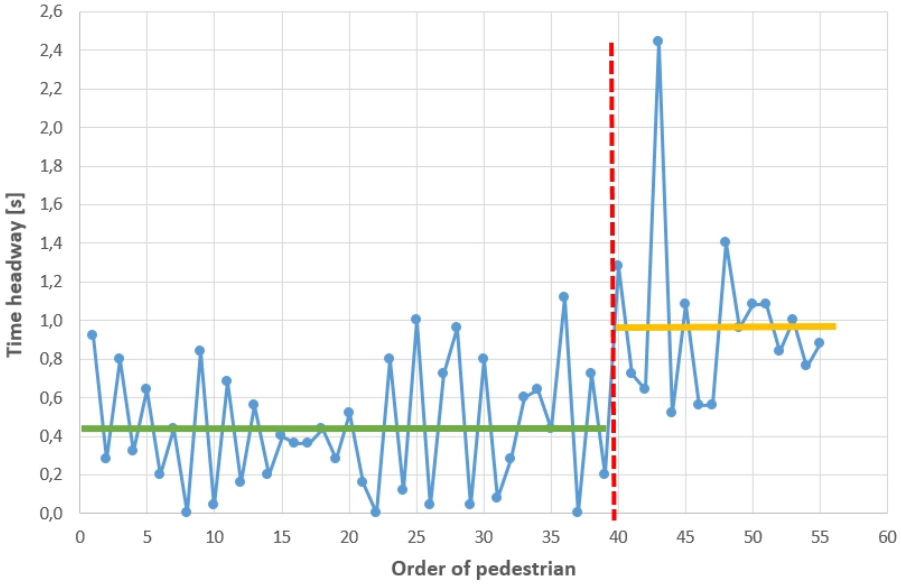


Figure 3.28: The time development of time headways in scenario A-2-II trial 1. The green line visualize mean headway value within main phase, yellow line the mean headway within tail phase and red dotted lines represents the phase separation.

| Scenario | main phase mean [s/ped] | tail mean [s/ped] | tail prop [%] |
|---|---|---|---|
| A-1-I | 0.64 | 1.35 | 17 |
| A-1-II | 0.50 | 1.14 | 19 |
| A-2-I | 0.51 | 1.16 | 19 |
| A-2-II | 0.43 | 1.07 | 31 |

Table 3.6: Microscopic results of Experiment E1. Values were averaged over two trials and two main exits, where available.

Initial phase randomly affects all trials, thus data from this phase was not used for further analysis.

Averaging these features among the scenarios (Table 3.6) brings numbers sufficient to understand the effect of settings:

- A-1-I was low in both main phase and the tail
- A-1-II was faster in both phases by 20% relatively to A-1-I (effect of waiting)
- A-2-I waster in both phases by 20% relatively to A-1-I (effect of bigger crowd)
- A-2-II was faster in both phases by 30% relatively to A-1-I (combination of previous effects), the macroscopic performance is worse due to the higher proportion of tail phase

The combination of close doors and one exit available in scenario A-2-II caused that lower

deck passengers filled the exit room, thus they blocked the door and the upper deck passengers had to wait at the stairs. When this room was available again, upper deck passengers started the evacuation, but due the bottlenecks inside the train, only one half of exit capacity was used. This caused higher proportion of tail phase which significantly increased travel time. The performance of pedestrians was better than during other scenarios thus the overall observation was in line with the others.

As seen from Table 3.6, combining lowest mean time headways with lowest tail proportion could bring more efficient evacuation. In case the upper deck and lower deck passengers would be balanced and therefore the tail proportion would be 19%, the scenario A-2-II, the total evacuation time could be lower by 5 s.

### 3.3.3 Egress Experiment 2

In March 2018, the second experiment extending the parametric space by:

- heterogeneity of passengers: high school students / population sample (B)
- exit width: 0.60 m – 1.34 m
- exit type: platform / stairs / terrain

It involved 90 volunteers at the age of 1 to 70 years. This time, different scenario took place in each half of train (Figure 3.29) and with respect to larger set of parametric combinations (30), only one trial was realized for each.

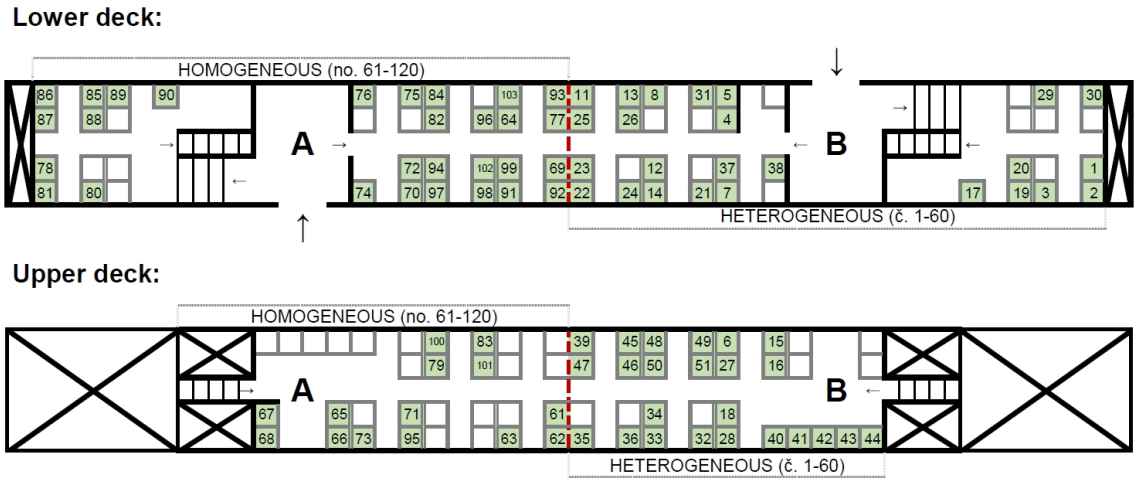


Figure 3.29: Layout of the second experiment.

Macroscopic observation visualized in Figure 3.30 will be statistically decomposed in detail within another study. For now one can say that the evacuation time decreases with increasing exit width almost linearly, young students are a bit faster than regular the population sample and jump to the terrain makes the evacuation slower than platform and even stairs approach.

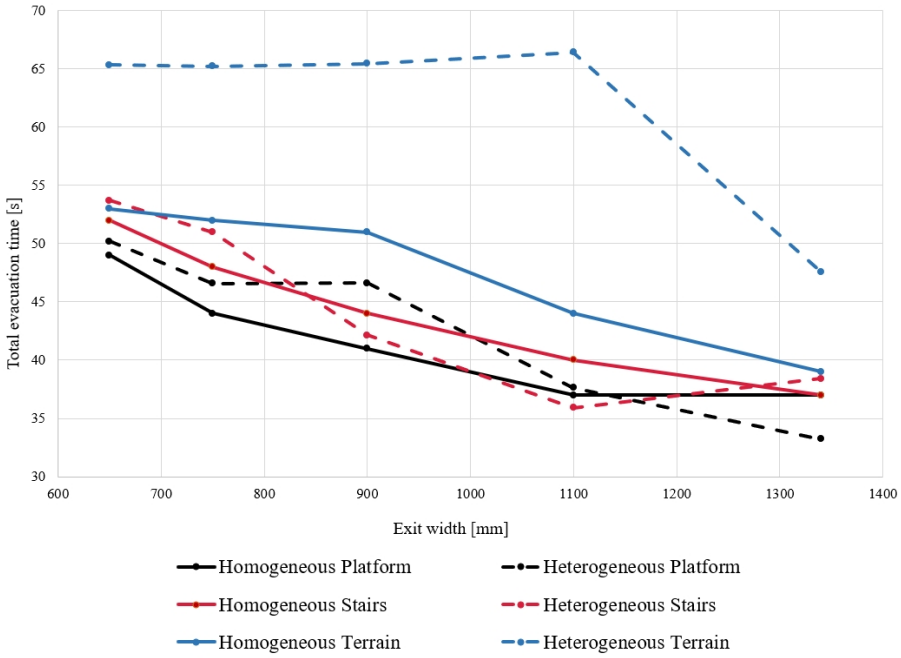


Figure 3.30: Evacuation time with respect to all parameters, experiment.

Again, headway analysis brings more light to the mechanism behind the evacuation time dynamics. This time, crowd size and the waiting time are not a factor, the motivation is the same for all trials. On the other, the changeable exit width dramatically affects the possibility of independent passing of two lines and the exit type and heterogeneity could affect the mean time headway.

The headway charts visualized in Figure 3.31 confirms the expected behavior yet quite interesting way. It seems that the headways do not hold arbitrary values, but they exist within several classes with low variation (0 s, 1 s, 3 s and 4 s).

A few classic patters were detected – constant trend along 1 s indicates one line motion, saw like patter alternating 1 s and 0 s class corresponds to two line motion with no phase shift as described in previous sections.

Then, the phase transition from one line to two lines motion induced by the exit width variation is driven by more frequent 0 s class rather than continuously decreasing headway. This is obvious in case of homogeneous group egressing to terrain and applicable for other trials as well.

Moreover, the negative effects of less efficient exit types affects the headways the same fashion – instead of systematically higher headways, one can observe more frequent headways from class 2 s, 3 s or even higher. This indicates the situation that a pedestrian needs several time units to leave the train. Such behavior was detected mainly for heterogeneous group and jump-to-terrain exit type.

Similarly to egress experiment 1, the behavior of all trials changes when all lower deck pedestrians leave. Characteristically higher headways of tail phase are again explainable by higher probability of 2 s or 3 s classes rather that by systematic shift.

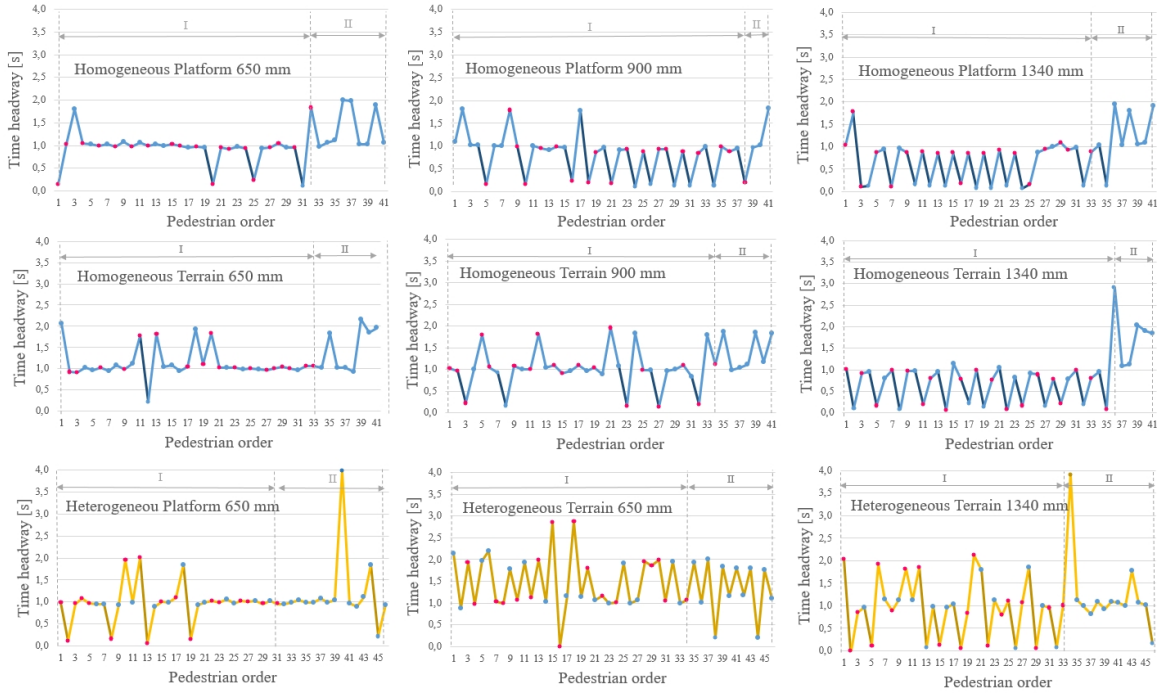


Figure 3.31: Headway study, second experiment.

This observation is common for all trials of egress experiment 2. Instead of mean headway, each trial may be characterized by proportion of headway classes. As seen in Figure 3.31, such representation would corresponds to the headway charts much better than averaging applied in egress experiment 1.

### 3.3.4 Conclusions

This section illustrates the microscopical analysis of pedestrian headways used to explain the impact of scenario parameters to the evacuation time.

First, each round was split to the main phase and tail phase. The tail phase is characterized by significantly higher headways related to the main phase cased by the lack of participants in front of the exit. It is shown that the proportion of this phases strongly influences the evacuation time.

Moreover, headways inside the phases depends to the scenarios as well as the motivation of pedestrians differs with the motivation. On the other hand, the scenario with the lowest headways reached the highest proportion of tail phase, which decreased the total performance. Assuming a scenario combining low headways and low proportion of tail phase, the total evacuation time could be 10% lower than observed.

These observation was common for both experiments, even several features differs. While the first one indicated independent line motion in lines, moving in pairs is rather observed in the second one. To be more specific, the higher flow observed for wider door or more efficient exit type is related more to frequent observation of short headway rather then lower

median headway value.

In general, the total evacuation time differs with the probability of consecutive egress of two pedestrians or, on the other end of the scale, with the probability that one pedestrian would need more time steps to leave. That explain the worst performance of heterogeneous group egressing to the terrain. In this case the high evacuation time is caused by the special assistance needed for several participants delaying the evacuation by seconds.

## 3.4 Local Behavior

In previous section, the performance of one path was evaluated with respect to the state in the room averaged over the passing time. Even the quantities as travel time or exit angle were individualized and explained by the occupation, we are still far from really microscopic study of the specific pedestrian's motion in given moment. Such approach (presented in [23, 27, 26]) will be build in following section.

To reach this goal, we have to use language of actual velocity, direction and individual density. As mentioned in section 2.2.1, the density distribution is characterized by the kernel selection – we will work with the conic one (2.18) which has several desired features as decreasing trend with increasing distance, limited support and independence of one pedestrian to the others.

But as shown upwards, the correlation between velocity and density differs from expectations.

### 3.4.1 Broken Velocity-density Paradigm

Theoretically (and even in measurement [124] the relation of velocity and density is evident: pedestrians walk by their optimal velocity whenever they are able to. With increasing density, it is more and more demanding to keep the desired velocity. Thus, pedestrians have to slow down and even stop when the motion is impossible due to the dense crowd around. From this perspective, we expect to observe strong negative correlation between velocity and density during all phases of the pedestrian movement.

However, the velocity-density study shows very different results. The selected trajectory illustrated in the Figure 3.32 is characteristic by long slowing down interval caused by overtaking the crowd – the velocity decreases at the beginning from 1.5 m/s to 1 m/s (Figure 3.33). Avoiding the crowd phase is followed by joining the crowd and continuous decrease in velocity from 1 m/s to 0.2 m/s, meanwhile the density increases from 0.5 ped/m$^2$ up to 3 ped/m$^2$ based on parameters, especially the range. Then, the density levels but the velocity increases as the pedestrian approaches the exit – and this is something unexpected.

To see the source of positive or negative correlation, it is beneficial to study rolling correlation for segments of each trajectory $R_t(\rho_{\omega_\alpha}, v_\alpha)$ and $R_t(v_\alpha, v_\beta)$ – rolling window with memory time $\tau = 1.5$ s and $\tau = 2.5$ s respectively enables to obtain this point of view.

In the language of rolling correlation (see Figure 3.34), three phases of movement are observed. There is a strong positive correlation between velocity and long-range density in free flow area, which can be explained by competitiveness between pedestrians – the occur-

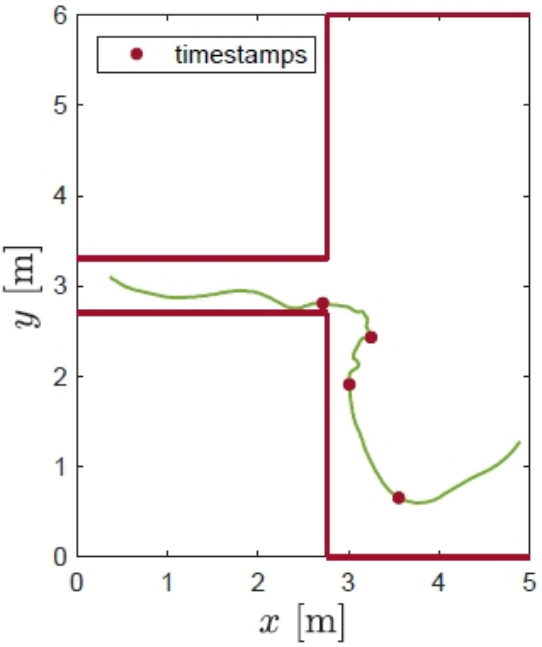


Figure 3.32: Trajectory 1240.

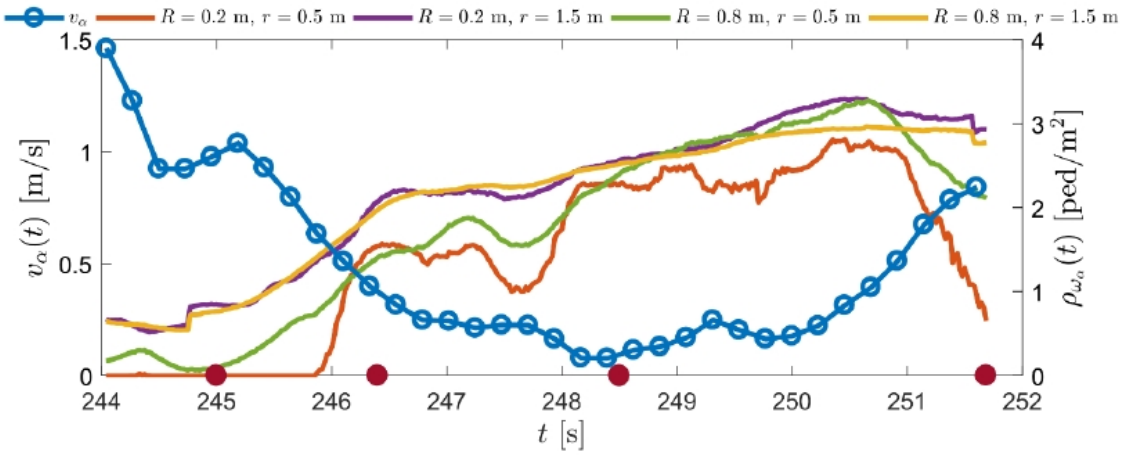


Figure 3.33: Velocity and four densities with different blur $R$ and range $r$ parameters. First drop of velocity (1.5 m/s to 1 m/s) at the beginning of avoiding the crowd is followed by continuous decrease of velocity (1 m/s to 0.2 m/s) while joining the crowd, meanwhile the density increases from 0.5 ped/m$^2$ up to 3 ped/m$^2$ based on parameters. Timestamps are placed at the positions corresponding to the spots of the chosen path in Figure 3.32.

rence of another pedestrian motivates the pedestrian to move faster, and this phenomenon is more noticeable in long-range density.

Strong negative correlation between velocity and all densities in avoiding and joining the crowd phase corresponds to adjusting velocity to higher density. The decrease in velocity

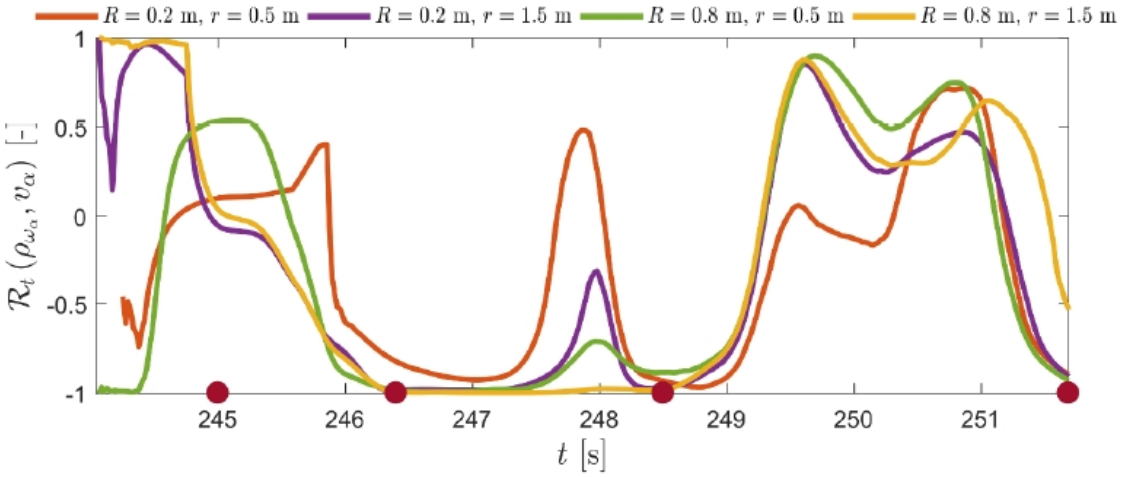


Figure 3.34: Pearson rolling correlation coefficient of densities for four blur $R$ and range $r$ combinations and velocity (memory time $\tau = 1.56$ s). Timestamps are placed at the positions corresponding to the spots of the chosen path in Figure 3.32.

fits the increasing trend of long-range densities better because of the fact that pedestrians decelerate few seconds before the first contact with the crowd and only the long-range densities cover this distance.

The correlation peak near $t = 248$ s illustrates the differences between various parametric choices. As shown in Figure 2.10, short-range densities are affected by temporary increased distance to another pedestrian decreasing the density. And as the velocity is still decreasing, the result is mentioned peak of rolling correlation to neutral or even positive zone for the short-range case.[1]

From long-range perspective, the density is decreased only slightly and the effect is more significant for low blur models – due to the sensitiveness of the correlation. Such stability of long-range density models with high blur is very useful to bridge insignificant deviations of pedestrian paths - this is the reason why we use these values of parameters in the further text.

The positive correlation of velocity and all densities in the cluster area indicates that the mechanism of motion in the crowd significantly differs from the previous phases, and therefore the density (even the individual one) cannot be used to predict the actual velocity of any pedestrian. We have to introduce different concept to describe the movement in this phase - see next sessions.

The very last part of the examined path reverts to the negative trend. In the exit area, the density drops due to the empty space in a forthcoming corridor and the pedestrian starts to walk faster which is in an agreement with the expected negative correlation.

Generally the individual density inside the crowd is rather constant. The crowd edge area

[1] The detail analysis shows that the long term decrease of velocity stops and for 0.2 s velocity almost levels. This indicates that pedestrian reacted to the density fluctuation the expected way - still the negative correlation should be observed. The mentioned neutral/positive peak is cause by asynchronicity between velocity and short range / small radius densities, what is another reason not to use them.

where the density increase from almost zero to the maximal value lengths only several meters as shown in the session 3.1.8. The slight increasing trend toward the exist may be observed, but the scale is not significant.

That implies that the future steps of any pedestrian are not predictable by their reaction to the surroundings as has been discussed earlier. Obviously pedestrians need a space to move to, but they do not have to see a space to start movement. They can move because their predecessor moves - that will provide the space to finish a step.

The positive correlation observed in the experiment is just a coincidence - the velocity deep in the crowd is definitely not higher because of the density is higher. The correlation it self does not imply causality.

### 3.4.2 Follower-leader Concept

In the crowd, a pedestrian often copies the movement of their predecessor standing close ahead – the flow motion is usually carried by just one line, while the others barely move. While one half of crowd stands, the second moves just because someone ahead was able to make several steps. The situation is the same as in case of queues, but the structure is more chaotic – usually several people try to follow the one who moves.

For such system, a follow the leader model similar to vehicular traffic [119, 134] may be much more successful that velocity – density causality. Unfortunately crowd represent much more complex system that an ordinary road, therefore to define leaders and followers is no straight forward task.

Let us denote the pedestrian $\alpha$ and his predecessor $\beta$. Pedestrian $\beta$ is labeled as a leader for pedestrian $\alpha$ in a time point when $\alpha$ approaches $\beta$ at a specific distance (0.75 m) fulfilling the assumption that $\beta$ is closer to the exit than $\alpha$ ($\beta$ is in the $\alpha$ field of vision).

It is worth noting that a leader for one pedestrian can be at the same point in time a follower of another. For instance, if there is one linear queue of ten pedestrians (pedestrian one is the closest to the exit), our concept sees it as nine leaders (pedestrians one to nine) and nine followers (pedestrian two to ten). Representing this multi-chaotic queue by a graph structure, we would obtain a tree, where the root (at the exit) has no leader, the pedestrians in the body of the tree are the both, leaders and followers, and finally the leaves are pure followers. Such tree creates branches any time two or more pedestrians follow one predecessor – that means a queue splits.

This approach is not related to controlled evacuation models, where leaders are often defined in advance and have a special role during an evacuation. Although the leader and the follower have the same goal, there does not have to be any psychological link between them in this concept - a pedestrian becomes a leader not by his own will, but due to the existence of a follower.

We will go back to mentioned path 1240 (Figure 3.32). Let us highlighted the point where this pedestrian $\alpha$ becomes a follower in the chart of velocity and density. As seen in Figure 3.35, this spot corresponds to the densest area and the point when his velocity drops almost to zero – just before the pedestrian adapts to new conditions.

The Figure 3.36 visualizes the velocity-density correlation $R_t(\rho_{\omega_\alpha}, v_\alpha)$ together with the follower-leader velocity correlation $R_t(v_\alpha, v_\beta)$. As discussed in previous paragraphs, the

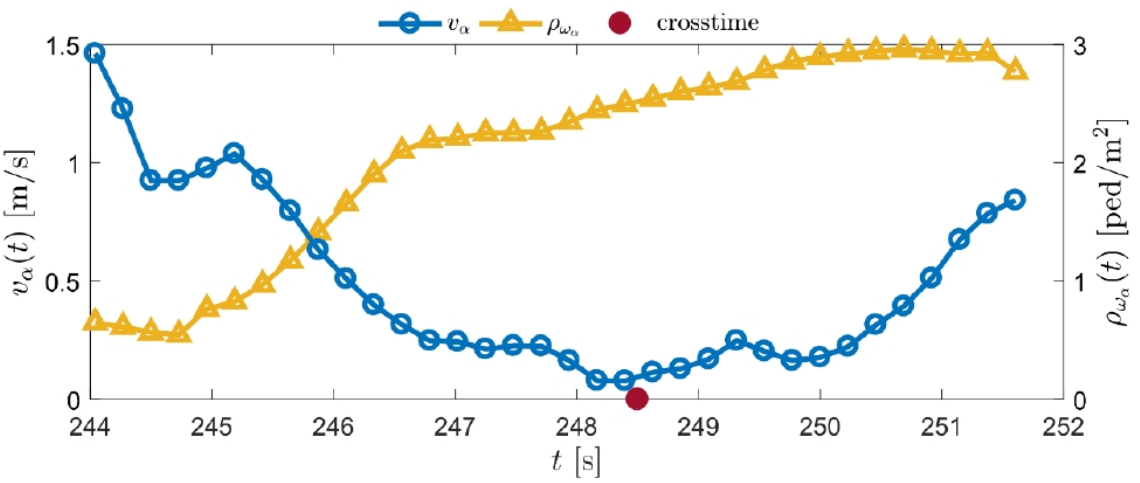


Figure 3.35: Trend of velocity and long range large radius density of path 1240 3.32. The spot represent the first approach of pedestrian $\alpha$ to a leader $\beta$.

positive correlation between the individual density and the velocity in the crowd area is just a coincidence. On the contrary, the correlation between velocities reflects the situation better.

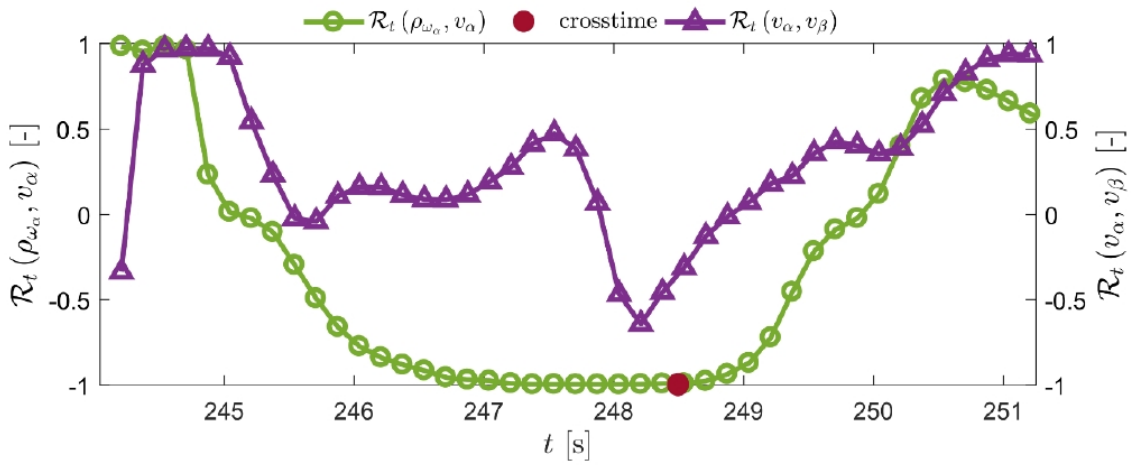


Figure 3.36: Trend of velocity and long range large radius density of path 1240 3.32. The spot represent the first approach of pedestrian $\alpha$ to a leader $\beta$.

Short time after the spot, $R_t(\rho_{\omega_\alpha}, v_\alpha)$ is negative as pedestrians competes to the exit position. Pedestrian $\beta$ won the conflict and pedestrian $\beta$ started to follow. Since that time correlation turns positive as their velocities perfectly fit.

### 3.4.3 Generalization

So far, we deal just with one trajectory. In this section, we will replicate investigated phenomena for all pedestrians who passed the room under conditions with free flow at the beginning and congestion at the end. All trajectories were scaled using normalized travel time (2.6) and both, the velocity – density correlation and follower – leader velocity correlation were evaluated.

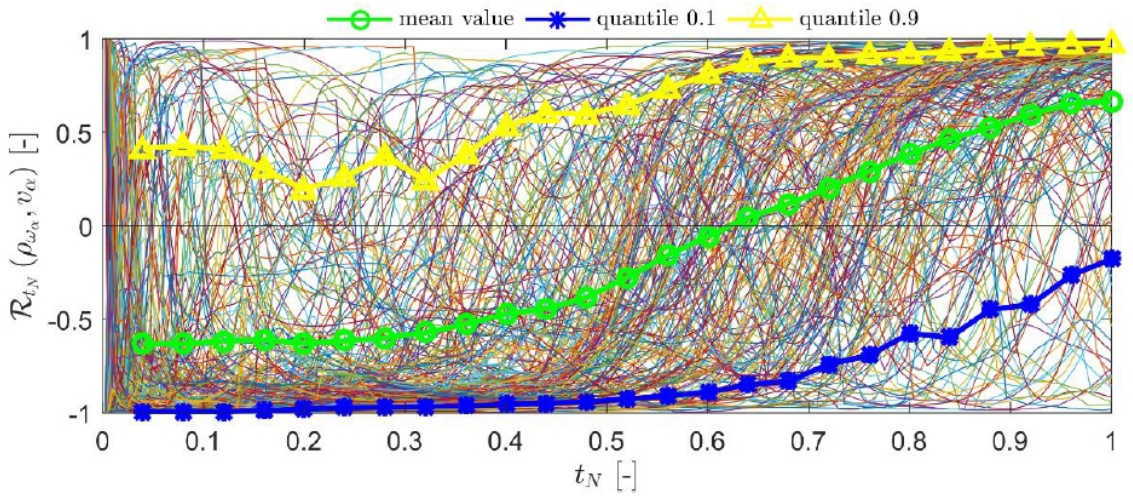


Figure 3.37: Correlation between individual density and velocity for each pedestrian corresponding to travel time $\in (7, 15)$ s and mean occupancy $\in (7, 15)$ ped.

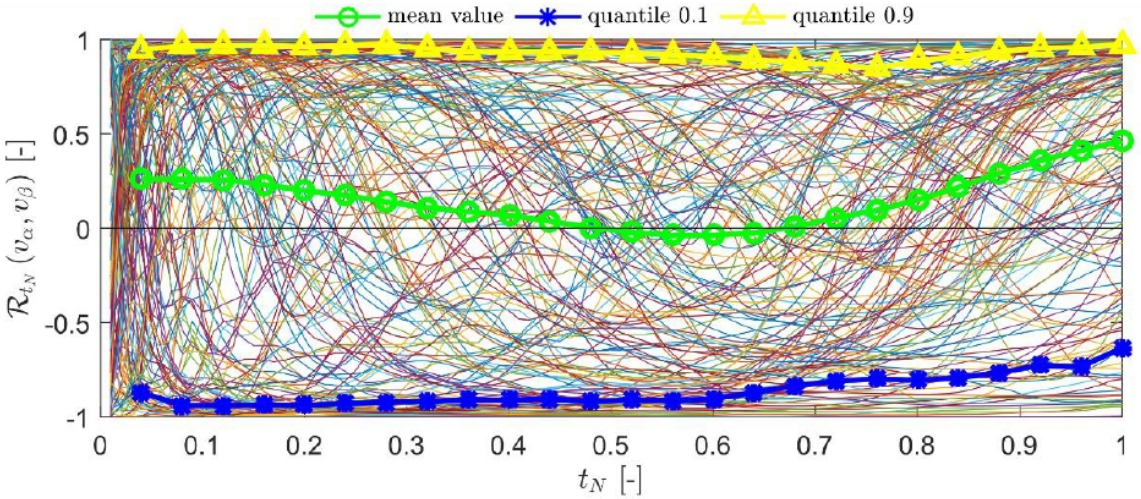


Figure 3.38: Correlation between follower and leader velocities for each pedestrian corresponding to travel time $\in (7, 15)$ s and mean occupancy $\in (7, 15)$ ped.

The results for $R_t(\rho_{\omega_\alpha}, v_\alpha)$ (Figure 3.37) are in compliance with the preceding text. Expected negative value of mean velocity-density correlation scaled in the normalized time

was observed for $t_N$ between 0.2 and 0.6, i.e. in the joining the crowd phase. This negative correlation completely turns positive when the most paths is fully joined the crowd for $t_N$ between 0.5 and 0.7.

The positive value of mean correlation $R_t(v_\alpha, v_\beta)$ (Figure 3.38) in the first part of records agrees with the fact that every pedestrian and their leader come to the crowd from free flow where they are affected by the same conditions. The middle part, the phase of joining the crowd, is averaged to zero value which turns into strictly positive correlation in the crowd area.

Although there are many paths with the significant value of follower-leader velocity correlation in all phases, the mean value shows a trend just in the crowd area, i.e. in the phase where velocity-density relation fails. This fact indicates that the follower-leader relation is not stable in time, averaging brings the values close to zero.

Obviously neither follower-leader velocity nor velocity-density approach itself fully explains pedestrian behavior. However, together they cover all path in complement.

### 3.4.4 Flow Conservation Law

In previous sections, the velocity – density driving force was replaced by follower–leader concept corresponding better to the observations in the crowd area. However, it does not explain positive $R_t(\rho_{\omega_\alpha}, v_\alpha)$ observed due to the increasing velocity with decreasing distance to the exit. To solve this, we have to start with fundamentals.

The corollary of the flow conservation law can be derived directly from hydrodynamic approximation (3.4) assuming non-turbulent flow. If we consider semi-circular cross-sections (see Figure 3.39), every pedestrian crosses each separating curve just once.

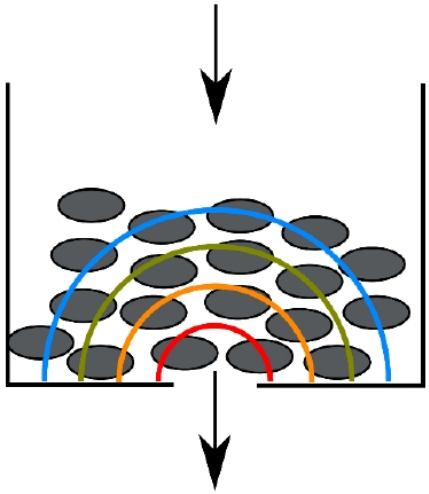

Figure 3.39: Illustration for the flow conservation law.

The absolute flow through all these cross-sections has to be the same. For any selected pair of them (denoted with indexes 1,2), following equality must be fulfilled

$$\rho_1 v_1 d_1 = \rho_2 v_2 d_2, \tag{3.10}$$

therefore

$$\frac{v_1}{v_2} = \frac{d_2}{d_1} \cdot \frac{\rho_1}{\rho_2}. \tag{3.11}$$

As we shown, the density in the crowd is almost constant (only slightly increasing towards the exit), thus $\rho_2/\rho_1 \approx 1$. Moreover, length of a semicircular cross-section $d = \pi r$. Applying these to (3.11), the relation between the velocity and the distance to the exit becomes evident:

$$\frac{v_1}{v_2} \approx \frac{r_2}{r_1}. \tag{3.12}$$

In other words, the mean velocity linearly decrease with increasing distance to the exit ans linearly grows the number of people sharing the flow, i.e. the capacity of the bottleneck.

To conclude this research we should not say that the velocity – density was replaced by the flow conservation law. We just showed that there are two independent factors limiting pedestrian flow and naturally more severe one is applied.

In the bottleneck crowd situation, the flow conservation law prevails. No matter the velocity-density relation further the exit may enable higher velocity, the value is overridden by this stricter limit as many pedestrians share the flow produced by on pedestrian just passing the exit.

## 3.5 Time Headway Analysis

As shown in previous sections, time headways play an important role to evaluate pedestrian flow and in general to understand crowd dynamics.

In this section, we will check the headway distribution measured during the E4 by different detectors [33], introduce advanced statistics characterizing crowd from physical perspective [18] and extend the data set to more complex geometries [17].

### 3.5.1 Detectors in front of the Exit

Recalling the detector placement in E4 (Figure 2.2), detectors D1 and D0 are large enough to enable passing of multiple participants. The input to the system was realized by three independent entrances simulating geometric distribution.

Such design brought conditions to observe headway values close to zero as well as large gaps exceeding five seconds, see histograms in Figure 3.40. Charts indicate exponential-like behavior, but statistical tests summarized in Table 3.7 rejects this hypothesis for half of performed runs.

In case of D0, we can't reject the exponential hypothesis for five rounds. Putting aside round eight with high number of out-layers, the high p-value of tests is related to high pedestrian inflow. This observation was replicated even for D1, where four rounds weren't rejected. Again, the rounds with rejected exponential hypothesis belong to the low inflow cases.

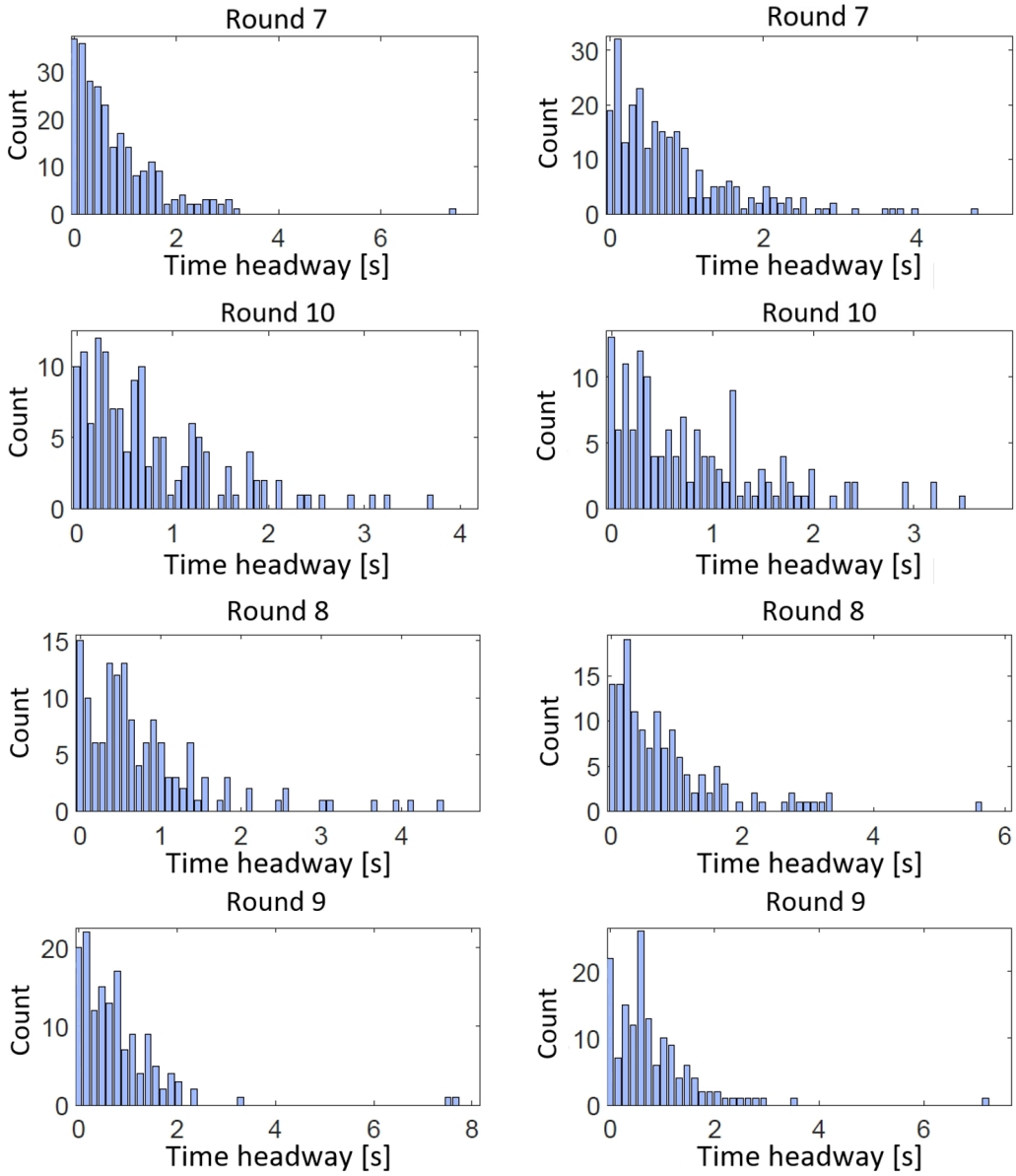


Figure 3.40: Comparison of time headways of selected rounds measured in detectors D0 (left) and D1 (right).

The crucial feature to reject this hypothesis is the proportion of super-low headways. In general, this proportion is lower in D0 case as this detector is closer to the exit and the crowd interaction effects occur. On the other hand we have observed even a switch in the different direction for round 8.

### 3.5.2 Detector at the Exit

Headways at the exit are frequently studied (e.g. [63, 94]) as they described the critical moment of egress process.

| Round | D0 | | | D1 | | |
|---|---|---|---|---|---|---|
| Test | Lillierfors | K–S | Chi2 | Lillierfors | K–S | Chi2 |
| 2 | $< 0.001$ | 0.002 | 0.011 | $< 0.001$ | $< 0.001$ | $< 0.001$ |
| 3 | 0.003 | 0.036 | 0.009 | 0.002 | 0.024 | 0.004 |
| 4 | $< 0.001$ | 0.004 | $< 0.001$ | 0.004 | 0.040 | **0.055** |
| 5 | $< 0.001$ | 0.004 | $< 0.001$ | $< 0.001$ | $< 0.001$ | $< 0.001$ |
| 6 | **0.111** | **0.293** | **0.080** | 0.041 | **0.164** | **0.504** |
| 7 | **0.226** | **0.443** | **0.232** | **0.419** | **0.647** | **0.341** |
| 8 | 0.009 | **0.069** | **0.333** | **0.500** | **0.716** | **0.501** |
| 9 | **0.262** | **0.484** | **0.071** | $< 0.001$ | 0.017 | **0.138** |
| 10 | **0.500** | **0.742** | **0.182** | **0.500** | **0.713** | **0.646** |
| 11 | **0.141** | **0.339** | **0.058** | **0.500** | **0.745** | **0.466** |

Table 3.7: p-values of evaluated tests verifying exponential hypothesis.

In the E4, the exit width was fixed to 0.6 m, thus only one pedestrian could pass in given moment. Extremely low probability of time headways below 0.3 s are therefore the no-go requirement for any considered distribution.

The importance of initial distribution decreases with increasing distance from entrances and with increasing density. In case crowd occurs in front of the exit, the system behaves as (chaotic) queue with multiple pedestrians eligible to exit.

Histograms from Figure 3.41 fulfills these theoretical expectations, accumulating the headways around the value 0.7 s. Even the round 5 characterized by low inflow follows this criteria, but the shape of the distribution differ as a kind of entry exponential distribution persisted. The differences between low and high inflow rounds make the selection of optimal distribution complicated.

In this section, we will evaluate the fit of 16 distribution to our data using the Bayes information criteria:

$$BIC = k\ln(n) - 2\ln(L), \tag{3.13}$$

where $L$ is the maximize likelihood function value of model $M$, i.e. $L = p(x|\theta, M)$, and $\theta$ are parameters eligible to optimizing process. Variable $x$ denotes the headway values, $n$ stands for the number of headways and $k$ refers to the number of parameters.

The results are summarized in Table 3.8. The difference in BIC grater than 6 points is considered as significant, greater by 10 points as noticeable [75]. From this perspective, log-logistic distribution defined as

$$f(x|\mu,\sigma) = \frac{1}{\sigma}\frac{1}{x}\frac{e^z}{(1+e^z)^2}; \quad x \geq 0, \tag{3.14}$$

where

$$z = \frac{\ln(x) - \mu}{\sigma} \tag{3.15}$$

is significantly better than other distributions for all rounds but rounds 2, 9 and 10 where GEV (generalized extreme value) distribution is slightly better.

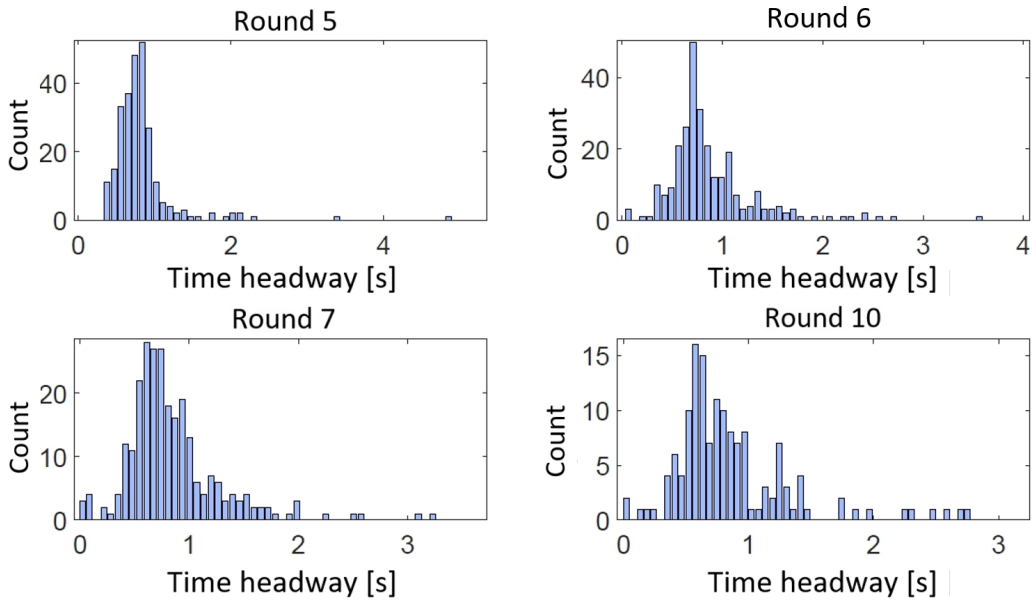


Figure 3.41: Time headway histograms of selected rounds measured in detector D2.

| Distribution | 2 | 3 | 4 | 5 | 6 | 7 | 8 | 9 | 10 | 11 |
|---|---|---|---|---|---|---|---|---|---|---|
| Loglogistic | 209 | 36 | 115 | 31 | 202 | 242 | 147 | 166 | 157 | 169 |
| GEV | 195 | 59 | 132 | 45 | 221 | 247 | 154 | 168 | 159 | 183 |
| Student | 248 | 57 | 115 | 42 | 222 | 246 | 172 | 179 | 167 | 191 |
| Lognormal | 217 | 60 | 216 | 70 | 246 | 310 | 163 | 202 | 198 | 188 |
| Inverse Gauss | 218 | 66 | 347 | 79 | 279 | 397 | 176 | 261 | 262 | 197 |
| Gamma | 252 | 71 | 164 | 121 | 238 | 267 | 157 | 179 | 171 | 195 |
| Logistic | 304 | 85 | 154 | 127 | 257 | 270 | 180 | 193 | 181 | 229 |
| Weibull | 288 | 135 | 202 | 237 | 281 | 285 | 171 | 190 | 180 | 228 |
| Normal | 364 | 142 | 211 | 294 | 321 | 324 | 196 | 223 | 209 | 10,3 |
| Exponential | 349 | 445 | 503 | 451 | 491 | 458 | 263 | 270 | 259 | 362 |
| Extreme value | 506 | 347 | 410 | 657 | 544 | 521 | 288 | 342 | 301 | 434 |

Table 3.8: Values of BIC for several distributions evaluated for time headways measured in detector D2.

Four distributions with the best fit are visualized in Figure 3.42. Student distribution does not fulfill the requirement of low probability near zero headway value, thus it can be eliminated. Other three candidates seems suitable for applications [76].

According to $\chi^2$ test results summarized in 3.9, we may reject the hypothesis that heayways correspond to log–logistic distribution for all low inflow rounds. On the other hand, rounds with dense crowd at the exit produced p-value far from rejecting threshold, thus this distribution seems to be strong candidate for high density situation.

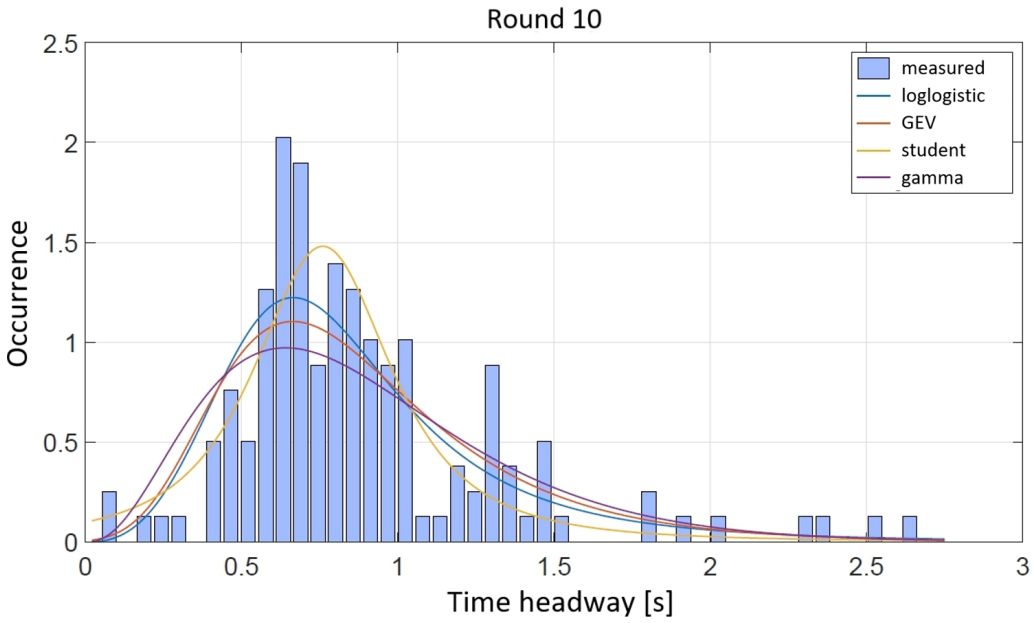


Figure 3.42: Time headway histogram measured in detector D2 for round 10 together with four best fitted distributions.

| Round | 2 | 3 | 4 | 5 | 6 | 7 | 8 | 9 | 10 | 11 |
|---|---|---|---|---|---|---|---|---|---|---|
| D2 | 0.006 | 0.001 | 0.002 | 0.863 | 0.460 | 0.206 | 0.022 | 0.853 | 0.237 | 0.001 |

Table 3.9: P–value of $\chi^2$ test evaluated for the log-logistic distribution fit on the D2 headway values.

### 3.5.3 Reflection of Territorial Social Forces

Generally, the main goal of this study fully published in [18] is to find a theoretical elucidation of time headway distribution. Quantities detected for various experimental/empirical systems may then lead (similar to [86, 87]) to a quantitative adjustment of interaction forces in the social force models. More specifically, the main objectives of this work can be established as follows.

- We aim to report on a series of original pedestrian experiments arranged for revealing quantitative properties of microstructure in one-dimensional pedestrians traffic. Besides headway distributions we will also analyze advanced statistical properties (e.g. statistical rigidity [89]).
- We aim to confirm/reject the hypothesis that statistical properties of pedestrian flows are similar to those detected in vehicular traffic (see [88, 92, 91, 120]). Furthermore, we aim to compare levels of synchronization in both systems.
- We intend to introduce relevant mathematical predictions for experimental/empirical headway distributions and the associated statistical rigidity (similar to [43]).

- Using mathematical estimations for headway distribution and analytically derived rigidity we intend to improve the existing knowledge of distance dependence of interaction forces acting between pedestrians (published in [73]).

### 3.5.4 Link between Headways and Force

In typical social force based models (like in [62, 61]) the acceleration equation includes four basic types of forces: 1) acceleration term describing tendency to reach the desired area as soon as possible (with a certain desired velocity); 2) interaction term describing the psychological tendency of two pedestrians keeping sufficient distance between one another; 3) repulsive term describing interaction with borders/walls/obstacles; 4) fluctuation term arising from accidental or deliberate deviations from the usual rules of motion.

As evident, global detection and validation of all acceleration/deceleration factors is not realistic because of the complexity of the system investigated. For this reason, it is necessary to restrict the issue of crowd dynamics to minor tasks only. One of the possibilities to do so is to formulate a simplified version of pedestrian flow where some of the above-mentioned effects are suppressed. Therefore, for the purpose of this work we take into consideration unidirectional one-lane flows of walkers whose movement can be classified as non-panic, i.e. comfortable and safe movement of people through a narrow corridor. Such restriction is convenient and, at the same time, essential for completion of the aforementioned tasks. Thus, proceeding in a similar way to [64, 73, 71, 132] we have performed several experiments (see section 3.5.6) suitable for revealing statistical distributions of time gaps between walkers.

Let us denote by $t_j$ the passage time of $j$th pedestrian, $j \in \{0, 1, \ldots, N\}$. Then we can define the re-scaled time headway as

$$\tau_j = \frac{N(t_j - t_{j-1})}{t_N - t_0}. \tag{3.16}$$

Thus we obtain a set $\{\tau_j : j = 1, 2, \ldots, N\}$ of all successive (re-scaled) headways with an average value equal to one. This set represents the fundamental subject of our investigations.

The scaling procedure is introduced for several obvious reasons. Firstly, the re-scaling to the unit mean headway allows to compare data from various sources/countries/situations without any substantial loss of generality. Secondly, such a procedure is well established in the physics of traffic (e.g. [89, 92]), where it is applied to analytic predictions of vehicular microstructure. Thirdly, it is well known from Random Matrix Theory [103] that the scaling procedure (as a significant part of the general procedure called *unfolding* – see [93]) reveals a universality in the spectra of random matrices. Besides others, such approach has been useful in finding a relation between vehicular samples (or public transport samples) and certain classes of random matrices (see [93, 84, 85, 38].

Choosing an appropriate division of a time axis $\Delta_\tau$, one can define the empirical/experimental histogram function

$$H(\tau|\Delta_\tau) := \frac{|\{j : \lfloor \tau/\Delta_\tau \rfloor \leqslant \tau_j/\Delta_\tau < \lceil \tau/\Delta_\tau \rceil\}|}{N}, \tag{3.17}$$

as an estimation of the probability density function of the time headway distribution. Here $\lfloor\ \rfloor$, $\lceil\ \rceil$ stand for the floor/ceiling functions respectively, and $|\ |$ stands for cardinality. For

greater clarity, if necessary, the graphical representation of the histogram function (step function) may be replaced by a scatter chart depicting point-set $\{(\Delta_\tau/2 + k\Delta_\tau; H(\Delta_\tau/2 + k\Delta_\tau|\Delta_\tau) \in \mathbf{R}^2 : k = 0, 1, \ldots\}$.

For unidirectional flows in a narrower corridor (where overtaking is improbable/prohibited) one can expect that the most decisive dynamic factor is the territorial social force reflecting a repulsive effect between *private spheres* of two persons. Such territorial effect (see [127]) can be expressed by a mathematical formula/graph (similar to [64, 73]), which is the desired output. Since these territorial forces influence decision-making of walkers, their action must be reflected in the headway distribution. Thus, there exists a direct link between the territorial forces and microstructure of pedestrian crowds. This link is definitely intricate, however, a simplified conception can be obtained (in analogy with [86, 87, 92]) by the following considerations.

In one-dimensional flows private spheres are reduced to *private intervals,* which allows to introduce repulsive forces in a simplified form $f_{j,k}(s_{j,k})$, where $s_{j,k}$ is the distance between walkers ($j$th and $k$th). Although this force (measuring how $j$th person is influenced by $k$th person) is not known, some of its properties are expectable:

1) $f(0_+) = +\infty$ due to impossibility of overtaking

2) there exists $s_0 > 0$ so that for all $s > s_0$ it holds that $f(s) = 0$

2b) $\lim_{s\to 0_+} f(s) = 0$

3) in all cases $f_{j,k}(s) = 0$ for all $s$ and all $k = j, j+1, j+2, \ldots$

4) in all cases $f_{j,j-1}(s) \gg f_{j,j-2}(s)$ for all $s$

Thus, such behavior can be classified as short-ranged because the dominant force is initiated by a predecessor.

For correctness, let us remark that all these considerations are valid for the afore-mentioned one-lane unidirectional scenarios only. Velocity differences are not considered. For purposes of analytic derivations (instead of individual formulas for every $f_{j,k}(s)$) we use the common force description: $f(s)$.

For taking into account accidental deviations we introduce a stochastic variant of the ensemble, where the level of stochasticity is regulated by the coefficient of resistivity $\beta \geq 0$. This parameter reflects the global state of the system determined by the density of walkers, corridor width, initial arrangement of walkers, and so on. Such a simplistic approach brings a significant profit: analytic derivation of associated headway distribution.

As proven in [86, 87] and generalized in [89, 90] the headway distribution (abbreviated by THD) of such an ensemble reads

$$\wp(\tau|\beta) = A\Theta(\tau)\mathsf{e}^{-\beta\phi(\tau)}\mathsf{e}^{-D\tau}, \tag{3.18}$$

where

$$\phi(\tau) = -\int_0^\tau f(s)\ \mathtt{d}s, \tag{3.19}$$

$\Theta(x)$ is Heaviside's unit-step function, and $A, D$ are constants for proper normalization and scaling. It is worth noting that although the one-parametric probability density (3.18) has

been derived for thermal equilibrium of particle gas with symmetrical interactions the papers [92, 91, 133] justified the possibility of approximating some driven many-particle systems by Hamiltonian systems. Indeed, the paper [133] proves that analytic gap distributions like (3.18) can be derived from a simple non-isotropic thermodynamic model of driven particles.

Thus, detection of empirical/experimental headways and relevant statistical estimations of associated THD may lead to calibration of the force model used. This will be the subject of the following sections. The importance of the knowledge of THD for the model calibration is summarized in article [98]. The time headway distribution in pedestrian bottleneck flow has been studied in [43] and [94]. However, the stress of these studies was given to the estimation of statistical model parameters.

### 3.5.5 Principal Attribute of Socio-physical Headway Distributions

Alternatively, one can view the detection of headway distributions from a more theoretical perspective. Omitting the detailed empirical background or theoretical models of pedestrian flows we now aim to reveal functional restrictions resulting from a purely mathematical point of view, i.e. the goal is to detect certain principal attributes of socio-physical headway distributions. From such a perspective we are dealing with an ensemble of particles whose mutual interactions are short/middle-ranged (for the correct explanation please see the note at page 2 in [92]), which means that distant particles are not interacting in any way. Mathematically, these systems may be identified as quasi-poissonian and it can then be proven rigorously (see the Appendix in the paper [18]) that associated headway distributions necessarily belong to class B of balanced distribution ([92, 93, 91]). Therefore any socio-physical headway distribution fulfills the criteria for balanced distribution. A probability density function $g(x)$ is called *balanced* if there exists $\omega > 0$ so that

$$\forall \varkappa \in (0, \omega): \quad \lim_{x \to +\infty} g(x) \mathsf{e}^{\varkappa x} = 0, \tag{3.20}$$

and

$$\forall \varkappa > \omega: \quad \lim_{x \to +\infty} g(x) \mathsf{e}^{\varkappa x} = +\infty. \tag{3.21}$$

The number $\omega$ is then called *the balancing index* and denoted by $\mathrm{inb}(g)$. Representatives of the set B are, for example, exponential distribution, Erlang distribution, Gamma distribution, and generalized inverse Gaussian distribution. Contrariwise, log-normal distribution or normal distribution does not belong to B.

To conclude, theoretically-based predictions for socio-physical headway distributions should show a balanced tail. This is, as justified above, a general property of all quasi-poissonian ensembles. Therefore, any proposal for functions estimating empirical headway distributions in traffic/pedestrian systems must comply with the above-mentioned criterion *(the balancing criterion)*.

### 3.5.6 Scenarios of Experiments and Description of Empirical Measurements

The presented study is based on four independent data collections: three experimental and one empirical. Although some measurements were not primarily designed for the time

headway studies, the layout of the monitored areas and recording methods allowed to collect the time headway data according to the above mentioned restrictions, i.e., unidirectional, one-lane flow without overtaking. It is worth noting that the one-lane non-overtaking flow was achieved by different means: It was not possible in the passing-through experiment and Kretz bottleneck experiment due to the narrow corridor. It was forbidden in the following-walkers experiment. It was extremely rare in the shopping center observation due to quite narrow corridor and social conventions. The detailed description of scenarios follows below.

### The Passing-through Experiment

Time headways measured during E4 at three spots of the outflow corridor were used as primary data source. Detectors were placed directly at the exit (Detector 1), 1 m downstream from the exit (Detector 2), and 2 m downstream from the exit (Detector 3). As mentioned in previous analysis and will be shown below, the bottleneck acts like a synchronization element because in the corridor (downstream from the exit) the territorial social force prevails against the acceleration force pushing pedestrian towards and through the exit in order that they may escape the uncomfortable zone.

This experiment is further referred to as First, Second, and Third Detector.

### The Following-walkers Experiment (Walkers on the Line)

The following-walkers experiment was performed in January 2015 at the Brno University of Technology (Faculty of Civil Engineering). Twenty two pedestrians were instructed to walk in a linear formation, each pedestrian following their predecessor. It means that pedestrians walked in a line, following the leader, who was choosing the path. Time headways have been extracted from the video records at a given cross-section. From the essence of the experiment it is obvious that motivation of pedestrians to move forward was lower than in the passing-through experiment. Therefore, the level of synchronization was higher because the territorial social force dominated over the acceleration term.

This experiment is further referred to as Walkers on the line.

### Shopping Center Observation

The data observed empirically have been provided by Pavel Křiváň, who recorded the flow in a shopping center in Pardubice. Operators of the center built corridors in the lobby due to reconstructions underway in the central part of the lobby. Furthermore, the visitors were instructed to choose the given corridor for the given direction of motion and follow the one-way signs. This situation was recorded for several days. Nevertheless, for the purpose of this article, only rush hours records have been used in order to assure constant flow of pedestrians, which motivated the visitors to keep the ordered walking direction. To eliminate the influence of pedestrians entering or leaving the pedestrian stream, a virtual detector for time headway measurements was placed at a significant distance from entrances to individual shops.

This observation is further referred to as Empirical Headways.

#### Pedestrian Flows through a Bottleneck

The fourth data sample was provided by Tobias Kretz. The flow through bottlenecks of various width has been studied in [94] in order to provide a dependence between the bottleneck width and pedestrian flow through it. This article makes use of data related only to flow through bottlenecks 40, 50, and 60 cm in width.

This experiment is further referred to as Kretz et al.

#### Data Processing

Previously mentioned experiments have been recorded on camera. The video footage has been processed autocratically using image recognition techniques (First – Third Detector) or manually (Walkers on the line, Empirical Headways, Kretz et al.). For further analysis, the time series $(t_j)_{j=0}^{N}$ of crossings of certain virtual detector have been used. For each run of the experiment, the crossing times have been transformed to sequences of scaled time headways $(\tau_j)_{j=0}^{N}$ (see Eq. (3.16) and discussion below). The scaling to mean value equal to one enables the comparison of the interaction essence in different data samples.

The scaled sequences (for given experiment) have been aggregated to one sequence, which was used for further statistical analysis (headway distribution, spectral rigidity). This procedure is justified by the assumption that the successive headways can be considered as independent. This is discussed in more detail in section 3.5.10. This procedure enabled to gain sufficient amount of information even from experiments with low number of pedestrians and low number of records in individual runs of the experiment.

A preliminary analysis of THD is visualized in figure 3.43. Besides headways gauged especially for this paper we also plot (for illustration) THD analyzed from previous researches published in [71, 132, 94]. It is of note to point to the incompatibility between the histogram (shown in figure 3.43) plotted for data obtained by Jezbera et.al. [71] and histograms plotted for other sources. According to the authors of the article [71], this conspicuous discrepancy can be attributed to an inaccurate measurement method.

### 3.5.7 Analytic Estimations of Territorial Social Forces

Following the general strategy presented in section 3.5.4, we intend to examine elementary estimations - if any - for territorial social forces $f(s)$ for which the analytically-determined headway distributions correspond to empirical/experimental histogram functions. Actually, attempts to estimate the force action are not entirely new. In the articles [94, 43, 64, 73] their authors investigate either headway distribution or suggest statistical distribution models or suggest distance dependence of the interaction forces. On the contrary, our paper presents a theoretically-substantiated link between territorial social forces and distribution of time gaps.

First, we suggest (with respect to the previous considerations) two natural choices for a force description: logarithmic and hyperbolic potential. The logarithmic potential $\phi(s) = -\log(s)$ corresponds to repulsion decreasing with the distance according to $f(s) = s^{-1}$. The corresponding quantities are further marked with subscript L. The hyperbolic potential $\phi(s) = s^{-1}$ results in a stronger repulsion force $f(s) = s^{-2}$. The corresponding quantities

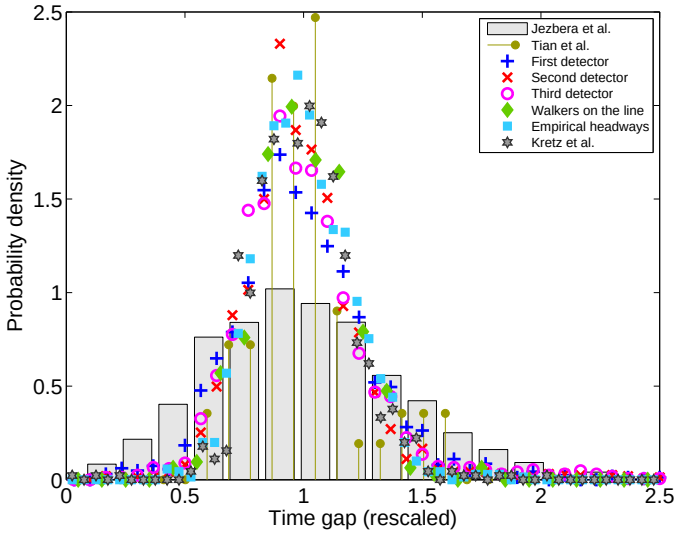


Figure 3.43: The experimental/empirical headway distributions. The signs represent the probability density of scaled time gaps among neighboring walkers passing a detector. As announced in the legend, the bars, stems, and hexagrams correspond to researches published in [71, 132, 94], respectively. The other signs display headway distributions analyzed from original experiments presented in this paper. Analogous trends in headway distribution has been also detected in [43].

are marked with subscript $\mathtt{H}$. The associated headway distributions read

$$\wp_{\mathtt{L}}(\tau|\beta) = \Theta(\tau)\frac{(\beta+1)^{\beta+1}}{\Gamma(\beta+1)}\tau^{\beta}\mathsf{e}^{-(\beta+1)\tau}; \tag{3.22}$$

$$\wp_{\mathtt{H}}(\tau|\beta) = A\Theta(\tau)\mathsf{e}^{-\frac{\beta}{\tau}-D\tau}; \tag{3.23}$$

where

$$D = \beta + \frac{3-\mathsf{e}^{-\sqrt{\beta}}}{2}; \quad A^{-1} = 2\sqrt{\frac{\beta}{D}}\mathcal{K}_1\big(2\sqrt{D\beta}\big).$$

Here $\mathcal{K}_1(x)$ stands for Macdonald's function of the first order. Note that both distributions belong to the family of balanced distributions discussed in section 3.5.5. We remark that distribution (3.22) has already been found in [43] being a suitable candidate for a time headway distribution of pedestrian groups.

Practically, in figure 3.44 the PDFs (3.22) and (3.23) are plotted against the empirically/experimentally obtained data of time headways. Parameter $\beta$ of the considered distribution families has been estimated by means of the minimum-distance estimation method i.e., $\hat{\beta} = \operatorname{argmin}_{\beta\in[0,\infty)}\tilde{\varrho}(\beta)$. In figure 3.44 it is evident that the empirical/experimental headways are very convincingly described by both approximations (see also table 3.10). In fact (as seen if comparing the last two columns in table 3.10 and if calculating distance $\varrho$ between both estimations), it is hard to distinguish between the approaches proposed because both curves (calibrated to data) are extremely close. A smaller amount of data precludes recognition of more detailed nuances in THD. Therefore, the THD analysis seems to be insufficient to make a decision between logarithmic and hyperbolic potentials.

| Detector | # | Mean Headway $[ms]$ | $\hat{\beta}_{\mathtt{L}}$ | $\hat{\beta}_{\mathtt{H}}$ | $\tilde{\varrho}(\hat{\beta}_{\mathtt{L}})$ | $\tilde{\varrho}(\hat{\beta}_{\mathtt{H}})$ |
|---|---|---|---|---|---|---|
| First detector | 2452 | 739 | 13.87 | 6.51 | 0.0628 | 0.0637 |
| Second detector | 2440 | 745 | 21.82 | 10.43 | 0.114 | 0.1004 |
| Third detector | 2531 | 761 | 17.01 | 8.02 | 0.1022 | 0.0829 |
| Walkers on the line | 316 | 708 | 23.65 | 11.46 | 0.0391 | 0.0553 |
| Empirical headways | 1406 | 858 | 23.56 | 11.37 | 0.0202 | 0.0379 |
| Kretz et al. | 901 | 1140/980/870 | 27.55 | 13.28 | 0.0374 | 0.033 |

Table 3.10: Quantitative summary of pedestrian experiments and minimum distance estimations.

### 3.5.8 Statistical Rigidity and Compressibility

Although analyzing and estimating headway distributions is a natural way to inspect the microstructure of pedestrian crowds, the formal background of such investigations is disputable. Measurements, data processing, and automatic evaluation techniques are burdened by systematic errors and extensive inaccuracies.

Therefore, we search for any logical alternative which should be a) directly measurable; b) less prone to inaccuracies; c) mathematically well-established. So a natural candidate then seems to be statistical rigidity defined/studied in [89, 88, 92, 71, 90, 103]. In pedestrian dynamics statistical rigidity represents (formally speaking) a variance of pedestrian flux (see also [71]). Obviously, pedestrian flow is understood to be the number of pedestrians passing any fixed point during a given time interval. Therefore, the fundamental quantity for flux enumeration is a random variable $N(T)$ representing number of pedestrians crossing a detector during a time interval $T$. Statistical nature of $N(T)$ generates fluctuations of individual realizations of $N(T)$. They are standardly described by a quantity called statistical rigidity defined by

$$\Delta(T) = \sum_{k=0}^{\infty} (k - T)^2 \, \mathbb{P}[N(T) = k], \tag{3.24}$$

where $\mathbb{P}[N(T) = k]$ stands for probability that number of pedestrians detected during $T$ is exactly equal to $k$. We also add that $\langle N(T) \rangle = T$, which is because the mean headway (as explained in the previous sections) is strictly set to one. Formula (3.24) represents a pseudo-variance of $N(T)$ around the average value $\langle N(T) \rangle$. Since in the particles/agents interaction systems condition $\langle N(T) \rangle = \mathbb{E}(N(T))$ is not usually met, the quantity (3.24) is not a standard variance. For systems with uncorrelated subsequent headways (see also section 3.5.10) there exists (see [92]) a direct link between headway distribution (or its Laplace image $G(s) = \mathfrak{L}[g]$) and rigidity. According to appendix 2 published in [18], it holds that

$$\mathfrak{L}[\Delta(T)] = \frac{2}{s^3} + \frac{(s-2)G(s) + 2sG'(s) + (s+2)G^2(s)}{s^2(G(s)-1)^2}. \tag{3.25}$$

According to [89, 90, 92], the rigidity satisfies a condition $\Delta(T) = \chi T + \mu + \mathcal{O}(T^{-1})$, and, therefore, it can be (extremely accurately) approximated by the linear function $\Delta(T) \approx \chi T + \mu$ for $T \gg 0$. For both above-mentioned headway distributions the relevant asymp-

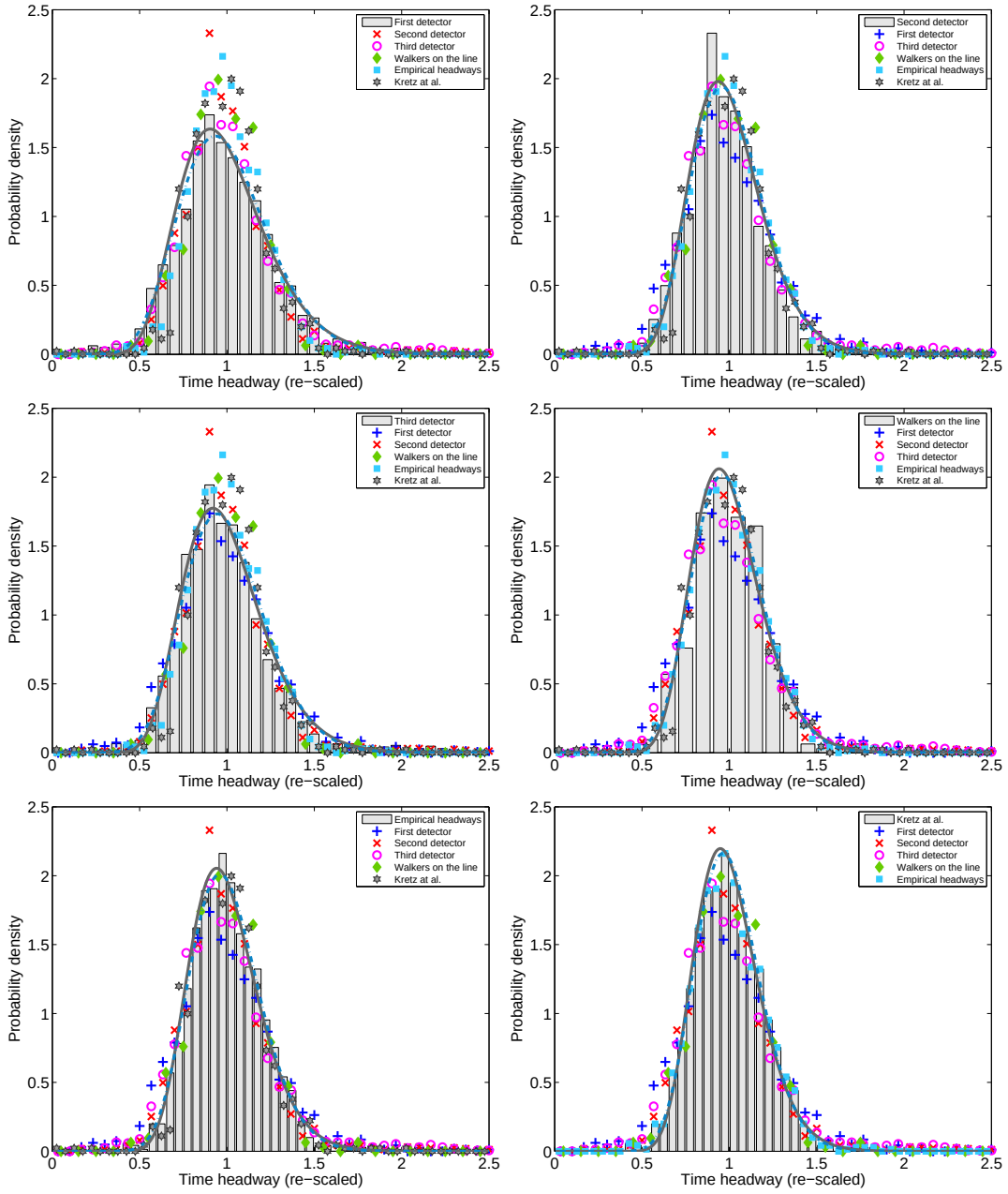


Figure 3.44: Analytical estimations of empirical/experimental headway distributions. Black curve visualizes a graph of the function (3.23) enumerated for the parameter $\hat{\beta}_{\mathrm{H}}$ estimated by MDE (see table 3.10). Blue (dash-dotted) curve displays a course of the theoretical prediction (3.22) with the estimated parameter $\hat{\beta}_{\mathrm{L}}$. Histograms represent distributions subjected to estimations (see legend). Signs (showing headway distributions measured for rest experiments – see figure 3.43) are drawn for clarity.

totical behavior has been derived in [92, 89]. It holds (after applying (3.25)) that

$$\Delta_{\mathrm{L}}(T) \approx \frac{T}{\beta+1} + \frac{\beta\,(\beta+2)}{6(\beta+1)^2}; \tag{3.26}$$

$$\Delta_{\mathtt{H}}(T) \approx \frac{2+\sqrt{D\beta}}{2D(1+\sqrt{D\beta})}T + \frac{6\sqrt{D\beta}+D\beta(21+4D\beta+16\sqrt{D\beta})}{24(1+\sqrt{D\beta})^4}. \tag{3.27}$$

Slope $\chi$ of this linear asymptote is usually referred to as compressibility, whose specific value (lying between 0 and 1) corresponds to the level of synchronization between mutual positions of elements (pedestrians, vehicles). For systems, where interactions between agents are weak, one can expect a low level of synchronization, i.e. $\chi \approx 1$. However, if the agent's interactions are more intensive, the level of synchronization increases and, therefore, compressibility decreases. The rigidity analysis applied to all data sources available is shown in figure 3.45. The graphical outputs show interesting distinctions between various pedestrian data as well as distinctions between vehicular and pedestrian traffic. In some of the investigated systems (shopping center data, Kretz data) compressibility is rapidly subdued, which corresponds to a stronger force action and/or lower level of randomness between walkers.

Moreover, figure 3.45 provides an interesting comparison between pedestrian and vehicular streams. Although the basic interaction principles are the same in both systems, different levels of fluctuations are responsible for significantly different values of compressibility. At first sight, this is a surprising finding because a wrong maneuver of a driver has much more serious consequences than of a walker. Therefore, one can expect increased vigilance of drivers, which intuitively should lead to a more systematic arrangement of vehicles. However, this study definitely refutes such behavior. Since, however, compressibility $\chi$ is strictly decreasing with resistivity $\beta$ the figure 3.45 demonstrates that pedestrian systems (contrary to vehicular systems) are much more resistant to statistical fluctuations, which means that ensembles of walkers are substantially closer to deterministic systems than vehicular systems. This observation can be explained by the fact that maneuvering of drivers is, as expected, much more variable than the maneuvering of walkers, which is due to a larger variance of speeds. Also, driving a vehicle is not so natural for humans as ordinary walking.

### 3.5.9 Compressibility-based Estimations

Owing to the fact that tests of statistical rigidity are, without any doubt, more compelling (not burdened by inaccuracies) than those using headways, we use statistical rigidity as the main instrument for making a decision which potentials (logarithmic/hyperbolic) or balanced distributions (3.22)/(3.23) are more suitable for statistical description of crowd microstructure. Thus, estimating the compressibility of pedestrian data (using simple linear regression applied to linear tails in graphs of statistical rigidity) we calculate values

$$\hat{\beta}_{\mathtt{L}} = \frac{1}{\chi} - 1, \tag{3.28}$$

$$\hat{\beta}_{\mathtt{H}} = \hat{\beta}_{\mathtt{H}}(\chi) \quad \& \quad 2+\sqrt{\hat{\beta}_{\mathtt{H}}\, D(\hat{\beta}_{\mathtt{H}})} = 2\chi D(\hat{\beta}_{\mathtt{H}}) \left(1+\sqrt{\hat{\beta}_{\mathtt{H}}\, D(\hat{\beta}_{\mathtt{H}})}\right) \tag{3.29}$$

of estimated values $\hat{\beta}_{\mathtt{L}}$ and $\hat{\beta}_{\mathtt{H}}$ for both potentials. Knowing $\hat{\beta}_{\mathtt{L}}$, $\hat{\beta}_{\mathtt{H}}$ we then calculate the statistical distance

$$\varrho_{\mathtt{L/H}} := \left(\int_0^{\infty}\left(\int_0^{x}(\wp(y|\hat{\beta}_{\mathtt{L/H}}) - H(y|\Delta_\tau))\,\mathtt{d}y\right)^2 \mathtt{d}x\right)^{1/2} \tag{3.30}$$

between the estimated theoretical distribution and empirical/experimental time headway distribution. Values $\varrho_{\mathrm{L}}$ and $\varrho_{\mathrm{H}}$ (expressed for six data sources) can then be used for final decision which of the two considered potentials (or distribution models) is more suitable for theoretical estimations of territorial social interactions acting inside a group of moving individuals.

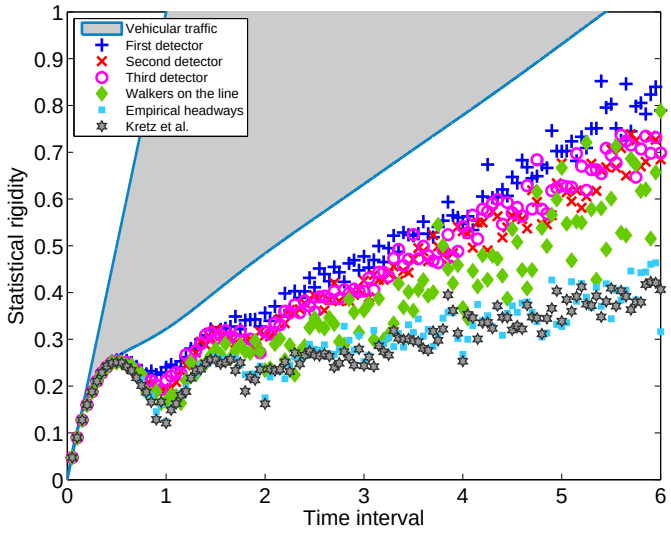


Figure 3.45: Statistical rigidity in empirical/experimental data. Graphs of the statistical rigidity analyzed for all available pedestrian data (see legend for details). The gray zone shows a region of vehicular rigidities, i.e. empirical statistical rigidity detected for vehicular traffic is usually (according to [89, 92, 88, 90]) a curve lying in this zone.

As quantified in table 3.11 in all cases (except for shopping center observations) the statistical distance $\varrho_{\mathrm{L}}$ (assuming gamma-distributed headways) is greater than $\varrho_{\mathrm{H}}$ (assuming GIG-distributed headways). It seems therefore that force description based on hyperbolical repulsion is closer to reality than the description using a logarithmical potential. The same conclusion has been drawn (in [86, 88, 92]) for vehicular streams as well. Relatively high values of these distances confirm the expected premise that statistical analysis of pedestrian headways is less informative, which is a logical consequence of the fact that digital processing (automatic detection) of gaps between walkers is quite inaccurate. On the other hand, calculations of statistical rigidity (based on counting walkers passing by a given point at a given time interval) are more accurate, by an order of magnitude.

### 3.5.10 Assumption of Statistical Independence for Headways

Note that all the previous considerations (i.e. predominantly analytical derivations for statistical rigidity) are valid only under the assumption that the neighboring spacings are independent. Therefore, it is essential (for practical applications) to test whether such a premise is reasonable or not. Thus, we test if statistical rigidity of the analyzed data sources is or is not influenced by random changes of the order of headways. Since randomly shuffled headways (analyzed for systems with short- or middle-ranged cooperation) are independent.

| Detector | $\chi$ | $\hat{\beta}_{\mathtt{L}}$ | $\hat{\beta}_{\mathtt{H}}$ | $\varrho_{\mathtt{L}}$ | $\varrho_{\mathtt{H}}$ | $\alpha$ |
|---|---|---|---|---|---|---|
| D1 | 0.118 | 7.475 | 3.547 | 0.2006 | 0.1869 | 0.01928 |
| D2 | 0.098 | 9.220 | 4.445 | 0.2647 | 0.2417 | 0.00572 |
| D3 | 0.103 | 8.756 | 4.205 | 0.2135 | 0.1886 | 0.01065 |
| Line | 0.097 | 9.265 | 4.467 | 0.2676 | 0.2600 | 0.05790 |
| SC | 0.044 | 21.861 | 10.851 | 0.0394 | 0.0450 | 0.00248 |
| Kretz | 0.044 | 21.678 | 10.747 | 0.0904 | 0.0799 | 0.01154 |

Table 3.11: Summary of compressibility-based estimations.

A slight deviation is detected for walkers on the line, which is caused by insufficient length of data sample (compare the numbers in the second column of table 3.10).

To be specific, let us consider vector $\vec{\tau} = (\tau_1, \tau_2, \ldots, \tau_N)$ of successive headways arranged in the original order (chronologically with respect to the time of measurement). Let $\pi$ be a randomly generated permutation of $\{1, 2, \ldots, N\}$. Then $\vec{\varkappa} = (\varkappa_1, \varkappa_2, \ldots, \varkappa_N) := (\tau_{\pi(1)}, \tau_{\pi(2)}, \ldots, \tau_{\pi(N)})$ is the vector of randomly shuffled headways, where all statistical links between successive headways $\varkappa_k$, $\varkappa_{k+1}$ have been broken by the afore-mentioned randomization. It is well known (from Random Matrix Theory) that vectors of dependent headways show a significant deviation from the formula derived for independent headways. Therefore, an angular deviation between linear asymptotes $\chi_{\vec{\tau}} T + \mu_{\vec{\tau}} \approx \Delta_{\vec{\tau}}$ and $\chi_{\vec{\varkappa}} T + \mu_{\vec{\varkappa}} \approx \Delta_{\vec{\varkappa}}$ reflects a certain measure of dependence in $\vec{\tau}$. Practically, such deviation can be quantified by

$$\alpha = |\chi_{\vec{\tau}} - \chi_{\vec{\varkappa}}|. \tag{3.31}$$

If $\alpha > \alpha_0$, where $\alpha_0$ is a normal deviation (here we consider $\alpha_0 \approx 0.02$); then the detected deviation is statistically significant and the analyzed headways can be classified as dependent. The last column of table 3.11 summarizes numerical outputs of the method proposed.

### 3.5.11 Conclusions

At first, we have shown that statistical distribution of time gaps between neighboring pedestrians can be convincingly described by some probability density belonging to a family of balanced distributions (e.g. gamma distribution or GIG distribution). This knowledge generalizes the recent results published in [43], and, in practice, it can be used for quantitative assessments of pedestrian models or for predictions of corridor capacities.

By introducing a stochastic force-based scheme (controlled by coefficient of statistical resistivity $\beta$) we relate the detected headway distribution with the associated force description. In other words, we estimate the territorial social forces (and their dependence on distances between walkers) by making the use of knowledge of spatio-temporal arrangement of individuals in pedestrian groups.

Useful information about the statistical nature of systems investigated is obtained by calculation of coefficient $\beta$ quantifying measure of statistical resistivity, i.e. measuring the nearness to deterministic arrangement of pedestrian locations.

A deeper insight into the pedestrian flow microstructure is made possible by a thorough analysis of statistical rigidity. The efficiency of an instrument of statistical rigidity is apparent when comparing the compressibility among all systems observed. Indeed, although the time headway distributions in all systems are relatively close, a course of the rigidity reveals mutual nuances. They are caused by different levels of compressibility. As far as the passing-through experiment is concerned, figure 3.45 shows that compressibility $\chi$ depends on the location of the detector, which indicates changes in pedestrian synchronization in the course of time. This supports the idea that with time pedestrian headways evolve so that compressibility decreases. The level of synchronization for walkers in a line in a free area is visibly larger than in corridors with a boundary. Stronger synchronization is detected for empirical flows measured in a narrow corridor and for passage through a door.

Both methods, however, suffer from relatively inaccurate detection of time gaps between individuals, which is a well-known problem of crowd modeling.

Moreover, new interesting knowledge has been obtained by comparing of compressibility between vehicular and pedestrian streams. It follows from figure 3.45 that synchronization of walkers is much more intensive than that of cars. The effect is the same for statistical resistivity. Such difference is given by the fact that vehicular flows allow (due to larger variances of speed) a greater fluctuation level than pedestrian flows. Thus, the suggested approach allows to differentiate between various agent's systems using a set of headways only, which is a great benefit.

From the practical point of view, the suggested methodology based on tests of statistical rigidity seems to be a suitable instrument for theoretical validations of various pedestrian models. The low values of compressibility reveals that the repulsion force between pedestrians has hard-core-like nature. This should be taken into account in model formulation, which means that the potential generated by the model agent should be very high in the close neighborhood of the agents and should vanish very fast with distance to the agent. The compressibility value could be then used for proper parameters calibration.

### 3.5.12 Synchronization Effects

In the E4 experiment, we have analyzed the flow at different spots in the room (in the free flow area, in the crowd, at the exit, in the corridor behind the exit) and even the total flow was the same (law of conservation the flow), we have observed significant differences in micro-structure analyzed from time headways perspective (2.35).

This section extends previous microscopic studies to more complex scenarios of multiple consecutive bottlenecks with merging of pedestrian streams. The analyzed data were acquired in two types of experiments conducted at CTU: double-deck rail car egress experiments and laboratory egress experiments where four groups merged at two levels of bottlenecks to egress at one general exit.

To describe the phenomena of synchronization and the structure of crowd, the time-headway distribution is examined at each bottleneck. The gradual synchronization of time-headways is shown to appear in the network of rooms connected by doors. On the contrary, the train egress shows rather spontaneous lane formation in the corridor-like structure leading to a synchronized two-lane flow.

Provided results can be used in the field of hand-calculations as presented in our study [24]

or in building evacuation time study [118]. The arrival and service times defining behavior of such model are usually random variables with some "handy" distribution which meets the criteria that the mean value is equal to inverse maximal flow of the bottleneck according to equation (2.35). The definition of such distribution of the arrivals and service times is the subject of the following part of this section.

### Observations

As proposed by [51], pedestrians in the E2-4 experiments [8] were entering the system according to the exponential distribution with the mean value corresponding to the desired inflow. From the queuing principle we assumed the time-headways to be distributed according to the exponential-like distribution with the mean value corresponding to the bottleneck outflow capacity.

Unexpectedly, we have observed [9] that the exponential-like distribution changes significantly as described in Figure 3.46. The low values of the time-headways have low probability, the main part of the probability density function is narrowly placed around the mean value. Most of the pedestrians kept the same specific distance to the predecessors.

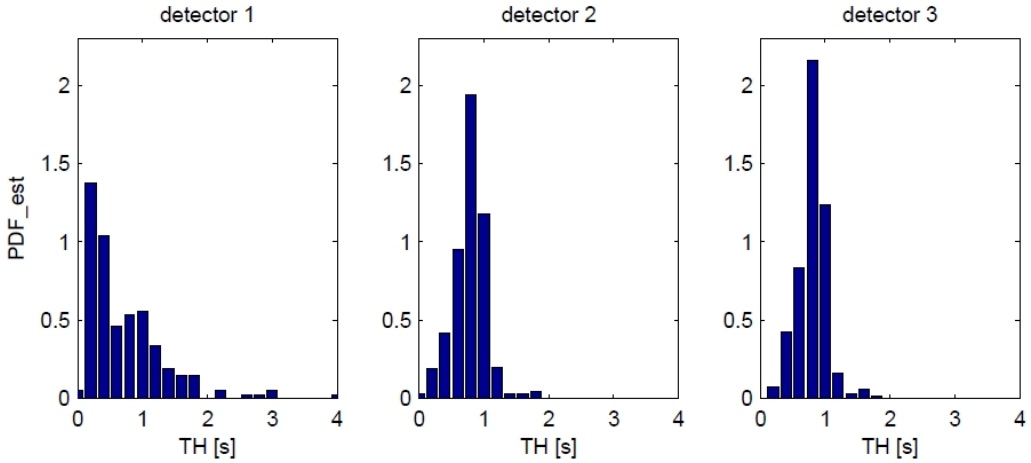


Figure 3.46: Synchronization of the headways within one bottleneck (left part of Figure 3.47). Histogram estimations of the probability density function of time-headways measured at three detectors: 1 – pedestrians joining the crowed, 2 – exit door, 3 – corridor behind the exit.

This observation motivated us to revise the concept of random arrivals. An additional experiments involving flow through multiple consecutive bottlenecks during the egress of a lecture hall were organized (denoted as E56). The experimental set-up consisted of 7 rooms connected in a way to create a binary-tree-like structure: four bottlenecks lead to two rooms which lead to one common room in front of the main exit as depicted in Figure 3.47. The time-headways have been aggregated for each level of the tree.

Corresponding histograms are visualized in Figure 3.48. Exponential distribution is not detected in any level. Moreover, the results of the analysis show that the variance of the time-headway distribution decreases as the level of the tree decreases (we consider the level

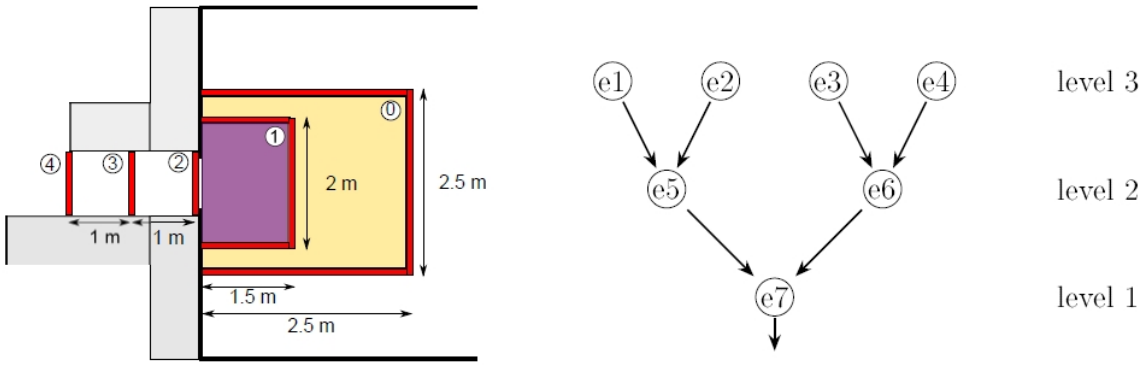


Figure 3.47: Schematic description of laboratory experiments. Left: positions of detectors illustrating the synchronization effect of a particular bottleneck. Right: schema of the experimental setup used in the study hall egress through tree-shape structure of bottlenecks experiment.

decreasing in the direction of the pedestrian flow). Hence, we conclude that the bottlenecks act as a synchronization element in the pedestrian flow.

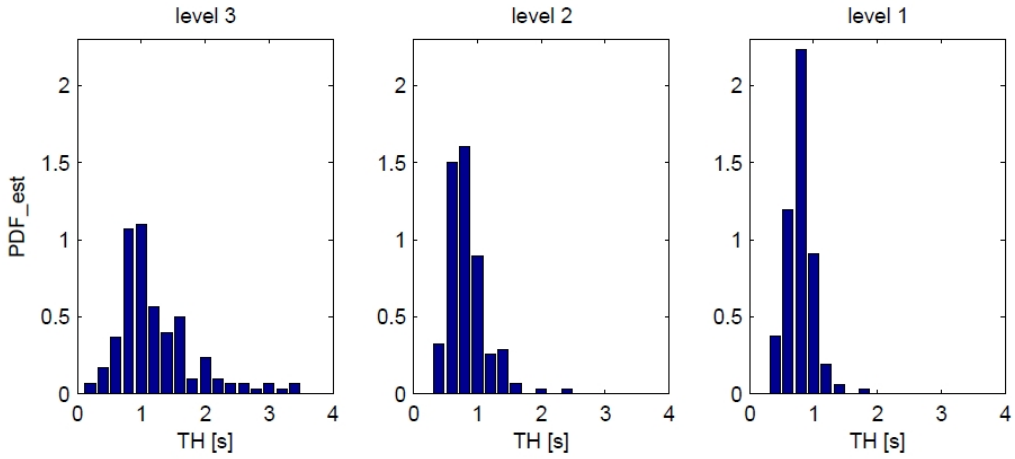


Figure 3.48: Synchronization of headways in consecutive bottlenecks. The histogram estimations of the probability density function for time-headways are plotted for three levels of the experiment. The door widths were 750 mm in level 1 and 700 mm in levels 2 and 3

For the train egress experiment, the time-headway histograms for bottlenecks No. 1, 3, and 4 (see Figure 3.26) are plotted in Figure 3.49. Since the distribution of time-headways related to exit No. 4 seems to be significantly wider than the one corresponding to bottlenecks No. 1 and 3, we can first wrongly interpret an opposite trend. The right interpretation lies in the width of the bottleneck. The width of No. 4 (1300 mm) is approximately twice width comparing to the previous bottlenecks No. 1 (650 mm) and No. 3 (840 mm).

Obviously the time headway distribution is much more similar to exponential than in case of E56 (possibly due to the lower density in front). Moreover, the wider the exit is the more

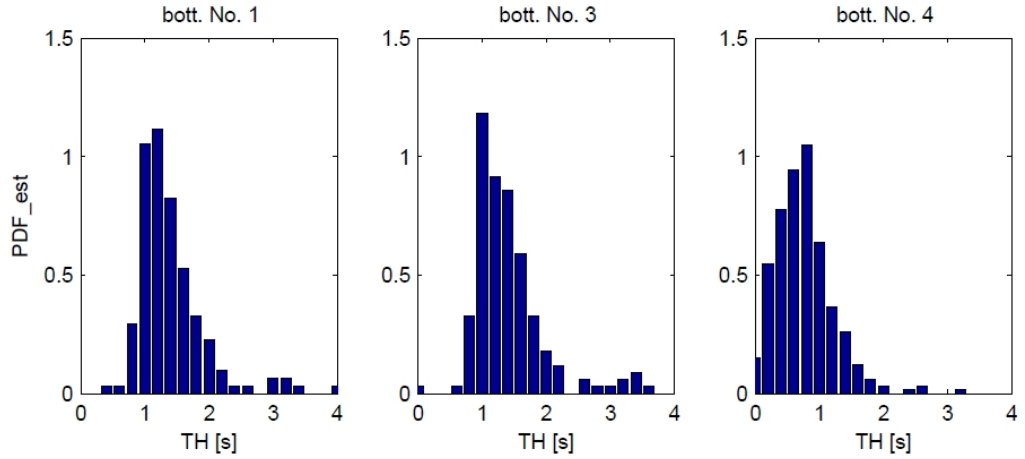


Figure 3.49: Time-headway distribution in the train experiment. The histogram estimations of probability density functions are plotted for bottlenecks No. 1, 3, and 4. The wider distribution at No. 4 can be clearly seen.

exponential (less normal) the distribution is.

The exit No. 4 is sufficiently wide to enable the egress of two passengers almost simultaneously. The time-headway distribution corresponding to the exit No. 4 can be therefore considered as a mixture of two distributions, first related to the headways between pairs and second related to the headways between pedestrians in a pair.

To summarize, in the case of narrow bottlenecks where more than one pedestrian can pass at the same time only rarely, the synchronization of pedestrians is reflected in the decrease of the time-headway variance, i.e., pedestrians are consecutively adopting the motion of their predecessor. In the case of wide bottleneck as in the train study, the synchronization of the motion is reflected in the pair-like movement (i.e., alternation of extremely short and relatively high time-headways) and the spontaneous formation of two lanes.

# Chapter 4

# Review of Present Models and Theory

Modeling of crowd motion or, more general, any kind of traffic is an important part of urbanity planning process. From the engineering perspective, there are just few features that must a model fulfill: reliability, simple calibration, reasonable calculation demands and ability to return desired quantities. Different model types are more appropriate for different requested outputs [122], but usually there are multiple ways how to achieve them.

The spectrum of desired model outputs may be quite wide. On the macroscopic level, we are mostly interested in flow. Such variable is affected by the pedestrian density (number of people in given area), geometry and pedestrian mindset (motivation, knowledge of given facility and cultural aspects). The total evacuation time is another crucial quantity from engineering perspective, it may be replaced by the evacuation time of desired sub-population (all clients, 98% of all people, ...).

In more detail, we may focus on trajectory level producing individual evacuation time, local densities, velocity distribution in space and many more fancy features. From scientific perspective such microscopic research brings additional information and more precise derivation of macroscopic quantities. Moreover, microscopic observation may explain why the system generates given pattern.

On the other hand, microscopic models always require more computational power, their validation is more demanding and they are difficult to calibrate or to correctly set up initial and boundary conditions. That's why engineers prefer to use simple, well known models, even they might be outdated. The transition to modern approach requires special motivation, thus the scientific state of the art is quite ahead on engineering .. as always.

## 4.1 Related Models

Historically there are multiple research streams, each of them dominated some period in past, based on fashion and available computational capacity:

- **Hand calculations**. Applying queuing theory or "physical" mechanics, we can answer many elemental questions. E.g. from given inflow and bottleneck capacity (max-

imal flow), one can predict whether the evacuation will be smooth or whether a congestion would appear.

- **Grid models**. These models discrete in space and time are using simple movements rules. Reasonable discretization allows even microscopic approach, as will be shown later on implemented cellular automata model.

- **Force based models**. The interaction agents $\alpha$ and infrastructure $\beta$ may be defined as the set of social forces, e.g.

$$m\ddot{x} = m(\dot{x} - v_{\alpha}^{opt}) + \sum_{\beta} f_{\alpha\beta} + \sum_{b} F_{\alpha b}, \tag{4.1}$$

  where $v^{opt}$ is the preferred velocity, $f_{\alpha\beta}$ refers to agent interaction and $F_{\alpha b}$ to interaction with infrastructure. Similarly to classic mechanics, the resolution of this large set of equations provides detail movement description. This approach successful in simple geometries, but too demanding for large scale simulations.

- **Thermodynamic models**. Similarly to their physical precursors, placed agents into thermal pool (with given temperature) to simulate movement in stochastic environment. The interaction of agents is defined by reaction potential that impacts total energy $H$. The probability density of states of the system is then evaluated as

$$P(\vec{x}, \dot{\vec{x}}) \propto e^{-\frac{1}{k\mathrm{T}} \cdot H(\vec{x}, \dot{\vec{x}})}, \tag{4.2}$$

  where $k$ stands for Boltzmann constant. Such model is used to predict the behavior of steady state, e.g. space or time headways may be analytically derived.

- **Agent based models**. The most modern approach is based on intelligent agent moving in continuous space and time according predefined rules. This approach combines advantages of all above mentioned approaches yet it may be difficult to calibrate.

- **Data driven models**. Another quite new approach based on machine learning technology. With sufficiently large database, model could predict the next movements based on some smart mix of historical trajectories. Unfortunately the ability to process situation that is not in database is questionable.

This work is focused on a cellular automata model, partially in comparison with agent based model. Both were implemented on microscopical level but they have quite different rules as they are facing different challenges given by different spatial limits.

## 4.2 Principles of Cellular Automata

Crowd dynamics models based on cellular automata have some significant advantages over the other kinds of pedestrian movement models – their simplicity. Movement of occupants is modeled by set of fairly simple rules[109]. Moreover, one can easily establish sufficient balance between efficiency and accuracy, that makes CA-based models suitable e.g to large scale data–driven simulation e.g. [135]. However, the usage of CA based models is connected with a number of issues, related mostly with coarse discretization of space and time [10].

### 4.2.1 Original CA concept

The base element of a cellular automata model is a cell (i.e. cellular automaton), which is described by his state and actualization rules respecting the state of his surrounding. These rules are constant in whole area and do not depend on time. To be more precise, CA model is defined by the set (State, Neighborhood, Rulebook).

The surrounding of a cell $x$ might be quite general, but usually consist of nearest cells $y$:

$$d(x, y) < \mathrm{C}, \tag{4.3}$$

where $d(x, y)$ is distance from $x$ to $y$ (the distance should incorporate bypassing the obstacles). Constant C is the range of a surrounding, usually it is a small natural number. Here we note that the cell itself is usually considered as a part of its surroundings.

The most commons are Von Neumann's surrounding using only orthogonal directions and Moore's surroundings adding diagonal directions, see Figure 4.1 for illustration.

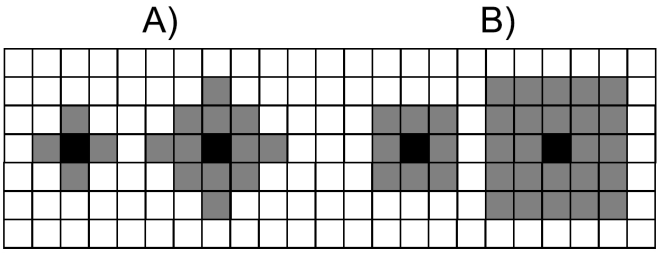


Figure 4.1: The illustrations of surroundings used for pedestrians movement modeling: A) Von Neumann's surrounding with the distance one and two, B) Moore's surrounding with the distance one and two.

As there are usually two states of a cell, the rule book uses binary coding to define the state of neighborhood and the definition of the next state. See Figure 4.2 for illustration of one rule in 1D system, for more details see e.g. [143].

### 4.2.2 CA Models of Pedestrian Motion

Applying CA to modeling of pedestrian motion, several things should be specified the state of a cell is vacant or occupied (by one agent, lets avoid obstacles for simplicity ). As the pedestrian can't freely appear or disappear, the number of occupied cells is constant (putting aside the entry and exit cell with special rules for now).

This restriction limits the rule system – it has to fulfill the condition that update of one cell (A) from occupied to vacant must be followed by update of some vacant cell (B) to the state occupied. Such situation is interpreted as the motion of an agent from cell A to cell B.

That cased the modification of general CA concept to state where agents move in the lattice. The actualization rules of agents may be much more complicated than deterministic pattern matching on nearest neighborhood. Moreover, different types of agents and cells can occur

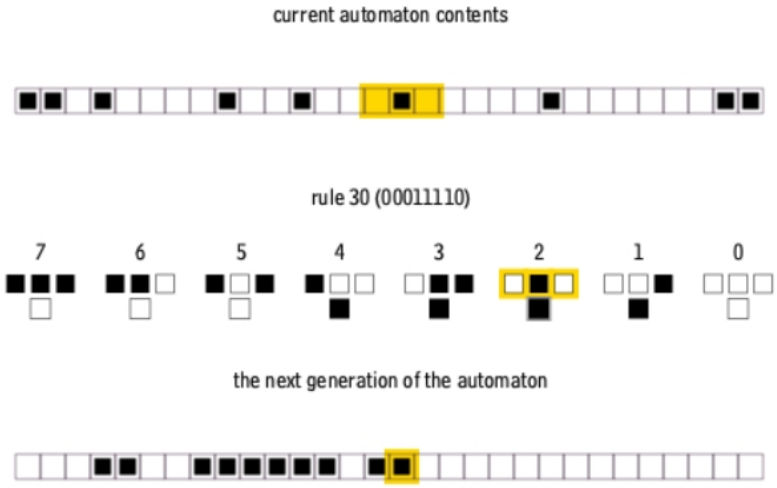


Figure 4.2: The illustrations of rule 30. In 1D system with nearest neighbor surroundings, there is only 8 configuration. For each of them, we have to define whether given cell would be occupied or empty. With fixed orientation, it is simple to interpret this 8 bits as a binary code representing number. I.e. the 8 digit binary code of the number 30 is 00011110, indicating that configuration 0, 5, 6 and 7 would generate empty cell while configuration 1, 2, 3 and 4 stands for occupied cell.

in the system, each type may have special actualization rules. Due to these facts, the term "agent system" is often used in literature instead.

Generally, we can distinguish two kinds of surroundings – target surrounding and reaction surrounding. The target surrounding is a set of cells, which an agent can reach in one step. It is connected to the length of the step. The reaction surrounding consists of cells, which affect the decision of given agent.

It is beneficial to define both surroundings small to keep decision rules simple and computational demands low. Usually agent can reach only nearest cell an even the reaction surrounding used to consist of several cells. Therefore the information about the distant object (as exits) must be coded in all cells to incorporate it to the decision process.

The cellular automata are categorized by the process of actualization to parallel and sequential. In case of parallel update, the actualization of all cells runs simultaneously, this can cause conflicts. This phenomenon is wanted, it is an instrument how a model produces collisions. The sequential update means, that the cells are updated sequentially, in strictly given order or randomly.

## 4.3 Review of Floor Field Models

Modeling of pedestrian movement using cellular automata is a young branch of study. One of the first articles [49] published in 2000 presents elemental decision making process. The track of each agent is determined by checkpoints, which an agent follows. During his journey, he reacts to his surrounding – he selects empty cells and adapts his velocity with respect to

local density.

Two years later, the group from the University of Köln presented an article [77], introducing the concept of Floor field model. This model was modified [109], [53], today, the F.A.S.T. model (Floor field and Agent-based Simulation Tool model [95], [96]) represents the top simulation tool.

This model was used to simulate some specific phenomena, e.g. [97] deals with the pedestrian behavior in counterflow, [51] studies the motion through multiple bottleneck, [54] deals with the influence of the inflow to the system or [79] investigates the impact of the bottleneck width to the outflow.

Some other works were presented together with Floor field model to supplement it. We talk about the influence of physical forces [65] and the prediction to avoid conflict in the counterflow [131] or [59]. These principles will be described further.

Many other models simulate pedestrian movement and uncover untouched phenomena, e.g. article [57] deals with the modeling of obstacles, articles [145], [146] and [147] propose alternative methods for discretization and article [121] talks about the symmetry. Similarly to the traffic models, the follow-the-leader approach can be used, see [58]. Agent's behavior may be differentiate according to specific role, group affiliation [40] or cognitive abilities [42].

To model the pedestrian movement, the proxemics theory and social distance approach can be also used, see [136] or [138]. [83] and [82] model the evacuation with respect to the local Guidelines, this work includes complex geometry with stairways.

The work [149] concerns with the evacuation of a complex building. It describes the different ways how to manage the numeric simulations for individuals parts (floors, buildings) effectively.

## 4.4 Floor Field Model

Floor field model [45] is a cellular automaton inspired by the chemotaxis of ants. The ants mark their trace by the pheromones to guide others to the food. The model codes analogically the paths of each pedestrian, this phenomenon provides the long–range interaction.

The whole family of models utilizes different floor fields(FF) to store any information needed for the decision process. Vast majority of them uses *static FF* - i.e. gradient potential field that lead occupants to points of attraction. Other types of fields models different aspects of pedestrians behavior: *dynamic FF* - is responsible for mimicking the following others behavior, *wall FF and proxemics FF* describes repulsive forces from obstacles and other pedestrians respectively, *anticipation FF* introduces in advance collision avoidance, while *force FF* introduce pushing behavior for CA based models. Superposition of chosen set of mentioned fields is used as main factor that drive pedestrian movement. For details see [119] and references therein.

In this work, we have analyzed the model as defined in the dissertation of Tobias Kretz [96].

### 4.4.1 Definition

The space is divided by rectangular lattice into square cells with dimensions $0.4\,\mathrm{m} \times 0.4\,\mathrm{m}$. The time is also discrete, the actualization runs parallel for all pedestrians.

The actualization progress in three substeps:

1. the selection of an exit
2. the selection of target cell
3. the movement towards the chosen cell

#### Selection of an Exit

Each step begins with the choice of the exit, which become a target during subsequent decision. The probability, that agent $\alpha$ chooses the exit $E$ is given by equation:

$$p_E^\alpha = N \frac{1 + \delta_{\alpha,E} k_E(\alpha)}{d(\alpha, E)^2}\,, \tag{4.4}$$

where $\delta_{\alpha,E}$ is the indicator that agent $\alpha$ has chosen the exit $E$ last time (it is equal to 1 in case he did and it is equal to 0 if he did not). The coefficient $k_E(\alpha)$ is persistence of agent $\alpha$ to exit $E$, $d(\alpha, E)$ is the distance and $N$ the normalization constant.

The distance $d(x, E)$ of cell $x$ towards the exit $E$ is given by Dijskra's algorithm on discrete lattice. This algorithm enumerates the minimal number of steps to reach the exit $E$ from every cells in a lattice, with respect to the geometry of building and obstacles.

#### Selection of Target Cell

During the decision process, the profitability of each cell in a surroundings of given agent is evaluated.

The "complete" surroundings (see Figure 4.3), which is used in this model, is determined by maximal velocity ($v_{max}$) of an agent. It is defined as a set of cells, which can an agent reach using maximally ($v_{max}$) steps in von Neuman's or Moore's surrounding (see Figure 4.1). The way of alternation of von Neuman's or Moore's surrounding is elected so that the motion keep spherical symmetry.

The probability that an agent chooses the cell $i$ is given by equation:

$$p_i = N \cdot (1 - n_i) \cdot e^{k_s \cdot S_i} e^{k_d \cdot D_i} e^{-k_I \cdot F_i} e^{-k_w \cdot W_i} e^{k_p \cdot N_i}\,, \tag{4.5}$$

where $N$ is the normalization constant and $n_i$ is the occupation number ($n_i = 1 \ldots$ occupied cell, $n_i = 0 \ldots$ empty cell), which express the fact that agent is allowed to select only empty cell.

In the latest articles, the expression $(1 - n_i)$ is substituted by $(1 - \Phi \cdot n_i)$, where $\Phi \in \langle 0, 1 \rangle$ is the weight of occupation. With this modification, an agent can select even an occupied cell, this concept is used in this project.

Each exponent describes the influence of one field:

| | | | | | |
|---|---|---|---|---|---|
| 5 | 5 | | | | |
| 4 | 4 | 5 | 5 | | |
| 3 | 3 | 4 | 4 | 5 | |
| 2 | 2 | 3 | 4 | 5 | |
| 1 | 1 | 2 | 3 | 4 | 5 |
| 0 | 1 | 2 | 3 | 4 | 5 |

Figure 4.3: One quarter of complete surroundings with respect to maximal velocity (up to 5 cell/step). An agent can reach the cell with number equal or less than its maximal velocity.

- the static floor field $S$ ensures the motivation of an agent to move towards the exit. The value $S_i$ is determined by the distance to the exit. To support the randomness in decision process, the values in static field are rounded to integer values
- the dynamic floor field $D$ contains the vector information about the motion of others, it enables modeling of herding behavior
- the inertia effects $I$ reflects the physical possibilities of pedestrians. E.g. pedestrians change the velocity rather than turn
- the repulsive effects of walls $W$, which is given by the distance of nearest wall
- the influence of nearby agents $N$ – agent prefers a places with lower local density

The coefficients $k_X$ describes the sensitivity of an agent to field $X$. These "weights" express the relative importance of given fields and their value presents the individual parameters of each agent.

#### Movement towards Chosen Cell

When all agents have chosen the target cells, the phase of movement begins. Two different approaches are presented:

- jumping to the target cell is a simple, but not realistic method. An agent is putted into the target cell even if there is not a free path. When two or more agents try to move to the same cell, conflict happens. In this case, one pedestrian is chosen randomly to move and others stay. But with probability $\mu$ (friction coefficient), conflict remains unsolved and no one moves.
- motion cell by cell better corresponds to the real behavior. Sequentially (in given order or random), each agent tries to reach his chosen cell in $v_{max}$ steps. This journey runs deterministically – in each substep, an agent chooses from his nearest neighborhood the unoccupied cell closest to the target cell. It is suggested to keep trajectories of agents to uncover the conflicts from crossing paths. The cell, which was once occupied, remains blocked until the end of actualization.

### 4.4.2 Discussion

The essential impact to the behavior of this model has the maximal velocity. As seen in Figure 4.3, the neighborhood keeps the spherical symmetry up from the $v_{max} = 5$. It confirms the simulations presented in Figure 4.4.

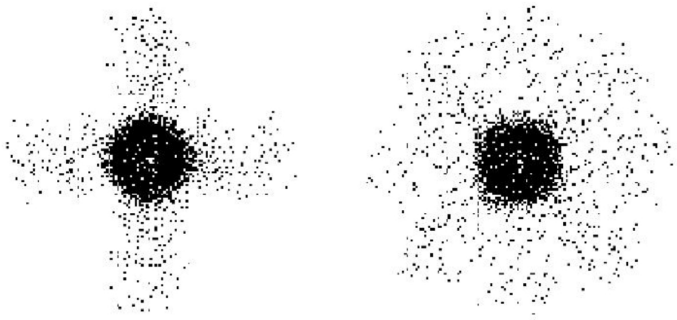

Figure 4.4: The comparison of simulation with different maximal velocities to test the symmetry. Left: $v_{max} = 1$, right: $v_{max} = 5$. (taken from [96])

The maximal velocity also influences the value of the time span. One step contains $v_{max}$ substeps, thus when one substep consumes 0.2 s, the time span is equal $v_{max} \cdot 0.2\,\mathrm{s}$. Therefore higher maximal velocity implies lower frequency of decision.

The influence of dynamical field is well observed during the simulation of guided evacuation. It is a situation of two groups with different level of knowledge of the environment. First group (guides) is characterized by large $k_S$, low $k_D$ and high influence on dynamic field. On the other hand, the followers has low $k_S$, large $k_D$ and low influence on dynamic field. The evacuation of 1000 person from labyrinth runs faster by 35% in case there are 100 leaders (the comparison of average 95 quantile).

The effects of wall repulsion and inertial forces are illustrated in Figure 4.5. As seen, the snaphshot with both effects looks high realistic.

The usage of this model illustrates Figure 4.6, where a simulation of an infrastructure is presented. The significant congestion was uncovered even in unexpected places.

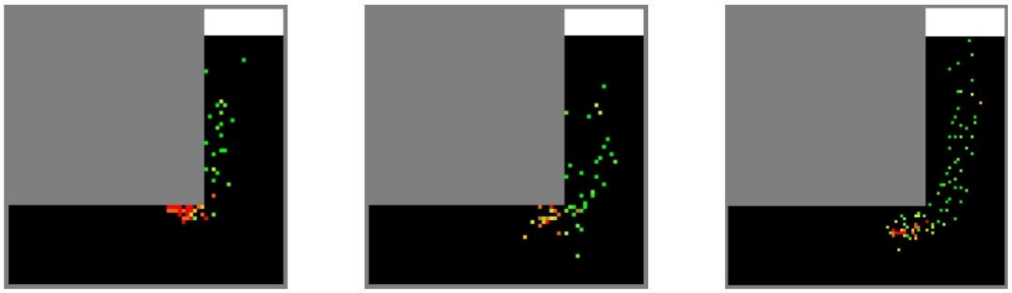

Figure 4.5: The influence of wall repulsion and inertia forces repulsions. First slide: without these effects, second slide: effect of inertia, third slide: effect of wall repulsion. (taken from [96])

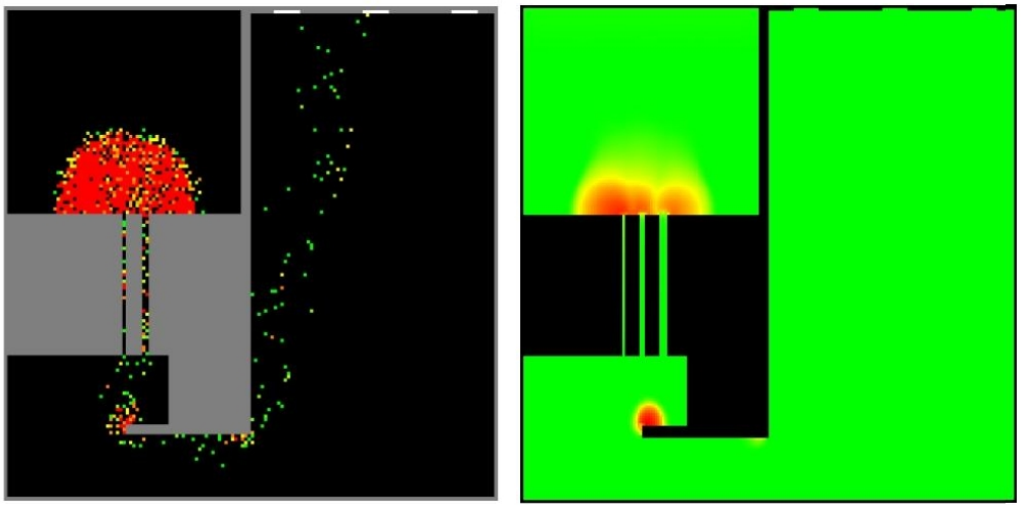

Figure 4.6: The visualization of egress simulation. Left: the actual velocity of agents (red – standing, green – movement with $v_{max}$. Right: a significant congestion (red value – 20% under high dense conditions). (taken from [96])

## 4.5 Related Models

In this section, models which supplement F.A.S.T. model are presented.

### 4.5.1 Physical Forces in Floor Field Model

The "Swarm force model" [65] enhances the floor field model with model of propagation of physical forces.

Force is generated by "pushing" the agents, which causes the creation of force bosons. These virtual particles are stored to the force field, where they can propagate and influence the agents. The force field represents both, the magnitude and the direction of force.

First, it is necessary to modify the decision making process. The equation (4.5) does not allow the selection of an occupied cell. This model proposes to change it, the selection of occupied cell is possible, but with probability penalization. The probability that an agent selects the cell $i$ is following:

$$p_i = N \cdot (1 - \Phi_i) \cdot e^{k_s \cdot S_i} e^{k_d \cdot D_i}, \tag{4.6}$$

the exponential part corresponds with the definition of F.A.S.T. model, the constant $\Phi_i$ is a vacancy factor ($\Phi_i = 0 \ldots$ empty cell, $\Phi_i = 0.5 \ldots$ occupied cell). Index $i \in \{1, 2, 3, 4\}$ refers to the four nearest cells, which only are allowed to be a target for decision.

If an agent selects an occupied cell, the effect of pushing appears. Such agent stays in his cell and drops several force bosons (their number is determined by the capacity for pushing). Each time step, force bosons propagate to the surroundings (the simulation of inter-personal contacts). The force is dissipated when it reaches empty cell or a wall.

The force field influenced the model by two ways:

- in case that the number of force bosons reaches some threshold (three times larger than the capacity for pushing), the decision making process disappears and agent choose the cell in the direction of the force.
- when the total number of bosons in one occupied cell reaches even higher threshold ($\varphi$), an agent becomes injured. Injured agent cannot move and stays in his actual cell as an obstacle until the end of simulation.

### 4.5.2 Anticipation in Floor Field Model

The anticipation is defined as "the ability of avoiding collisions with other pedestrians considering their future walking way" (see [131]). To avoid conflict with other agents, it is necessary to:

1. predict the movement and find the areas of conflict
2. change the velocity or direction to avoid the predicted conflict

To predict the movement, the effort to reach the target the shortest way is expected. Thus, an agent should walk along the gradient of static floor field. Further we define nearest $d_A$ cells ($d_A \in \mathbb{N}$ is a parameter of this model) on this virtual path as the reserved cells.

To store the information about reserved cells, a vector anticipation floor field (AFF) is defined. It keeps the number of agents, which head to the given cell, with respect to their direction (def.: $A_i^{(n)}$ is the value of AFF in cell $i$ from direction $n \in \{1, 2, 3, 4\}$ ). Then, during decision process, an agent reacts to the agents from different direction: $E_i^{(m)} = \sum_{n \neq m} A_i^{(n)}$ ($m$ refers to his direction).

The equation (4.6), which determines the probability of selection the cell $i$ in standard floor field model, is supplemented by anticipation:

$$p_i = N \cdot (1 - \Phi_i) \cdot e^{k_s \cdot S_i} e^{k_d \cdot D_i} e^{-k_A \cdot E_i^{(m)}}, \tag{4.7}$$

where $k_A$ is the sensitivity to the anticipation.

Here we note, that the process of reserving the cells runs before each decision making processes and the information is valid only through one step of the algorithm.

### 4.5.3 Real–Coded Cellular Automata

The cellular automata models limit the direction of agents to several possible values. Contrarily the real–coded model (see [145, 146, 147]), developed originally for lattice gas automata, solves this problem by special actualization rules.

The position of agent $i$ (denote $x_i$) is still discrete, but the magnitude of velocity ($v_i$) and its direction are continuously distributed.

The update process runs according to following four rules, which are applied to randomly chosen agent:

1. the streaming process: new (continuous) position $x_i' = x_i + v_i$ of agent $i$ is calculated.
2. the re-position on the grid: to set the agent to a matrix, the distance to four nearest cell is counted. The selection of new (grid) position runs randomly, the probabilities linearly depend on the distances to each cell.
3. the solution of conflict: in case, that his next (grid) position is occupied, agent $i$ stays on position $x_i$. Instead of motion, he changes his direction (he randomly turns by 45°).
4. adjusting the direction: due to the re-position, it is necessary to set the direction towards the exit again.

The decision making process presented in this work is quite simple, but it can be modified up to the style of FF model. The idea of partial continuous movement eliminates the greatest trouble of cellular automata.

# Chapter 5

# Designed Model

The model used for this study comes out from the Floor-Field cellular model with several modifications introduced in [5, 4] and studied in more detail in [7], here extended by the aggressiveness element [12]. The playground of the model is represented by the rectangular two-dimensional matrix consisting of cells that may be either occupied by one agent or empty. Agents are moving along the lattice by hopping from their current cell to any neighboring cell.

Even the desired velocity of each agent may be different (in agreement with [41]), the timespan of model is set to 0.3 s giving the free flow velocity up to 6 m/s. The pedestrian update is parallel, each pedestrian pick up desired cell based on calculated profitability and some random element. The profitability used to be composed of the distance to the exit, occupancy, conflict anticipation and other quantities.

Similarly to the latest models [81] or [37], pedestrians are allowed to choose an occupied cell. In such case, agent has to wait until the blocking agent moves or until next decision. This specification supports the ability pedestrians to hold formations.

In contrast to large scale simulations presented in [121] or [149], the goal of this work is to model essential phenomena of pedestrian motion, therefore one rectangular room with one exit and one entry is more convenient.

Following sections are dedicated to basic model elements and the simulations are summarized in consecutive chapter.

## 5.1 Space Elements

The base element of the model is the lattice $\mathbb{L}$ of square cell with edge from 0.4 to 0.5 m long. Each cell is identified by vector of position $\vec{x} = (x_r, x_c)$, where $x_r$ corresponds to rows and $x_c$ corresponds to columns.

Special type of cell is the exit, an agent leaves the model by entering there. The exit is considered as always empty, but only one agent can enter during one step of algorithm, here is no difference from ordinary cells.

The entry is realized by a cell (or cells) in front of the wall that can generate a pedestrian. For most of following studies, the entrance follows a desired distribution $p_{in}$. Each step, an

algorithm decides whether new pedestrian should be generated. In that case, new pedestrian is added to the entrance queue and any timestep when the entrance is empty, one pedestrian from this queue entered the room.

Another type of cell is a wall or an obstacles. These cells are excluded from the movement or decision process, model keeps them just for visualization.

In presented model, the motion is limited to the agent's surrounding. We use the Moore's neighborhood (see Figure 5.1) for both, decision making and movement. More precisely, an agent in the cell $\vec{x}$ can choose to jump to the cell $\vec{y} \in \mathcal{N}(\vec{x})$ defined as

$$\mathcal{N}(\vec{x}) = \left\{ \vec{y} \in \mathbb{L};\ \max_{j=1,2} |x_j - y_j| \leq R \right\} \tag{5.1}$$

where $R$ stand for the range of neighborhood. Moore's neighborhood was selected due to the ability to make diagonal steps, with all consequences that will be discussed in next sections.

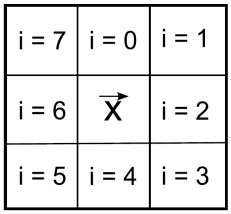


Figure 5.1: Moore's neighborhood (with range $R = 1$) of cell $\vec{x}$, with indexation used.

Even the range of model used in this project is set to $R = 1$, i.e. nearest neighborhood, the real horizon of pedestrian vision is larger. Cells from neighborhood have coded information about the exit position and motion of near by agents, as described further.

## 5.2 Decision Process

Decision process forms the first part of agents actualization. Each active agent chooses desired position from reachable cells of its surrounding (i.e. excluding walls or obstacles) and this decision is noted. If an agent chooses empty cell, it is added to waiting list of this cell. If it chooses cell occupied by an other agent, a bond to this blocker is created, the original agent becomes "bonded". Whole process is visualized in Figure 5.2.

Agents choose their target cells $\vec{y}$ from $\mathcal{N}(\vec{x})$ stochastically according to probabilistic distribution $P(\vec{y} \mid \vec{x};\ \text{state of } \mathcal{N}(\vec{x}))$ that reflects the "attractiveness" of the cell $\vec{y}$ to the agent. When situation is clear, we will use the notation $p(x, y) =: p_i$ where $i$ is the index $\vec{y}$ in the neighborhood of $\vec{x}$, as defined in Figure 5.1.

Analogically to the Floor Field model, part of the "attractiveness" is expressed by the static potential field $U : L \to \mathbb{R}$ that assigns value $U(\vec{x})$ to every cell $\vec{x}$ in the sense that the agent is attracted to the cell with lower potential. Commonly, the potential field is generated by the exit and is static over time. The probability of hopping from $\vec{x}$ to $\vec{y}$ fulfills $p_i \propto \exp\{-k_U U_i\}$, where $k_U \in \langle 0, \inf \rangle$ stands for the parameter of sensitivity to the

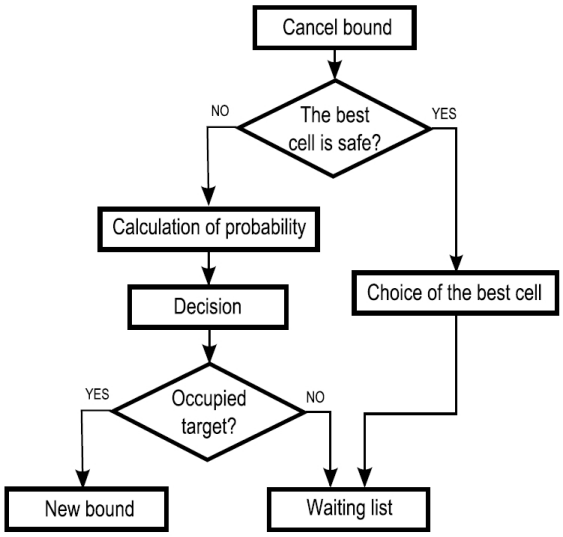


Figure 5.2: Diagram of decision process of one agent. The process of bond annulations precedes the decision, which is in detail described in Figure 5.3. If the cell with higher potential (referred to as the best) is empty and occupation is not predicted, agent chooses it. Consequences of decision depend on the state of target cell. If it is empty, agent is added to waiting list. Otherwise, it is bonded to the agent who is blocking him.

potential. The potential itself is defined as scaled negative distance to the exit.

$$U(\vec{x}) = -\mathrm{F} \cdot r(\vec{e}, \vec{x})\,, \tag{5.2}$$

where $r(\vec{e}, \vec{x})$ is Euclidean distance:

$$r(\vec{e}, \vec{x}) = \sqrt{(e_r - x_r)^2 + (e_c - x_c)^2}\,. \tag{5.3}$$

Linear relation ensures that the probability distribution that an agent pick given cell from his surrounding generated by attractiveness does not change with the distance of the agent to the exit. Nonetheless, for specific purposes, an arbitrary shape of potential may be implemented, see section 6.1.

As the probability depends on the product of "force" and sensitivity $p_i \propto \exp\{-k_U U(y)\} = \exp\{-k_U \cdot F \cdot r(\vec{e}, \vec{y})\}$, we will further consider $F = 1$ as default and modify only $k_U$.

The decision starts by finding the cell with the highest potential (denoted $m$):

$$m = \mathrm{argmax}_{i \in \{0 \ldots 7\}} U_i\,, \tag{5.4}$$

where the indexes refer to the cells from the surrounding (see Figure 5.1).

The calculation of probability $\bar{p}_i$ that an agent will choose given cell from his surrounding depends on the state of the cell $m$. If both, the prediction and occupation number of this cell is equal to zero, the agent chooses $m$ deterministically, otherwise the probability of motion to cell $i$ may be interpreted as the profitability of this cell (5.9).

The probabilistic choice of the target cell is further influenced by the occupancy of neighboring cells ($O_{\vec{x}}(\vec{y}) = O_i$). Note that the value of occupation is relative in the way that the cell where agent $\alpha$ stands is occupied for everyone but agent $\alpha$. The possibility to select

An occupied cell is considered to be less attractive, nevertheless, it is meaningful to allow the choice of an occupied cell while the principle of bonds is present (explanation of the principle of bonds follows below). This principle is related to the parameter of sensitivity to occupation $k_O$, which combines two strategies: to stay in line and wait for the motion of the predecessor ($k_O = 0$), or to try to run around the crowd ($k_O = 1$).

The decision process may be influenced by the predicted state of considered cells. To describe this influence, let us first define the term movement prediction. In the essence, agent $\alpha$ is predicted to move in the same direction as he did in his previous step, i.e, we define the predicted position of an agent as

$$\vec{x}_\alpha^P(t+1) := \begin{cases} 2\vec{x}(t) - \vec{x}(t-1) & \text{if } 2\vec{x}(t) - \vec{x}(t-1) \in L\,, \\ \vec{x}(t) & \text{otherwise}\,. \end{cases} \tag{5.5}$$

This allows us to define the dynamical field $\eta(\vec{y}, t)$ of the occupancy prediction of the cell $\vec{y}$ from the point of view of agent $\alpha$ sitting in $\vec{x}$ as

$$\eta_{\vec{x}}^P(\vec{x}, t) := \begin{cases} 0 & \text{if } \{\forall \beta \neq \alpha \,|\, \vec{y}_\beta^P(t+1) = \vec{x}\} = \emptyset\,, \\ 1 & \text{otherwise}\,. \end{cases} \tag{5.6}$$

Us usual, the coefficient of sensitivity to predicted occupancy is referred to as $k_\eta$.

Furthermore, the movement in diagonal direction is penalized in order to suppress the zig-zag motion in free flow regime and support the symmetry of the motion with respect to the lattice orientation. The diagonal steps deforms the probability distribution of deviation from straight trajectory. When the straight direction to the goal follows diagonal steps, potential deviations would be orthogonal, i.e. shorter steps. Such steps would be much less beneficial thus the probability of these deviations would be low. In contrary when the straight direction to the goal follows orthogonal steps, potential diagonal deviation would move pedestrian further. Even the straight step would bring a pedestrian closer than diagonal deviations, the difference would not be significant, see illustration further on Figure 6.8. To compensate this issue, we have to adjust profitability metric by diagonal penalization.

$$D(\vec{x}, \vec{y}) = \begin{cases} C \ldots i \in \{1, 3, 5, 7\} \\ 1 \ldots i \in \{0, 2, 4, 6\}\,, \end{cases} \tag{5.7}$$

$C$ is the global constant.

This leads to the final form of decision process:

$$\bar{p_i} = \begin{cases} \delta_{im} \;\ldots\; n_m = r_m = 0 \\ P(\vec{y} \,|\, \vec{x}) \quad \ldots\; otherwise\,. \end{cases} \tag{5.8}$$

Expression $\delta_{ij}$ represents Kronecker delta, which is equal 1 if $i = j$ and 0 otherwise. The probability $P_i = P(\vec{y} \,|\, \vec{x})$ is defined as:

$$P(\vec{y} \,|\, \vec{x}) = \frac{\exp\big\{-k_S S(\vec{y})\big\}\big(1 - k_O O_{\vec{x}}(\vec{y})\big)\big(1 - k_\eta \eta_{\vec{x}}(\vec{y})\big)\big(1 - D(\vec{\vec{x}}, \vec{\vec{y}})\big)}{\sum_{\vec{z} \in \mathcal{N}(\vec{x})} \exp\big\{-k_S S(\vec{z})\big\}\big(1 - k_O O_{\vec{x}}(\vec{z})\big)\big(1 - k_\eta \eta_{\vec{x}}(\vec{z})\big)\big(1 - D(\vec{x}, \vec{z})\big)}\,. \tag{5.9}$$

The visualization of decision process for several specific settings is provided in Figure 5.3.

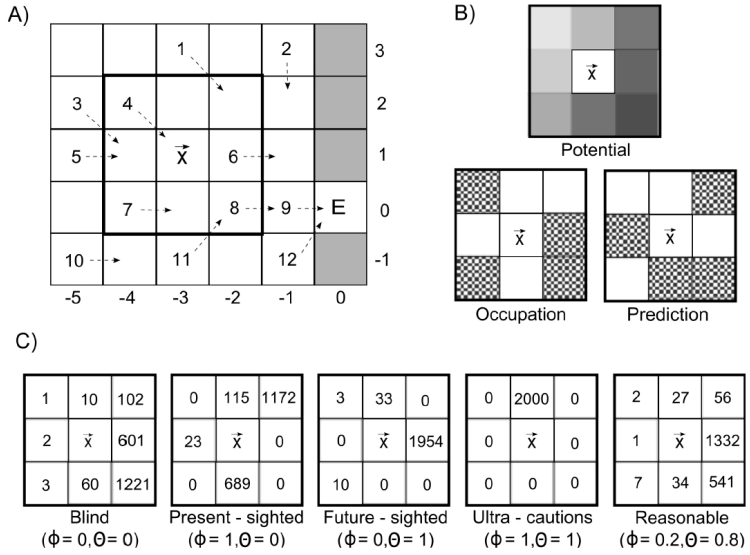


Figure 5.3: Example illustrating principle of the decision process. Subfigure A visualizes wider surrounding of an agent in cell $\vec{x}$. Integer numbers represent agents and dashed arrows their predicted movement. The probability distribution $p_i$ given by (5.9) is determined by potential, occupation and conflict prediction. The subfigure B visualizes these parameters. The darker color the higher potential (closer to exit), hatched area means penalization in stated category. The final cell attractiveness strongly depends on coefficients of sensitivity to stated parameters. While potential represent static conditions, occupation and prediction of conflict reflect agent strategy. Final probabilities for different settings of sensitivity parameters $k_O, k_\eta$ are shown in subfigure C. For each of them, 2000 decisions were divided into the cells according to (5.9). Different strategies lead to different distribution of the probability. "Blind" agent responds only to potential; "present", resp. "future" variant excludes occupied, resp. predicted cells. The variant "ultra cautious" accepts only position, which is empty and also predicted to be empty. Presented model uses the variant "reasonable", which corresponds to the observations. The sensitivity to potential $k_U = 3$.

It is worth noting that the site $\vec{x}$ belongs to the neighborhood $\mathcal{N}(\vec{x})$, therefore the equation (5.9) applies to $P(\vec{x} \mid \vec{x})$ as well. It is obvious that this process is fully parallel for active agents – the decision of agents does not influence the result. At the end of this phase, the time of agent's next actualization is calculated from his frequency (5.12). Even the equations and techniques are far from physics, the defined probability and whole updating scheme is not to far from gradient-driven motion in potential field.

## 5.3 Time

Aside the decision process, the study focuses on the influence of updating scheme. Updating schemes used in this work are inspired by the asynchronous cellular automata schemes presented in [46]. We use similar approach to the "clocked" scheme, i.e., every agent has assigned it's own timer which ticks at different rates for different agents. Furthermore, when the principle of bounds is incorporated ($k_O = 1$), the timer is influenced by the motion of

other agents, as will be mentioned below and is discussed in [5].

The time interval between events can be irregular, both globally and even focusing on single agent. Therefore it is appropriate to define a function generating the next actualization time of each agent. One can start with simple form:

$$t_{n+1} = t_n + f_j^{-1}\,, \tag{5.10}$$

where $f_j$ is the actualization frequency of agent $j$, the sequence $\{t_n\}_{n=1}^{\inf}$ is evaluated for each pedestrian. This time is written to the timeline, as illustrates Figure 5.4.

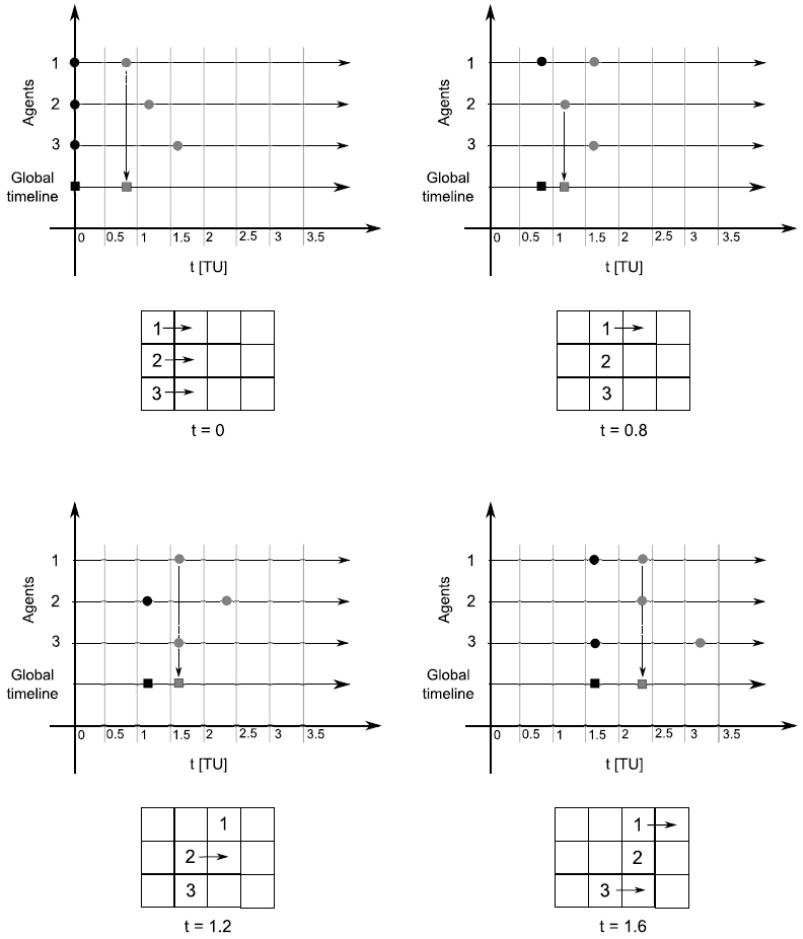


Figure 5.4: Example illustrating principle of timeline. Black color of circles (agents time) and squares (global time) represents active objects, gray color indicates the time of next activity of each element. Three agents with different frequencies ($0.8^{-1}$, $1.2^{-1}$, $1.6^{-1}$) became to move in time $t = 0$. For all of them, next actualization time is calculated according to the equation (5.12) and the time of nearest event in timeline is actualized (arrow). Time moves to $t = 0.8$, only agent 1 is active, he makes a step and his next actualization time is counted. After actualization of time ($t = 1.2$), only agent 2 moves. Next global time is $t = 1.6$, where agents 1 and 3 are active, the subsequent events are solved analogically.

Used updating scheme combines the advantages of fully-parallel update approach leading to

necessary conflicts and the asynchronous clocked scheme [46] enabling the agents to move at different rates. This general concept will be called the *adaptive time span*.

There is a specific time sequence $(t_{i,n})_{n\in\mathbb{N}_0}$ unique for every agent. This sequence determines the moments when agent $i$ is *activated* to actualize his position according to above mentioned rules. Looking at the system as a whole, the system state is actualized at times $(t_m)_{m\in\mathbb{N}_0}$, where

$$t_{m+1} := \min_{j\in\hat{N}}\{t_{j,n} \,|\, t_{j,n} > t_m \,,\, n \in \mathbb{N}_0\}\,. \tag{5.11}$$

This equations means that the time of next actualization is chosen as the nearest event defined by the updating sequences of all agents.

A common example of such concept is that the sequence $t_{i,n}$ is driven by the Poisson process, i.e., the increments $t_{i,n+1} - t_{i,n}$ are exponentially distributed. The principle used in our model comes out of the idea that each agent has its own desired frequency of actualization $f_i$ characterized by the desired time increment $\tau_i = f_i^{-1}$. This leads, in an ideal case without correlations between agents, to the sequence $t_{j,n} = n\tau_j$. As will be shown below, the presented conflict solution changes this sequence slightly due to the adaptation to the movement of agents in the neighborhood. Similar idea is considered in [142] to simulate heterogeneous system with two kinds of agents.

As mentioned in previous section, agent may move to orthogonal or diagonal direction, thus there are two possible lengths of step. By diagonal step, agent moves $\sqrt{2}$ further than by orthogonal one. To conserve the pedestrian velocity, we have to compensate it by adjusting time consumption of these steps – they will take $\sqrt{2}$ times longer.

To hold agents on stable level of synchronization, we used approximation $\sqrt{2} \approx 3/2$ that keeps all pedestrians in discrete (semi-integer) steps. Time unit was cut to half and an agent moves each second or third tick, with respect to the type of step it realized. That leads to the updating function in shape

$$t_{n+1} = t_n + f_j^{-1} + \frac{1}{2} I_d \cdot f_j^{-1}\,, \tag{5.12}$$

where $I_d$ is the identifier of diagonal movement. The effect of rational approximation is visualized in Figure 5.5.

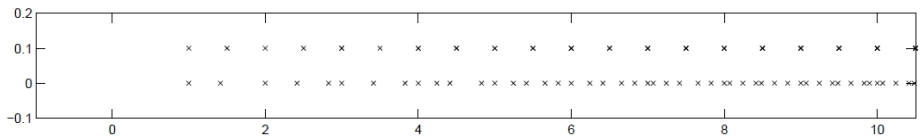


Figure 5.5: Illustration of adaptive time span with the rational approximation of $\sqrt{2}$ (top) and without it (bottom).

Assuming heterogeneous population where $f_j$ really differs among pedestrians, completely asynchronous update would mitigate all conflicts, thus we defined different approach. Each pedestrian still has its own $t_{n+1}$, but the model clock are ticking by predefined period $\tau$. All agents with their $t_{n+1}$ within given tick are updated at once, but their $t_{n+2}$ is calculated from previous $t_{n+1}$, see schema on Figure 5.10. The time steps would be still independent but

from the purpose of model dynamics all events within one time frame would be considered as concurrent.

In language of symbols, let us denote $A(t) = \{j \in \hat{N} \,|\, \exists n \in \mathbb{N}_0, t_{j,n} = t\}$ the set of active agents at time $t$. Let us consider the situation that agent $i$ creates a bond $(i \to \vec{x})$ at $t_{i,n}$, because $\vec{x}$ is occupied by agent $j$. As times evolves, two possibilities may occur. Firstly, agent $j$ stays in $\vec{x}$ until $t_{i,n} + \tau_i$. In this case, the bond $(i \to \vec{x})$ is canceled, the actualization time of $i$ is set to $t_{i,n+1} := t_{i,n} + \tau_i$ and the decision process of $i$ at $t_{i,n+1}$ goes according to above mentioned rules. Secondly, agent $j$ moves from $\vec{x}$ within the time interval $(t_{i,n}, t_{i,n} + \tau_i)$. In that case we set

$$t_{i,n+1} := \min\{t \in (t_{i,n}, t_{i,n} + \tau_i) \,|\, \xi_j(t) \neq \vec{x}\} \quad \text{and} \quad \xi_i^*(t_{i,n+1}) := \vec{x}. \tag{5.13}$$

Here should be noted that the model period must be shorter that than the period of fastest agent.

This concept is quite robust, thus it might be used to even more complex dynamics. So far, we have imagined constant actualization frequency for any agent. This assumption may be released, the algorithm enables variable actualization frequency that may react to environmental parameters (type of surface, visibility, ...) as well as to dynamic features (local pedestrian density, fatigue, ...). But we haven't use this option due to the demanding calibration. As discussed in analytic chapters, the velocity-density relation is still quite unknown and definitely it depends on a lot variables. Rather than pick up the most promising curve and (possibly) calibrate model to inappropriate situation, we have decided to reach desired behavior by other way. But it doesn't mean that dynamic actualization frequency is bad idea in general.

For various studies two cases are distinguished: homogeneous and heterogeneous. In the homogeneous case, all agents have the same own period $\tau = 0.3$ s (1.33 $\mathrm{ms}^{-1}$ in free flow); in heterogeneous case two kinds of agents are considered: faster agents with $\tau_1 = 0.3$ s and slower agents with $\tau_2 = 0.4$ s (1.00 $\mathrm{ms}^{-1}$ in free flow) with the ratio of occurrence 50%. Then the value of model clock $\tau = 0.3$ s corresponds to the synchronous update (slower agents "miss" one of four steps) and $\tau = 0.05$ corresponds to the asynchronous update.

## 5.4 Dynamics

For each timeframe written on above mentioned timeline, the updating scheme can be described by following loop:

1. Cleaning of exits
2. Selection of active agents in given time frame
3. Decision process of active agents
4. Conflicts solution and motion
5. Bond evaluation and motion
6. Input of new agents

While the first three items are trivial from model dynamic perspective, conflicts and bonds (visualized in Figure 5.6) are more interesting.

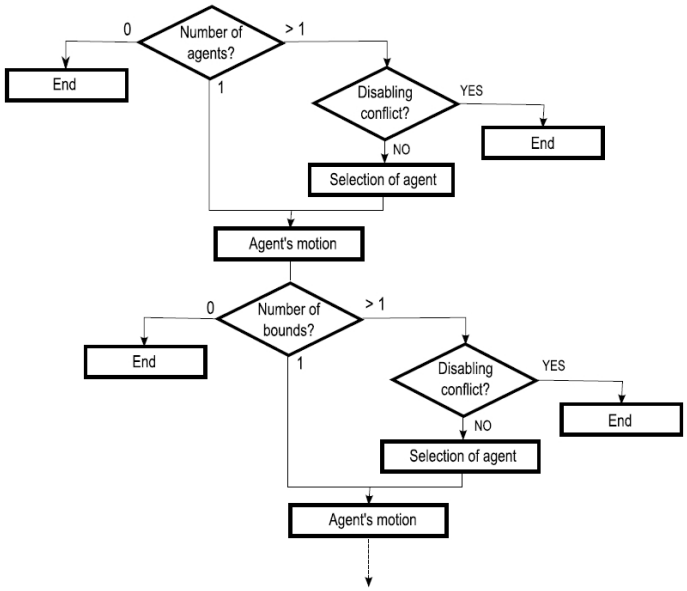


Figure 5.6: Diagram of conflicts solution in one cell and the subsequent motion. The first question is: How many agents are in the waiting list. If there is just one agent, he moves directly. In case that there are more agents, conflict happens. With probability $\mu$, the conflict disables the motion. Otherwise, one of the agents is chosen randomly to move. His motion can cause motion of agents bounded to him. Again, possible conflict must be solved before motion. This sequence is repeated until there is not bounded agent or until conflict stops the movement.

The critical essence of parallel updating scheme is inevitable accompanied by conflicts, when more agents decide to enter the same cell. In such case, one of the agents is usually chosen at random to win the conflict. There are more approaches, how the randomness is executed, e.g. uniformly, or proportionally to the hopping probabilities [45]. Important role in models of pedestrian evacuation play the unresolved conflicts, i.e., the aim to attempt the same cell leads to the blocking of the motion. This is captured by the friction parameter $\mu$ denoting the probability that none of the agent wins the conflict. An improvement is given by the friction function [148], which raises the friction according to the number of conflicting agents.

For purposes of this work, we introduce the choice of the winning agent based on his ability to win conflicts represented by an additional parameter $\gamma \in [0, 1]$, which is referred to as the aggressiveness. Similar heterogeneity in agents behavior has been used in [144], where the "aggressiveness" has been represented by the willingness to overtake.

The conflict is always won by agents with highest $\gamma$ among conflicting agents. If there are two or more agents with the highest $\gamma$, the friction parameter $\mu$ plays a role. In this article we assume that the higher is the aggressiveness $\gamma$, the less should be the probability that none of the agents wins the conflict. Therefore, the conflict is not solved with probability $\mu(1-\gamma)$ (none of the agents move). With complement probability $1 - \mu(1 - \gamma)$ the conflict resolves

to the motion of one of the agents. This agent is chosen randomly with equal probability from all agents involved in the conflict having the highest $\gamma$. The conflict solution among heterogeneous group of agents is depicted in Figure 5.7.

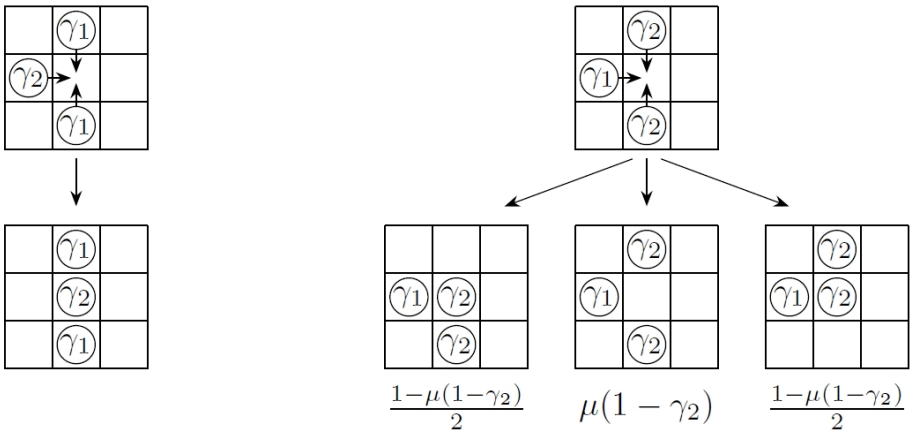


Figure 5.7: Conflict solution for $\gamma_1 < \gamma_2$. Left: More aggressive wins the conflict over two less aggressive. Right: The conflict of two more aggressive can resolve by the blocking of the movement.

The bonds principle is closely related to the possibility of choosing an occupied cell ($k_O \neq 1$). If an agent chooses as his target cell an occupied cell then the *bond* to the blocking agent is created. The bound holds until the blocker moves or until the blocked agent is activated. In the case of the earlier movement of the blocker (i.e., if the blocker moves within the algorithm step before the activation of the blocked agent), the blocked agent follows the blocking agent immediately outside his activation step, see illustration on Figure 5.8. This principal supports the motion in lines and is further discussed in [4] or [5].

The set of bonded person works like waiting list – more than one agent induces conflict, which is solved according to previous rule. Chosen agent moves and other bonds are canceled. Again, if the chosen agent was a blocker, another agent can move. So the model can come to deep recursion, which is limited by number of agents. The principle of waiting lists

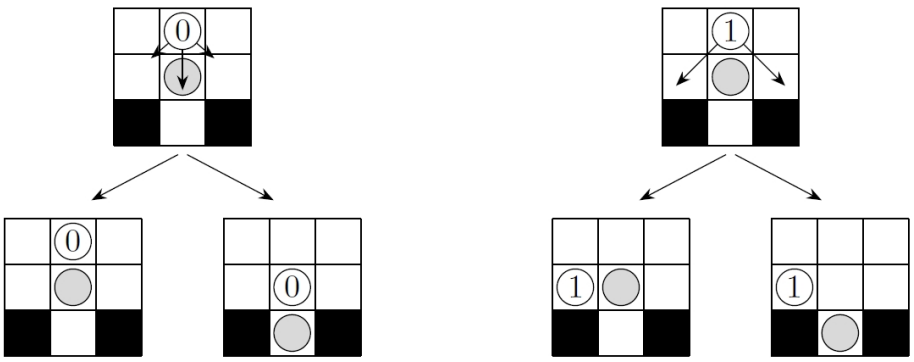


Figure 5.8: Choice of the target cell with respect to sensitivity to occupancy. Left: $k_O = 0$, bond is created. In case blocking agent moves, blocked agent moves as well. Otherwise, they stay. Right: $k_O = 1$, motion to second most attractive cell. Rear agent moves anyway.

and bonds is illustrated in Figure 5.9.

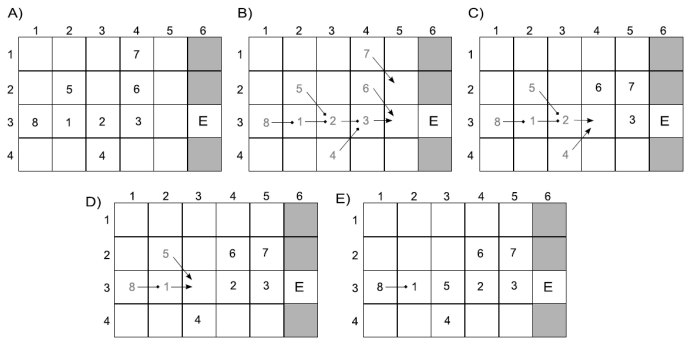


Figure 5.9: Example illustrating principle of waiting lists and bounds during one step. First slide shows agent's position at the beginning of the step. Second slide displays decision of all agents – triangled arrows represents waiting lists and squared arrows represents bounds (synchronization is expected). The process of decision is not discussed in this illustration (see figure 5.3). Only waiting list of cell [2,5] contains just one agent, so he can move. Two agents target to cell [3,5], therefore conflict happens. According to the depicted situation, conflict did not disable the movement. Agent (3) is chosen randomly to move – third slide. Agents (2,4) are bonded to agent (3), his motion causes their action. The conflict is not blocking, agent (2) was chosen randomly – fourth slide. Again, two agents are bonded to him, but according to a draw, their conflict blocks the movement. Agent (1) stays, thus agent (8) remains bonded to him – fifth slide.

Figure 5.10 illustrates how bounds influence the activity of agents. The principle of bounds participates in agents synchronization. Faster agents may be blocked by slower ones, hence they have to wait until their movement. From macroscopic perspective it could look like homogeneous group. Moreover, when a blocker and a blocked agent have the same actualization frequency, their following movement will be synchronized.

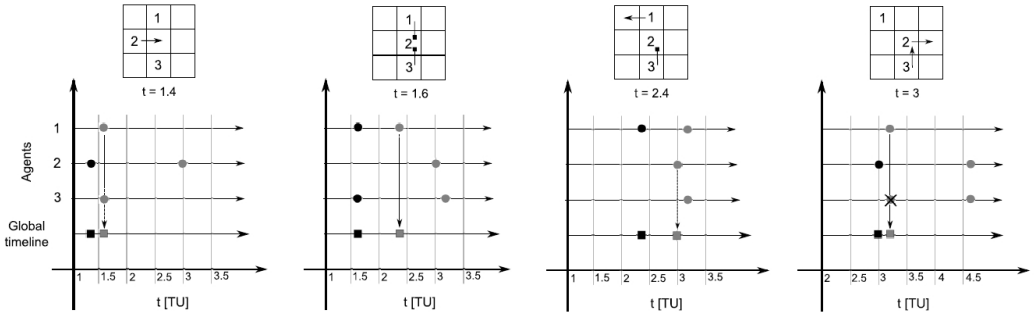


Figure 5.10: Example illustrating the timeline with bonds. This situation describes the cross of three agents. Agent 1 is fast ($f_1 = 0.8^{-1}$), agents 2 and 3 are two times slower, $f_{2,3} = 1.6^{-1}$. The movement of agents 1 and 3 is synchronized, agent 2 is ahead. It is visualized in first slide (time $t = 1.4$), where only agent 2 is actualized. In time $t = 1.6$, both agents, 1 and 3, chooses the cell occupied by agent 2 and make bounds. Agent 1 is fast and he is actualized again in time $t = 2.4$: the bond is broken, he chooses empty cell and moves there. Agent 2 moves in time $t = 3$, therefore bonded agent 3 jumps to this displaced cell. He makes a move out of his step, his next actualization time is recalculated by (5.12) with respect to actual time. This phenomenon leads to synchronization of agents 2 and 3.

## 5.5 Discussion

Proposed model contains many fixed or optional parameters (see Table 5.1), their influence will be discussed further.

Model has three coefficients of sensitivity: to potential, occupation and prediction number. The value of this triplet needs to be assessed.

The effect of sensitivity to occupation is the best observable – in case that an agent could never choose occupied cell ($k_O = 1$), model would not approximate the state of congestion, when whole group moves without any gaps between agents. On the other hand it is obvious, that when person decides between two equal cells and one is occupied, he chooses the empty one with much more probability.

The sensitivity to potential influences the stochasticity of decision. The higher the value is, the higher is the probability of choosing the cells in the exit direction.

The effect of sensitivity to prediction number can be observed only indirectly, prediction reduces the number of conflicts.

The friction coefficient, which simulates conflicts, plays an interesting role mainly under high density situations. In case of congestion, almost all agent's actualizations are accompanied by a conflict. When the density is low, there are only a few conflicts and therefore this parameter is not important. The dependence of evacuation time on this coefficient is visualized on figure 5.11.

The friction effect interacts with two other principles, which were implemented to the model. Adaptive time span and dynamic timeline allow asynchronized motion of agents. But this freedom reduces the number of conflicts – conflict happens only if more agents actualize in

| Quantity | Default value | Description |
|---|---|---|
| $\mathbb{L}$ | Edge 0.4 m | Lattice |
| $\vec{x} = (x_r, x_c)$ | | Position of cell |
| $\mathcal{N}(\vec{x})$ | Moore | Neighborhood |
| $R$ | 1 | Range of neighborhood |
| $p_{in}$ | Exponential | Entrance probability |
| $P(\vec{y} \mid \vec{x}) =: p_i$ | | Hopping probability |
| $\bar{p_i}$ | | Cell selection formula |
| $U(\vec{x})$ | Spherical | Static potential |
| $k_U$ | 3 | Sensitivity to potential |
| $F$ | 1 | Force of the exit |
| $r(\vec{e}, \vec{x})$ | Euclidean | Distance to the exit |
| $O_{\vec{x}}(\vec{y}) =: O_i$ | Boolean | Occupancy of cell |
| $k_O$ | 0.2 | Sensitivity to occupancy |
| $\vec{x}_\alpha^P(t+1)$ | | Predicted position |
| $\eta_{\vec{x}}^P(\vec{x}, t)$ | Boolean | Prediction number |
| $k_\eta$ | 0.7 | Sensitivity to prediction |
| $D(\vec{x}, \vec{y})$ | Boolean | Diagonal motion |
| $C$ | 0.2 | Diagonal probability penalization |
| $\tau$ | 0.3 s | Model period |
| $\tau_i = f_i^{-1}$ | 0.25 – 0.4 s | Agents period / frequency |
| $\tau_i^D$ | 0.5 $\tau_i$ | Diagonal time penalization |
| $\mu$ | 0.9 | Friction parameter |
| $\gamma_i$ | 0 – 1 | Aggressiveness of agent |

Table 5.1: Parameter values and description

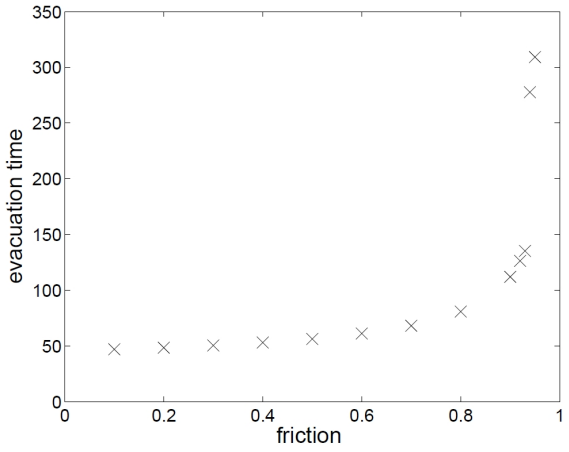


Figure 5.11: The dependency of evacuation time on the friction coefficient $\mu$. A crowd of 30 agent were arranged along the wall 10 m far from doors on the opposite side, simulating the experiment E1, setting A. The values of parameters are following: $C = 0.2$, $k_U = 3$, $k_O = 0.2$, $k_\eta = 0.7$.

the same time. Due to the different velocity of agents and diagonal penalization, certain degree of asynchronization is necessary and therefore this effect must be reflected.

The second conflict element is the principle of bounds, especially its effect in congested state. When an agent moves, it enables consequently motion of all line, which is bounded to him. Due to this phenomenon, the motion is more frequent than one could expect with given values of parameters.

The principle of bonds plays important role for synchronization of movement. As mentioned in section 5.3, two asynchronous agents with the same actualization frequency became synchronous, after successful motion of both participants of bond. Paradoxically, the principle of bonds is resolving conflicts, but also it participates on increasing of their number.

The elimination of asymmetry in the model caused significant intervention to the decision process – the probability of choosing a diagonal cell is penalized by multiplication constant $C = 0.2$ (thus 80% penalization). But the exponential function in the equation (5.9) strongly benefits the diagonal cell, which allow $\sqrt{2}$ times longer step. The step length affects the potential in the argument of exponential, therefore this penalization only compensates such benefit.

At the end, the potential modification to complex geometry should be discussed. First, the distance must be modified to respect convex shape of room, e.g. the distance field generated by Dijskra's algorithm in [96]. This approach enables also an effective avoidance of obstacles. Second, the connection between rooms could be modeled by oriented graph, an multilevel approach for traffic is described in [68].

# Chapter 6

# Simulations

The purpose of this chapter is to demonstrate several mechanisms developed to support microscopical aspects of pedestrian movement in cellular models. Each section focuses on some model feature, it illustrates the effect of proposed improvements and discuss parametric setup.

We will start with initial calibration and discuss the symmetry – these studies are based on two simple experiments E1 and E2. Then we will move to more advanced simulations covering heterogeneity, phase transition or complex geometry supported by experiments E3, E4, E5, E6.

The purpose of this work is not to recommend an optimal set of parameters, but (we believe) it gives to the reader all information to decide what set of parameters he/she should use to reproduce desired behavior. The values of model parameters has been setting up and modified for years. With changes in simulation design, some features were highlighted or suppressed, thus there is no standard method describing calibration of our model in general. Actually, there are no standards to calibrate any model, we could find just several test cases that a model should fulfill. This course was set even by government authorities in several European countries [153].

The detail process of model calibration for a continuous rule based mode has been developed just now in cooperation with Jana Vacková. It is based on independent calibration episodes where each episode focuses on small group of set of parameters [32].

## 6.1 Initial Calibration

When the model was implemented, we have organized simple "leave the room" experiment. In each of 29 experimental rounds, 30 of 70 participants took predefined positions at one side of a room and on a signal, the walked out through the door at opposite side.

During this process, following phenomena were observed (see left part of Figure 6.1):

1. Pedestrians hold the lines and wait rather than walking around the crowd, thus occupation is not important, but the prediction and bounding principle is significant
2. Pedestrians are not forced to form a cluster near exit; multi-line (chaotic) queue is

formed instead

3. The movement is relatively deterministic

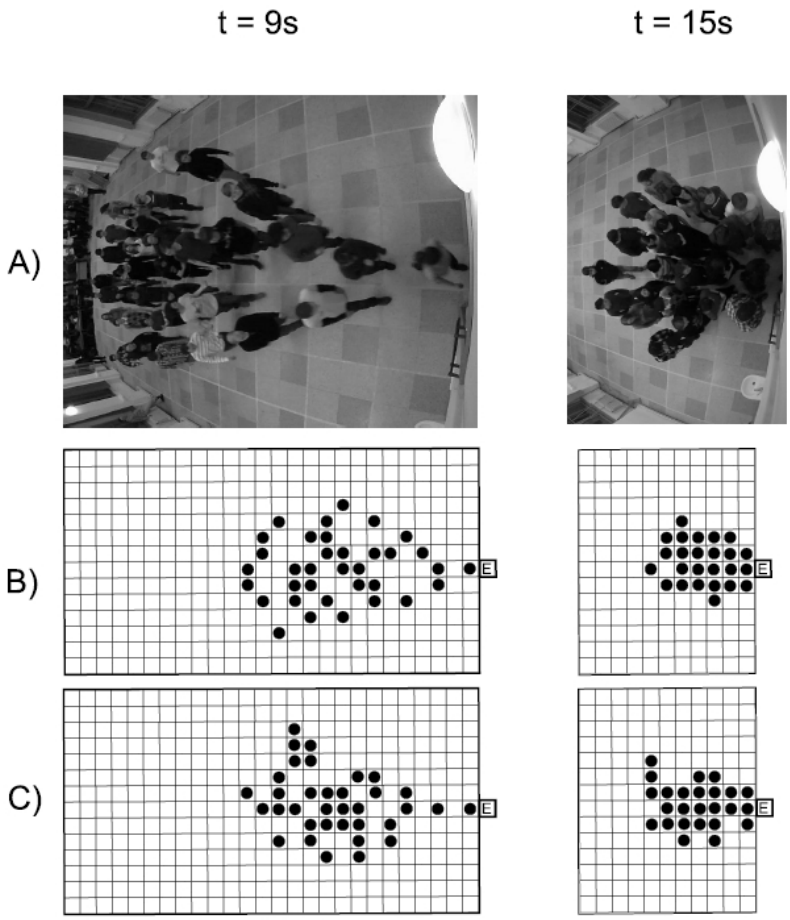


Figure 6.1: Visualization of progress of one round, pedestrians walked (left) and run (right). Pictures A come from frontal camera, 9 s after initialization, when first person approaches the exit and 15 s after initialization, when compact cluster is developed. Subfigures B project previous pictures to lattice representation and subfigures C represent corresponding realization of the simulation.

In the simulation we have considered homogeneous synchronous update, $\tau_i \forall i \in \hat{N} = \tau = 0.31$ s. The other quantities were set with respect to the shape of the crowd, lack of overtaking and low value of conflict, as shown in Table 6.1

| potential | occupation | movement | friction | diag. pen. | time unit |
|---|---|---|---|---|---|
| $k_U$ | $k_O$ | $k_M$ | $\mu$ | c | $TU$ |
| 3 | 0.2 | 0.7 | 0.9 | 0.2 | 0.31 s |

Table 6.1: Values of parameters used for the cooperative simulation

Furthermore, considering the essence of the experiment, moral barriers connected to social conventions avoided the participants to create semi-spherical cluster in front of the exit, which is expected in panic-like situations (see e.g. [62], [119], etc.). The participants were not motivated to leave the room earlier than others, therefore there has not been observed any drastic fight at the door. As shown in Figure 6.2, the spontaneous development of lines was observed instead.

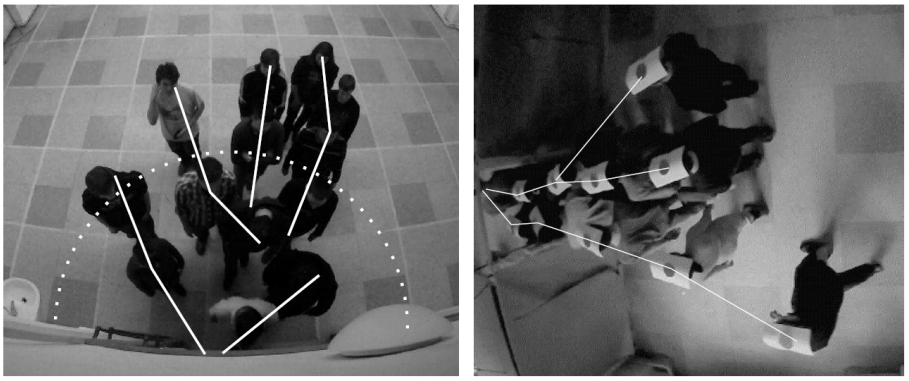

Figure 6.2: Spontaneous line formation in front of the exit observed during experiments.

Later in the experiment, the running was allowed thus the mood among participants turned to be more competitive[1]. We observed much more examples of overtaking and conflicts, the spherical shape of cluster formed near the exit. In that case, sensitivity to occupation become more relevant, the recommended values of the sensitivity parameters should be changed: Table 6.2

| potential | occupation | movement | friction | diag. pen. | time unit |
|---|---|---|---|---|---|
| $k_U$ | $k_O$ | $k_M$ | $\mu$ | c | $TU$ |
| 3 | 0.9 | 0.9 | 0.9 | 0.2 | 0.31 s |

Table 6.2: Values of parameters used for the competitive simulation

Here we note that the friction parameter seems to be extremely high, but his influence is weakened by the concept of bonds. Unresolved conflicts serve mostly as the means enabling to switch between lines in the chaotic queue in front of the exit.

Usually the potential $U(\vec{x})$ is defined in the spherical form $U(\vec{x}) = |\vec{x}-\vec{e}\|_2$, where $\|.\|_2$ is the euclidean norm and $\vec{e}$ is the position of the exit cell mostly set to $\vec{e} = (0, 0)$. The cooperative "movement in lines" inspired us to deform the spherical form of potential iso-value curves [3, 14] to shape

$$\varrho(\vec{e}, \vec{x}) = \sqrt{\frac{10(e_{\text{line}} - x_{\text{line}})^2}{e_{\text{column}} - x_{\text{column}}} + (e_{\text{column}} - x_{\text{column}})^2} \ . \tag{6.1}$$

[1]For this part of the experiment, we chose just few of participants, all volunteered. We have instructed to behave carefully even within this competitive setup. Anyway, the were not able to obey the rule to avoid physical conflict, thus only several rounds of this setup was executed.

visualizes by the iso-value curves presented in Figure 6.3. Such potential optimizes the reproduction of observed funnel-like shape of crowd by the simulations, but it brings another (hardly calibrated) set of parameters. As the overtaking and line formation can be controlled by sensitivity parameters, we will used the standard spherical potential in all simulations described further.

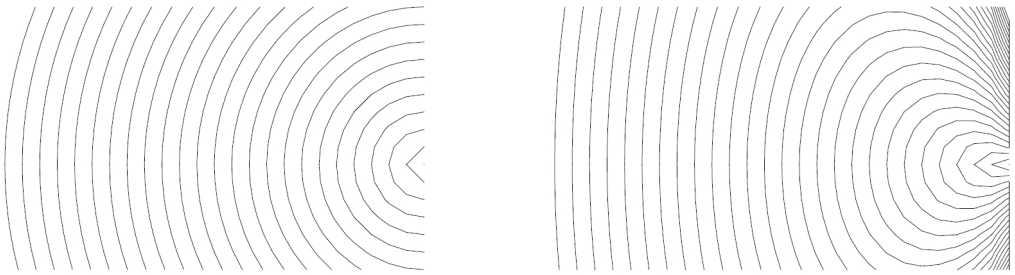


Figure 6.3: Demonstration of suggested potential.

Here we note that the equation (6.1) is applicable to define the required potential modification only for normal conditions without obstacles, where the average direction of pedestrian cloud center towards exit is in the positive $x$ direction. The generalization to more complex geometries requires more detailed experimental study and further discussion.

## 6.2 Symmetry

The independence of the motion to the lattice is obvious natural requirement. The travel time should be the same as the distance is the same no matter whether an agent moves north, south, east or west. Such requirement was tested on the travel time dependence on the motion-grid angle as visualized in 6.4. The correct result is "independence".

As defined in previous chapter, we try to reach the symmetry using hopping probability penalization and agent's period penalization.

### 6.2.1 Probability Penalization

Applying diagonal penalization to decision probability, we could reach the same travel time for all desired angles even without time penalization, see 6.5.

Symmetry of the movement is influenced by the strength of exit (or sensitivity to potential). By increasing the strength the behavior becomes more deterministic, agents tend strongly to follow the shortest path. It implies that constant value of diagonal penalization cannot remove asymmetry in general. Fortunately it is necessary to remove the asymmetry just for reasonable interval of strength parameter. Model must by symmetric in areas corresponding to "real motion", and it is neither perfectly deterministic nor chaotic.

During testing, we determined the optimal value of diagonal penalization $C = 0.15$. This value assures that the number of steps does not depend on angle in area of used strength

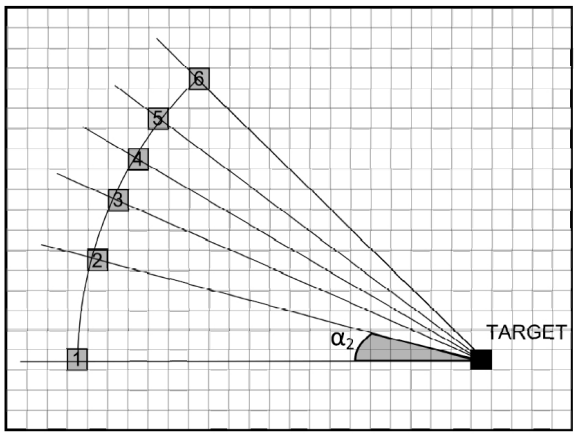


Figure 6.4: Design of testing the symmetry. The euclidean distance of points 1 – 6 to the target is the same (20 cells), hence the time distance must be equal.

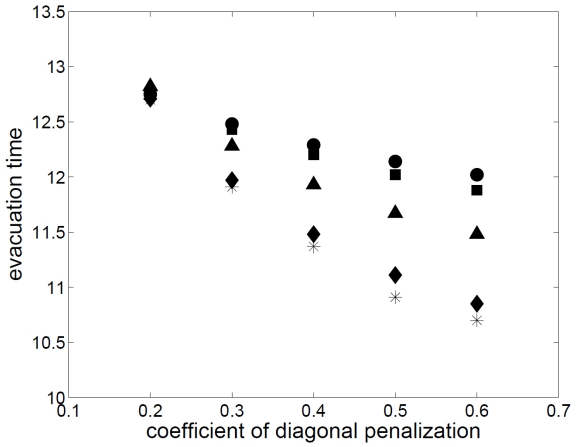


Figure 6.5: Influence of diagonal penalization coefficient to travel time. 100 000 simulations ran for 5 initial positions according to Figure 6.4, 10 cells far from attractor (position labels: 1 – circle, 3 – square, 4 – triangle, 5 – diamond, 6 – star), the strength of exit was set to $k_O = 0.2$, $k_\eta = 0.7$, $k_U = 1$, $F = 2$. Lower value of coefficient corresponds to higher penalization.

of the exit (see the graph in Figure 6.6). The model uses strength from interval $F \in \langle 2, 3 \rangle$, where value $F = 2$ corresponds to chaotic behavior and the value $F = 3$ represents almost deterministic movement. The chaoticity was assessed with respect to the number of random deviations.

This solution has unfortunately crucial disadvantage: In case of diagonal direction to target cell, one diagonal step is, with some level of randomness, followed by a pair of horizontal and vertical steps. On average, three time steps are used to travel $2 \cdot \sqrt{2} \approx 3$ distance units, that is ok. But the alternations of diagonal and orthogonal steps cause a rough trajectory with frequent changes of actual direction. That is in conflict with observed straight movement. As our goal is to model even microscopic features, we have to introduce another approach.

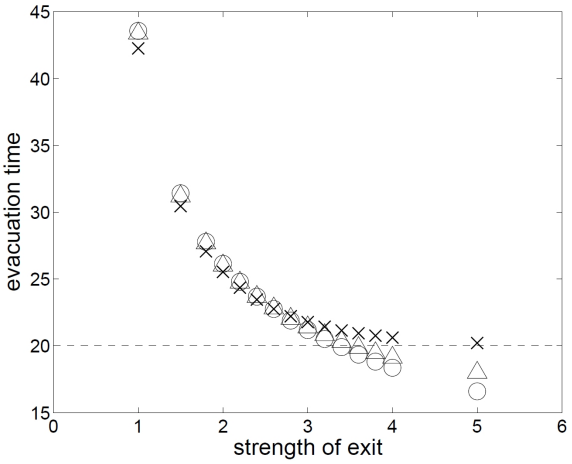


Figure 6.6: Travel time with respect to strength of attractor, the hopping probability of diagonal movement is penalized ($C = 0.15$). Marks represent different angles, see Figure 6.4 – labels $\times, \triangle, \circ$ represent starting position 1,4,6. For each of them, 10 000 simulations were performed for different strengths. The values of other parameters are following: $k_O = 0.2$, $k_\eta = 0.7$, $k_U = 1$.

### 6.2.2 Time Penalization

Another idea is to release strict time management and adjust time consumption of a step with respect to the step length. It brings several complication, but as already explained in section 5.3, this approach has multiple benefits.

As seen in Figure 6.7, the evacuation time after applying $\tau_i^D = 0.5$ is still relatively different for different angles. The minimal time does not drop under 20 s as expected with respect to the distance, but the time for "orthogonal" directions is too high.

The figure 6.8 illustrates the most likely deviations from straight direction for both, orthogonal and diagonal movement. It is evident that the deviations are less profitable in case of diagonal direction, due to the higher difference of the distance to the exit. Therefore the probability of deviations is higher for orthogonal movement that cause higher travel time.

Even time penalization does not decrease the asymmetry to the required level, it seems optimal solution should combine both approaches.

### 6.2.3 Synthesis

As a final solution, we have calibrated probability penalization for values of the strength of the exit $F \in \langle 1, 4 \rangle$ with activated time penalization. The dependency of travel time to the strength of attractor was evaluated for multiple values of $C$, as seen in the Figure 6.9, the asymmetry vanished for the probability penalization set to $C = 0.2$.

Here we should note that this value differs from the value of penalization introduced in previous section. It is natural as first approach normalized the system without the time penalization.

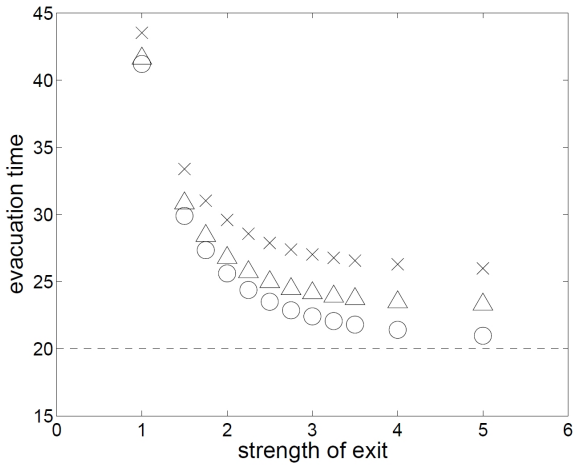


Figure 6.7: The graph of evacuation time (measured in real time) with respect to the strength of the exit. The influence of time penalization was included, in contrary to probability penalization ($C = 1$). Markers represent different angles, see Figure 6.4 – labels $\times$, $\triangle$, resp. $\circ$ represent starting position 1, 4 resp. 6. For each of them, 10 000 simulations were performed. The values of other parameters are following: $k_O = 0.2$, $k_\eta = 0.7$, $k_U = 1$.

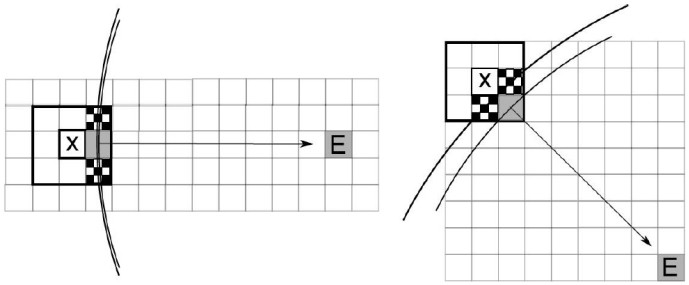


Figure 6.8: Most likely deviations from straight direction. Gray color represents the best cell, squared cells illustrate given deviations.

## 6.3 Heterogeneity in Parameters

One of the most important observation from our experimental study E4 is the fact that the pedestrian differs. It does not sound like a big surprise, but the dramatic differences of evacuation time among the participants passing the room in the same time deserves to be reflected in the model.

### 6.3.1 Heterogeneity in Velocity and Aggressiveness

The effect of the aggressiveness has been studied by means of the simulation in paper [12]. Results stressed in this article come from the simulations with parameters given by Table 6.3. The values of $\tau_i$ and $\gamma_i$ are distributed among agents uniformly and independently on each other.

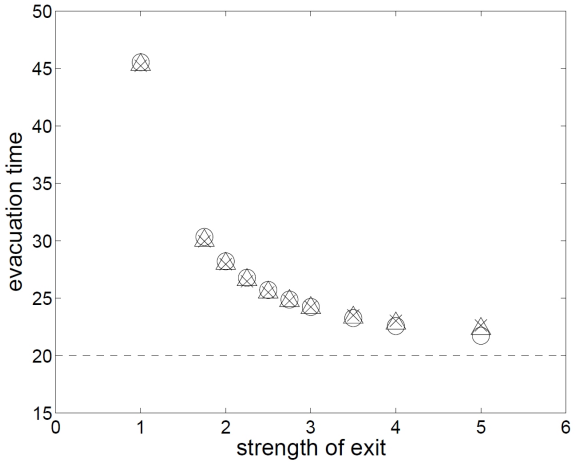


Figure 6.9: Evacuation time with respect to the strength of exit. The influence of both time penalization and probability penalization ($C = 0.2$) was included. The marks represent different angles, see Figure 6.4 – labels $\times, \triangle, \circ$ represent starting position 1,4,6. For each of them, 10 000 simulations were performed. The values of other parameters are following: $k_O = 0.2$, $k_\eta = 0.7$, $k_U = 1$.

| $k_S$ | $k_O$ | $k_D$ | $h$ | $\mu$ | $\tau$ | $\gamma$ |
|---|---|---|---|---|---|---|
| 3.5 | 1 | 0.7 | 0.1 s | 0.5 | $\{.25, .4\}$ | $\{0, 1\}$ |

Table 6.3: Values of parameters used for simulation of aggressiveness Only.

The simulation set-up has been designed according to the experiment, i.e., the room of the size 7.2 m $\times$ 4.4 m has been modeled by the rectangular lattice 18 sites long and 11 sites wide. The size of one cell therefore corresponds to 0.4 m $\times$ 0.4 m. The exit is placed in the middle of the shorter wall, the open boundary is modeled by a multiple entrance on the opposite wall. New agents are entering the lattice stochastically with the mean inflow rate $\alpha$ [pedestrians/second]. The inflow rate is a controlled parameter. For more detailed description of the simulation we refer the reader to [7].

It has been shown that such system evinces the boundary induced phase transition from the free flow (low number of agents in the lattice) to the congestion regime (high number of pedestrians in the lattice) via the transient phase (number of pedestrians fluctuating between the low and high value). Therefore, wise choice of different inflow rates $\alpha$ covering the all three phases, enables us to study the dependence of the travel time $TT$ on the average number of agents in the lattice $N_{\text{mean}}$. When simulating with parameters from Table 6.3, the correct choice of inflow rate is $\alpha \in [1, 3]$.

Figure 6.10 shows the dependence of the travel time $TT = T_{\text{out}} - T_{\text{in}}$ on the average number of agents in the lattice $N_{\text{mean}}$ calculated according to (2.2). Measured data consisting of pairs $(N_{\text{mean}}, TT)$ are aggregated over simulations for inflow rate values $\alpha \in \{1, 1.5, 1.8, 2.0, 2.3, 2.7, 3.0\}$; for each inflow $\alpha$ twenty runs of the simulation have been performed. Each run simulates 1000 s of the introduced scenario starting with empty room. Agents were distributed into four groups according their own period $\tau$ and aggressiveness $\gamma$, namely "fast aggressive" ($\tau = 0.25$, $\gamma = 1$), "fast calm" ($\tau = 0.25$, $\gamma = 0$), "slow aggressive"

($\tau = 0.4$, $\gamma = 1$), and "slow calm" ($\tau = 0.4$, $\gamma = 0$).

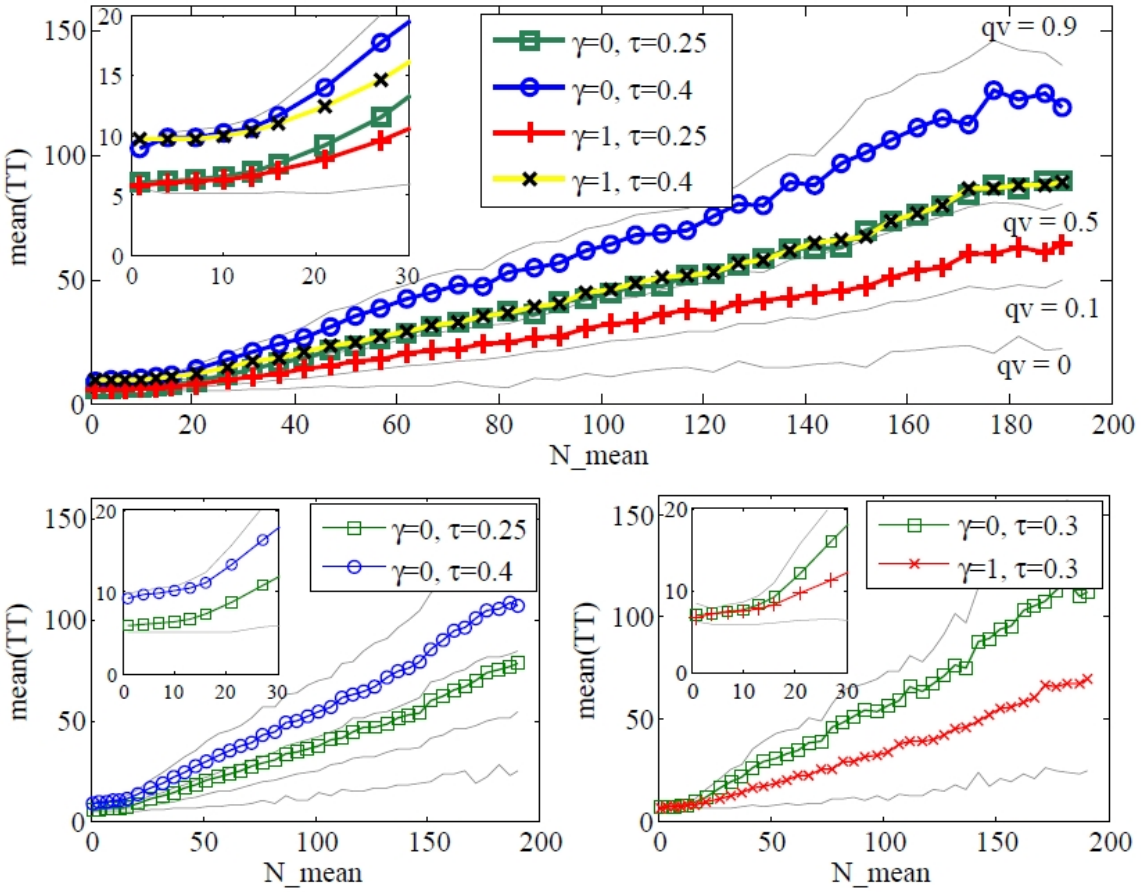


Figure 6.10: Dependence of the mean travel time $TT$ on the average occupancy $N_{\text{mean}}$ for each group of agents. Gray lines represent the quantiles of the travel time regardless to the groups. Top: heterogeneity in both, $\gamma$ and $\tau$. Bottom left: heterogeneity in $\tau$. Bottom right: heterogeneity in $\gamma$.

In the graph of the Figure 6.10 we can see the average travel time for each group calculated with respect to the occupancy of the room. It is evident that for low occupancy up to 10 agents in the room the mean travel time for each group levels at a value corresponding to the free flow velocity given by the own updating period. For the occupancy above 20 agents in the lattice, the linear growth of the mean travel time with respect to $N_{\text{mean}}$ is obvious. Furthermore, the average travel time for fast-calm corresponds to the travel time of slow aggressive. The Figure 6.10 shows two auxiliary graphs presenting the dependence of $TT$ on $N_{\text{mean}}$ for systems with homogeneity in $\gamma$ (left) or in $\tau$ (right). From the graphs we can conclude that the heterogeneity in aggressiveness $\gamma$ reproduces the desired variance in the slope of the graph without the non-realistic high variance in free flow generated by the heterogeneity of own updating frequency.

The influence is even more evident from the graph in Figure 6.11 representing a plot of all travel time entries with respect to the time of the exiting $T_{\text{out}}$. Right graph shows the box-plots of the travel time for four groups measured after 500 s from the initiation, i.e., in the steady phase of the system. We can see that in this view, the aggressiveness plays

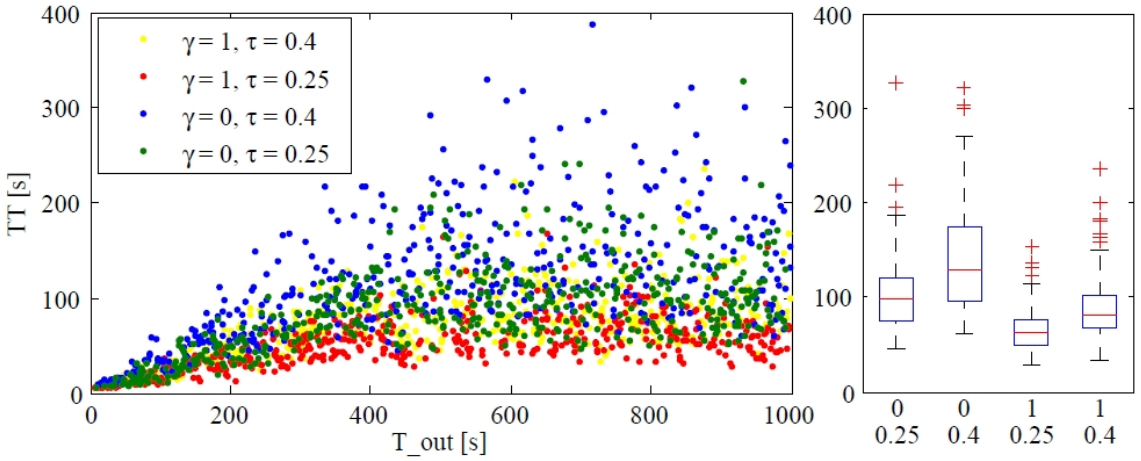


Figure 6.11: Left: Development of travel time $TT$ in time for one run of the simulation. The value $TT$ is plotted against the time of the exit $T_{\text{out}}$ to ensure that values corresponding to the same time stem from similar conditions near the exit. Inflow rate $\alpha = 3$ ped/s. The agent group is indicated by the color. Right: Box-plots of the travel time for entries with $T_{\text{in}} > 500$ s (i.e. in the steady state).

more important role that the desired velocity of agents.

### 6.3.2 Heterogeneity in Sensitivity to Occupation

Main goal of this section is to append the heterogeneity in the sensitivity of occupation to the arrangement presented in previous section. As summarizes in the article [14] we focus on the heterogeneity in free-flow velocity (represented by own frequency), aggressiveness, and sensitivity to occupation.

#### Experimental Setup

In order to have comparable results to the experiment, the parameters have been calibrated to give similar values of important macroscopic quantities as free flow velocity (1.57 m/s in experiment) and maximal outflow (1.4 ped/s in experiment). The used set of parameters is given in Table 6.4.

The free flow simulation (without interactions) is directly influenced by $k_U$, $C$ and $\tau_i$. The diagonal penalization $C$ together with time penalization of diagonal motion have been tested in previous research. The values of $k_S$ and $\tau_i$ have been chosen to agree with the mean and variance of the free-flow velocity. Here we note that the pedestrians in the experiment walked relatively fast (1.57 m/s), which motivated us to set the algorithm step $\tau = 0.2$ s of real time to balance significant decrease of velocity in congested regime.

The motion of agents in crowd is influenced by parameters $\mu$, $\gamma_i$, and $k_O$. These parameters have been calibrated to fit the maximal outflow from the exit in congested situation, i.e, the exit capacity (1.4 ped/s). The significant decrease of velocity in crowd is modeled by means of relatively high friction $\mu = .9$. Here we note that such high friction is necessary

| Parameter | Value | Range | Description |
|---|---|---|---|
| $\Delta m$ [cm] | 0.4 | | Lattice constant |
| $k_U$ | 3.5 | $[0, \infty)$ | Sensitivity to potential |
| $C$ | 0.7 | $[0, 1]$ | Penalization of diag. motion |
| $\mu$ | 0.9 | $[0, 1]$ | Friction parameter |
| $\tau$ [s] | 0.2 | $(0, \infty)$ | Length of one time step |
| $\tau_i$ [s] | 0.2 | $(0, \infty)$ | Homogeneous own period |
| | $\{0.15, 0.4\}$ | | Heterogeneous own period |
| $\gamma_i$ | 0.14 | $[0, 1]$ | Homogeneous aggressiveness |
| | $\{0, 1\}$ | | Heterogeneous aggressiveness |
| $k_O$ | 0.9 | $[0, 1]$ | Homog. sensitivity to occupation |
| | $\{0.1, 0.95\}$ | | Heter. sensitivity to occupation |

Table 6.4: Parameter values and description

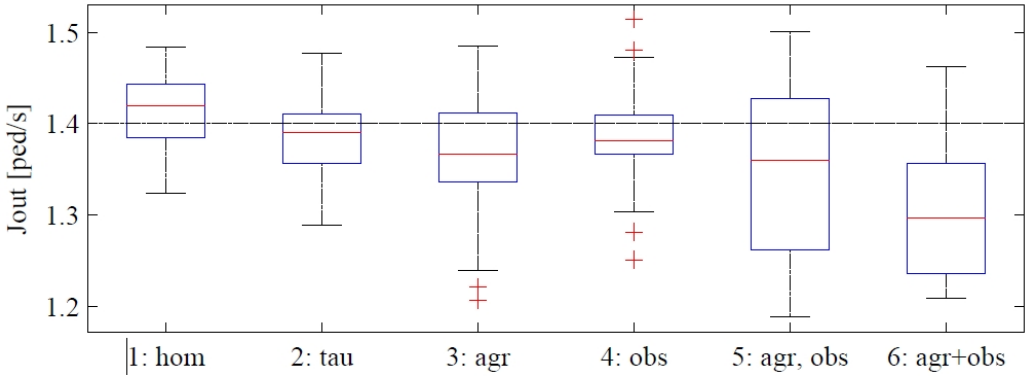


Figure 6.12: The box-plots of outflow $J_{\text{out}}$ from the congested room ($N = 50$) measured for 20 runs of the simulation experiment for each parameter set. The box gives information about .25, .5, and .75 quantile.

to compensate the conflict solution mechanism related to aggressiveness and the motion in lines related to the sensitivity to occupation.

Our goal is to illustrate the effects of heterogeneity in chosen parameters. Therefore, the values of outflow had not been calibrated directly to the value 1.4 m/s, but sufficiently close to it, see Figure 6.12. Such approach enables to fit the homogeneous and heterogeneous values of each parameter independently and therefore can be used in all considered scenarios – 1: hom (homogeneous in all parameters), 2: tau (heterogeneous in velocity), 3: agr (heterogeneous in aggressiveness), 4: obs (heterogeneous in sensitivity to occupation), 5: agr,obs (heterogeneous in aggressiveness and occupation independently), 6: agr+obs (heterogeneous in aggressiveness and occupation with dependence, i.e., there are only two groups of agents: aggressive more sensitive to occupation and non-aggressive less sensitive to occupation).

The simulation was performed for system with periodic boundaries, i.e., the egress of an agent causes the entrance of another one (contrary to [12], where open boundaries were used giving the same results). The properties of agents $(\tau_i, \gamma_i, k_O)$ were drawn from uni-

form distribution on the groups of parameters. For each set of parameters the simulations were executed for the occupancy $N \in \{1, 3, 5, 7, 10, 12, 14, 17, 20, 30, 40, 45, 50, 75, 100\}$. The simulation was carried on until 1000 agents walked through the exit and it was repeated 20 times. All quantities are averaged.

### Simulation Results

In Table 6.5 the measured values of free flow velocity $v_0$ (velocity for agents under the occupancy $N \leq 4$), maximal outflow $J_{\text{out}}$, and average travel-time $\overline{TT}_N$ for all 6 settings are compared to the experimental values. From the values we can see that the average travel-time is slightly, but not significantly, overestimated by the model. The lower free-flow velocity in case (2: tau) is caused by the heterogeneity in velocity; This set of parameters does not allow to fit both, the free-flow velocity and the outflow. The reason lies in the synchronous update with $\tau = 0.2$ s. As will be discussed below, the heterogeneity in velocity defined by the own frequency is not desirable for the presented model with respect to the performed experiment.

| | Exp. | 1:hom | 2:tau | 3:agr | 4:obs | 5:agr,obs | 6:agr+obs |
|---|---|---|---|---|---|---|---|
| $v_0$ [m/s] | 1.57 | 1.11 | 1.57 | 1.57 | 1.57 | 1.57 | 1.57 |
| $J_{\text{out}}$ [ped/s] | 1.40 | 1.42 | 1.39 | 1.37 | 1.38 | 1.35 | 1.30 |
| $\overline{TT}_{45}$ [s] | 24.31 | 30.74 | 30.76 | 30.72 | 31.17 | 32.01 | 33.05 |
| $\overline{TT}_{100}$ [s] | – | 67.74 | 66.83 | 67.84 | 67.52 | 67.63 | 70.59 |

Table 6.5: Average quantities measured for different parameter settings.

The main stress is given to the travel-time study and dependence on the average occupancy $N_{\text{mean}}$, which reflects the heterogeneity in the reaction to the crowd. The $TT - N_{\text{mean}}$ plots for studied parameter sets are given in Figure 6.13. In the graphs the mean travel time is plotted according by groups with the same parameters, the overall mean and quantiles are present for completeness. From the graphs it is evident that the model is able to mimic the piece-wise linear dependence (3.5) of $TT$ on $N_{\text{mean}}$, which is present in the experimental study. The break-point of the model is in agreement with the experimental observation at the value $N = 7$.

We can see quite good agreement with the experiment regarding the trend of the dependence of $TT$ on the occupancy not only in average but also in the minimal and maximal measured values, see Figure 3.15. Due to to significantly lower volume of data from the experiment it is reasonable to compare the 0.1 and 0.9 quantiles. Here we note that the lower average $TT$ in experiment (24.31 s) than produced by the model (approx. 30 s) is caused by the small volume of data related to $N \approx 45$ in the experiment – such crowded conditions were kept for relatively short time due to the small number of participants (75).

We can see that the differences in the slope of the linear dependence can be observed in all heterogeneous scenarios. Nevertheless, for further studies we have neglected the heterogeneity in the own updating period $\tau_i$, related to velocity. Even the homogeneous setting of free-flow velocity can reproduce variances in the free-flow travel-time in sufficient manner due to the stochastic nature of Floor-Field model. Therefore, another heterogeneity in the parameter $\tau_i$ is redundant. On the other hand, the concept can be used in case of

evident heterogeneity where the desired velocity significantly differs [80, 128].

The heterogeneity in aggressiveness parameter $\gamma_i$ becomes evident in occupancy $N \in (10, 50)$, the effect does not rise significantly for higher occupancy, see sub-figure 3. Complementary evinces itself the heterogeneity in sensitivity to occupancy $k_O$ (sub-figure) 4, which becomes most evident for occupancy $N > 50$. Interesting results brings the combination of these two parameters. The scenario 5 shows that the heterogeneity in $\gamma_i$ and $k_O$ combines both effects from 3 and 4 in superposition manner. The scenario 6 (aggressiveness and occupancy are dependent) shows the highest difference in the slope of $TT$.

Here we note that the sensitivity to occupation should be interpreted as the willingness to join an existing queue in order to move along this queue. It is therefore reasonable to suppose that the aggressive behavior is related to the willingness to overtake, i.e., $k_O \to 1$.

For further comparison let us focus on the distribution of the relative travel time $TT_R$. In Figure 6.14 we can see the histograms of $TT_R$ for scenarios 1, 3, and 6, i.e., with increasing heterogeneity. We can make a conclusion that with increasing heterogeneity the relative frequency of low values of $TT_R$ (first bin) increases. Similarly, the modus of the distribution is closer to lower values for higher heterogeneity (bins 4, 3, 2).

Looking at the histograms of $TT_R$ related to heterogeneous scenarios, we conclude that the final distribution can be considered as a mixture of two uni-modal distribution corresponding to two groups of agents, which seems to be the case of the experiment as well.

Although some differences between scenarios 3 and 6 are evident, they might be considered as marginal in comparison with the homogeneous case 1. Let us therefore focus on another aspect observed during the experiment – the path choice. In Figure 6.15 we can see the snapshots from the simulation showing a representing situation of the simulation. In scenario 3, the more aggressive agents are more successful in pushing through the crowd, but they do not evince any preference in path-choice. In scenario 6, the aggressive agents prefer walking around the crowd and hopping to the exit from the left or right. As a consequence, less aggressive agents standing in lines remain often trapped few cell away from the exit, as often observed during the experiment.

### Summary and Conclusions

In this section we have shown that the heterogeneity in the ability to win conflicts is necessary to reproduce experimentally observed behavior in cellular models. Such property can be useful for proper modeling of an evacuation of a complex structure, where the heterogeneity in the ability to win conflicts is expected. In such cases a group of people can remain trapped within the facility for unjustifiable long time, although the average flows and evacuation times fulfill the expectations.

The introduced aspects of heterogeneity can be summarized as follows:

1. **Velocity:** The heterogeneity in velocity causes undesired bi-modal histogram in the free-flow regime. The observed heterogeneity in pedestrian sample can be sufficiently modeled by the stochastic nature of the decisions, the variance in the travel time is then related to the number of deviations from the direct path. Nevertheless, the concept can be used in dramatically heterogeneous scenario where the average speed of one group of pedestrians is two times higher than the average velocity of other

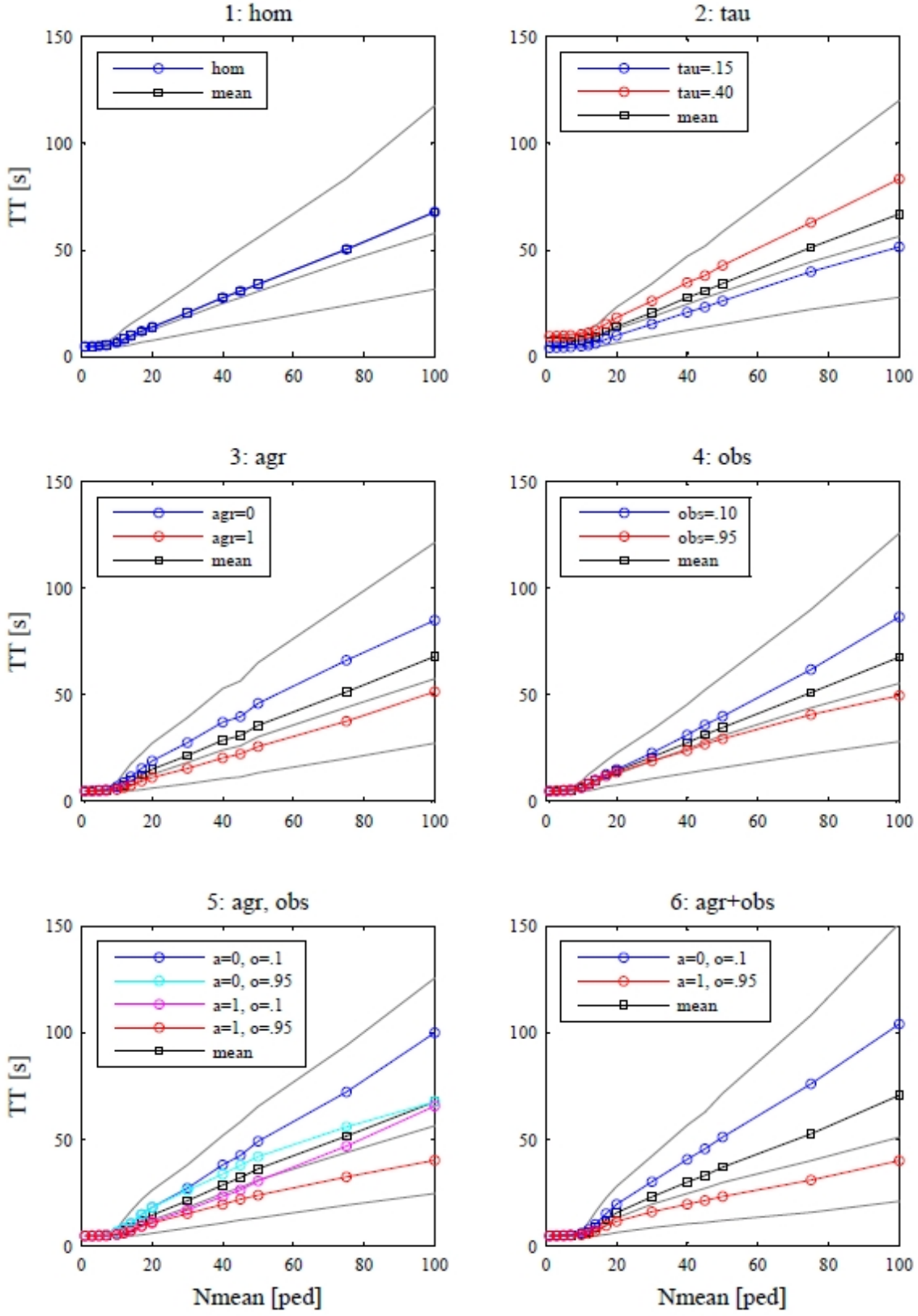


Figure 6.13: Average travel against mean occupancy plotted by groups. Black line represents the mean over all entries, gray lines correspond to 0.1, 0.5, and 0.9 quantiles. Colors distinguish individual groups, the values of heterogeneous parameters are given in legends.

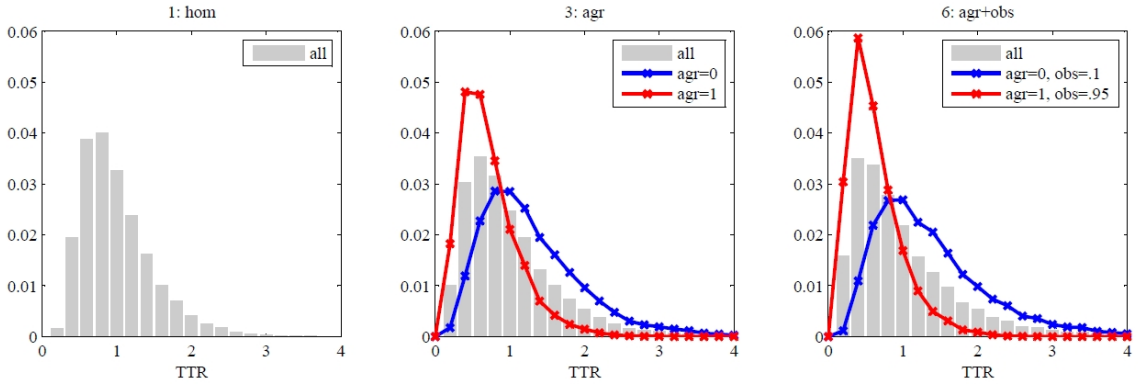


Figure 6.14: normalized histograms of relative travel-time $TT_R$ for scenarios 1: hom, 3: agr, and 6: agr+obs.

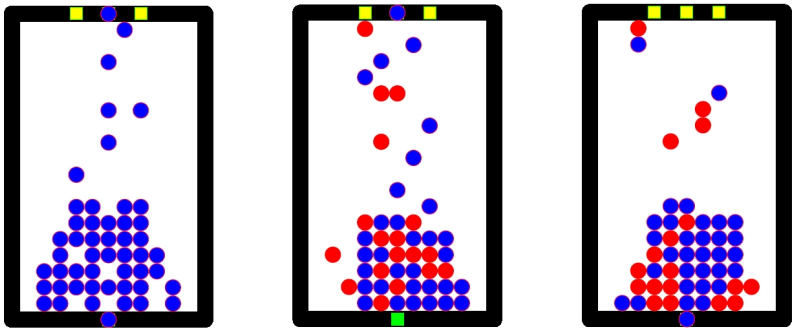

Figure 6.15: Snapshots from the simulation of scenarios 1: hom, 3: agr, and 6: agr+obs approximately 60 s after initiation. By red dots are marked more aggressive pedestrians.

group. Here we note that this conclusion is valid for models with parallel (or partially parallel) update enabling the presented conflict solution. In case of asynchronous update the heterogeneity in desired speed plays important role, as e.g. in [140].

2. **Aggressiveness:** This conflict-solution method, where the conflict is won by the agent with higher value of aggressiveness, seems to be very efficient to reproduce the high variance of the $TT$ in the congested regime. In combination with the heterogeneity of the velocity we are able to simulate a situation when slower agent is more aggressive than a fast one. It is important to note that the term aggressiveness may be a little bit misleading, since it corresponds to the ability to win conflicts, which may be given by some rules of preference as well.

3. **Sensitivity to Occupancy:** This aspect influences mainly the space usage by the agent in given conditions. The lower the sensitivity is, the higher is the average $TT$ for the agent, since he waits in lines and can be overtaken and trapped in front of the exit. This parameter plays very important role in combination with the parameter of aggressiveness.

## 6.4 Phase transition

### 6.4.1 First Insight

The above mentioned model has been used to simulate the phase transition analogically to [54], where a situation of a rectangular room with one entrance and one exit has been introduced. The phase transition occurs due to the change of the inflow parameter $\alpha$. In [54], the situation was studied by means of simple Floor Field model with aggressiveness parameter $\zeta$. In this section, we present the experiment "passing through", which was inspired by the setting mentioned above.

Within E3, eight inflow settings have been considered. The setting is characterized by the number of entering pedestrians $n_s$ and the mean value of time headway $\mu_s$. From these the average inflow current $J_{\text{in}}$ can be calculated as $J_{\text{in}} = n_s/\mu_s$ pedestrians per second. As we have used the time unit corresponding to 0.31 s as the algorithm step, we define $\alpha_{\text{exp}} = J_{\text{in}} \cdot 0.31$ pedestrians per model time unit (TU). This value gives the average inflow rate per time step, which is used for simulations. That means $\alpha_{\text{exp}}$ should represent the probability of the injection of new pedestrian to the system within one $TU$. Experimentally measured values are given in Table 6.6.

| setting | $\mu_s$ | $n_s$ | $J_{\text{in}}$ | $\alpha_{\text{exp}}$ | observed state |
|---|---|---|---|---|---|
| 1 | 1.78 | 2 | 1.12 | 0.35 | free flow |
| 2 | 1.68 | 2 | 1.19 | 0.37 | free flow |
| 3 | 1.59 | 2 | 1.26 | 0.39 | free flow |
| 4 | 1.43 | 2 | 1.40 | 0.43 | temporary cluster |
| 5 | 1.85 | 3 | 1.62 | 0.50 | stable cluster |
| 6 | 1.72 | 3 | 1.74 | 0.54 | congestion |
| 7 | 1.66 | 3 | 1.81 | 0.56 | congestion |
| 8 | 1.57 | 3 | 1.91 | 0.59 | congestion |

Table 6.6: Experimental setting: inflow rates

As seen from Table 6.6, the settings were classified according to macroscopic observations: free flow regime, congested regime, and meta-stable regime. In the free flow regime (settings 1, 2, and 3) pedestrians walked freely through the room and did not block each other in front of the bottleneck. In meta-stable regime, occasional conflict in front of the exit resulted to a small cluster formation, which melted after short time period (setting 4) or stabilized, but fluctuated around 5 pedestrians in the cluster (setting 5). By increasing the inflow rate, the competition at the door significantly blocks the motion and rapidly increases size of the stable cluster which fills in significant part of the room (settings 6, 7, and 8).

Analogical observation was made by the simulations using the model described in previous section. The transition from free regime to the stable congestion was observed at the inflow rate $\alpha_{\text{sim}} \in \langle 0.42, 0.46 \rangle$ pedestrians per second, which corresponds to the experimental observation. At the critical values of $\alpha_{\text{sim}}$, the creation and melting of the temporary cluster was highly supported by the asynchronous update and bounds principle.

These observations motivated us to investigate the phase transition in detail.

### 6.4.2 Detailed Observation

The study [10] focuses on the critical behavior, where the increasing inflow of pedestrians leads to the clogging inside the room and significant drop of the flow. Consider a rather small rectangular room with one small exit and one multiple entrance. Pedestrians are entering the room with known (or given) intensity $\alpha$ [pedestrians/second] in order to pass through and walk out of the exit. Such scenario has been investigated in [52] by means of a simple version of Floor-Field model [77, 96] with friction function [148]. Similarly to the well known one-dimensional TASEP model [48], a boundary induced phase transition from free flow to congested regime has been observed as well as the metastable transient state at the transition point between those two phases.

This article introduces a transformation of the presented modifications into the language of CA with isochronous steps. By means of the numerical calculations of the CA, the influence of bonds, asynchronous update, and heterogeneity to the inflow induced phase transition from free flow to congestion is studied and compared to the experiments.

The existence of the so called low and high density phase in dependence on the boundary parameters is a typical feature of cellular models based on hopping of particles. In this section we aim to investigate the transition from the low to the high density in stated models. As shown e.g. in [52], the transition is very sensitive to model parameters and divides the parametric space into phases.

The parameter $k_U$ has been set to the value $k_U = 3.5$ to balance the deterministic motion in free flow and stochastic behavior in the congested cluster (see [4] or [5]). As will be explained in detail below, for purposes of this article two values of $k_O$ have been chosen: $k_O = 1$ corresponding to the situation that occupied cells are excluded from the decision process and $k_O = 0$ incorporating the possibility of choosing an occupied cell, which is closely related to the principle of bounds. Analogically, $k_D = 1$ corresponds to the von Neumann neighborhood and $k_D = 0.7$ corresponds to the Moore neighborhood with certain diagonal movement penalization [4].

#### Phases Classification

The term density refers to the ratio of occupied cells to the number of all cells in the lattice. Let us in the following denote the number of occupied cells in time $t$ as

$$N_t = \sum_{x \in \mathbb{L}} \mathbf{1}_{\{\tau_t(x) > 0\}} \,, \tag{6.2}$$

where $\mathbf{1}$ is the identifier of the event. The number of occupied cells (referred to as the occupancy) will in the following play the role of the density, since the number of cells of the CA remains constant.

One way to study such system is to investigate its' steady-state properties. Since the process is assumed to be ergodic, steady state occupancy corresponds to the long time average denoted as $N_\infty$. The intuitive look at the open boundary system suggests that the steady-state occupancy increases linearly with the inflow alpha until it reaches the capacity of the exit, which leads to the complete filling of the room. This jump in the $N_\infty - \alpha$ diagram may be understood as the transition from the free flow (linear dependence) to the congested regime (filled room).

We aim to investigate such transition based on the observation of system with rather low number of cells observed in a finite time horizon, since it corresponds to the measured experiments. In such case, the transition is rather smooth than jump-like.

To classify the phases properly, we use the sample average occupation $\langle N_t \rangle = \frac{1}{K} \sum_{k=1}^{K} N_{t;k}$ averaging the actual occupation $N_t$ over $K = 30$ trajectories of the stochastic model.

Classification of the phases is then as follows:

1. *Free flow*: Low inflow leads to the absence of interactions near the exit. Only a temporary increase of the number of occupied cells may occur in front of the exit. $N_t$ levels at low value $N_\infty$. The steady-state occupancy $N_\infty$ increases linearly with $\alpha$.
2. *Congestion*: The inflow $\alpha$ exceeds the exit capacity and individuals fill-in almost the whole lattice. $N_t$ stabilizes, levels around high value $N_\infty$. The steady-state occupancy $N_\infty$ is independent on $\alpha$.
3. *Transient phase*: Individual trajectories of the model can correspond to both above mentioned phases. The variance of $N_t$ is high in the sense of the sample variance as well as in the time variance along one trajectory.

Representative trajectories corresponding to individual phases are depicted in Figure 6.16.

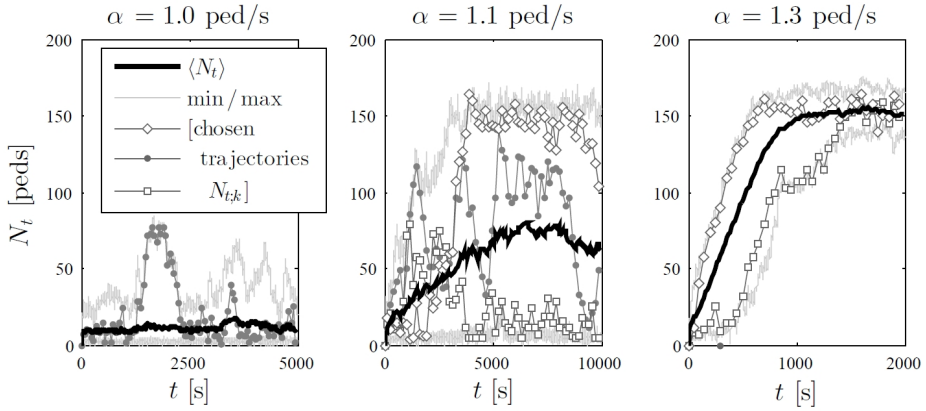


Figure 6.16: Time evolution of the average occupancy $\langle N_t \rangle$ (black line), minimal and maximal occupancy $\min_k N_{t;k}$, resp. $\max_k N_{t;k}$ (gray lines), in comparison to individual samples: above the average ($\diamond$), oscillating ($\bullet$), and below the average ($\square$). $h = 0.3$, $k_O = 0$, homogeneous. Free flow (left), transition (middle), congestion (right).

### Simulation and Considered Settings

The model has been studied by means of computer simulation for 18 different settings of model parameters in order to investigate their influence on the boundary induced phase transition. Investigated features are: time-step length $\tau$, i.e., synchronism of the update; principle of bonds, i.e., possibility of choosing the occupied cell represented by parameter $k_O$; and heterogeneity of the own frequency $\tau_i$. Other parameters have been fixed.

Based on the previous studies [52, 5] the fixed parameters have been set to following values: $\mu = 0.7$ – high friction to slow down the motion within the crowd, $k_S = 3.5$ – to balance the

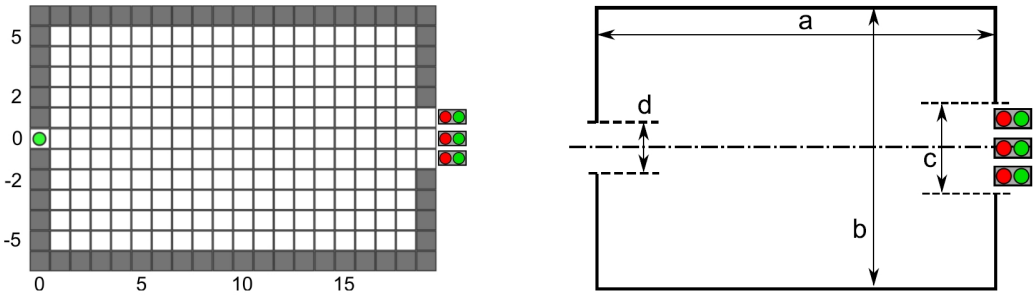


Figure 6.17: The room with parameters $a = 7.2$ m, $b = 4.4$ m, $c = 1.3$ m; $d = 0.5$ m is modeled by the rectangular lattice 11×18 cells, i.e., $w = 5$, $l = 18$.

deterministic and fully probabilistic choice of the target cell, $k_D = 0.7$ – due to symmetry analyses.

The time-step length has been chosen from the set $\tau =: h \in \{0.1, 0.2, 0.3\}$ s, i.e., from the asynchronous to synchronous update (mean value of $\tau_i$ is 0.3 s). The occupancy parameter $k_O \in \{0, 0.5, 1\}$, 0 means that occupation does not influence the probability (5.9), 1 means that the occupied cell is never chosen as a target cell. Homogeneous sample is characterized by the uniform own frequency $\tau_i = 0.3$ s, heterogeneous sample consists of individuals with own frequencies $\tau_i \in \{0.2, 0.4\}$ s.

All simulations started with empty room, i.e., all cells are unoccupied at the beginning.

As mentioned above, we focus on the simulation of passing through a room with the entrance on one side and the exit on the opposite side. To match the experiments described in [5] and [6], the room was equipped with one exit of the width corresponding to one cell and three entrances placed on the opposite wall to the exit, as illustrated in Figure 6.17. The inflow is controlled by the inflow parameter $\alpha$, which determines the number of pedestrians coming to the entrance per one second (i.e., if the room capacity is reached, agents are accumulated in front of the entrance). For purposes of the simulation, the room 7.2 m long and 4.4 m wide has been chosen. The cellular model used for the simulation is described below.

To simulate and control the randomized inflow of pedestrians into the room, geometric distribution was used. The number of steps between the input of two consecutive agents to one entrance $I_j$ is given stochastically by the geometric distribution, i.e., the probability of another agent coming to the row in front of the entrance $I_j$ is

$$p(k) = (\alpha h/3)(1 - \alpha h/3)^{k-1}\,, \tag{6.3}$$

where $h$ is the length of the algorithm step, which depends on the used updating scheme, as described below.

### Simulation Results

For each settings 15 scenarios corresponding to different values of inflow rate $\alpha \in [0.5, 3]$ have been investigated by means of the computer simulation. The statistics is based on the

sample average over $K = 30$ trajectories of each scenario. The dependence of the steady-state occupancy $N_\infty$ on the inflow rate $\alpha$ is depicted in Figure 6.18 for 9 settings with homogeneous own frequency (As follows from the graphs in Figure 6.20, the heterogeneity has only marginal influence to the phase transition).

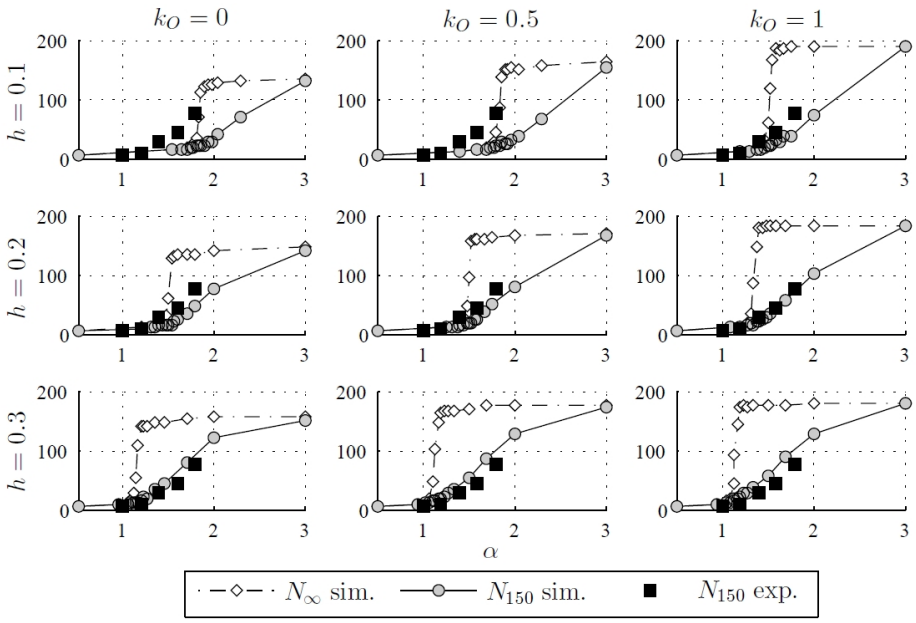


Figure 6.18: The dependence of $N_\infty$ ($\diamond$) and $N_{150}$ ($\circ$) on the inflow $\alpha$ in comparison to the experimental results ($\blacksquare$) from 150 s of the measurement.

For completeness the graphs are accompanied by the average occupancy $N_{150}$ in time $t = 150$ s in order to compare the simulation to the experimental results. Due to time demanding nature of the experiment, each run of the experiment was stopped after the number of pedestrian inside the room stabilized (in free flow or transition regime) or when the pedestrians were not able to enter the room according to given inflow rate (in congestion regime – majority of volunteers was inside the room). Therefore, 150 s seems to be good reference point for all runs of the experiment, for more detail see [8, 11].

Crucial feature in the phase transition is the critical inflow $\alpha_c$ corresponding to the transient state at the border between the free flow phase and congestion phase. To detect the transition by means of the simulation we have used the properties of the time of the first pass over the steady-state occupancy, defined as

$$T_k = \inf\{t \in [0, +\infty) \mid N_{t;k} \geq N_\infty\}\,. \tag{6.4}$$

From the mechanism of the phase transition it follows that the average time of the first pass $\langle T \rangle = \frac{1}{K} T_k$ increases with $\alpha$ in free flow and decreases with $\alpha$ in the congestion phase. Therefore, the critical inflow $\alpha_c$ is determined by the change of these trends, as depicted in Figure 6.19.

In Figure 6.20, the values of steady-state occupancy $N_\infty$ and critical inflow rate $\alpha_c$ are plotted according to considered settings. From these observations, several conclusions can be drawn:

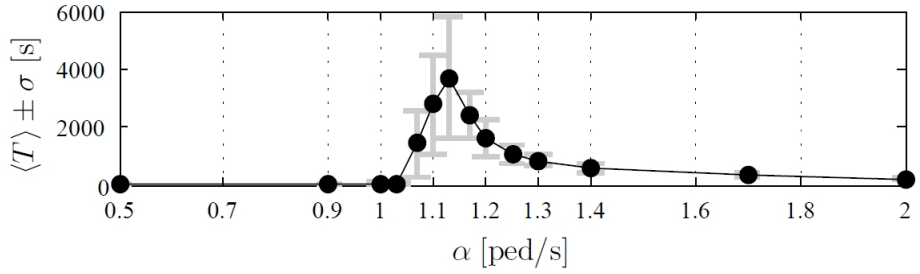


Figure 6.19: Determination of $\alpha_c$ by means of the time to the first pass of $N_{t;k}$ over the value $N_\infty$. Highest average $\langle T \rangle$ and highest variance of $T$ correspond to the upper estimation of the critical inflow $\alpha_c$. Example for $h = 0.3$, $k_O = 0$, homogeneous.

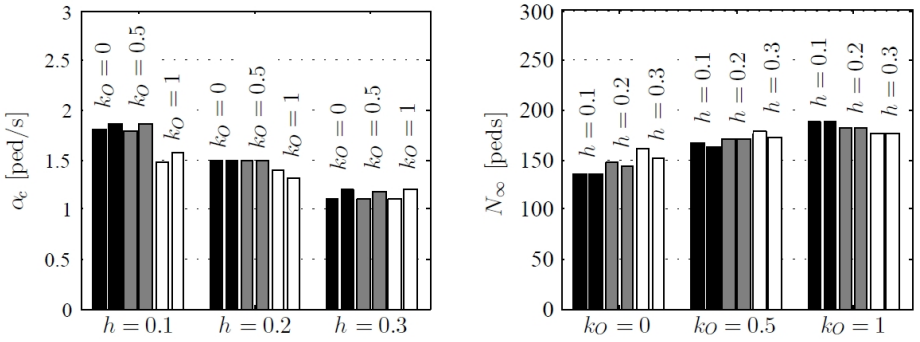


Figure 6.20: Comparison of individual settings according to investigated parameter. Left column of the same color corresponds to the homogeneous, right to the heterogeneous setting.

1. The Heterogeneity of the individuals does not have significant influence to the phase transition.

2. The principle of bonds influences mainly the steady-state occupancy $N_\infty$, but has not significant influence to the critical inflow rate $\alpha_c$. The more significant are the bonds in the model (decreasing $k_O$), the lower is the maximal occupancy. This can be interpreted in the way that individuals prefer standing in lines and have not such effort to fill the empty but disadvantageous cells.

3. The length of the time-step $h$ influences mainly the critical inflow rate $\alpha_c$, but does not significantly influence the maximal occupation. The more asynchronous the update is (lower $h$), the higher is the critical inflow, i.e., the higher is the outflow from the room, which corresponds to the room capacity. It is worth noting that the value of critical inflow $\alpha_c$ is highly influenced by the update rules for the exit cell $E$. In the original article [7], the exit cell has been emptied immediately after it was entered by the egressing individual. This leads to unrealistic high outflow for asynchronous update. Nevertheless, this feature may be used for smoother modeling of the varying exit width than is allowed by the size of the lattice cells.

| Heterogenous | Homogenous |
|---|---|
| HET: $\tau_1 = 0.3$ s, $\tau_2 = 0.4$ s | HOM: $\tau = 0.3$ s |
| No bounds | Bounds |
| F: $k_D = 1.0$ | O: $k_D = 0.0$ |
| Moore | von Neumann |
| M: $k_O = 0.7$ | N: $k_D = 1.0$ |
| Synchronous | Asynchronous |
| S: $h = 0.3$ | A: $h = 0.05$ |
| High friction | Low friction |
| H: $\mu = 0.7$ | L: $\mu = 0.2$ |

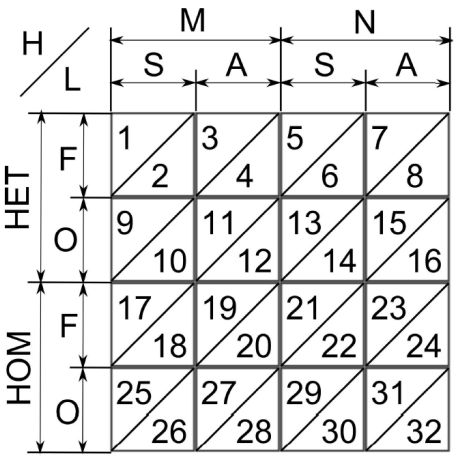


Table 6.7: Numbering of specific settings and given parameters. In the following figures, the setting is identified by the corresponding position as shown in the right part of the table, odd numbers represent high friction. Therefore, setting 11 means heterogeneity, bounds, asynchronous update, Moore neighborhood, and high friction.

### 6.4.3 Parametric Study

In [52] the transition from low density to high density phase in dependence on inflow parameter $\alpha$ has been investigated with respect to the friction function parameter $\zeta$. In this section (published in [7]) we focus on such dependence on the model type classified according to Table 6.7. The investigation is far from complete parameter investigation or validation. We aim above all to point out characteristic features and mechanism of the transition.

We distinguish 32 combinations of different representative settings according to Heterogeneity/Homogeneity; With/Without bounds; Moore/von Neumann neighborhood; Synchronous/Asynchronous update; High/Low friction. The numbering of given settings together with specific values of parameters is given in Table 6.7.

As we aim to investigate the system in the steady state, we have let the model to evolve for a long period. By the free flow setting we understand such set of parameters under which the room does not become overfilled by the agents. The congested setting is characterized by the creation of stable cluster in front of the exit, which size grows to the capacity of the room. By the transition from the free flow to the congestion phase we understand the change from free flow to congestion setting by increasing inflow parameter $\alpha$.

#### Results

For each of the 32 settings, simulations with variety of inflow parameters $\alpha$ have been performed. Three basic characteristics have been measured in the steady state: travel time, room occupancy and real inflow into the room. By the travel time we understand the time an agent spent in the room, i.e., from the time of the entrance (which is different from the time of coming to the row in front of the exit) to the time of leaving the room through the exit; room occupancy denotes the average number of agents inside the room, and the real inflow stands for the number of pedestrians entering the room per second. This quantity corresponds in the steady state to the average flow.

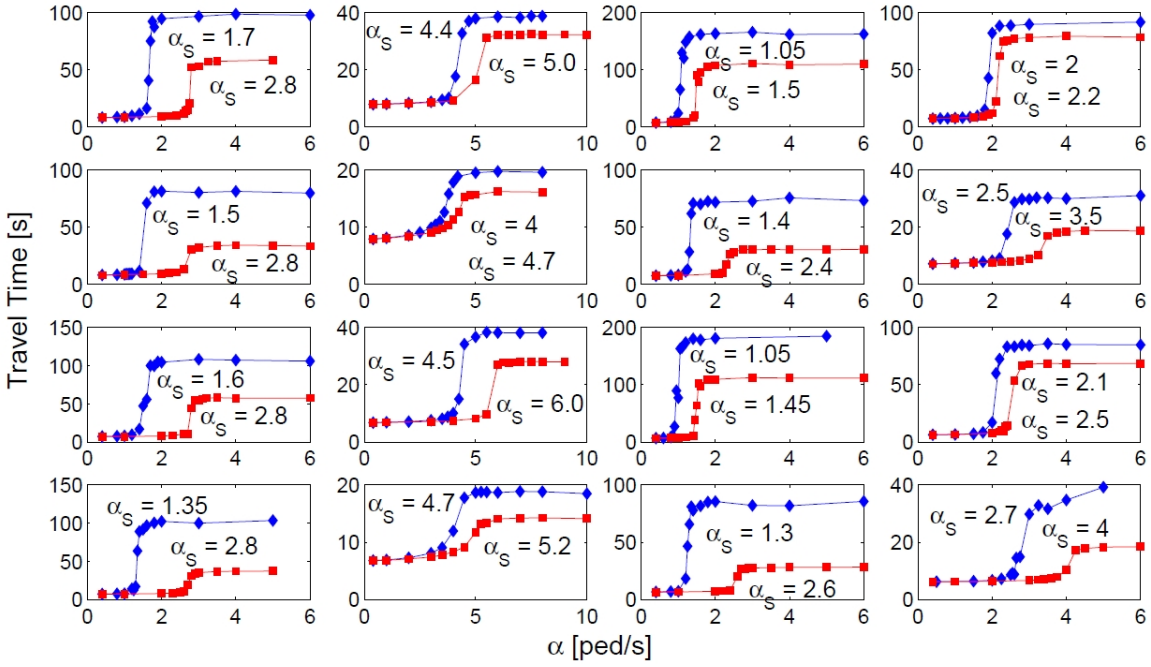


Figure 6.21: Travel time with respect to $\alpha$. The graph position corresponds to Table 6.7. Blue diamonds represent $\mu = 0.7$ and red squares $\mu = 0.2$

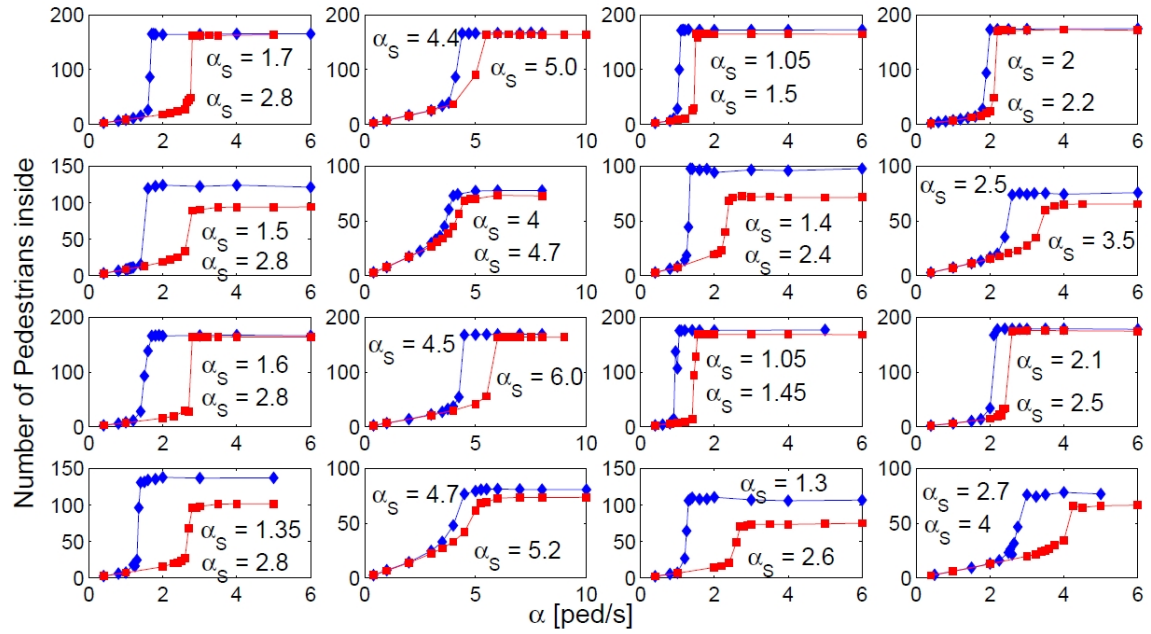


Figure 6.22: Occupancy with respect to $\alpha$. The graph position corresponds to Table 6.7. Blue diamonds represent $\mu = 0.7$ and red squares $\mu = 0.2$

From the simulation results in Figures 6.21 and 6.22, several conclusions can be made:

- Appropriate values of saturation inflow $\alpha_S$ are added to the graphs. We can read that the "capacity" of the room is not necessarily close to the number of cells $11 \times 18 = 198$. When the bonds principle is implemented (row 2 and 4, numbers 9-16 and 26-32), the maximal number of pedestrians is significantly lower. This can be explained by the possibility of choosing an occupied cell. Agents partially stand in lines and only several of them are trying to run over the crowd.

- Another important aspect is the shape of the curves near the saturation point. In the majority of the settings the average travel time levels before the saturation point (number of pedestrians increases linearly). The change of the curves towards the saturation value is sharp, jump-like. In settings with bonds and asynchronous updates (numbers 11/12, 15/16, 27/28, and 31/32) is the transition much smoother with respect to inflow $\alpha$. The travel time increases slightly before the saturation point and smoothly reaches the maximum corresponding to the saturation. This phenomenon is more obvious in the case of Moore neighborhood (columns 1 and 2), as expected. the smooth shape of the travel time curve in the case of bounds can be explained by the motion in lines which is supported by this principle. Agents are rather waiting in lines then walk around each other. In the higher inflow case ($2.0 < \alpha < 4.0$) leads to slight increase of the travel time, but suppresses the overall delay caused by the friction.

- From the observations it follows that the heterogeneity of the system does not qualitatively nor quantitatively influence the system on the macroscopic bases captured by the travel time, occupancy, or saturation point. This is mainly caused by two aspects. Firstly, the macroscopic quantities are compared by means of aggregated data, which suppresses the heterogeneity nature. Secondly, the heterogeneity in the setting is given by the 50-50 distribution of velocities $\tau_1$ and $\tau_2$ keeping the decision process intact (there are no aggressive pedestrians etc.). Nevertheless, in microscopic point of view does the heterogeneity influence the histograms of travel time in the free flow with $\alpha \ll \alpha_S$ as shown in Figure 6.23.

- The friction parameter influences mainly the behavior of the system with synchronous updates. Although the value $\mu = 0.7$ seems to be unrealistic (values between 0.2 and 0.3 are commonly used as e.g. in [78]), in the settings incorporating bonds and/or asynchronous update the number of conflicts is suppressed, therefore it is important to increase the friction to maintain the ratio of conflicts per time unit.

In Figure 6.24 four representatives are compared with two sets of experimental data. In agreement with [5], the transition from free flow to stable cluster was observed at inflow rate $\alpha \in (1.3, 1.6)$ ped/s.

**Conclusion**

Three characteristics have been used as the indicator of the saturation point and shape of the transition: average travel time, average occupancy of the room and average inflow. The analyses of the settings 11/12, 15/16, 27/28, and 31/32 (bounds and asynchronous update) shows that the transition does not have to be sharp and jump-like. In the mentioned settings the transition is rather smooth with respect to the inflow $\alpha$.

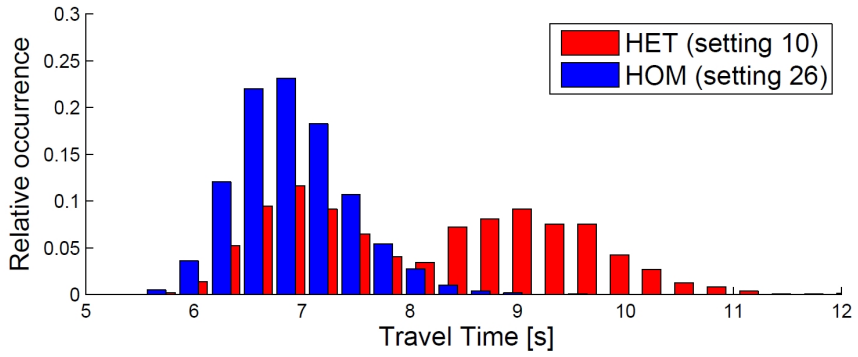


Figure 6.23: Travel time histograms for free flow $\alpha = 0.4$ ped/s.

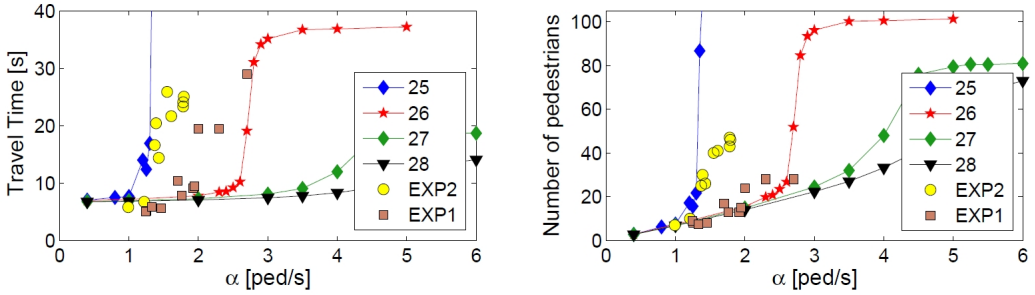


Figure 6.24: Comparison of selected settings with experiments (yellow circles and orange squares).

From the evaluation of experiments it follows that setting with higher friction corresponds better to the identified saturation point $\alpha_S \approx 1.4$ ped/s when principle of bounds is implemented. Furthermore, the synchronous update leads to better correspondence as well, as can be shown in Figure 6.24, where synchronous settings 25/26 are compared to asynchronous settings 27/28. The asynchronous update significantly suppresses the conflicts and therefore increases the maximal outflow from the room which leads to unrealistic high value of the saturation $\alpha \approx 4$ ped/s.

From the above mentioned analysis supported by the simple observation of the microscopic motion we conclude that the synchronous update with bounds, high friction, and Moore neighborhood is in the best correspondence with performed experiments.

## 6.5 Merge Simulations: Comparison with Social Distances Model

In this section [13], simulation results from two advanced CA based crowd dynamics models, namely Social Distances Model [140] and Floor Field model with Bonds Principle (further referred as Bonds Floor Field Model) [4] are investigated using experimental data. Two experiments regarding pedestrian egress from simple network of rooms with multiple consecutive bottlenecks was executed in Prague and Krakow. Simulation results comparison is the basis for discussion about models properties.

### 6.5.1 Experiment

This study leans over data from two conducted experiments, which focus on the egress of a group of pedestrians from a small network of rooms with multiple consecutive bottlenecks. In both experiments several groups of university students were instructed to egress the classrooms and leave the monitored part of the facility using one exit. The experimental layout is schematically depicted in Figure 6.25.

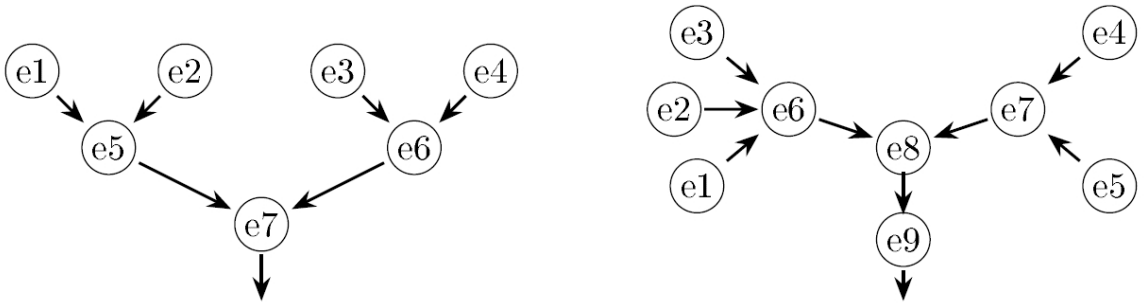


Figure 6.25: Schema of the experiment PRG (left), KRK (right). Arrows indicate the direction of motion.

Important characteristic of the experiments is joining of pedestrian streams, i.e., pedestrians from more entrances walked towards one exit. Key quantity used for the comparison of the models with experiment is the cumulative flow $J_j^{\mathrm{cum}}(t)$ through each exit denoting at each time $t$ the number of pedestrian, who passed through the exit $j$ until time $t$.

**PRG experiment** was conducted in Prague in the lecture hall of the Czech Technical University with help of 54 students. In the lecture hall, four staircases (exits 1-4) lead to two gathering places. Two exits 5 and 6 lead from the gathering points to the vestibule with one exit 7. The widths of the bottlenecks are 70 cm for exits 5 and 6, 75 cm for exit 7. The egress was repeated three times, the evacuation time was between 40 and 42 s. See E6 in intro or appendix for details.

**KRK experiment** was conducted in Krakow on one floor of the AGH University. Three rooms (exits 1-3) lead to a common hallway, which leads through exit 6 to the staircase hall. Similarly, two rooms (exits 4 and 5) lead to a hallway attached to the staircase hall on the

opposite side. The staircase hall leads to the stairs through exit 8, the stairs go downwards one floor leading to another hall through exit 9. The widths of the bottlenecks are 75 cm for exits 6 and 7, 177 cm for exits 8 and 9. The egress was repeated two times, 54 and 51 participants took place in this runs, respectively. In the first run the streams from exits 6 and 7 did not merge - corridor before exit 6 is longer than corresponding corridor before exit 7. Therefore, in the second run the part related to exit 7 was delayed by 11 seconds in order to obtain the merging behavior. The total evacuation time was 61 and 62 s.

### 6.5.2 Cellular Models

Two advanced CA models have been used to simulate the above mentioned experiments. The first one has been defined investigated on previous 50 pages, the second one was developed in AGH Krakow.

The main concept behind Social Distances Model (SDM) is incorporation of proxemics theory into CA crowd dynamics models. It is achieved by use of smaller cells - squares 25 x 25 cm$^2$, and elliptical representation of pedestrians with axis equals to 45 and 27 cm [137]. One cell can be occupied by one pedestrian and the center of cell coincides with the center of a pedestrian on the cell. Eight different orientations of pedestrian is allowed (0°, 45°, 90°, 135°, 180°, 225°, 270°and 315°).

It is worth noting, that with such a representation, the size of pedestrian is over 52% bigger (953,775 $cm^2$) that the size of the cell (625 $cm^2$). Therefore, according to its orientation pedestrians occupying adjacent cells can overlap. Here the *compressibility parameter* is introduced. It indicates pedestrians tolerance for high density (overlapping with another pedestrian). It, defines allowed and forbidden positions on the grid according to neighbors position and orientation. Low value of *compresibility parameter* bring the situation when pedestrians wants to keep their personal space, while high values allow pedestrians to get closer.

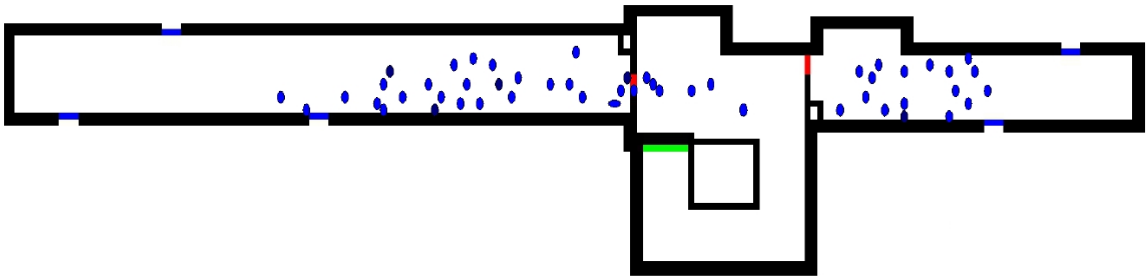

Figure 6.26: Discretization of space of the KRK experiment for the Social Distances Model.

What is interesting, our recent research[115] shows that tolerance for close neighbors depend on its position according to pedestrian. Neighbors on the sides can be ignored, even if they are relatively close, while the ones in front of (behind) are strongly avoided. However, it is not yet implemented in model.

SDM is based on typical Floor Field Model. Two kinds of floor field are included into the model: static FF which defines POIs, as well as dynamic FF which take into account

[2]Typical cells in CA models are 40 x 40 cm.

proxemics issues. Additional parameters are added in order to model wall avoidance and inertia effect.

Pedestrian can have the different desired speed. Desired speed is related with the number of steps that can be made in each second of simulation - from 1 to 8 steps. Thus, desired speed vary from $0.25\frac{m}{s}$ up to $2\frac{m}{s}$. The distribution of desired speed is the main calibration parameter for this model.

Detailed algorithm of floor field calculation and motion rules definition is provided in [140] Taking into account massive evacuation we proposed a dedicated version of the model [139].

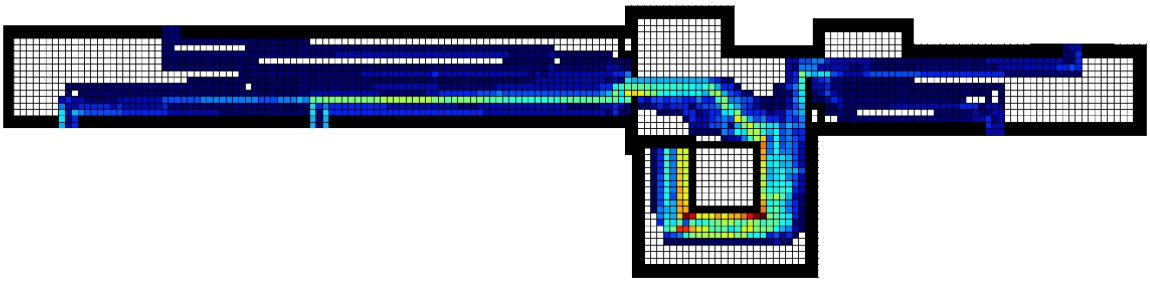

Figure 6.27: Pedestrians occurrence frequency during single simulation of KRK experiment using SDM. The hotter the color the more time given cell was visited.

### 6.5.3 Comparison with Experimental Data

Both models have been applied to the geometries related to the above mentioned experiments. The aim was to study, whether the models can reproduce same cumulative outflow from the main exit given that the inflow through the border/leaves exits (1-4 or 1-5) is known. Agents representing pedestrians are entering the system through the leaves exits in the same times as measured in the experiment.

#### Bonds FF and Experiment

For the simulation by means of the FF model with Bonds Principle we have chosen the homogeneous set of parameters noted in Table 6.4 calibrated for the simulation of one room with open boundaries.

In comparison to the above mention study, the value of the friction $\mu$ has been changed from 0.9 to 0.8 in order to reflect the fact that the widths of the bottlenecks related to exits 5 and 6 (PRG) and 6 and 7 (KRK) were higher than in the previous experiment (The exits are modeled by one cell corridors of the width 40 cm. Since it was impossible for two pedestrians to pass simultaneously in the experiment, the width is rather improved by lower friction then two cells corridor.). Secondly, in the case of KRK experiment, the own period of pedestrians $\tau_i$ has been changed from 0.2 s to 0.25 s, because the free flow velocity of pedestrians in the KRK experiment was lower than in the PRG experiment.

In Figure 6.28 you can see the comparison of cumulative flow from the experiment with several realisations of the stochastic Bonds FF model (BFF) for the PRG experiment (left) and the KRK experiment (right). We can see good agreement of the model data with the

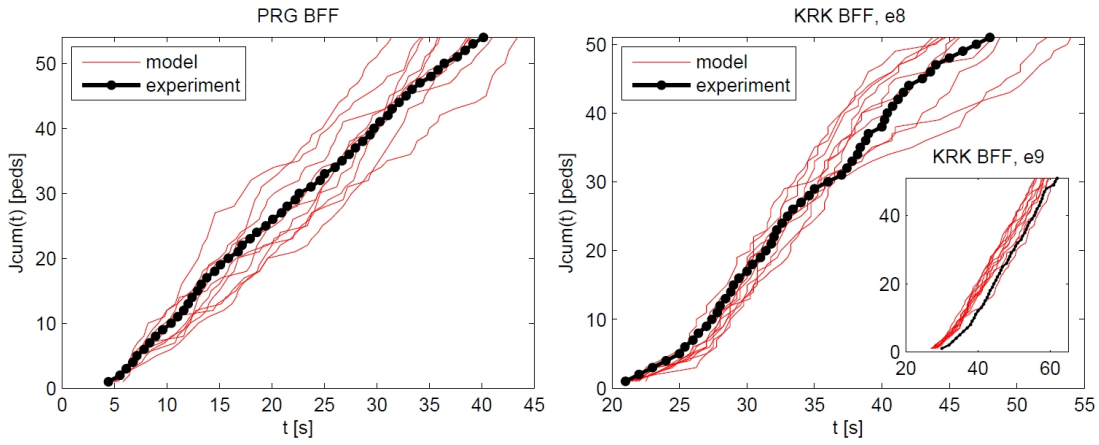


Figure 6.28: Comparison of cumulative flow from the experiments (black circles) and the BFF model (red lines). Left is the PRG experiment, first run, exit 7. Right is the KRK experiment, second run, exits 8 and 9.

experiment. It is worth noting that the model produces faster evacuation for the KRK experiment when considering the motion from exit 8 to exit 9, i.e., on the stairs. Here the model is not able reflect the slow-down of pedestrians while walking on stairs.

#### Social Distances Model and Experiment

Both experiments are modeled as non-competitive egress [140]. Moreover, since non significant clogs are present the compressibility parameter is set to 0 - ellipses that represent pedestrians can not overlap. The main parameter used for calibration is the desired maximal speed $v_{max}$ and its standard deviation $\sigma$. For both experiments the best results was obtained for $v_{max} = 1.25$ m/s. For Prague experiment deviation was set to $\sigma = 0.25$ m/s, while for Krakow experiment we use $\sigma = 0.1$ m/s.

In Figure 6.29 one can see comparison of experimental results with ten runs of its simulation. Good agreement between data and results can be observed. One can notice the influence of deviation $\sigma$ parameter - the spread of results is much higher for Prague experiment than for Krakow one. On the other hand, simulation results for Krakow are slightly shifted - egress in simulation is always faster than in real data. This phenomenon can be explained mainly by discretization of pedestrians velocity.

### 6.5.4 Summary and Conclusions

Two advanced CA models of crowd dynamics, Social Distances Model (SDM) and Bonds Floor Field Model (BFF), have been used for the simulation of an egress of simple network of rooms. The simulations have been compared to the measured data from two original experiments organized in Prague and Krakow.

The goal is to simulate the egress from a complex facility through a common exit given that the occupation flow from primary rooms (lecture halls, class rooms) is known or can be anticipated sufficiently precise. The performed experiments were designed correspondingly

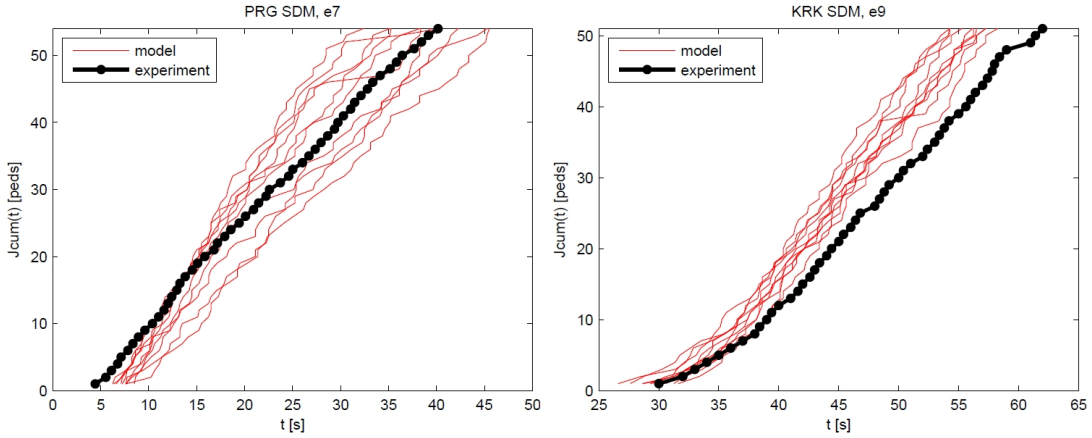


Figure 6.29: Comparison of cumulative flow from the experiments (black circles) and the SDM model (red lines). Left is the PRG experiment, first run, exit 7. Right is the KRK experiment, second run, exit 9.

to such anticipation. As the main comparison tool the cumulative outflow from the main exit has been used. By the cumulative outflow we understand the number of egressed pedestrians over time.

As shown in Section 6.5.3, the simulation results are in good agreement with the measured experimental data. Nevertheless, the stochastic nature of the models causes some variances in the individual trajectories of the simulation.

In Bonds Floor Field model, the stochasticity is caused mainly by the mechanism of conflict solution related to the situation when more agents are entering the same cell. This happens mostly in the cluster in front of the exit and therefore the conflict solution directly influences the exit capacity.

The stochasticity in Social Distances Model is contrarily caused by the deviation of the desired velocity related mainly to the motion in free flow. Such stochasticity can be controlled by appropriate choice of agents properties. Presented simulations for different experiments show the influence of parameter calibration (e.g. desired velocity and its standard deviation).

An important question to be answered is, whether the variance in evacuation times can be observed in reality. Such information can be helpful for appropriate choice of the model parameters. This is the goal of our further study, which requires to conduct the same experiment in various conditions, at different time, with different group of pedestrians.

## 6.6 Summary

Calibration and verification of the model was performed using experimental data obtained from in-house realized scenarios and, moreover, the experimental from Germany and Poland were available as well. It is not that complicated to calibrate parametrized model to fit few macroscopic quantities, but the satisfied match on microscopic features is much more complicated task.

Modifications described in previous chapters helped to find a set of parameters with reasonable level of heterogeneity that model results fits experimental observations not only in mean value but even on the distribution level. Such agreement is important in order to simulate the behavior of slowest pedestrians that are the most vulnerable during critical situations.

The data from Krakow validated the flexibility of the model, i.e. the ability to use the model for different arrangement and the set of participants that were used for calibration. The results turned to be positive, only minor adjustments caused by slower participants were needed to reach the fit between model and Krakow experiment.

As mentioned in the introduction, the fundamental model outcome is the predicted type of steady state. Except known congestion state and free flow, developed model has reproduced even metastable state described in the analytic chapter. As illustrated in previous sections, this state is metastable, but still observable in long term horizon.

# Chapter 7

# Summary

The assignment of this thesis focused mainly on the improvements of the cellular automata model in order to support the individualistic features. The combination of conducted experiments, data analysis and model enhancements verified in previous project enriched the model by the heterogeneity in velocity, aggressiveness and path selection. All these features were presented on prestigious conferences and published in impacted magazines. In parallel, the analytic conclusions were presented and published as well, mainly the heterogeneity, phase transition or time headway analysis.

Described success on the main rail opened the door for international cooperation on related projects. In cooperation with AGH Krakow and technical support from TU Munich, we have realized experimental and model analysis of merging of pedestrian streams. These results confirmed that both, cellular model and experimental knowledge base established in the main project is robust enough to handle complex infrastructure.

The second large follow up focused on the train evacuation. We were invited by the UCEEB CTU to help with the data analysis of train evacuation experiment. Originally simple task was extended to three years project included organizing another train evacuation experiment, providing micro and macroscopic data analysis and developing sensitivity model. The data from this project exposed another level of heterogeneity among the pedestrians/passengers and highlighted the need of individual data analysis to explain engineering level observations.

From academical perspective the project fulfilled its purposes. The author learned and applied multiple advanced techniques including image processing, statistical analysis or object programming as well as the leadership, project planning or presenting the results. All these skills were used even for unrelated projects brought to the attention from different academic directions. More over, the author was supervising three master students and he was providing courses for undergraduates related to this topic. Presented research was established within the department and was used even for propagation of the faculty to the public.

Even this project (including previous degrees) consumed ten years of research and the author had a support of more than ten colleagues, there are many interesting pedestrian question left unanswered. Several times we have touched the velocity - density paradigm that obviously works only under specific conditions, but this work just summarized experimental

observations and left complex analysis to someone else.

In general, we have shown the possibilities how apply the cellular model, how to improve it and how to bypass its weaknesses. But at some point we had to admit that other models may be appropriate in some specific situations. E.g. continuous agent based model that has been developed now within our research group benefits from its cellular ancestor. It has the ambition to mimic pedestrian behavior even better than presented model, but it seems the calibration costs would be high. The other pole is occupied by the hand calculation technique known for years that are able to answer engineering questions with the reliability that is frequently sufficient.

The main impact of this project seems to be the illustration that a microscopic analysis can uncover important information that vanishes in total or averaged numbers. In this thesis, such observations were highlighted and, moreover, the methods how to enhance any cellular model were proposed. Ultimately, any safety engineering institution may use it (similarly to may other proposals from scientific community) and build it to the applied methodology. The number of publications and citations indicate that some impact was already reached.

# Bibliography


[1] M. Bukáček, *Models of Granular Systems with Middle-Ranged Interactions*, Bachelor thesis, Czech Technical University in Prague, Czech Republic, 2011

[2] M. Bukáček, *Cellular Model of Pedestrian Dynamics with Adaptive Time Span*, Master thesis, Czech Technical University in Prague, Czech Republic, 2013

[3] P. Hrabák, M. Bukáček and M. Krbálek, *Cellular Model of Room Evacuation Based on Occupancy and Movement Prediction*, Lecture Notes in Computer Science 7495, 709–718, 2012

[4] P. Hrabák, M. Bukáček and M. Krbálek, *Cellular Model of Room Evacuation Based on Occupancy and Movement Prediction, Comparison with Experimental Study*, Journal of Cellular Automata 8, 383 – 395, 2013

[5] M. Bukáček, P. Hrabák and M. Krbálek, *Cellular Model of Pedestrian Dynamics with Adaptive Time Span*, Lecture Notes in Computer Science 8385, 669 – 678, 2014

[6] M. Bukáček, P. Hrabák and M. Krbálek, *Experimental Analysis of Two-Dimensional Pedestrian Flow in front of the Bottleneck*, In: Traffic and Granular Flow '13, 93 – 101, Springer, 2014

[7] M. Bukáček and P. Hrabák, *Case Study of Phase Transition in Cellular Models of Pedestrian Flow*, Lecture Notes in Computer Science 8751, 508 – 517, 2014

[8] M. Bukáček, P. Hrabák and M. Krbálek, *Experimental Study of Phase Transition in Pedestrian Flow*, Transportation Research Procedia 2, 105 – 113, 2014

[9] M. Kotrba, M. Bukáček, *Individual Approach to Evaluate Density and Flow in Egress Experiment*, In: SPMS 2015, pp. 97–105, 2015

[10] M. Bukáček and P. Hrabák, *Boundary Induced Phase Transition in Cellular Automata Models of Pedestrian Flow*, Journal of Cellular Automata 11/4, 327 – 338, 2016

[11] P. Hrabák, M. Bukáček and M. Krbálek, *Individual Microscopic Results Of Bottleneck Experiments*, In: Traffic and Granular Flow '15, 105–112, 2016

[12] M. Bukáček and P. Hrabák, *Conflict Solution According to Aggressiveness of Agents in Floor-Field-Based Model*, Lecture Notes in Computer Science 9574, 507 – 516, 2016

[13] P. Hrabák, J. Porzicky, M. Bukáček at all, *Advanced CA Crowd Models of Multiple Consecutive Bottlenecks*, Lecture Notes in Computer Science 9863, 396 – 404, 2016

[14] P. Hrabák and M. Bukáček, *Influence of Agents Heterogeneity in Cellular Model of Evacuation*, Journal of Computer Science 2017(21), 486–493, 2017

[15] M. Bukáček, P. Hrabák and M. Krbálek, *Microscopic Travel Time Analysis of Bottleneck Experiments*, Transportmetrica A 14(5-6), 375-391, 2018

[16] J. Porzicky, P. Hrabák, M. Bukáček at all, *Data Driven Method of Pedestrian Flow Estimation for Evacuation Scenario using Queuing Model*, In: EG-ICE 2016 proceedings, accepted

[17] M. Bukáček, H. Najmanová and P. Hrabák, *The Effects of Synchronization of Pedestrian Flow through Multiple Bottlenecks – Train Egress Study*, In: Pedestrian and Evacuation Dynamics 2016, 105–112, 2016

[18] M. Krbálek, P. Hrabák and M. Bukáček, *Pedestrian Headways – Reflection of Territorial Social Forces*, Physica A 490 (1), 38–49, 2018

[19] M. Bukáček, P. Hrabák, M. Krbálek, *Microscopic Travel Time Analysis of Bottleneck Experiments*, Transportmetrica A 14 (5–6), 375–391, 2018

[20] H. Najmanová, P. Hejtmánek, M. Bukáček, *Fire Safety of Passenger Trains: Experimental Analysis of Evacuation from CityElefant Double-deck Unit*, In: International Conference of Fire Safety 2016, 294–301, 2016

[21] M. Bukáček, V. Pešková, H. Najmanová, *Double-Deck Rail Car Egress Experiment: Microscopic Analysis of Pedestrian Time Headways*, In: Springer Proceedings in Physics: TGF 2019, 449–455, 2020

[22] H. Najmanová, L. Kuklík, V. Pešková, M. Bukáček, P. Hrabák, D. Vašata *Fire Safety of Passenger Trains: Experimental and Sensitivity Study of Evacuation from a Double-deck Train Unit*, in revision process

[23] M. Bukáček, J. Vacková, *Evaluation of Pedestrian Density Distribution with Respect to the Velocity Response*, In. Traffic and Granular Flow '17, 235–243, 2019

[24] P. Hrabák, M. Bukáček, P. Kielar, A. Borrmann, *Pedestrian Flow through Complex Infrastructure, Experiments and Mass-Transport Processes*, In. Traffic and Granular Flow '17, 159–166, 2019

[25] P. Kielar, P. Hrabák, M. Bukáček, A. Borrmann, *Using Raspberry Pi for Measuring Pedestrian Visiting Patterns via WiFi-Signals in Uncontrolled Field Studies*, In. Traffic and Granular Flow '17, 245–253, 2019

[26] J. Vacková, M. Bukáček, *Follower-Leader Concept in Microscopic Analysis of Pedestrian Movement in a Crowd*, Collective Dynamics 5, 496-498, 2020

[27] J. Vacková, M. Bukáček, *The Microscopic Analysis of Velocity-Density Paradigm*, In: Aplimat 2019, 1210–1222, 2020

[28] M. Bukáček, J. Vacková, *Statistical Analysis of Old Kingdom of Egypt* In: Aplimat 2019, 120–133, 2020

[29] M. Oharek, M. Bukáček, *Analysis of the Ancient Egyptian Society with Utilization of Decision Tree*, In: SPMS 2019, 93–106, 2019

[30] B. Paterek, M. Bukáček, *Clustering in Egyptian Ancient Society Analysis*, In: SPMS 2019, 107–114, 2019

[31] J. Vacková, M. Bukáček, *Ruling Principles for Decision-Based Pedestrian Model*, In: SPMS 2019, 141–154, 2019

[32] J. Vacková, M. Bukáček, *Social and Physical Pedestrian Sizes and their Impact on the Decision-Based Modeling*, In: FEMTC 2020, virtual, 1–11, 2020

[33] M. Kotrba, *Study of Macroscopic and Microscopic Quantities Describing the Pedestrians Movement*, Master thesis, Czech Technical University in Prague, Czech Republic, 2018

[34] M. Oharek, *Stochastic Methods Combining Neural Networks with Random Forests and their Applications to Medical Data Analysis*, Master thesis, Czech Technical University in Prague, Czech Republic, 2020

[35] M. Džabarjan, *Development of Alternative Methods for Density Calculation and Analysis of their Impact to the Fundamental Diagram*, Master thesis, Czech Technical University in Prague, Czech Republic, 2021

[36] J. Anděl, *Statisické metody*, Matfyzpress, 1998, ISBN: 80-85863-27-8

[37] C. Arita, J. Cividini, C. Appert-Rolland, *Shuffle Updates in an Evacuation Problem*, Transportation Research Procedia 2, 309–317, 2014

[38] J. Baik , A. Borodin , P. Deift, T Suidan, *A Model for the Bus System in Cuernavaca (Mexico)*, Journal of Physic A 39(28), 8965–8975, 2006

[39] R. Bailo, J. Carrillo, P. Degond, *Pedestrian Models Based on Rational Behaviour*, In: Crowd Dynamics (1), 259–292, 2018

[40] S. Bandini, L. Manenti, S. Manzoni, *Generation of Pedestrian Groups Distributions with Probabilistic Cellular Automata*, Lecture Notes in Computer Science 7495, 299–308, 2012

[41] S. Bandini, L. Crociani, G. Vizzari, *Heterogeneous Pedestrian Walking Speed in Discrete Simulation Models*, In: Traffic and Granular Flow '13, 273 – 279, 2015

[42] S. Bandini, M. L. Federici, G. Vizzari, *Situated Cellular Agents Approach To Crowd Modeling And Simulation*, Cybernetic Systems 38/7, 729–753, 2007

[43] N.W.F. Bode, E.A. Codling, *Statistical Models for Pedestrian Behavior in Front of Bottlenecks*, In: Traffic and Granular Flow '15, 81–88, 2016

[44] M. Boltes, J. Zhang, A. Seyfried, B. Steffen, *T-junction: Experiments, Trajectory Collection, and Analysis*, In: ICCV Workshops, 158–165, 2011

[45] C. Burstedde, K. Klauck, A. Schadschneider, J Zittartz, *Simulation of Pedestrian Dynamics using a Two-Dimensional Cellular Automaton*, Physica A 295/3–4, 507–525, 2001

[46] D. Cornforth, D. G. Green, D. Newth, *Ordered Asynchronous Processes in Multi-agent Systems*, Physica D 204/1–2, 70–82, 2005

[47] M. Campanella, S.P. Hoogendoorn, W. Daamen *Effects of heterogeneity on self-organized pedestrian flows*, Transportation Research Record 2124, 148–156, 2009

[48] B. Derrida *An exactly soluble non-equilibrium system: The asymmetric simple exclusion process*, Physics Reports 301/1–3, 65–83, 1998

[49] J. Dijkstra, H.J.P. Timmermans, A.J. Jessurun, *A Multi-Agent Cellular Automata System for Visualising Simulated Pedestrian Activity*, In: ACRI 2000 Proceedings, 29–36, 2000

[50] D. Duives, W. Daamen, S. Hoogendoorn, *Anticipation behavior upstream of a bottleneck*, Transportation Research Procedia 2, 43–50, 2014

[51] T. Ezaki, D. Yanagisawa, K. Nishinari, *Pedestrian Flow through Multiple Bottlenecks*, Physical Review E 86 (2), 026118, 2012

[52] T. Ezaki, D. Yanagisawa, K. Nishinari, *Analysis on a Single Segment of Evacuation Network*, Journal of Cellular Automata 8/5–6, 347–359, 2013

[53] T. Ezaki, D. Yanagisawa, K. Ohtsuka and K. Nishinari, *Simulation of Space Acquisition Process of Pedestrians using Proxemic Floor Field Model*, Physica A 391 (1-2), 291–299, 2012

[54] T. Ezaki, D. Yanagisawa, *Metastability in Pedestrian Evacuation*, Lecture Note in Computer Science 7495, 776–784, 2012

[55] K. Fridolf, D. Bilsson, H. Frantzich, *Evacuation of a Metro Train in an Underground Rail Transportation System: Flow Rate Capacity of Train Exits, Tunnel Walking Speeds and Exit Choice*, Fire Technology 52 (5), 1481–1518, 2016

[56] A. Garcimartin, D. R. Parisi, J. Pastor, C. Martin-Gomez, I. Zuriguel, *Flow of Pedestrians through Narrow Doors with Different Competitiveness*, Journal of Statistical Mechanics: Theory and Experiment (4), 043402, 2016

[57] I. G. Georgoudas, G. Koltsidas at all, *A Cellular Automaton Model for Crowd Evacuation and Its Auto-Obstacle Avoidance Attribute*, Lecture Notes in Computer Science 6350, 455–464, 2010

[58] Ch. Vihas, I. G. Georgoudas, G. Ch. Sirakoulis, *Follow-the-Leader Cellular Automata Based Model Directing Crowd Movement*, Lecture Notes in Computer Science 7495, 752–762, 2012

[59] H. Gotoh, E. Harada, E. Andoh, *Simulation of Pedestrian Contra-Flow by Multi-Agent DEM Model with Self-Evasive Action Model*, Safety Science 50/2, 326–332, 2012

[60] M. Haghani, M. Sarvi, *Identifying Latent Classes of Pedestrian Crowd Evacuees*, Transportation Research Record: Journal of the Transportation Research Board 2560, 67–74, 2016

[61] D. Helbing, P. Molnár, *Social Force Model for Pedestrian Dynamics*, Physical Review E 51 (5), 4282–4286, 1995

[62] D. Helbing, I. Farkash, T. Vicsek, *Simulating Dynamical Features of Escape Panic*, Letters to Nature 407, 487–490, 2000

[63] D. Helbing, L. Buzna, A. Johansson, T. Werner, *Self-Organized Pedestrian Crowd Dynamics: Experiments, Simulations, and Design Solutions*, In: Transportation Science, 1–24, 2005

[64] D. Helbing, A. Johansson, *Pedestrian, Crowd and Evacuation Dynamics*, Encyclopedia of Complexity and Systems Science, Springer, 2009

[65] C. M. Henein, T. White, *Macroscopic Effects of Microscopic Forces between Agents in Crowd Models*, Physica A 373, 694–712, 2007

[66] U. Chattaraj, A. Seyfried, P. Chakroborty, *Comparison of Pedestrian Fundamental Diagram across Cultures*, Advances in Complex Systems 12(03), 393–405, 2009

[67] B. Inditsky, H. Bodmann, H. Fleck, *Elements of Visual Performance Contrast Metric – Visibility Lobes – Eye Movements*, Lighting Research and Technology 14(4), 218–231, 1982

[68] V. Ivanac, B. D. Ďaši, Z. Vanjak, *Construction of Cellular Automata Lattice Based on the Semantics of an Urban Traffic Network*, Lecture Notes in Computer Science 7495, 795–806, 2012

[69] X. Ji, X. Zhou, B. Ran, *A Cell-Based Study on Pedestrian Acceleration and Overtaking in a Transfer Station Corridor*, Physica A 392 (8), 1828–1839, 2013

[70] A. Jelić, C. Appert-Rolland, S. Lemercier, J. Pettré, *Properties of Pedestrians Walking in Line: Fundamental Diagrams*, Physical Review E 85 (3), 036111, 2012

[71] D. Jezbera, D. Kordek, J. Kříž, P. Šeba, P. Šroll, *Walkers on the Circle*, Journal of Statistical Mechanic, L01001, 1–10, 2010

[72] A. Johansson, D. Helbing and H. Z. Al-Abideen, *Dynamics of Crowd Disasters: An Empirical Study*, Physical Review E 75, 046109, 2007

[73] A. Johansson, D. Helbing, P.K. Shukla, *Specification of the Social Force Pedestrian Model by Evolutionary Adjustment to Video Tracking Data*, Advances in Complex Systems 10, 271–288, 2007

[74] W. Kang, Y. Han, *A Simple and Realistic Pedestrian Model for Crowd Simulation and Application* arXiv preprint, arXiv:1708.03080, 2017

[75] R. E. Kass, A. E. Raftery, *Bayes Factors*, Journal of the American Statistical Association 90(430), 773–795, 1995

[76] V. Kautský. *Grouping Function of DUE Class Random Matrices*, Master thesis, Czech Technical University in Prague, Czech Republic, 2016

[77] A. Kirchner, A. Schadschneider, *Simulation of Evacuation Processes using a Bionics-Inspired Cellular Automaton Model for Pedestrian Dynamics*, Physica A 312 (1-2), 260–276, 2002

[78] A. Kirchner, K. Nishinari, A. Schadschneider, *Friction Effects and Clogging in a Cellular Automaton Model for Pedestrian Dynamics*, Physical Review E 67/5, 056122, 2003

[79] E. Kirik, T. Vitova, *On Validation of the SIgMA.CA Pedestrian Dynamics Model with Bottleneck Flow*, Lecture Notes in Computer Science 7495, 719–727, 2012

[80] P. Kleczek, J. Was, *Simmulation of Pedestrian Behavior in Shopping Mall*, Lecture Notes in Computer Science 8751, 650–659, 2014

[81] H. Klüpfel, M. Schreckenberg, T. Meyer-konig, *Models for Crowd Movement and Egress Simulation*, preprint, 2004

[82] N. Shinozaki, S. Koyama, S. Morishita, *Evacuation Simulation from Rooms through a Pathway and a Starway by Cellular Automata Based on the Public Guideline*, Lecture notes in computer science 7495, 743–751, 2012

[83] S. Koyama, N. Shinozaki, S. Morishita, *Modeling of Walking through Pathways and a Stairway by Cellular Automata Based on the Guideline for Evacuation*, Lecture Notes in Computer Science 7495, 728–737, 2012

[84] M. Krbálek, P. Šeba, *Statistical Properties of the City Transport in Cuernavaca (Mexico) and Random Matrix Ensembles*, Journal of Physics A 33, 229–233, 2000

[85] M. Krbálek, P. Šeba, *Headway Statistics of Public Transport in Mexican Cities*, Journal of Physics A 36, 1–5, 2003

[86] M. Krbálek, D. Helbing, *Determination of Interaction Potentials in Freeway Traffic from Steady-State Statistics*, Physica A 333, 370–378, 2004

[87] M. Krbálek, *Equilibrium Distributions in a Thermodynamical Traffic Gas*, Journal of Physics A 40, 5813–5821, 2007

[88] M. Krbálek, *Inter-Vehicle Gap Statistics on Signal-Controlled Crossroads*, Journal of Physics A 41, 205004, 2008

[89] M. Krbálek, P. Šeba, *Spectral Rigidity of Vehicular Streams (Random Matrix Theory Approach)*, Journal of Physics A 42, 345001, 2009

[90] M. Krbálek, *Analytical Derivation of Time Spectral Rigidity for Thermodynamic Traffic Gas*, Kybernetika 46 (6), 1108–1121, 2010

[91] M. Krbálek, *Theoretical Predictions for Vehicular Headways and Their Clusters*, Journal of Physics A 46, 4451011, 2013

[92] M. Krbálek, J. Šleis, *Vehicular Headways on Signalized Intersections: Theory, Models, and Reality*, Journal of Physics A 48, 015101, 2015

[93] M. Krbálek, T. Hobza, *Inner Structure of Vehicular Ensembles and Random Matrix Theory*, Physics Letters A 380 (21), 1839–1847, 2016

[94] T. Kretz, A. Grunebohm, M. Schreckenberg, *Experimental Study of Pedestrian Flow through a Bottleneck*, Journal of Statistical Mechanics 10, 1–20, 2006

[95] T. Kretz, M. Schreckenberg, *The F.A.S.T. – Model*, In: ACRI 2006 Proceedings, Lecture Notes in Computer Science 4173, 712–715, 2006

[96] T. Kretz, *Pedestrian Traffic, Simulation and Experiments*, Doctoral Thesis, Universitat Duisburg-Essen, Germany, 2007

[97] T. Kretz, M. Kaufman, M. Schreckenberg, *Counterflow Extension for the F.A.S.T.-Model*, Lecture Notes in Computer Science 5191, 555–558, 2008.

[98] L. Li, X.M. Chen, *Vehicle Headway Modeling and its Inferences in Macroscopic/Microscopic Traffic Flow Theory: A Survey*, Transportation Research Part C: Emerging Technologies 76, 170–188, 2011

[99] W. Liao, A. Tordeux, A. Seyfried, *Measuring the Steady State of Pedestrian Flow in Bottleneck Experiments*, Physica A 461, 248–261, 2016

[100] R. Lovreglio, E. Ronchi, D. Nilsson, *An Evacuation Decision Model Based on Perceived Risk, Social Influence and Behavioural Uncertainty*, Simulation Modeling Practice and Theory 66, 226–242, 2016

[101] R. Lubaś, J. Porzycki, J. Was, M. Mycek, *Validation and Verification of CA-Based Pedestrian Dynamics Models*, JCA 11 (4), 285–298, 2016

[102] S. Markos, J. K. Pollard, *Passenger Train Emergency Systems: Single-Level Commuter Rail Car Egress Experiments*, Technical Reports .DOT/FRA/ORD-10/11, Federal Railroad Administration, 2015

[103] M.L. Mehta, *Random matrices*, Academic Press, 2004

[104] M. Moussaid, D. Helbing, G. Theraulaz, *How Simple Rules Determine Pedestrian Behavior and Crowd disasters*, Proceedings of the National Academy of Sciences 108 (17), 6884–6888, 2011

[105] H. C. Muir, D. M. Bottomley, C. Marrison, *Effects of Motivation and Cabin Configuration on Emergency Aircraft Evacuation Behavior and Rates of Egress*, The International Journal of Aviation Psychology 6(1), 57–77, 1996

[106] K. Muller, *Die Gestaltung und Bemessung von Fluchtwegen fur die Evakuierung von Personen aus Gebauden*, Doctoral Thesis, Technische Hochschule Magdeburg, Germany, 1981

[107] R. Nagai, M. Fukamachi, T. Nagatani, *Evacuation of Crawlers and Walkers From Corridor Through an Exit*, Physica A 367, 449–460, 2006

[108] H. E. Nelson and F. W. Mowrer, *Emergency movement*, In: SFPE Handbook of Fire Protection Engineering 14, 367–367, 2002

[109] K. Nishinari at all, *Extended Floor Field CA Model for Evacuation Dynamics*, IEICE Transaction on Information and Systems 87D, 726–732, 2004

[110] K. Nishinari, A. Kirchner, A. Namazi and A. Schadschneider, *Simulations of Evacuation by an Extended Floor Field CA Model*, In: Traffic and Granular Flow '03, 405–410, 2005

[111] S. J. Older, *Movement of pedestrians on footways in shopping streets*, Traffic Engineering and Control 10, 160–163, 1968

[112] Oswald, M., Kirchberger, H., Lebeda C.: Evacuation of a High Floor Metro Train in a Tunnel Situation: Experimental Findings. In: Pedestrian and Evacuation Dynamics 2008, 67–81, 2010

[113] A. Owaidaha, D. Olarua, M. Bennamouna, F. Sohelb, N. Khan, *Review of Modelling and Simulating Crowds at Mass Gathering Events: Hajj as a Case Study*, Journal of Artificial Societies and Social Simulation 22 (2), 1–9, 2019

[114] J. Porzycki, M. Mycek, R. Lubaś, J. Was, *Pedestrian Spatial Self-organization According to its Nearest Neighbor Position*, Transportation Research Procedia 2, 201–206, 2014

[115] J. Porzycki, M. Mycek, R. Lubaś, J. Was, *Pedestrian Spatial Self-organization According to its Nearest Neighbor Position*, In PED'14, Transportation Research Procedia 2, 201–206, 2014

[116] J. Poryzcki, J. Was, L. Hedayatifar, F. Hassanibesheli, K. Kulakowski, *Velocity Correlations and Spatial Dependencies Between Neighbors in a Unidirectional Flow of Pedestrians*, Physical Review E 96(2-1),022307, 2017

[117] V. M. Predtechenskii, A. I. Milinskii, *Planing for Foot Traffic Flow in Buildings*, Amerind Publishing, 1978

[118] A. Schadschneider, A. Seyfried, *Empirical Results for Pedestrian Dynamics and their Implications for Cellular Automata Models*, In: Pedestrian Behavior - Models, Data Collection and Applications, 27–43, 2009

[119] A. Schadschneider, D. Chowdhury and K. Nishinari, *Stochastic Transport in Complex Systems*, Elsevier, 2010

[120] A. Schadschneider, W. Klingsch, H. Klüpfel, T. Kretz, Ch. Rogsch, A. Seyfried, *Evacuation Dynamics: Empirical Results, Modeling and Applications, Extreme Environmental Events: Complexity in Forecasting and Early Warning*, Springer, 2011

[121] M. Schultz, S. Lehmann, H. Fricke, *A Discrete Microscopic Model for Pedestrian Dynamics to Manage Emergency Situations in Airport Terminals*,In: Pedestrian and Evacuation Dynamics '05, 189–199, 2007

[122] A. Seyfried, B. Steffen, T. Lippert, *Basics of Modeling the Pedestrian Flow*, Physica A 368(1), 232–238, 2006

[123] A. Seyfried, B. Steffen, *Empirical Data for Pedestrian Flow Through Bottlenecks*, In: Traffic and Granular Flow 07, 189–199, 2009

[124] A. Seyfried, M. Boltes, *Enhanced Empirical Data for the Fundamental Diagram and the Flow Through Bottlenecks*, In: PED '08, 145–156, 2009

[125] A. Seyfried, O. Passon, B. Steffen, M. Boltes, T. Rupprecht, *New Insights into Pedestrian Flow Through Bottlenecks*, Transportation Science 43 (3), 395–406, 2009

[126] A. Seyfried, A. Portz, A. Schadschneider, *Phase Coexistence in Congested States of Pedestrian Dynamics*, Lecture Notes in Computer Science 6350: 496–505, 2010

[127] A.E. Scheflen, N. Ashcraft, *Human Territories: How We Behave in Space-Time*, Prentice-Hall, 1976

[128] E. Spartalis, I.G. Georgoudas, G.Ch. Sirakulis,*CA Crowd Modeling for a Retirement House Evacuation with Guidance*, Lecture Notes in Computer Science 8751, 481–491, 2014

[129] B. Steffen, A. Seyfried, *Methods for Measuring Pedestrian Density, Flow, Speed and Direction with Minimal Scatter*, Physica A 389(9), 1902–1910, 2010

[130] B. Steffen, M. Chraibi, *Multiscale Simulation of Pedestrians for Faster Than Real Time Modeling in Large Events*, Lecture Notes in Computer Science 8751, 492–500, 2014

[131] Y. Sumaa, D. Yanagisawa, K. Nishinari, *Anticipation Effect in Pedestrian Dynamics: Modeling and Experiments*, Physica A 391, 248–263, 2012

[132] W. Tian, W.G. Song, J. Ma, Z. Fang, A. Seyfried, J. Liddle, *Experimental Study of Pedestrian Behaviors in a Corridor Based on Digital Image Processing*, Fire Safety Journal 47, 8–15, 2012

[133] M. Treiber, D. Helbing, *Hamilton-like Statistics in Onedimensional Driven Dissipative Many-Particle Systems*, The European Physical Journal B 68, 607–618, 2009

[134] M. Treiber, A. Kesting, *Traffic Flow Dynamics: Data, Models and Simulation*, Springer, 2013

[135] G. Vizzari, L. Manenti, *An Agent-Based Model for Pedestrian and Group Dynamics: Experimental and Real-World Scenarios*, In: AAMAS, 1341–1342, 2012

[136] J. Was, B. Gudowski, P. J. Matuszyk, *Social Distance Model of Pedestrian Dynamics*, Lecture Notes in Computer Science 4173, 492–501, 2006

[137] J. Was, B. Gudowski, P. J. Matuszyk, *New Cellular Automata Model of Pedestrian Representation*, Lecture Notes in Computer Science 4173, 724–727, 2006

[138] J. Was, R. Lubas, W. Mysliwiec, *Proxemics in Discrete Simulation of Evacuation*, Lecture Notes in Computer Science 7495, 768–775, 2012

[139] J. Was, R. Lubaś, *Adapting Social Distances Model for Mass Evacuation Simulation*, Journal of Cellular Automata 8/5-6: 395–405, 2013

[140] J. Was, R. Lubaś *Towards Realistic and Effective Agent-Based Models of Crowd Dynamics*, Neurocomputing 146, 199–209, 2014

[141] U. Weidmann, *Transporttechnik der Fusganger*, ETH Zurich, 1993

[142] W. G. Weng, T. Chen, H. Y. Yuan, W. C. Fan, *Cellular Automaton Simulation of Pedestrian Counter Flow with Different Walk Velocities*, Physical Review E 74/3, 036102, 2006

[143] S. Wolfram, *A New Kind of Science*, Wolfram media, 2001

[144] X. Ji, X. Zhou, B. Ran, *A Cell-Based Study on Pedestrian Acceleration and Overtaking in a Transfer Station Corridor*, Physica A 392/8, 1828–1839, 2013

[145] K. Yamamoto, S. Kokubo, K. Nishinari, *New Approach for Pedestrian Dynamics by Real-Coded Cellular Automata (RCA)*, Lecture Notes in Computer Science 4173, 728–731, 2006

[146] K. Yamamoto, S. Kokubo, K. Nishinari, *Simulation for Pedestrian Dynamics by Real-Coded Cellular Automata (RCA)*, Physica A 379, 654–660, 2007

[147] K. Yamamoto, *Evacuation Simulation in Floor Field by Real-Coded Cellular Automata*, Lecture Notes in Computer Science 5191, 571–574, 2008

[148] D. Yanagisawa, A. Kimura, A. Tomoeda, R. Nishi, Y. Suma, K. Ohtsuka, K. Nishinari, *Introduction of Frictional and Turning Function for Pedestrian Outflow with an Obstacle*, Physical Review E 80/3, 036110, 2009

[149] J. P. Yuan, *Integrated Network Approach of Evacuation Simulation for Large Complex Buildings*, Fire Safety Journal 44/2, 266–275, 2009

[150] J. Zhang, A. Seyfried, *Quantification of Bottleneck Effects for Different Types of Facilities*, In PED'14, Transportation Research Procedia 2, 51–59, 2014

[151] J. Zhang, A. Seyfried, *Experimental Studies of Pedestrian Flows under Different Boundary Conditions*, 17th International IEEE Conference on Intelligent Transportation Systems (ITSC), 542–547, 2014

[152] K. Zhu, Q. Shi, *Experimental Study on Choice Behavior of Pedestrians during Building Evacuation*, Procedia Engineering 135, 207–216, 2016

[153] ISO 20414:2020, Fire Safety Engineering — Verification and Validation Protocol for Building Fire Evacuation Models, ICS 13.220.01, International Organization for Standardization, 2020